July 2021

# Finite Element Numerical Modeling and Parametric Study of Geosynthetic Reinforced Pile-Supported Embankments

Abdallah Ikbarieh
*Louisiana State University and Agricultural and Mechanical College*

# FINITE ELEMENT NUMERICAL MODELING AND PARAMETRIC STUDY OF GEOSYNTHETIC REINFORCED PILE-SUPPORTED EMBANKMENTS

A Thesis

Submitted to the Graduate Faculty of the
Louisiana State University and
Agricultural and Mechanical College
in partial fulfillment of the
requirements for the degree of
Master of Science in Civil Engineering

in

The Department of Civil and Environmental Engineering

by
Abdallah Ghaleb Ikbarieh
B.Sc., Jordan University of Science and Technology, 2018
August 2021

## Acknowledgments

Without all the support, guidance, motivation, and love of many people, all this work throughout my master's degree would have never been accomplished. First of all, I would like to express my deepest appreciation and gratitude to my advisor Professor Murad Abu-Farsakh for his tremendous support, motivation, guidance, and constructive criticisms throughout this research work. His leadership, wisdom, dedication, hard work, and involvement in this study made it possible. I will always be inspired by his personality, extraordinary experiences, and outstanding academic achievements.

My gratitude extends to Professor George Z. Voyiadjis, my co-advisor, for his valuable support, fruitful discussions, great conversations, and for sharing his knowledge throughout my research work. Finally, I would like to thank Professor Shengli Chen for his support and for accepting to be on my committee.

My thanks also go to all staff of Louisiana State University (LSU) and Louisiana Transportation Research Center (LTRC). I would like to express my gratitude to my research group mates for sharing the office and helping me to accomplish this work. Special thanks go to Dr. Ismaail Ghaaowd for his help and support in the first stage of work. My thanks also go to Dr. Ning Luo for supporting me through my research work. My sincere gratitude goes to my friends Hussein Alqrinawi, Hassan Amer, Abedalqader Idries, Salman Abusalman, Ariful Hassan Mojumder, and Hakam AL-Bataineh, who made this journey joyous and possible.

Last but not least, I would like to express my greatest appreciation and gratitude to my parents, Ghaleb and Najah, and my siblings Anwar, Sorayya, and Bader for their endless love and support throughout all the journeys in my entire life. I will always be indebted to you, and I would never be the person you see right now without being part of this family.

# Table of Contents

# Abstract

This study directed at investigating the performance of the pile-supported embankment system utilizing a geosynthetic reinforced load transfer platform (GRLTP) using Finite Element numerical modeling. A 2D Finite Element Modeling (FEM) methodology was first developed using PLAXIS 2D 2021 computer software and verified by well-documented case studies in the literature of this system. Second, a performance prediction was made for a field case study of the Amite River Project near French Settlement, which is located along Route LA 16 Livingston Parish in Louisiana State. A comprehensive FEM parametric study was then carried out to evaluate the performance of the system by changing the subsoil profiles, the GRLTP and the piles' extent under the embankment slope, embankment height, and pile spacing. Key performance measures included: settlement, lateral displacement, stress transfer, excess pore water pressure, and geosynthetic reinforcement strain. The subsoil profiles included very soft clay and very loose sand layers which were considered problematic layers. The GRLTP and the piles' extent were changed under the embankment slope as no support under the slope, one-quarter of the slope, mid-slope, three-quarters of the slope, and full length up to the embankment toe. Embankment heights were varied to be 3.05 m (10 ft), 6.10 m (20 ft), and 9.15 m (30 ft). An extensive parametric study of the performance of the system with changing the center-to-center pile spacing of 0.915 (3 ft), 1.22 m (4 ft), 1.525 m (5 ft), and 1.83 m (6 ft) was then conducted with each proposed embankment height. The results of the FEM parametric study showed a significant improvement in the system by utilizing a combination between timber piles and GRLTP in terms of the settlement, the differential settlement, and global stability. Better arching effect development was observed for the very soft clay cases compared to that of the very loose sand cases. Furthermore, the very loose sand cases showed less required GRLTP and piles to be extended under the slope compared to the very soft

clay cases. The FEM parametric study design recommendations were also compared with the Federal Highway Administration (FHWA) design recommendations for this system. The FHWA design recommendations showed an overestimation of the values obtained in the FEM parametric study for both the required horizontal distance between the outer pile edge and the embankment toe, and the required tensile stiffness of geosynthetics for support.

# CHAPTER 1.
# INTRODUCTION

## 1.1. Background and Description

It is common to encounter weak and soft clayey soils during the construction and execution of different geotechnical engineering projects. The main characteristics of these soils are low shear strength, high compressibility, and a tendency towards long-term consolidation settlement. Therefore, constructing big structures with significant loads on soft clay can lead to problems in both strength and serviceability limit states including bearing capacity failures, intolerable and differential settlement, lateral sliding, and slope failures. Many ground improvement techniques are used to limit or even these problems such as wick drains, surcharge loading, complete soil replacement. However, when time constraints play a vital role in the project's success, modern ground improvement techniques are needed to overcome these problems. Pile-supported embankments (also called column-supported embankments) with or without a geosynthetic reinforced load transfer platform (GRLTP) has been used by owners as an effective, economical (Magnan 1994) approach to deal with these concerns especially for the construction of highways, railways, wind turbines, buildings, storage tanks, and retaining walls (Chen et al. 2008). For the unreinforced pile-supported embankments, rigid piles such as driven piles and drilled shafts (Han and Gabr 2002; Liu et al. 2007. 2009; Chen et al. 2010; Briançon and Simon 2012), stone columns (Ambily and Gandhi 2007; Huang and Han 2009; Murugesan and Rajagopal 2010; Stuedlein and Holtz 2013; Zhou and Kong 2019), and deep mixed columns (Broms and Boman 1979; Han et al. 2002; Liu et al. 2012; Pongsivasathit et al. 2013; Jamsawang et al. 2016) are used to transfer the load of the embankment through the soft compressible soil layer to a firm foundation. However, this method requires closely spaced piles with large pile caps to ensure that the load from the

embankment is effectively transferred to the piles, and a small part of the load to the soft soil between piles. Moreover, inclined piles (battered piles) must be used to prevent lateral spreading. To reduce the cost, time, and construction difficulty of inclined piles, a GRLTP is used in order to minimize the number of piles required to support the embankment and to increase the efficiency of the design by redistributing internal load, and preventing punching effects. Figure 1.1 shows the typical detailing of the pile-supported embankment utilizing a GRLTP.

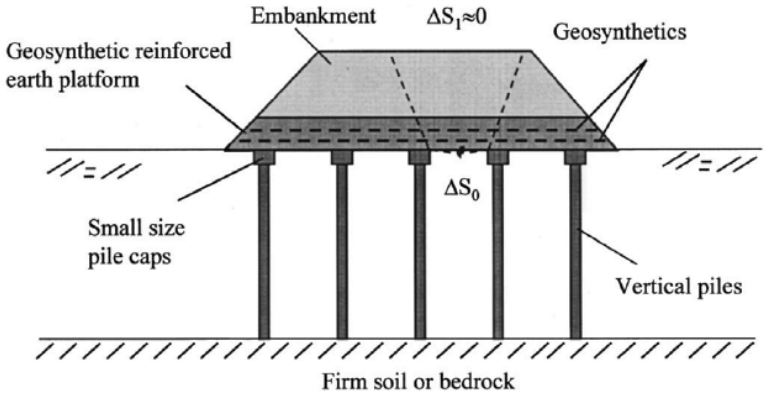


Figure 1.1. Typical detailing of the pile-supported embankment utilizing a GRLTP (Han and Gabr, 2002).

The GRLTP, located between the embankment and the piles, typically consists of granular fill reinforced by one or multiple layers of geosynthetic reinforcement, and helps to transfer load more efficiently to the piles. Above the platform, a non-select fill may be used to construct the remainder of the embankment. The main benefits of using a GRLTP are: increasing pile spacing, reducing the size of pile caps, and eliminating the use of inclined piles. Han (1999) reported that the area covered by pile caps could be reduced from 30-70% for the conventional system to 10-20% for the case of pile-supported embankments utilizing a GRLTP. Furthermore, the geosynthetics function as a separation between the subsoil and the embankment material, allow for drainage, enhance the mechanical properties of the soil with their high tensile strength, and counteract the lateral spreading at the embankment edges. A single layer of geosynthetic reinforcement of high

strength, or multiple layers of geosynthetic reinforcement with lower strength are typically used in the GRLTP.

Currently, there are two fundamental approaches to GRLTPs: the catenary method and the beam method. The catenary method considers the reinforcement to act as one layer at the interface between the subsoil, piles, and the embankment. Select fill may or may not be used above the geosynthetic, and the geosynthetic acts as a catenary. The beam method considers multiple (i.e., 3 or more) layers of reinforcement with a typical spacing of 150 mm (6 inches) to create a beam of reinforced soil.

During the construction of the embankment, differential settlement occurs between the rigid piles and the consolidated soft soil leading to a non-uniform vertical stress distribution across the base of the embankment. Greater vertical stresses occur on top of the pile more than the soft soil forming a soil arch between adjacent piles. Consequently, shear stresses are generated in the fill material, and through the arching effect, the vertical stresses are transferred from the soft foundation material onto the piles. Comparing the conventional pile-supported embankment with the reinforced pile-supported embankment, the subsoil between two adjacent piles settles approximately the same in the unreinforced system although the soil near the piles may experience less deformation due to the pile skin friction, resulting in a more or less uniformly distributed stress acting on the subsoil between piles. On the other hand, the pressure acting on the reinforcement between piles in the geosynthetic reinforced pile-supported embankment is distributed as follows: large load is exerted on the reinforcement strips located exactly between adjacent piles as they have the shortest span between piles, resulting in less settlement than other locations, and attracting greater load than elsewhere. Moreover, the pressure acting on a certain reinforcement strip is at the highest near the piles since it has lower deflection than in the middle between piles.

The vertical load transferred from the embankment is divided into three parts as shown in Figure 1.2. Load part A is the load transferred directly on top of the piles, load part B is the load applied on the reinforcement at the platform and transferred to the piles, and load part C is the subsoil support.

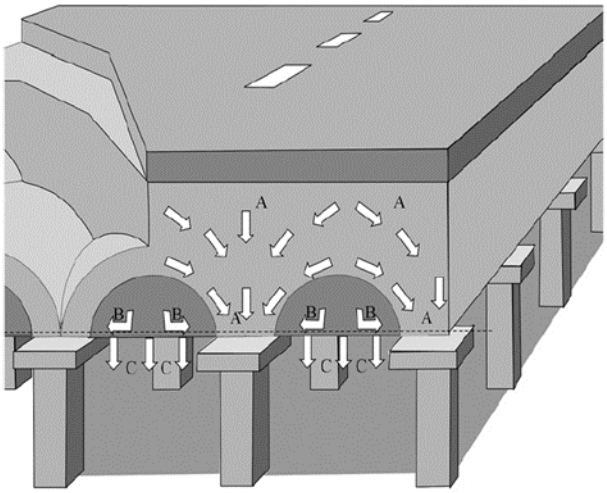


Figure 1.2. Vertical load divisions (Van Eekelen et al., 2011).

**1.2. Problem Statement**

Pile-supported embankment system utilizing a geosynthetic reinforced load transfer platform (GRLTP) has proven itself rule to be a cost-effective solution in a lot of projects which have problematic soil such as high compressible soils with low shear strength. Presently, there is disagreement in the literature on the methods and assumptions made to build the arching models and construction guidelines, and thus, reported results of soil arching models and stress distribution differ significantly in terms of the evaluation of the pile-supported embankment system with a GRLTP. Also, there are some researchers who did try to conduct parametric studies using numerical modeling techniques to evaluate the effect of changing different design parameters on the performance of the system. However, the number of researchers who took into consideration the pile configuration condition (end-bearing and floating piles) is low. Evaluating the

performance of pile-supported embankment utilizing the GRLTP is crucial for the design of embankment approaching bridges and other structures. Nevertheless, there is a scarcity of research performed in Louisiana or using Louisianan soil. This research is intended to predict the performance of one of the Louisiana Department of Transportation and Development (LA DOTD) proposed pile-supported embankments utilizing a GRLTP which is the Amite River project. Furthermore, an extensive parametric study will be conducted for soil stratification representing the subsoil condition of Louisiana subsurface soil. Also, as timber piles are commonly used in Louisiana, the performance of the system when the embankment is supported by timber piles and a GRLTP will be addressed in this study.

### 1.3. Research Objectives and Approach

The ultimate goals of this research are to evaluate the short-term (during construction) and long-term performance of pile-supported embankment utilizing GRLTP in the state of Louisiana, to assess the effect of changing different variables involved in the design, and to verify and modify important design factors and construction guidelines used in the design of the system. The main design factors are the pile design requirements, the GRLTP and piles' extent under the slope, acceptable embankment heights, acceptable center-to-center pile spacing, and the GRLTP configuration. These objectives are accomplished through conducting an extensive numerical modeling study using PLAXIS 2D Finite Element Software. First, different soil profiles are proposed and the piles are designed accordingly. Second, the GRLTP and the piles' extent is investigated by changing the embankment height, and the soil profile and condition. Assuming a 1V:2H side slope, the horizontal distance of the slope is 2H. Accordingly, the proposed GRLTP and piles' extent are 0.0H (at the embankment crest), 0.5H (one-quarter of the slope), 1.0H (mid-slope), 1.5H (three-quarters of the slope), and 2.0H (full length up to the embankment toe). The

embankment height is varied to be 3.05 m (10 ft), 6.10 m (20 ft), and 9.15 m (30 ft). Soil profiles are divided into two groups: Cases 1 and 2, and Cases 3 and 4. Cases 1 and 2 are where a very soft clay layer exists underneath the embankment, whereas Cases 3 and 4 are where a very loose sand layer exists underneath the embankment. Furthermore, the stress history of the very soft clay is included by investigating a normally consolidated (NC) and overconsolidated (OC) soil conditions. Table 1.1 shows the factorial table for the GRLTP and piles' extent' under the slope. This is followed by an extensive parametric study of the performance of the system with changing the center-to-center pile spacing of 0.915 (3 ft), 1.22 m (4 ft), 1.525 m (5 ft), and 1.83 m (6 ft) with each proposed embankment height. Table 1.2 shows the factorial table for the pile spacing parametric study.

Table 1.1. GRLTP and piles' extent parametric study factorial table.

| Soil Profile | H (m) | 3.05 | | 6.10 | | 9.15 | | Number of Models |
|---|---|---|---|---|---|---|---|---|
| | Soil Condition | NC | OC | NC | OC | NC | OC | |
| Cases 1 & 2 | GRLTP and Piles' Extent | 0.0H | 0.0H | - | - | - | - | 2 |
| | | 0.5H | 0.5H | 0.5H | 0.5H | - | - | 4 |
| | | 1.0H | 1.0H | 1.0H | 1.0H | - | - | 4 |
| | | 1.5H | 1.5H | 1.5H | 1.5H | 1.5H | 1.5H | 6 |
| | | 2.0H | 2.0H | 2.0H | 2.0H | 2.0H | 2.0H | 6 |
| Cases 3 & 4 | GRLTP and Piles' Extent | 0.0H | | 0.0H | | - | | 2 |
| | | 0.5H | | 0.5H | | - | | 2 |
| | | 1.0H | | 1.0H | | 1.0H | | 3 |
| | | 1.5H | | 1.5H | | 1.5H | | 3 |
| | | 2.0H | | 2.0H | | 2.0H | | 3 |
| Total | | | | | | | | 35 |

Table 1.2. Pile spacing parametric study factorial table.

| Soil Profile | H (m) | Spacing (m) | | | | Number of Models |
|---|---|---|---|---|---|---|
| Case 1 | 3.05 | 0.915 | 1.220 | 1.525 | 1.830 | 4 |
| | 6.10 | 0.915 | 1.220 | 1.525 | 1.830 | 4 |
| | 9.15 | 0.915 | 1.220 | 1.525 | 1.830 | 4 |
| Case 2 | 3.05 | 0.915 | 1.220 | 1.525 | 1.830 | 4 |
| | 6.10 | 0.915 | 1.220 | 1.525 | 1.830 | 4 |
| | 9.15 | 0.915 | 1.220 | 1.525 | 1.830 | 4 |
| Case 3 | 3.05 | 0.915 | 1.220 | 1.525 | 1.830 | 4 |
| | 6.10 | 0.915 | 1.220 | 1.525 | 1.830 | 4 |
| | 9.15 | 0.915 | 1.220 | 1.525 | 1.830 | 4 |
| Case 4 | 3.05 | 0.915 | 1.220 | 1.525 | 1.830 | 4 |
| | 6.10 | 0.915 | 1.220 | 1.525 | 1.830 | 4 |
| | 9.15 | 0.915 | 1.220 | 1.525 | 1.830 | 4 |
| Total | | | | | | 48 |

### 1.4. Outline

The outline for this Thesis is as following; Chapter 2 presents the literature review for the previous work on the design and numerical modeling studies of the pile-supported embankment system. Chapter 3 presents the Finite Element Modeling (FEM) methodology and the constitutive models. Chapter 4 presents the validation of the FEM methodology on well-documented case studies of the pile-supported embankments. Chapter 5 presents the prediction of the performance of the Amite River Project in the state of Louisiana. Chapter 6 presents the extensive parametric study and a comparison between the FEM recommendations and the Federal Highway Administration (FHWA) design recommendations. Chapter 7 presents the conclusions and recommendations.

# CHAPTER 2.
# LITERATURE REVIEW

## 2.1. Soil Arching

The soil arching has been studied by many researchers in the literature using field tests (Lin and Wong 1999; Liu et al. 2009; Chen et al. 2010; Zhang et al. 2016), laboratory model tests (Terzaghi 1943; Hewlett and Randolph 1988; Guido et al. 1987; Low et al. 1994; Jenck et al. 2005; McGuire et al. 2012; van Eekelen et al. 2012a, b) and numerical modeling (Han and Gabr 2002; Jenck et al. 2009; Le Hello and Villard 2009; Jones et al. 2010; Halvordson et al. 2010; Plaut and Filz 2010; Han et al. 2012; Zhang et al. 2013; Lai et al. 2014, 2018, 2020).

Two formulas were mainly used by many design engineers and researchers to evaluate the load distribution on the GRLTP, soft soil, and piles due to the arching effect: the Marston theory (Marston 1913) and the Terzaghi theory (Terzaghi 1943) which was adopted in methods of Jones et al. (1993) and Chen et al. (2008), and the hemispherical soil arching model by Hewlett and Randolph (1988) which was adopted in methods of Low et al. (1994), Kempfert et al. (1997), Abusharar et al. (2009), Zhuang et al. (2014), and van Eekelen et al. (2013). The first group of methods took into consideration the equilibrium equation for the embankment fill relative displacement and required friction between the soil columns upon piles and subsoil, and considered a rectangle (in two-dimensional (2D) conditions) or a cylinder (in three-dimensional (3D) conditions) as the influence area affected by the arch. The second group of methods used the limit equilibrium equations and assumed that the soil arching has a constant height and would reach the ultimate state either at the crown or at the pile head. Guido et al. (1987) and Carlson (1987) proposed methods assuming that the subsoil carries a portion of the embankment load below a fixed shape of the soil arch.

## 2.2. Pile-Supported Embankment System Design

Pile-supported embankment utilizing the GRLTP design must conform with strength and serviceability limit states. First, piles are designed to carry the vertical load due to the soil arching without failing, and thus, the total load (embankment load and surcharge load) is assumed to be carried by the piles. Second, pile group extent under the embankment slope must be determined to avert any slope instability. Third, the GRLTP is designed to resist and transfer the vertical load due to soil arching to the piles. Fourth, lateral sliding of embankment fill due to the lateral thrust at the edges must be evaluated and checked. Finally, the global stability of the whole system is addressed and evaluated against any potential failure mechanisms. For the serviceability limit state, the strain in the geosynthetic reinforcement must not exceed a maximum value of approximately 5% (Schaefer et al., 2017) to prevent differential settlement at the crest of the embankment. Furthermore, the settlement of the overall system is evaluated and checked against a certain level depending on the structure and its function.

### 2.2.1. Piles Design

Piles are selected to meet the constructability requirements, structural and geotechnical capacities, and the cost. The total load of the embankment and the surcharge load are assumed to be carried by the pile based on the tributary area for each pile. It has been found that the tributary area shape around the pile is a regular hexagon (Collin et al., 2005). However, this tributary area can be approximated to an equivalent circle having the same area as the hexagon. The effective (equivalent) diameter of the circle is 1.13 and 1.05 times the center-to-center pile spacing for square and circular pile arrangements, respectively. The required design vertical load ($Q$r) in the column is:

$$Q\text{r} = \pi\left({}^{De}/_{2}\right)^{2}(\gamma H + q) \tag{2.1}$$

Where $De$ is the effective tributary area diameter of the pile ($De$= 1.13s for square spacing, $De$= 1.05s for triangular spacing).

$H$ is the height of the embankment.

$q$ is the live and dead load surcharge (typically 12 kPa/250 psf).

$\gamma$ is the unit weight of the embankment soil.

s is the center-to-center pile spacing.

**2.2.2. Lateral Extent of Piles**

Piles should extend a sufficient distance near the toe of the embankment to prevent the potential of slope instability or differential settlement outside the supported area (Figure 2.1). The maximum horizontal distance between the extreme edge of the pile or the pile cap and the embankment toe, $L_p$, as follows (BS 8006, 2010):

$$L_p = H(n - tan\theta \mathrm{p}) \tag{2.2}$$

Where $n$ is the side slope of the embankment.

$\theta_\mathrm{p}$ is the angle (from vertical) between the outer edge of the outer-most column and the crest of the embankment ($\theta_\mathrm{p}$= $45° - \phi_{emb}/2$).

$\phi_\mathrm{emb}$ = effective friction angle of embankment fill.

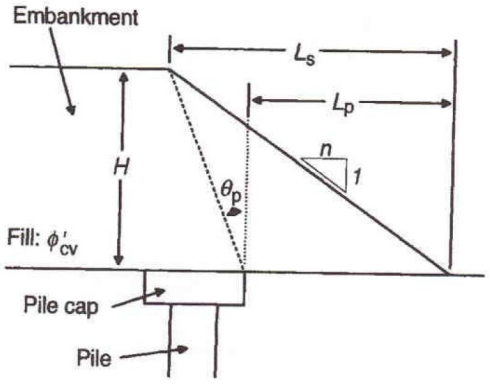


Figure 2.1. Lateral extent of piles under the embankment slope (BSI, 2010).

### 2.2.3. Lateral Spreading

Lateral spreading must be resisted by the subsoil strength or the geosynthetic reinforcement tensile strength (Figure 2.2). The lateral spreading ($P_{Lat}$) is determined as follows:

$$P_{Lat} = K_a \left[\gamma \left({H^2}/{2}\right) + qH\right] \quad (2.3)$$

Where $K_a$ is the coefficient of active earth pressure $[\tan^2(45° - \phi_{emb}/2)]$.

Moreover, the minimum length of reinforcement ($L_e$) beyond the crest and towards the toe of the embankment to maintain bonding between the reinforcement and surrounding material without sliding of the embankment is determined as follows:

$$L_e = \frac{P_{Lat}}{0.5\,\gamma H\, c_{iemb} tan\phi_{emb}} \quad (2.4)$$

Where $c_{iemb}$ is the coefficient of interaction for sliding between the geosynthetic reinforcement and embankment fill.

The resistance to lateral spreading without a geosynthetics reinforcement is determined by:

$$R_{ls} = (L_s)\, S_u \quad (2.5)$$

Where $S_u$ is the undrained shear strength of the foundation soil.

$L_s$ is the length of the side slope of the embankment.

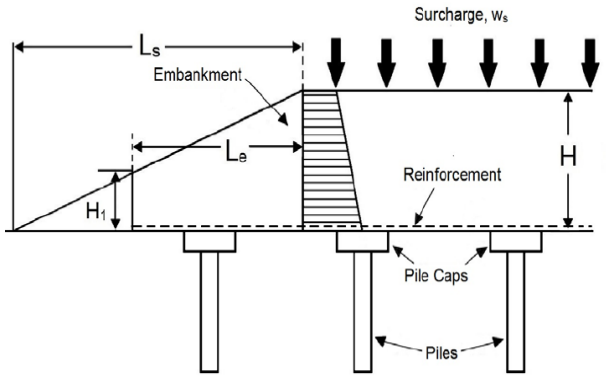


Figure 2.2. Lateral spreading effect at the embankment edges.

### 2.2.4. Load Transfer Platform Design

The vertical pressure acting on the GRLTP and the developed tension in the geosynthetic reinforcement have been studied by different researchers with different analysis methods. The vertical load carried by the geosynthetic reinforcement can be expressed in terms of the stress reduction ratio, $SRR$, which is defined as the average stress on the subgrade soil or geosynthetic reinforcement to the average vertical stress at the base of the embankment consisting of the embankment weight and the surcharge load $\left(SRR = \frac{\sigma_{soil}}{\gamma H+q}\right)$, where $\sigma_{soil}$ is the stress on the soil between columns or pile caps, γ is the unit weight of the embankment fill, $H$ is the embankment height, and $q$ is the surcharge pressure at the surface of the embankment. Accordingly, $\sigma_{soil}$ is used to calculate the tension developed in the geosynthetic reinforcement.

#### 2.2.4.1. British Standards Institution (BSI, 2010)

The British Standard "Code of practice for strengthened/reinforced soils and other fills" adopted an empirical method developed by Jones et al. (1990), which is based on Marston's equation (Marston 1913) for a positive projecting conduit. In this method, the stress acting on the piles is determined, and the remaining stress is assumed to be carried by the GRLTP. Nevertheless, this method assumes zero support from the subsoil (load part C=0). The stress distribution due to soil arching is governed by the pile type (friction piles, end bearing piles), width of the pile, and height of the embankment. If H>1.4(s-a), full arching will occur, and if H<1.4(s-a), partial arching is the resulting arch.

The vertical stress acting on the pile head is determined as follows:

$$\frac{p_c'}{\sigma_v'} = \left(\frac{C_c a}{H}\right)^2 \tag{2.6}$$

Where $p_c'$ is the vertical stress on the pile caps.

$\sigma_v'$ is the factored average vertical stress at the base of the embankment ($\sigma_v' = \gamma H + q$).

$C_c$ is the arching coefficient ($C_c$= 1.95$H/a$ – 0.18 for end bearing piles, and $C_c$= 1.5$H/a$ – 0.07 for friction and other piles).

$a$ is the pile width.

$H$ is the embankment height.

And thus load part A is:

$$A = p_c' a^2 = \left(\frac{C_c a}{H}\right)^2 \sigma_v' \, a^2 \tag{2.7}$$

For partial arching, pressure on GR ($p_r'$) can be obtained by subtracting the total load from the pile load divided by $s^2 - a^2$ as follows:

$$p_r' = \frac{(\gamma \mathrm{H} + \mathrm{q}) - p_c' a^2}{s^2 - a^2} = (\gamma \mathrm{H} + \mathrm{q}) X \tag{2.8}$$

And;

$$X = \frac{\left(s^2 - a^2 \frac{p_c'}{(\gamma \mathrm{H} + \mathrm{q})}\right)}{s^2 - a^2} \tag{2.9}$$

The distributed load $W_T$ (assuming a rectangular uniform distribution) carried by the reinforcement between adjacent pile caps (s-a):

$$W_T = \mathrm{s}(\gamma \mathrm{H} + \mathrm{q}) X \tag{2.10}$$

And thus load part B (assumed to be distributed on the area s-a and s) and SSR, respectively are:

$$B = 2W_T (\mathrm{s-a}) \tag{2.11}$$

And;

$$SSR = \frac{2WT (\mathrm{s-a})}{(s^2 - a^2)(\gamma \mathrm{H} + \mathrm{q})} \tag{2.12}$$

For full arching, the distributed load $W_T$ (assuming a rectangular uniform distribution) carried by the reinforcement between adjacent pile caps (s-a):

$$W_T = 1.4 \mathrm{s} \gamma (s - a) X \tag{2.13}$$

And thus load part B (assumed to be distributed on the area s-a and s) and SSR, respectively are:

$B = 2W_T(s\text{-}a) = 2.8s\gamma(s-a)^2X$ (2.14)

And;

$SSR = \frac{2.8s\gamma(s-a)^2X}{(s^2-a^2)(\gamma H + q)}$ (2.15)

The BS8006 (BSI, 2010) method uses the parabolic method for a square grid of piles. However, this method does not incorporate stress-strain compatibility. The tensile force developed in the geosynthetic reinforcement is determined using the tensioned membrane theory. This method recommends placing one or two layers of reinforcement above the piles. The tensile load in the geosynthetic per unit width, $T_{rp}$, developed under the vertical line load $W_T$ is:

$$T_{rp} = \frac{W_T(s-a)}{2a}\sqrt{1+\frac{1}{6\varepsilon}}; \quad (2.16)$$

The maximum mid-span deflection y of extensible reinforcement:

$$y = (s-a)\sqrt{\frac{3\varepsilon}{8}}, \ Practical\ maximum\ of\ 300\ mm \quad (2.17)$$

Therefore, the strain is:

$$\varepsilon = \frac{8y^2}{3(s-a)^2} \quad \text{(Practical upper limit 6\%)} \quad (2.18)$$

**2.2.4.2. Hewlett and Randolph (1988)**

Hewlett and Randolph (1988) proposed a semi-circular dome soil arching model to estimate the load carried by piles. This method is based on the limit equilibrium equations, has a constant soil arching height, and would reach the ultimate state either at the crown or at the pile head.

Hewlett and Randolph expressed the distributed load on reinforcement in terms of E, which is the proportion of the embankment weight carried by the piles. Hence the proportion of the embankment weight carried by the geosynthetic reinforcement may be determined (1−E). The condition of failure at the crown $E_{crown}$:

$$E_{crown} = 1 - \left[1 - \left(\frac{a}{s}\right)^2\right](A - AB + C); \quad (2.19)$$

$$A = \left[1 - \left(\frac{a}{s}\right)\right]^{2(K_p-1)}; B = \frac{s}{\sqrt{2}H}\left(\frac{2K_p-2}{2K_p-3}\right); C = \frac{s-a}{\sqrt{2}H}\left(\frac{2K_p-2}{2K_p-3}\right) \quad (2.20)$$

$$SSR = \left(1 - \frac{a}{s}\right)^{2(K_p-1)}\left(1 - \frac{s\,.\,2\,(K_p-1)}{\sqrt{2}\,.\,H\,.(2K_p-3)}\right) + \left(\frac{(s-a)\,.\,2\,.\,(K_p-1)}{\sqrt{2}\,.\,H\,.(2K_p-3)}\right) \quad (2.21)$$

The condition of failure at the pile cap $E_{cap}$:

$$E_{cap} = \frac{\beta}{\beta+1}; \beta = \frac{2K_p}{(K_p+1)(1+\frac{a}{s})}\left[\left(1 - \frac{a}{s}\right)^{-K_p} - \left(1 + \frac{K_p a}{s}\right)\right] \quad (2.22)$$

$$SSR = \frac{1}{\left(\frac{2K_p}{K_p+1}\right)\left[\left(1-\frac{a}{s}\right)^{1-K_p} - \left(1-\frac{a}{s}\right).\left(1+\frac{a}{s}.\,K_p\right)\right]+\left(1-\frac{a^2}{s^2}\right)} \quad (2.23)$$

Thus, the distributed load $W_T$ carried by the reinforcement between adjacent pile caps:

$$W_T = \frac{s(\gamma H+q)}{(S^2-a^2)}(1 - E_{min})s^2 \quad (2.24)$$

Where $K_p$ is the Rankine passive earth pressure coefficient ($K_p = \frac{1+sin\phi}{1-sin\phi}$).

$E_{min}$ is the minimum of $E_{crown}$ and $E_{cap}$.

**2.2.4.3. Carlson Method (1987)**

Carlson (1987) proposed a triangular soil-arching model which was adopted as the Swedish Method. The arching soil can be approximated by a wedge with an internal angle at the apex of the wedge equal to 30º. This method adopts a critical height (1.87(s-a)) approach such that any additional overburden above the top of the wedge is transferred directly to the columns.

Carlson (1987) calculates with the complete weight of the soil wedge, even when the height of the fill is limited (partial arching). In the case of incomplete arching, Carlson predicts a soil weight on the reinforcement that is too high even though the surcharge load is not taken into consideration. The two-dimensional stress reduction ratio, SRR (2D) is given as:

$$SSR_{2D} = \frac{s-a}{4\,.\,H\,.\,tan15^\circ} \quad (2.25)$$

#### 2.2.4.4. Guido Method (1987)

The Guido method (Guido, 1987) proposed a triangular soil-arching model assuming the load spreading forms an angle of 45°. The height of the triangle is 0.5(s-a) which does not reach the surface. The stress reduction ratio is calculated as follows:

$$SSR = \frac{s-a}{3.\sqrt{2}H} \quad (2.26)$$

#### 2.2.4.5. The Beam Method (Collin et al., 2005)

This method is a modification of the Adapted Guido Method of, and it assumes that the reinforced soil mass acts as a beam that consists of at least three layers of geosynthetic reinforcement. Each reinforcement layer carries the weight of the above LTP fill material within the soil wedge in the pyramid. The uniform vertical load of layer (n) of reinforcement ($W_{Tn}$) may be determined from the following equation:

$$W_{Tn} = [A_n + A_{n+1}]\, h_n\, \gamma / 2\, A_n \quad (2.27)$$

Where A is the Area at reinforcement layer n or n+1

$= [(s\text{-}d) - 2(\text{Reinforcement Vertical Spacing}/\tan 45)]^2$ (For square column spacing)

$= [(s\text{-}d) - 2(\text{Reinforcement Vertical Spacing}/\tan 45)]^2 \sin 60/2$ (For triangular column spacing)

The tensile load in the reinforcement is determined based on tension membrane theory and is given by:

$$T_{rpn} = W_{Tn}\, \Omega\, D/2 \quad (2.28)$$

Where D is the design span for tensioned membrane (D= 1.41 [(s-d) – 2(Σvertical spacing/tan45)] for square column spacing, D= 0.867 [(s-d) – 2(Σvertical spacing/tan45)] for triangular column spacing).

Ω is a dimensionless factor from tensioned membrane theory= 2.07, 1.47, 1.23, 1.08, and 0.97 for the reinforcement strain of 1%, 2%, 3%, 4%, and 5%, respectively.

### 2.2.4.6. The FHWA Ground Modification Methods – Reference Manual

The FHWA Ground Modification Methods – Reference Manual (Schaefer et al., 2017) adopted the load displacement compatibility (LDC) method developed by Smith (2005) and Filz and Smith (2006, 2007). This method can be used for both reinforced and unreinforced load transfer platforms. The net vertical stress acting up on the embankment base at the soil between the piles, $\sigma_{soil,geotop}$, and is expressed as $\sigma_{soil}$ for pile-supported embankments without geosynthetic reinforcement, can be evaluated using the Adapted Terzaghi Method (Russell and Pierpoint, 1997; Russell et al., 2003) as follows:

- For $H_1 + H_2 \leq H_{crit}$:

$$\sigma_{soil,geotop} \; or \; \sigma_{soil} = \frac{\gamma_1}{\alpha_1}(1 - e^{-\alpha_1 H_1}) + \frac{\gamma_2}{\alpha_2}(e^{-\alpha_1 H_1})(1 - e^{-\alpha_2 H_2}) + q\,(e^{-\alpha_1 H_1})(e^{-\alpha_2 H_2}) \quad (2.29)$$

- For $H_1 \leq H_{crit} \leq H_1 + H_2$:

$$\sigma_{soil,geotop} \; or \; \sigma_{soil} = \frac{\gamma_1}{\alpha_1}(1 - e^{-\alpha_1 H_1}) + \frac{\gamma_2}{\alpha_2}(e^{-\alpha_1 H_1})\left(1 - e^{-\alpha_2 (H_{crit} - H_1)}\right) + [q + (H_1 + H_2 - H_{crit})\gamma_2](e^{-\alpha_1 H_1})\left(e^{-\alpha_2 (H_{crit} - H_1)}\right) \quad (2.30)$$

- For $H_{crit} \leq H_1$:

$$\sigma_{soil,geotop} \; or \; \sigma_{soil} = \frac{\gamma_1}{\alpha_1}(1 - e^{-\alpha_1 H_1}) + [q + (H_1 - H_{crit})\gamma_1 + H_2\gamma_2](e^{-\alpha_1 H_1}) \quad (2.31)$$

And;

$$H_{crit} = \max \begin{Bmatrix} 1.5\,(s - a) \\ 1.15\,s' + 1.44\,d \end{Bmatrix} \quad (2.32)$$

$$\alpha_{1,2} = \frac{p\,K_{1,2}\,tan\phi_{1,2}}{A_{soil}} \quad (2.33)$$

Where $H_1$ and $H_2$ are the load transfer platform and the embankment thicknesses, respectively. $H_{crit}$ is the critical embankment height.

$\gamma_1$ and $\gamma_2$ are the load transfer platform material and the embankment material unit weights, respectively.

$q$ is the surcharge load.

$s$ is the center-to-center pile spacing.

$a$ is the pile equivalent width.

$d$ is the pile diameter.

$s'$ is the diagonal distance between the outer edge of the pile and the edge of the unit cell ($s' = s/\sqrt{2} - d/2$).

$p$ is the perimeter of the pile or pile cap.

$K_1$and $K_2$ are the load transfer platform and the embankment lateral earth pressure coefficients, respectively.

$\phi_1$ and $\phi_2$ are the load transfer platform material and the embankment material friction angles, respectively.

$A_{soil}$ is the area within the unit cell underlain by soil ($A_{soil} = A_{unitcell} - A_p$).

$A_{unitcell}$ is the area of the unit cell around a pile.

$A_p$ is the area of the pile.

The tension ($T$) in the geosynthetic reinforcement due to vertical loads can be evaluated as suggested by Filz et al. (2019) as follows:

$$6T^3 - 6T\left(\frac{\sigma_{net}\, A_{soil}}{p}\right)^2 - J\left(\frac{\sigma_{net}\, A_{soil}}{p}\right)^2 = 0 \qquad (2.34)$$

Where $\sigma_{net}$ is the net vertical stress acting on the geosynthetic.

$J$ is the sum of the stiffness of all geosynthetics.

It can be noted that the design methods to evaluate the vertical stress acting on the GRLTP and the developed tension in the geosynthetic reinforcement have some limitations. On one hand, both the

British Standards Institution and the Hewlett and Randolph methods do not consider the soil reaction. On the other hand, the Carlson method, the Guido method, and the beam method assume a constant height of the soil arch above the soil between the piles without considering the thickness of the GRLTP and the embankment above the GRLTP, and the subsoil condition. For the method adopted in the FHWA Ground Modification Methods – Reference Manual, the $SRR$ value is evaluated for the entire platform, as will be explained in Chapter 6.

### 2.3. Field Tests

Piled-supported embankments have been instrumented and reported by many researchers. Different types of tests have been utilized including full-scale experiments (Almeida et al., 2007; Sloan, 2011; Briançon and Simon, 2012; Xing et al., 2014), pilot-scale field tests (Oh and Shin, 2007), highway embankments (Liu et al., 2007; Haring et al., 2008; Chen et al., 2010; Zheng et al., 2011), and railway embankment tests (Cheng et al., 2014; Zhang et al., 2014). Some of these reported pile-supported embankments had a load transfer platform with or without a geosynthetic reinforcement, while the rest did not have any.

Almeida et al. (2007) reported a pile-supported embankment full-scale test utilizing geosynthetic reinforcement with two-dimensional and three-dimensional layouts of piles. Both excavated and non-excavated sections underneath the geogrids were tested. Almeida et al. (2007) found that the settlement between the pile caps increased with increasing the pile spacing. Furthermore, Almeida et al. (2007) observed that the settlement at the center of four piles is almost twice the settlement observed between two adjacent pile caps. It was also noted that the final settlement at the excavated section was reached before the end of construction, whereas the settlement observed in the non-excavated section was increasing slowly with time. For the strain in the geogrids, Almeida et al.

(2007) observed higher strain values new the face of the pile cap compared to that measured between the piles.

Chen et al. (2010) reported three cases of highway embankments supported by concrete piles with and without a geosynthetic reinforcement. Chen et al. (2010) observed a significant arching in the embankment resulting in higher observed stresses at the piles than those observed at the soil between the piles. It was also noted that no significant excess pore water pressure was observed compared to the embankment load with a fast rate of dissipation (Chen et al., 2010). Moreover, the system significantly improved the total and differential settlement performance with less settlements for the end bearing piles configurations.

Cheng et al. (2014) investigated the performance of the piled-supported embankment system utilizing a geosynthetic reinforcement. Cheng et al. (2014) observed that the increased load greatly affects the pore water pressure on shallow depths, but has a relatively small influence on deeper locations. It was also found that the rate of change of the lateral displacement is larger during the embankment construction compared to that after the end of construction (Cheng et al., 2014). In addition, the geosynthetic reinforced piled-supported embankment was found to enhance the stability of the system and diminish lateral displacement at the edges of the embankment significantly (Cheng et al., 2014).

**2.4. Numerical Modeling**

The pile-supported embankment utilizing a GRLTP is simulated in a full three-dimensional (3D) to represent the actual condition of the field. Nevertheless, the full 3D simulation of this system is not feasible in terms of time, and it requires high computer power (Smith and Filz, 2007; Ariyarathne et al., 2013). Consequently, reduced 3D models (Yoo and Kim, 2009; Jenck et al., 2009; Bhasi and Rajagopal, 2015), and 2D configuration analysis (Russell and Pierpoint, 1997;

Kempton et al., 1998; Han and Gabr, 2002; Huang and Han, 2010; Yu and Bathurst, 2017) are used to simulate case studies and perform parametric studies. Yoo and Kim (2009) reported that results of the reduced 3D simulation showed good agreement with results of the full 3D simulation. Furthermore, Bhasi and Rajagopal (2015) modeled the system using the 2D axisymmetric model considering a circular area around each pile element. However, obtained results from the reduced 3D model had more accuracy than those obtained from the 2D axisymmetric model (Bhasi and Rajagopal, 2015).

Comparisons between the equivalent two dimensional and the three dimensional FEM have been carried out by multiple researchers (Tan et al., 2008; Hassen et al., 2009; Ariyarathne et al., 2013; Chai et al., 2015). Results showed a relative difference between the measured settlements, lateral displacements, and bending moments between the 2D and 3D FEM analyses. In contrast, results by Hassen et al. (2009) and Tan et al. (2008) showed that equivalent 2D models could predict the performance of the pile-supported embankments in terms of the settlement, stress transfer, and excess pore water pressure. Generally, the equivalent 2D FEM approach is found to be suitable for simulating the pile-supported embankment system utilizing a GRLTP as will be discussed in Chapter 4.

Han and Gaber (2002) used FLAC (Fast Lagrangian Analysis of Continua) program to model piled embankment with load transfer platform. Typical pile diameter of 0.7 m, and center to center pile spacing of 3 m were used. Each single pile was modeled by an equivalent cylindrical area. A surcharge of 10 kPa was assumed as the traffic load on the embankment. The model included 6 meters of soft soil beneath the embankment. Although multiple layers of geosynthetic can be placed within the earth platform, one layer of geosynthetic is assumed in this study for simplicity. In this analysis, piles and geosynthetic are both considered linear elastic materials. Moreover, the

interfaces between piles and soil, and between geosynthetics and soil are assumed fully bonded for simplicity. The effect of the embankment height on the pile head and ground elevation was investigated. Two models were run (with load transfer platform and without). Results showed that the inclusion of the load transfer platform decreased the settlement to 25% of the embankment at the ground surface. Also, the authors found that as the geosynthetic stiffness increases, the maximum settlement decreases and becomes less important when the stiffness exceeds 4000 kN/m. In addition, the increase of the pile elastic modulus can reduce the maximum settlement. The arching phenomenon was investigated, and it was found that the increase in the embankment height increased stress concentration on the pile head. The geosynthetic stiffness had effects on the arcing ratio, stress concentration, differential settlement, and pile elastic modulus. Finally, the study investigated the geosynthetic tension force versus the distance from the center of the pile and found the maximum tension at the pile edge.

Huang and Han (2009) did a 3D coupled mechanical and hydraulic modeling of a well-documented bridge approach embankment which is supported by deep mixed (DM) columns utilizing a GRLTP. The GRLTP consisted of one layer of geotextile. The results of the reduced 3D model were compared with measured values in the field. Results showed good agreement between the numerical simulation results and the field measurements in terms of the total and differential settlements. Furthermore, observed total and differential settlements were more significant at the base of the embankment compared to that computed at the embankment crest. Huang and Han (2009) also found that the tension developed in the transverse direction was more significant than that in the longitudinal direction. Moreover, a fast dissipation of excess pore water pressure was observed due to the combination between the drainage and the stress transfer.

Huang and Han (2010) performed a parametric study based on coupled hydraulic and mechanical modeling to study the time-dependent behavior of geosynthetic-reinforced and pile-supported embankment using Finite Difference Modeling (FDM) FLAC software. The key performance measurements were maximum and differential settlements, the tension in the geosynthetic, and the degree of consolidation. The influencing factors considered in the parametric study were modulus and permeability of the soft soil, modulus and spacing of columns, tensile stiffness of the geosynthetic, and average construction rate. Huang and Han (2010) observed that it is over-conservative to use the settlement and the differential settlement on the crest of the embankment after construction as a reference to evaluate the performance of the geosynthetic reinforced piled embankments because these values are much smaller than those at the base of the embankment. Their results also showed that the construction rate had a significant influence on the GRCS embankment performance. Furthermore, it was found that the elastic modulus of the soft soil and the spacing of piles are the two most important design parameters for the performance of the geosynthetic reinforced piled embankments (Huang and Han, 2010).

Yu and Bathurst (2017) studied the performance of geosynthetic-reinforced column-supported embankments by using FDM with FLAC software. Key performance measurements were the reinforcement tensile loads and reinforcement vertical displacements. Yu and Bathurst (2017) observed that the reinforcement vertical displacement decreases by increasing each of the deep mixed column modulus, the soft foundation modulus, and reinforcement tensile stiffness. Yu and Bathurst (2017) also found that increasing the soft foundation modulus reduces the reinforcement tensile loads, while greater reinforcement tensile stiffness results in greater reinforcement tensile loads.

Pham et al. (2021) studied the performance of a geosynthetic-reinforced and pile-supported embankment by conducting three-dimensional Discrete Element Modeling (DEM) numerical analyses. Key performance measurements were the stress transfer from the subsoil to piles and its distribution, and the tension distribution in geosynthetic. Pham et al. (2021) found that the inclusion of the geosynthetic enhances the stress transfer from the subsoil to piles due to the tensioned membrane action which could reduce the possibility of the occurrence of soil yielding and differential settlement. Pham et al. (2021) also observed that the vertical stresses below the geosynthetic are significantly concentrated at the corner of the pile cap, while vertical stresses above the geosynthetic are more uniform. Moreover, the tension is not uniform along the geosynthetic and the maximum tension occurs at the pile cap edge. Pham et al. (2021) also found that soil between the piles underneath the embankment participates in the support resulting in less developed tension in the geosynthetic reinforcement.

# CHAPTER 3.
# 2D FINITE ELEMENT MODELING METHODOLOGY

## 3.1. Finite Element Modeling

The Finite Element (FE) technique is used in this study to simulate the performance of pile-supported embankments. This technique allows modeling and analyzing complex engineering problems that are not possible to solve using traditional methods. Engineering problems can be simulated as is in reality with this technique as it can deal with different materials with no boundaries for the problem size. Furthermore, the linear or nonlinear behavior of the materials involved in the problem can be simulated. However, mistakes can be easily made by the user in terms of the simulation methodology of the problem, bad use of constitutive models and material properties, and the boundary conditions. Thus, the user should pay attention and use the same exact condition of the real problem, so good and dependable results are obtained. This study will be conducted using PLAXIS 2D software. The main components of the Finite Element model to be introduced by the user are the problem geometry, the materials involved and their constitutive models, driving loads in the problem, boundary conditions, and interface simulation.

### 3.1.1. Geometry

The first step in the problem simulation is building the problem geometry. For this study, the geometry consists of the embankment, soil layers underneath the embankment, the piles, and the GRLTP. The dimensions of the soil layers and the embankment will be simulated as proposed by the numerical modeling study. The vertical and horizontal boundary of the model should be extended to a minimum distance where exceeding that distance will have a negligible effect on the deformation in the boundary.

### 3.1.2. Load

The driving loads will be gravity loads (self-weight of the embankment) and a static surcharge load to represent the highway traffic pointing downward. The initial stresses are generated using the $K_0$ procedure. The $K_0$ procedure calculates the stresses within the soil body as follows:

$$\sigma_{h_0} = K_0 \sigma_{v_0} \tag{3.1}$$

Where $\sigma_{h_0}$ is the horizontal earth pressure at rest, $K_0$ is the coefficient of earth pressure at rest, and $\sigma_{v_0}$ is the effective vertical overburden pressure.

### 3.1.3. Boundary Conditions

The global static equilibrium in the FE model is enforced by applying boundary conditions. Roller-type boundary conditions (the movement is prevented in the horizontal direction, while the movement is allowed in the vertical direction) are used at the horizontal boundaries on the sides of the model. Conversely, the bottom boundary is fixed in both directions. The FEM model is left to be free on the top boundary of the model.

### 3.1.4. Geosynthetic-Soil Interface and Pile-Soil Interface Behavior

The interaction at the interface between the GRLTP material and the geosynthetics, and between the timber piles and the surrounding soil must be simulated. PLAXIS program uses the linear elastic Mohr-Coulomb interface model to simulate the mechanical behavior of the interface between dissimilar materials. Node pairs are created at the interface between the soil and the structure in which each element has its own node. Both the gap and the slip displacements at the interaction between the node pair are simulated using elastic-perfectly plastic springs.

Interfaces using a linear elastic model with Mohr-coulomb failure criterion have properties of friction angle, dilation angle, cohesion, Young's modulus ($E$), Poisson's ratio ($v$), and tensile strength. These values can be set using a reduction factor ($R_i \leq 1.0$) applied to the soil materials

(the default value is $R_i$ = 1.0, i.e. a fully-bonded interface). The interface value properties are described in the following equations adopted from PLAXIS 2D 2021.

$$c_i = R_i c_i \tag{3.2}$$

$$tan\,\phi_i = R_i\, tan\,\phi_i \tag{3.3}$$

$$\psi_i = \begin{bmatrix} 0 & R_i < 1 \\ \psi_{soil} & R_i = 1 \end{bmatrix} \tag{3.4}$$

$$G_i = R_i^2 G_{soil} \tag{3.5}$$

$$v_i = 0.45 \tag{3.6}$$

$$E_i = 2G_i(1 + v_i) \tag{3.7}$$

$$E_{oed,i} = 2G_i \frac{(1-v_i)}{(1-2v_i)} \tag{3.8}$$

$$\sigma_{t,i} = R_i\, \sigma_{t,i} \tag{3.9}$$

Where $c_i$, $\phi_i$, $\psi_i$, $G_i$, $v_i$, $\sigma_{t,i}$, $E_i$ are the cohesion, friction angle, dilation angle, shear modulus, Poisson's ratio, tensile strength, and Young's modulus of the surrounding soil, respectively. The strength properties and the $R_{inter}$ value of the relevant material set are directly controlling the level at which (plastic) slipping occurs. For this FEM methodology, a strength reduction factor of 0.8 is applied at the interface between the GRLTP material and the geotextiles, and between the timber pile material and the surrounding soils. However, a strength reduction factor of 1.0 is applied at the interface between the GRLTP material and the geogrid to account for the interlocking of the gravelly material into the geogrid apertures.

### 3.2. Constitutive Models

Soil and rock tend to behave in a highly non-linear way under load. This non-linear stress-strain behavior can be modeled at several levels of sophistication. PLAXIS FEM software provides different models to simulate the behavior of soil. The models and their parameters that have been

used in the FEM of this study are discussed in detail below. Table 3.1 shows the materials and their corresponding constitutive model in this FEM study.

Table 3.1. Materials and their constitutive models.

| Material | Constitutive Model |
|---|---|
| Cohesive soils (clays) | Modified Cam Clay (MCC) model |
| Cohesionless soils (sands) | Mohr-Coulomb model |
| Embankment | Mohr-Coulomb model |
| GRLTP material | Hardening Soil (HS) model |
| Piles and geosynthetics | Linear Elastic model |

### 3.2.1. Modified Cam Clay (MCC) Model

The Modified Cam Clay (MCC) model is used to simulate the behavior of saturated clayey soils, especially the normally consolidated soft soils. The model assumes a logarithmic relationship between the void ratio and the mean effective stress. This model is used to simulate the behavior of cohesive soils (clay). The required parameters for the MCC model are summarized in Table 3.2. The slope of the critical state line in the $p' - q$ space ($p'$ is the mean effective stress, and $q$ is the deviatoric stress), $M$, as follows:

$$M = \frac{6 \sin \phi'}{3 - \sin \phi'} \tag{3.10}$$

Table 3.2. The MCC model input parameters.

| Parameter | Description |
|---|---|
| $\lambda$ | Cam-Clay compression index |
| $\kappa$ | Cam-Clay swelling index |
| $\nu_{ur}$ | Poisson's Ratio |
| $e_0$ | Initial void ratio for loading/unloading |
| $M$ | Tangent of the critical state line |
| $K_0^{nc}$ | Coefficient of lateral stress in normal consolidation derived from M |

### 3.2.2. The Mohr-Coulomb Model

The Mohr-Coulomb model is a linear elastic-perfectly plastic model, which can be used as a first approximation of soil behavior. The linear elastic part of the Mohr-Coulomb model is based on Hooke's law of isotropic elasticity loading and unloading/reloading. The perfectly plastic part is based on the Mohr-Coulomb failure criterion, formulated in a non-associated plasticity framework. This model is used to simulate the cohesionless soils (sands) and embankment material. The required parameters for the Mohr-Coulomb model are summarized in Table 3.3.

Table 3.3. Mohr-Coulomb model input parameters.

| Parameter | Description |
|---|---|
| $E$ | Young Modulus |
| $\nu$ | Poisson's Ratio |
| $c'$ | Cohesion |
| $\phi'$ | Friction angle |
| $\Psi$ | Dilatancy angle |

### 3.2.3. The Hardening Soil (HS) Model

The GRLTP nonlinear behavior is modeled using the elastoplastic hardening soil (HS) model. The hardening soil was developed under the framework of the theory of plasticity. In this model, stress-dependent stiffness is used to calculate the total strains, which is different for both loading and unloading/reloading. An isotropic hardening is assumed, depending on the plastic volumetric and shear strains. An associated flow rule is assumed for the cap hardening, and a non-associated flow rule is assumed when related to frictional hardening. The required parameters for the HS model are summarized in Table 3.4.

Table 3.4. Hardening soil model input parameters.

| Parameter | Description |
|---|---|
| $\phi'$ | Internal friction angle |
| $c'$ | Cohesion |
| $Rf$ | Failure ratio |
| $\Psi$ | Dilatancy angle |
| $E_{50}^{ref}$ | Reference secant stiffness from drained triaxial test |
| $E_{oed}^{ref}$ | Reference tangent stiffness from oedometer primary loading |
| $E_{ur}^{ref}$ | Reference unloading/reloading stiffness |
| $m$ | Exponential power |
| $v_{ur}$ | Unloading/reloading Poisson's ratio |
| $K_0^{nc}$ | Coefficient of earth pressure at rest |

## 3.3. Pore Water Pressure

Cohesive soils are modeled using the Undrained behavior in PLAXIS to allow for the development and dissipation of the excess pore water pressure in the soil layers. Conversely, cohesionless soils are modeled using the Drained behavior in PLAXIS due to the high hydraulic conductivity of these soils, so they serve as drainage layers.

### 3.4. Pile Simulation in 2D

The piles are simulated using plane strain walls of the original diameter (width) of the pile with an equivalent stiffness ($E_{eq}$) using the area replacement ratio (ARR) method reported by Huang et al. (2009):

$$E_{eq} = a_s E_p + (1 - a_s) E_s \tag{3.11}$$

Where $a_s$ is the area replacement ratio, which is equal to the area of the pile divided by the area of the unit cell ($A_p / A_{unit\ cell}$).

$E_p$ is the Young's modulus of the pile material.

$E_s$ is the stiffness of the surrounding soil.

The piles are simulated using a linear elastic model with the required parameters of only the Young's modulus ($E$) and the Poisson's ratio ($\nu$). Furthermore, it is expected that the excess pore water pressure dissipation will be underestimated due to the non-porous nature of the walls extending in the out-of-plane direction. Thus, the permeability of the piles was taken as the weighted mean of the hydraulic conductivity of the original surrounding soil and the pile material ($(k_v)_{pile} = 0$) as follows:

$$k_w = \frac{k_p A_p + k_s A_s}{A_w} \tag{3.12}$$

Where $k_w$ is the hydraulic conductivity of the wall.

$k_p$ is the hydraulic conductivity of the pile ($k_p = 0$).

$k_s$ is the hydraulic conductivity of the soil material surrounding the pile.

$A_w$ is the area of the wall.

$A_p$ is the area of the pile.

$A_s$ is the area of the soil ($A_s = A_w - A_p$).

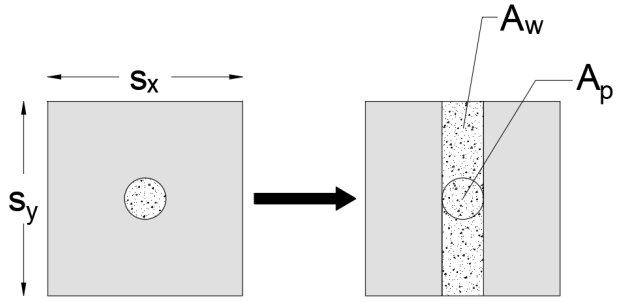


Figure 3.1. Plane strain wall configuration.

### 3.5. Geosynthetic Layers

The geosynthetic were simulated using the linear elastic geogrid elements. Only the tensile stiffness ($EA$) is the required parameter for the geosynthetic. Finally, an updated mesh analysis was used to account for the membrane effect in the geosynthetic layers.

# CHAPTER 4.
# NUMERICAL MODELING VALIDATION

## 4.1. Paris Case Study

A piled-supported embankment built on soft soil utilizing GRLTP was experimented within the French national research project, and is reported by Briançon and Simon (2012). This study emphasizes the benefits achieved with using GRLTPs. The full-scale experiment was located northeast of Paris, and had an area of 52 m by 23 m. The area was divided into four sections: (i) an embankment without any support (no piles or reinforcement), (ii) a non-reinforced piled-supported embankment, (iii) a piled-supported embankment utilizing GRLTP consisting of one layer of geotextiles, (iv) a piled-supported embankment utilizing GRLTP consisting of two layers of geogrids as shown in Figure 4.1. The sections are denoted as 1R, 2R, 3R, and 4R, respectively. The embankment full height is 5 m with a crown width of 8 m. The side slope is 3 H to 2 V. The augar displacement concrete piles having a diameter of 0.38 m with an average length of 8.3 m were used to reinforce the piled-supported sections and were arranged in a square configuration with 2 m center-to-center spacing. The load transfer platforms made by compacted gravel and reinforced by geosynthetics were used in sections 3R, and 4R having a thickness of 0.55 m, and 0.65 m, respectively (Figure 4.1c). The embankment material was a marly and chalky natural soil with a total unit weight of 18.5 kN⁄m3. Sensors were installed in the LTP, soft soil, and piles: earth pressure cells (E) to measure stress transfer, pore water pressure sensors (P) to measure interstitial pressure in the soft soil, magnetic probe extensometer (M) to measure settlement, settlement transducer (T) to measure the differential settlement between soil and pile at the pile head level, inclinometers (I) to measure lateral displacement near the embankment toe, and an optical device (Geodetect) to measure geosynthetic strains.

Detailed subsoil profile for this site is reported by Rowe and Liu (2015). The embankment was constructed on a soft soil layer with a thickness of 8-10.5 m and consisted mainly of, from top to bottom, a 1.5 m thick clayey fill (layers F1, F2), a 1 m thick soft marl and clay (layer F3), a 1.5 m thick clayey sand (layer F4), a 4 m thick plastic clay and sandy clay (layers F5, F6), a 1.5 m thick layer of slightly plastic sandy clay and stiff clay mixed with marl and gravel (layer F7), underlain by a compact gravel layer (Figure 4.1b). The groundwater table was found to be 2 m below the ground surface. This case study is simulated using Plaxis 2D FEM software and is compared by the performance measurements in the site and results computed by the 3D FEM reported by Rowe and Liu (2015).

(a)

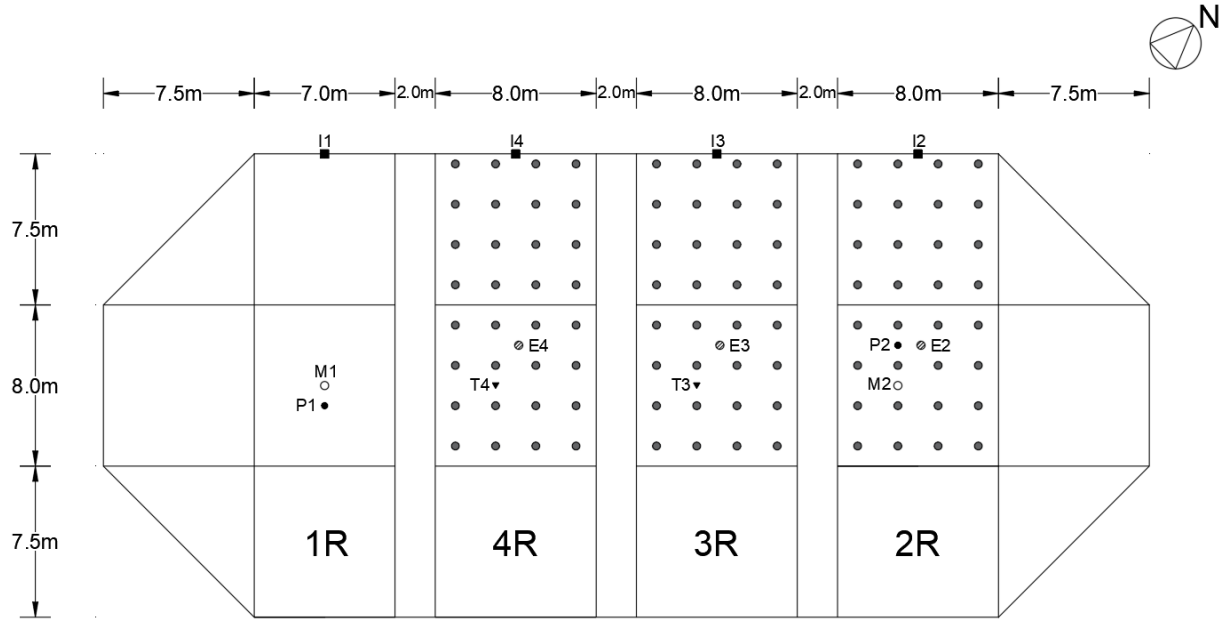


E: Earth pressure cell
P: Pore-water pressure sensor (-6 m)
M: Magnetic probe extensometer
T: Settlement transducer
Inc: Inclinometer
Piles

(b)

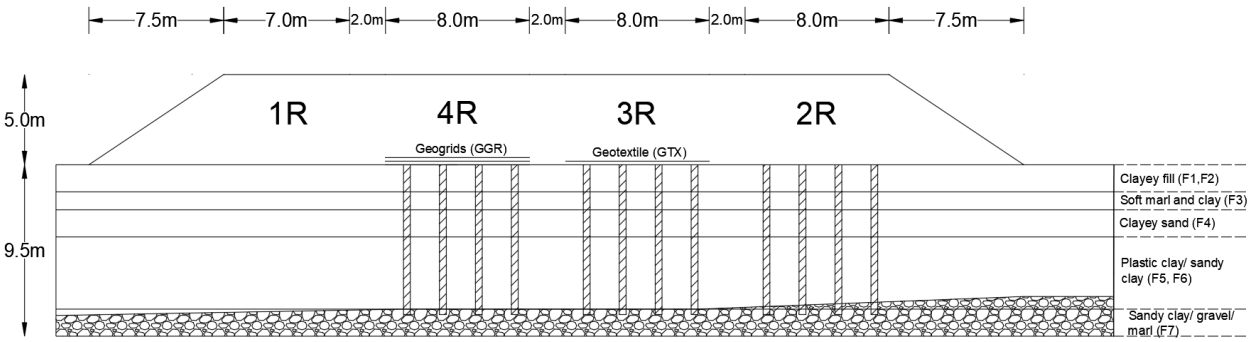


(c)

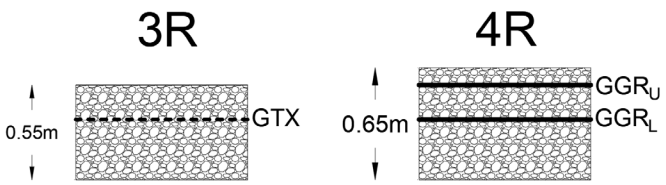


Figure 4.1. (a) Plan view of the experimental site and some of the monitoring locations; (b) typical site cross-section showing geometric characteristics and subsoil profile; (c) GRLTPs detailing in section 3R and 4R (Briançon and Simon, 2012).

### 4.1.1. Numerical Modeling

Four cases are modeled, case 1 with no support (1R), case 2 with piles only (2R), case 3 with piles and one layer geotextile (3R), and case 4 with piles and two layers of geogrids (4R). Rowe and Liu (2015) simulated the French case in a 3D configuration, while this study adopts the 2D configuration as described below. Detailed numerical modeling procedure, model geometry, and soil properties are adopted from Rowe and Liu (2015). An equivalent 2D Finite Element Modeling (FEM) has been carried out using PLAXIS 2D (2021) software. In this 2D modeling, piles are simulated as continuous plane strain walls having the same thickness as the pile diameter (0.38 m) with a reduced stiffness of 570 MPa according to the area replacement ratio (ARR) method given by Huang et al. (2009) and a Poisson's ratio of 0.2. For the constitutive modeling, the Modified Cam Clay model (MCC) was used to simulate the subsoil layers. The $M$ value is calculated using

equation (3.10). Table 4.1 summarizes the properties used for the subsoil material. The embankment fill and the LTP were modeled using the Mohr-Coloumb model (MC). The piles and geosynthetics were modeled using the linear elastic model. Table 4.2 shows the embankment, LTP, piles, and geosynthetic properties used in the modeling.

The bottom boundary of the FEM model is assumed to be fixed in both directions, and the horizontal boundaries are set to be fixed in the horizontal direction only (allowed vertically). To minimize the boundary effects on the analysis, the horizontal boundaries are extended one time the embankment width each side (i.e., three times the embankment width of 69 m), and the vertical boundary (layer F7) is extended 1 m for section 1R, 2 m for section 2R, 1.5 m for sections 3R and 4R. For the flow and drainage boundary conditions, the ground water table is set at -2m depth with free drainage along this plane. The bottom boundary is set to be closed (impermeable) because of the compact gravel layer, and flow is not permitted along the planes x= 0 and x=69 as they are extended an adequate distance on both sides.

In this numerical analysis, fifteen-node triangular elements with excess pore water pressure degrees of freedom at all nodes were adopted to simulate the soil below the water table, whereas., 15-node triangular elements without excess pore water pressure degrees of freedom at all nodes were used for the embankment fill, LTP, and soils above the water table. Moreover, five-node geogrid elements were used to simulate geosynthetics (geotextile and geogrids). Interface elements are utilized at the soil-pile and gravel-reinforcement interaction with assigning the interface friction angle to be the critical state friction angle ($\phi'_{cs}$) of the subsoil and the gravel in the load transfer platform, respectively. The lateral earth pressure coefficient is assumed to be the at-rest earth pressure coefficient as follows (Meyerhof, 1976):

$$K_o = (1 - \sin \phi'_{cs})\sqrt{OCR} \tag{4.1}$$

Table 4.1. Soft soil properties.

| Parameter | F1 | F2 | F3 | F4 | F5 | F6 | F7 |
|---|---|---|---|---|---|---|---|
| Thickness (m) | 0.75 | 0.75 | 1 | 1.5 | 2 | 2 | 1,1.5,2 |
| $\gamma$ (kN/m$^3$) | 19.6 | 19.6 | 14.1 | 19 | 20.5 | 20.5 | 20.8 |
| $M$ | 1.23 | 1.23 | 1.23 | 1.23 | 1.07 | 1.07 | 1.375 |
| $\lambda$ | 0.092 | 0.191 | 0.308 | 0.074 | 0.116 | 0.088 | 0.027 |
| $\kappa$ | 0.014 | 0.029 | 0.046 | 0.011 | 0.017 | 0.013 | 0.004 |
| $e_0$ | 0.78 | 1.35 | 2.0 | 0.67 | 0.92 | 0.76 | 0.69 |
| $k_v$ (m/s) | - | - | $8.8\times10^{-8}$ | $1.0\times10^{-6}$ | $6.1\times10^{-7}$ | $6.1\times10^{-7}$ | $6.6\times10^{-5}$ |
| $K_0$ | 1.668 | 0.986 | 0.686 | 0.574 | 0.662 | 0.619 | 0.52 |
| $K_s/K_0$ | 1.45 | 1.3 | 1.2 | 1.05 | 1.04 | 1.03 | 1.02 |

Table 4.2. Embankment, LTP, and geosynthetic properties.

| Parameter | Embankment | LTP | Geotextiles | Geogrids |
|---|---|---|---|---|
| Model | MC | MC | Linear Elastic | Linear Elastic |
| $\gamma$ (kN/m$^3$) | 18.5 | 20 | - | - |
| $\phi'$ (°) | 30 | 36 | - | - |
| $c$' (kPa) | 10 | 60 | - | - |
| $E$ (MPa) | 20 | 70 | - | - |
| $\nu$ | 0.3 | 0.3 | - | - |
| $EA$ (kN/m) | - | - | 800 | 500 |

To account for the pile driving and the soil disturbance, the lateral earth pressure coefficient ($K_s$) is modified to the lower range of $1K_o$to $2K_o$ for the normally consolidated and moderately consolidated clay (Meyerhof, 1976; Coduto, 2001), and $3K_o$ for the heavily overconsolidated clay using large displacement piles (O'Neill et al., 1981). Moreover, it is assumed that the horizontal hydraulic conductivity is equal to the vertical hydraulic conductivity, and both were reduced to 13% of the undisturbed hydraulic conductivity to account for soil disturbing after pile driving.

For the construction sequence, the model is brought to equilibrium then the piles are installed. The subsoil was left to consolidate for 33 days after pile installation, so no excess pore water pressure was observed at the time of embankment construction. Therefore, a fully drained condition is applied at the pile installation stage, so no excess pore pressures are generated. Consequently, the embankment is constructed in 17, 31, 31, and 24 days for cases 1R, 2R, 3R, and 4R, respectively. The fill loading rate adopted is the same as the actual field fill loading rate given by Rowe and Liu (2015). Finally, the soil is left to consolidate reaching 180 days after the embankment construction. Figure 4.2 shows the embankment, piles configuration, soil layers, and GRLTPs used in the numerical simulation for all the sections.

(a)

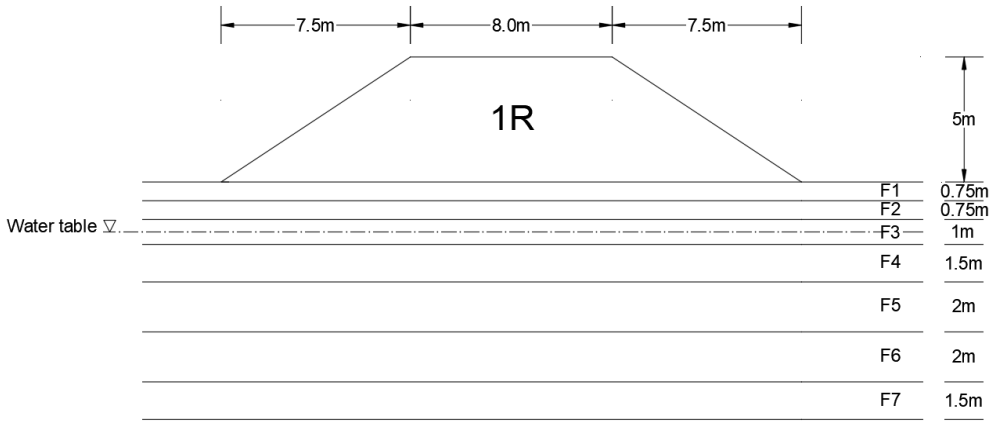

(b)

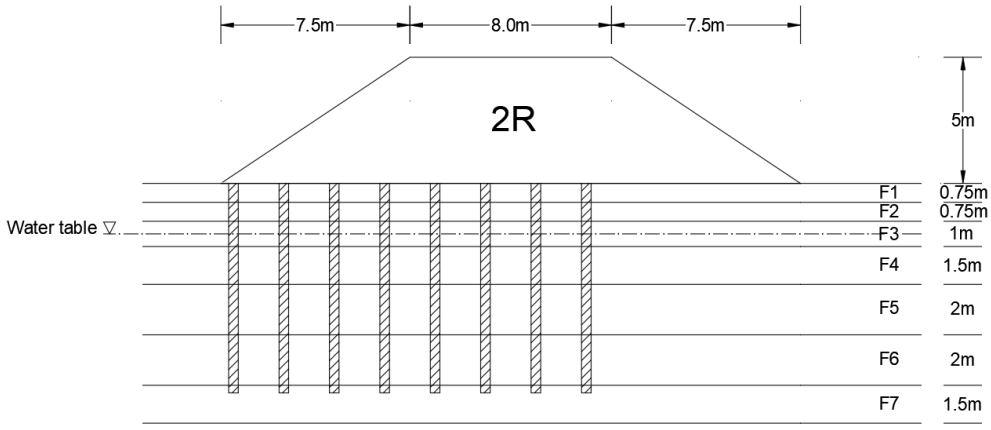


(c)

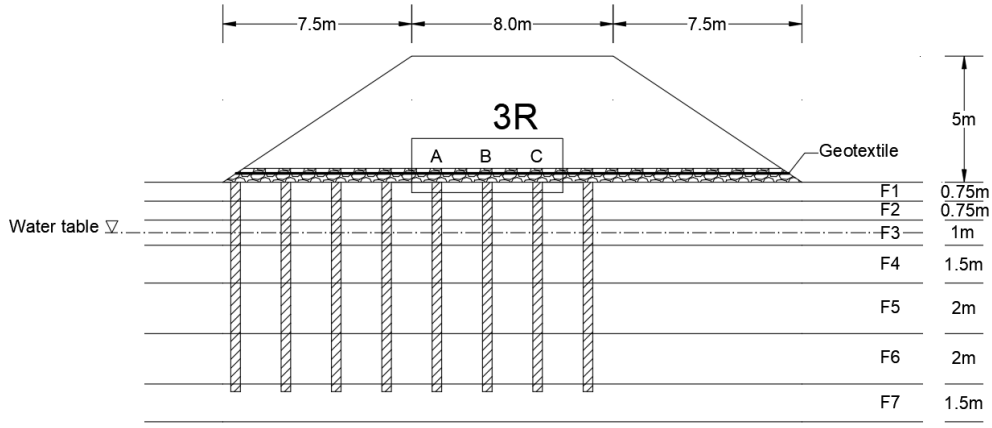


(d)

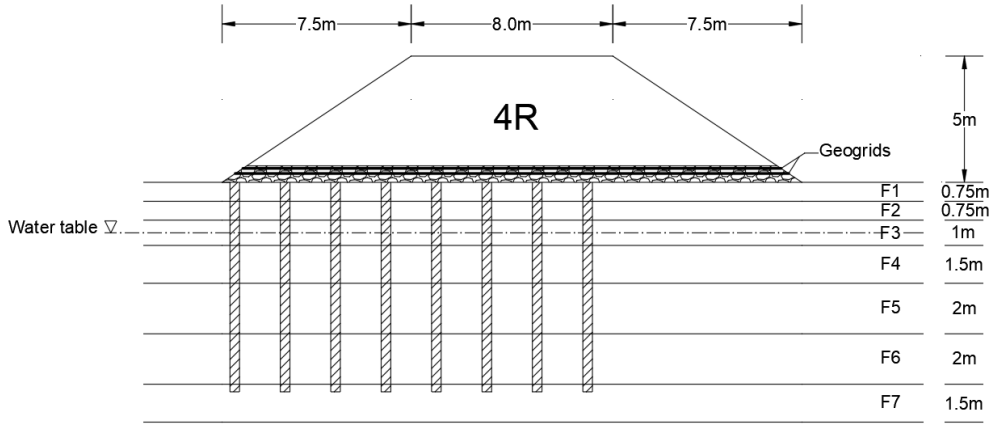


Figure 4.2. Cross-section of the site showing the embankment, piles, GRLTPs, and subsoils for section (a) 1R; (b) 2R; (c) 3R; (d) 4R.

### 4.1.2. Results

Computed results from numerical simulation are compared with the measured values from the field and with results published by Rowe and Liu (2015), which are referred herein as "R* 2015". Measurements include the settlement, excess pore water pressure, stress on soft soil, lateral displacement, and strain in the geosynthetics.

#### 4.1.2.1. Settlement

Computed settlements are compared with measured settlements from the magnetic probe extensometer (M1, M2). Figure 4.3 shows the settlement with time under the centerline of the embankment at different depths in section 1R. Computed settlements after 180 days were 280 mm, 186 mm, 69 mm, and 4 mm at depths of z=0 m, z= -2 m, z= -8 m, and z= -8 m, respectively. Results show good agreement with field measurements in terms of measured settlement and the time rate of consolidation. For instance, the maximum measured settlement at a depth of z= 0 m is 260 mm resulting in an overestimate of 7.69% for the 2D configuration in this study. In contrast, the 3D measurement reported by Rowe and Liu (2015) is 249 resulting in an underestimate of 4.23%. Figure 4.4 shows the settlement with time for the magnetic probe extensometer (2M) in section 2R. Calculated settlements were 95 mm, 46 mm, 22 mm, 2 mm at depths of z=0 m, z= -2 m, z= -5 m, and z= -8 m, respectively. The maximum calculated settlement and the time rate of consolidation are in good agreement with the measured values from the site. The maximum computed settlement at z= 0 m yielded an underestimate of 9.52% from the maximum measured value at the same location which was reported to be 105 mm. However, Rowe and Liu (2015) reported a value of 131 mm which gives an overestimation of 24.76% for the 3D configuration. This indicates that the 2D configuration used in this study overestimates the arching effect in a

tolerant way, indicating less stress transfer to the soil underneath the embankment resulting in less computed settlement.

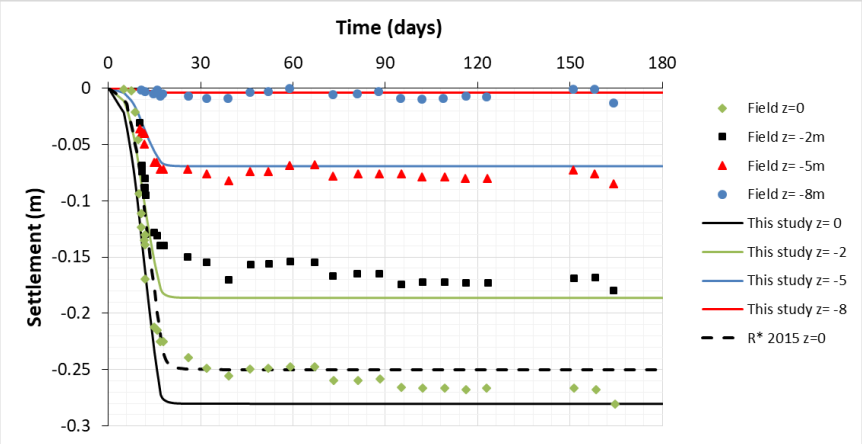


Figure 4.3. Settlement vs. time at different depths for section 1R.

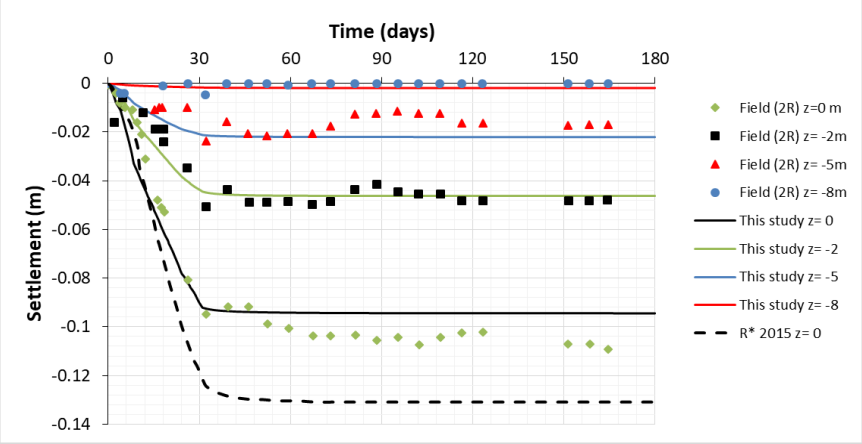


Figure 4.4. Settlement vs. time at different depths for section 2R.

Since the time rate of consolidation was not reported for sections 3R and 4R, only the maximum settlements at the locations of the settlement transducers T3 and T4 are compared in Table 4.3. Maximum computed settlements for sections 3R and 4R reached 59 mm, and 55 mm, respectively, after 180 days from the start of construction. Field settlements observed were 70 mm, and 65 mm for sections 3R, and 4R respectively, indicating an underestimate of the measurements obtained from this study of 15.71% and 15.38% for sections 3R and 4R, respectively. This implies that the

2D configuration used in this study overestimates the arching effect leaving the soil with less settlement. In contrast, reported 3D values from Rowe and Liu (2015) are 78 mm, and 71 mm for sections 3R and 4R, respectively, are overestimating the measured values from the field by 11.43% and 9.23% for the same sections. Furthermore, the inclusion of piles and GRLTPs improved the performance of the system in terms of the serviceability limit state as more embankment load is transferred to the piles due to the arching effect. For example, the inclusion of piles without the GRLTP in section 2R reduced the settlement to 33.9% of that computed in section 1R. Moreover, inclusions of piles with one layer of geotextile (section 3R) and two layers of geogrids (section 4R) reduced the original settlement from the computed settlement in section 1R to 21.1% and 19.6%, respectively. Comparing sections 3R (1 layer of geosynthetic) and section 4R (2 layers of geosynthetics), the addition of another geosynthetic layer for section 4R reduced the settlement to 93.2% only from that computed in section 3R. This can be attributed to the proximity of the stiffness of geosynthetics in both sections, 800 kN/m and 1000 kN/m for sections 3R and 4R, respectively.

Table 4.3. Settlement comparison between the experimental and numerical modeling studies.

| Case | 1R | 2R | 3R | 4R |
|---|---|---|---|---|
| Field Measurements (mm) | 260 | 105 | 70 | 65 |
| This Study (mm) | 280 | 95 | 59 | 55 |
| R* 2015 (mm) | 250 | 131 | 78 | 71 |

#### 4.1.2.2. Excess Pore Water Pressure

Figures 4.5a and 4.5b show piezometric levels (induced excess pore water pressure) with time for sensors P1 and P2 in sections 1R and 2R, respectively, at depth z= -6 m. Both figures show the increase in the excess pore water pressures due to embankment construction with time. The fast excess pore water pressure dissipation was due to the high hydraulic conductivity of the layers.

The computed maximum values were 5.6 kPa and 5.3 kPa for sections 1R and 2R, respectively, whereas the measured values were almost 5.4 for both sections, which are in good agreement with the computed values. Excess pore water pressure in the numerical modeling was dissipated faster than that in the field, and this indicates an overestimation in the hydraulic conductivities of the subsoil, as the permeability of the subsoil was not allowed to decrease with the reduction of the void ratio due to consolidation.

(a)

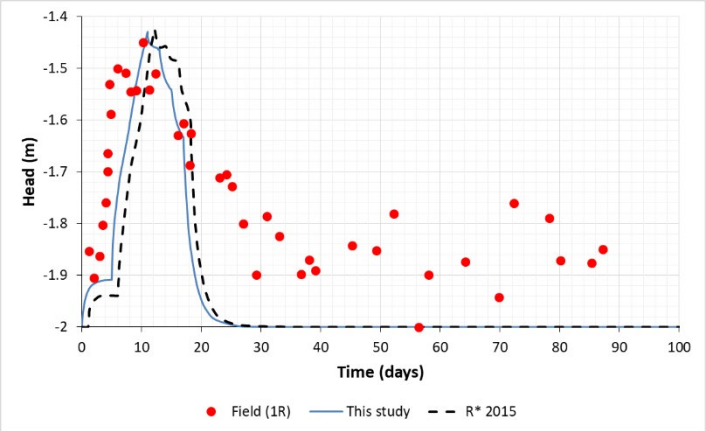


(b)

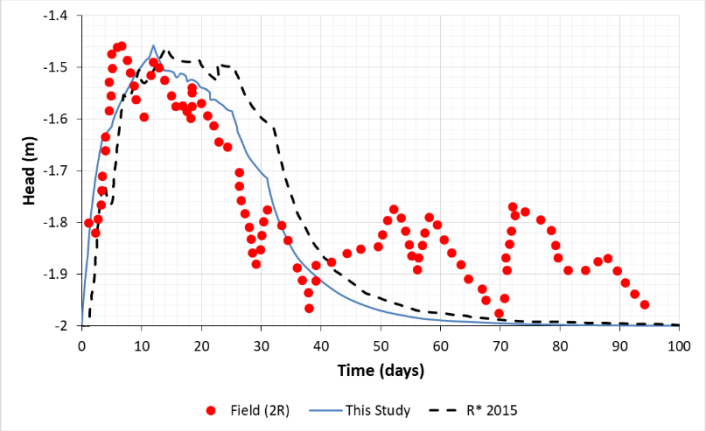


Figure 4.5. Peizometric levels with time for sensors (a) P1 in section R1; (b) P2 in section 2R.

#### 4.1.2.3. Stress on Soft Soil

Figures 4.6a, 4.6b, 4.6c show the stress with time in the subsoil between the piles at the embankment base for sensors E2, E3, and E4, respectively. All figures indicate an increase in the stress in the subsoil with the embankment filling until the end of construction (EOC). Peak computed values were 76.62 kPa, 50.7 kPa, and 45.6 kPa for pressure cells E2, E3, and E4, respectively, which are approximately 82%, 55%, and 49% of the total embankment load (≈93 kPa). This observation supports the idea that the GRLTPs facilitate the stress transfer to the piles and reduce stresses on the subsoil. Results from numerical modeling are in reasonable agreement with measured and the computed values from Rowe and Liu (2015) values, and the insignificant underestimation is due to an overestimation in the arching effect into the piles with less stress on the subsoil as discussed in the settlement section before.

(a)

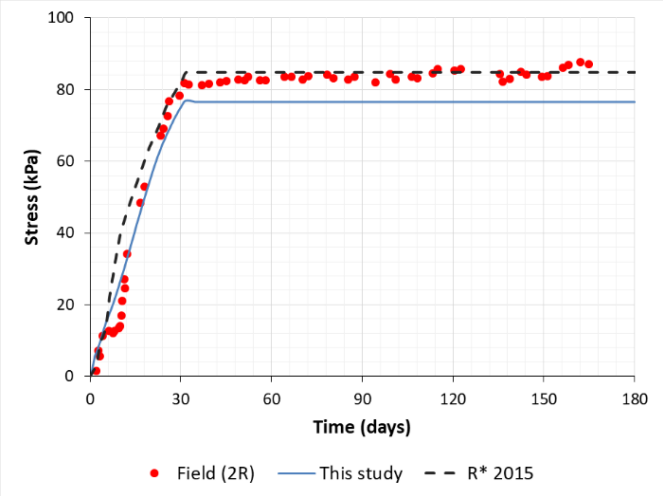

(b)

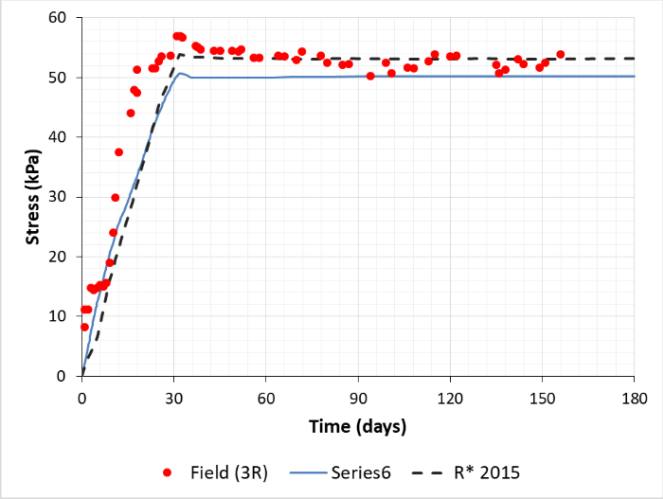


(c)

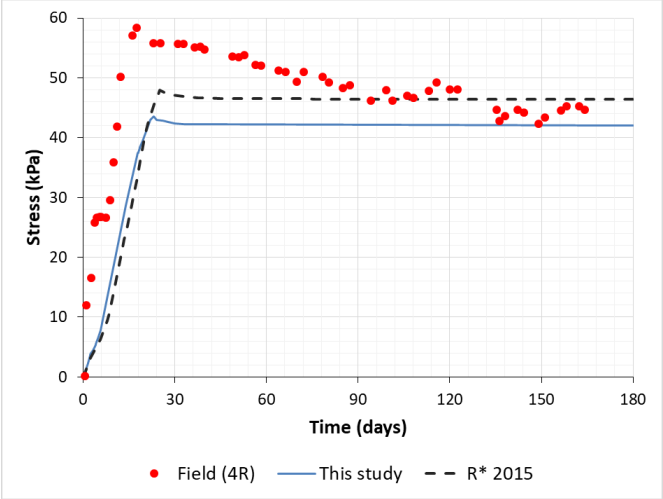


Figure 4.6. Stress on subsoil vs. time at the base of the embankment for pressure cells (a) E2 in section 2R; (b) E3 in section 3R; (c) E4 in section 4R.

#### 4.1.2.4. Lateral Displacement

Figure 4.7 shows the lateral displacement profiles near the toe of the embankment at 180 days inclinometers I1, I2, I3, and I4. The computed lateral displacements along depth from numerical modeling of this study overestimated the measured values from the field along the whole depth, but it reasonably captures the trend. This behavior is consistent with findings from other studies in

which the lateral deformations are hard to predict, and calculated values are frequently overestimated (Tavenas et al., 1979; Hinchberger and Rowe, 1998; Taechakumthorn and Rowe 2012; Rowe and Liu, 2015). For the 2D configuration in this study, this may be attributed to the reduced value of the stiffness of the pile material to account for the piles in the plane strain condition. Maximum measured lateral displacements were almost at a depth of 1.5 m from the ground surface for all sections at the same location of the weakest soil layer (F3). The calculated lateral displacement at a depth of 1.5 m below the ground surface is 36 mm, 21 mm, 18 mm, and 14 mm for sections 1R, 2R, 3R, and 4R, respectively. These values result in an overestimate of 19.7%, 31.3%, 28.6%, and 18.3%, for sections, 1R, 2R, 3R, and 4R, respectively, from the maximum measured values in the field (30 mm for section 1R, 16 mm for section 2R, 14 mm for section 3R, and 12 mm for section 4R). It can be noted from the numerical modeling results that the inclusion of the piles and the GRLTPs facilitated the resistance of the soil body to resist the lateral displacement near the toe as well as changing the maximum lateral displacement location to be at the ground surface. Moreover, sections 3R and 4R had better performance in terms of the lateral displacement as geosynthetics help with resisting the lateral spreading effect from the embankment loading.

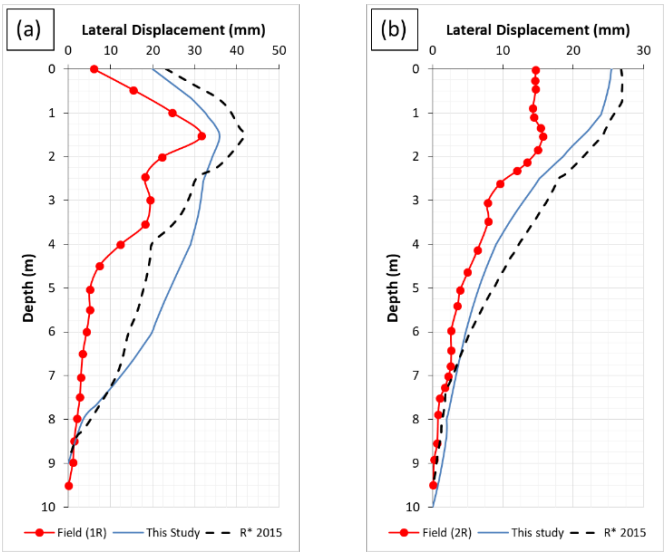

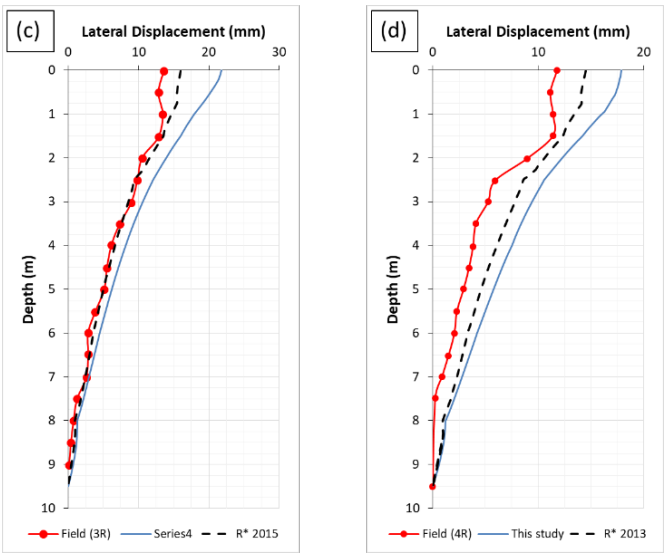


Figure 4.7. Lateral deformation profile vs. depth near the toe of the embankment at 180 days for inclinometers (a) I1 in section 1R; (b) I2 in section 2R; (c) I3 in section 3R; (d) I4 in section 4R.

#### 4.1.2.5. Strain in Geosynthetics

Rowe and Liu (2015) reported the computed values of the strains in geotextile and their locations as shown in Figure 4.3c with a closer look in Figure 4.8 as shown below. Thus, only the strain in the geotextile layer in section 3R is discussed herein. Figure 4.9 shows the strain in the geotextile layer in section 3R at the end of construction (EOC). Computed results from numerical modeling are in fair agreement with the measured values and computed values from Rowe and Liu (2015). Strains at the pile head are overestimated, whereas strains between the piles are underestimated. This observation may be attributed to the overestimation of the arching effect transferring more load towards the piles and less stress on the subsoil between the piles as discussed in the settlement and the stress on subsoil sections before. It can also be noted that the strains are higher as we move closer to the unsupported zone where there is no pile support.

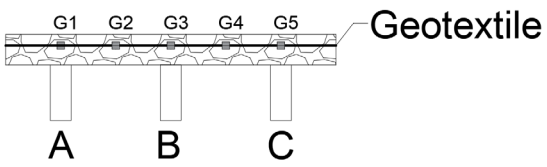


Figure 4.8. Locations of the computed strain in the geotextile layer in section 3R.

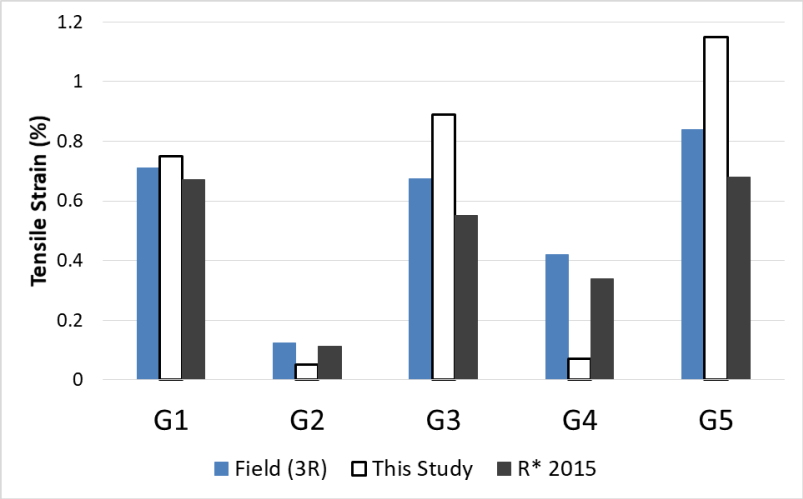


Figure 4.9. Strain in the geotextile layer in section 3R at the end of construction (EOC).

### 4.2. Shanghai Case Study

A case study of a highway pile-supported embankment built on soft soil utilizing a GRLTP was instrumented in Shanghai, China, and is reported by Liu et al. (2007). The site was located in a northern suburb of Shanghai. The embankment full height is 5.6 m and 120 m long with a crown width of 35 m. The side slope was 1 V to 1.5 H. The filling material used for the embankment was made of pulverized fuel ash and had a cohesion, friction angle, and unit weight of 10 kPa, 30°, and 18.5 kN/m$^3$, respectively. Cast-in-place annulus concrete piles were used to support the embankment, which had a length of 16 m and an outer diameter of 1.008 m with a thickness of 120 mm. The upper 0.5 m of the piles were solid, and annulus piles were utilized below that depth. Piles had a center-to-center spacing of 3.0 m and were arranged in a square pattern. The GRLTP was made of gravel and had a thickness of 0.5 m with a biaxial geogrid in the middle having a tensile strength of 90 kN/m and a maximum allowable strain of 8%. Sensors were installed in the LTP, soft soil, and piles: earth pressure cells (E) to measure vertical stress on the piles and surrounding soil, surface settlement plates (S) and subsurface settlement gauges (SS) to measure settlement, pore water pressure sensors (P) to measure excess pore water pressure due to

embankment loading, and inclinometer (I) to measure the lateral deformation near the toe of the embankment.

The subsoil consisted of, from top to bottom, a 1.5 thick coarse-grained fill, followed by a 2.3 m thick silty clay layer. The silty clay layer is underlain by a 10.2 m thick soft silty clay layer followed by a 2 m thick layer of medium silty clay layer. The soil profile ends with a sandy silt layer. In addition, the ground water table was found to be at a depth of 1.5 m from the ground surface. Figure 4.10 shows the cross-section of the highway embankment demonstrating the piles, GRLTP, subsoil, and the location of the key instrumentation measures, which were used for monitoring the performance of the system. This case study is simulated using Plaxis 2D FEM software and is compared by the performance measurements in the site and results computed by the 3D FEM reported by Liu et al. (2007).

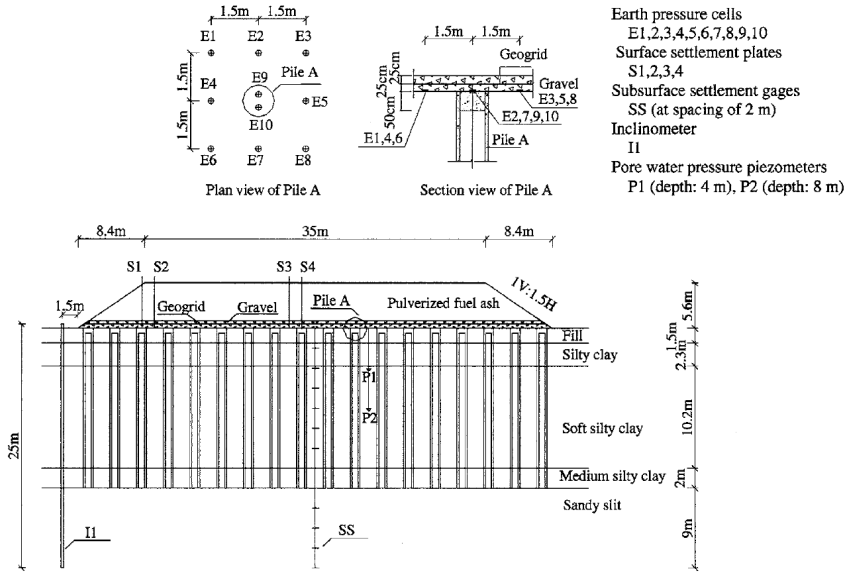


Figure 4.10. Instrumentation plan showing the embankment geometry, piles configuration, subsoil profile, and key instrumentation points (Liu et al., 2007).

### 4.2.1. Numerical Modeling

An equivalent 2D Finite Element Modeling (FEM) has been carried out using PLAXIS 2D (2021) software. Detailed numerical modeling procedure, model geometry, and soil properties are adopted from Liu et al. (2007). In this 2D modeling, solid concrete piles in the upper 0.5 m part are simulated as continuous plane strain walls having the same thickness as the pile diameter (1 m) with a reduced stiffness of 1.752 GPa according to the area replacement ratio (ARR) method given by Huang et al. (2009) and a Poisson's ratio of 0.2. The annulus concrete piles in the lower part below 1.5 m were simulated using embedded beam row elements which can be used to simulate pipe piles by assigning the out-of-plane spacing as the actual center-to-center pile spacing of 3 m, the actual cross-section of the annulus pile (outside diameter is 1 m and inner diameter is 0.76 m), and the actual stiffness of 20 GPa.

For the constitutive modeling, the Modified Cam Clay model (MCC) was used to simulate the subsoil layers except for the coarse-grained fill layer. Table 4.4 shows the properties used for the four layers simulated using the MCC model. The embankment fill, the LTP, and the coarse-grained fill layers were modeled using the Mohr-Coloumb model (MC). Table 4.5 shows the properties of the embankment, and LTP, and coarse-grained layer materials. The piles and geogrid layer were modeled using the linear elastic model. For the geogrid layer, the axial stiffness used is 1180 kN/m. Only half of the embankment is simulated due to symmetry around the centerline. The horizontal boundary is extended to 80 m (i.e., three times the embankment half-width), and the vertical boundary is extended up to 25 m, so boundary effects are minimized. The bottom boundary of the FEM model is assumed to be fixed in both directions, and the horizontal boundaries are set to be fixed in the horizontal direction only (allowed vertically). For the drainage boundary conditions, the ground water table is set at 1.5 m depth with free drainage along this plane. The bottom

boundary is set to be closed (impermeable), and flow is not permitted along the planes x= 0 (because of the embankment line of symmetry) and x= 80 (because the horizontal boundary is extended an adequate distance).

Table 4.4. Subsoil properties with the Modified Cam Clay (MCC) model.

| Material | Drainage type in Plaxis | $\lambda$ | $\kappa$ | $M$ | $e_o$ | $\nu$ | $k_v \times 10^{-4}$ (m/day) |
|---|---|---|---|---|---|---|---|
| Silty clay | Undrained (A) | 0.06 | 0.012 | 1.20 | 0.87 | 0.35 | 8.64 |
| Soft silty clay | Undrained (A) | 0.15 | 0.030 | 0.95 | 1.79 | 0.40 | 4.32 |
| Medium silty clay | Undrained (A) | 0.05 | 0.010 | 1.10 | 0.88 | 0.35 | 4.32 |
| Sandy silt | Undrained (A) | 0.03 | 0.005 | 0.28 | 0.97 | 0.35 | 43.2 |

Table 4.5. Embankment, LTP, and coarse-grained fill properties simulated using the Mohr-Coulomb (MC) model.

| Material | Drainage type in Plaxis | $c'$ (kPa) | $\phi'$ (°) | $\psi$ (°) | $E$ (MPa) | $\nu$ |
|---|---|---|---|---|---|---|
| Embankment | Drained material | 10 | 30 | 0 | 20 | 0.30 |
| LTP | Drained material | 10 | 40 | 0 | 20 | 0.30 |
| Coarse-grained curst | Drained material | 15 | 28 | 0 | 7 | 0.30 |

In this numerical analysis, fifteen-node triangular elements with excess pore water pressure degrees of freedom at all nodes were adopted to simulate the silty clay, soft silty clay, medium silty clay, and sandy silt layers, whereas 15-node triangular elements without excess pore water pressure degrees of freedom at all nodes were used for the embankment fill, LTP, and coarse-grained layers. Moreover, five-node geogrid elements were used to simulate the geogrid layer in

the LTP. Interface elements were utilized around the geogrid layer to simulate the interaction between the gravel and reinforcement with zero cohesion and the interface friction angle to be the same as the friction angle of the LTP material.

The lateral earth pressure coefficient is assumed to be the at-rest earth pressure coefficient assuming the layers to be normally consolidated. For the construction sequence, the embankment is constructed in 9 steps for a 55 days construction period as reported by Liu et al. (2007). The model is brought to equilibrium then the piles are installed. Finally, the soil is left to consolidate reaching 180 days after the embankment construction.

### 4.2.2. Results

Computed results from numerical simulation are compared with the measured values from the field and with results published by Liu et al. (2007). Measurements include the settlement, excess pore water pressure, vertical stress, lateral displacement, and strain in the geogrid layer.

#### 4.2.2.1. Settlement

Computed settlements are compared with measured settlements from the surface settlement plates (S1, S2, S3, and S4). Figure 4.11a and 4.11b show the settlement with time at settlement plates S2 and S3, and S1 and S4, respectively. S2 and S3 settlement plates are located at the soft soil between the piles, while S1 and S4 settlement plates are located at the pile heads. Results are in good agreement with the measured values in the field and the computed values by Liu et al. (2007). On one hand, the maximum measured settlements were approximately 65 mm and 89 mm for settlement plates S2 and S3, respectively. On the other hand, maximum settlements calculated in this study at 180 days are 58 mm (10.7% underestimation) and 80 mm (10.1% underestimation) for settlement plates S2 and S3, respectively. Moreover, the maximum settlements computed at

180 days for settlement plates S1 and S4 are 13 mm and 18 mm, respectively, which are in good agreement with the maximum values observed in the field of 14.5 mm and 19.7 mm, respectively.

(a)

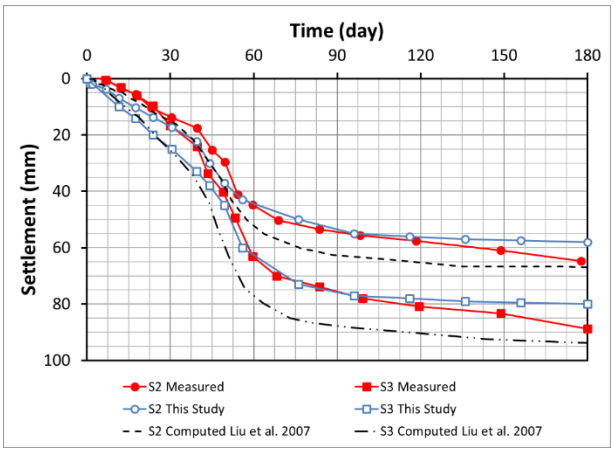


(b)

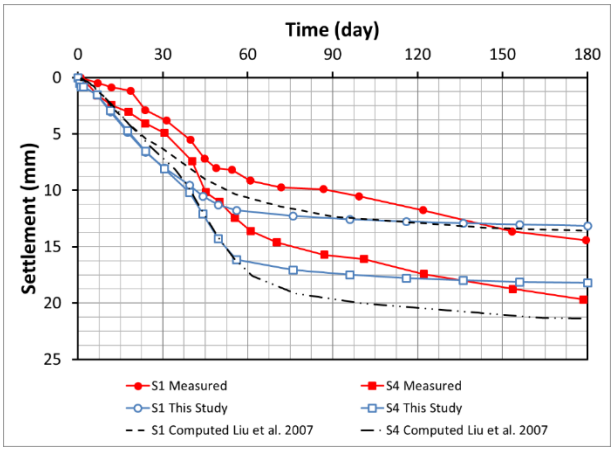


Figure 4.11. Settlement vs. time at settlement plates (a) S2 and S3; (b) S1 and S4.

#### 4.2.2.2. Excess Pore Water Pressure

Figure 4.12 shows the excess pore water pressure with time for sensors P1 and P2 measured at depths of 4 m and 8 m, respectively. Computed results in this study are in fair agreement with the results and the trend of both the measurements in the field and measurements by Liu et al. (2007). However, both calculated results for sensors P1 and P2 are underestimating the actual values

because of overestimation of the arching effect by transferring more load to the piles and less loads on the subsoil, which explains the underestimated settlement values too.

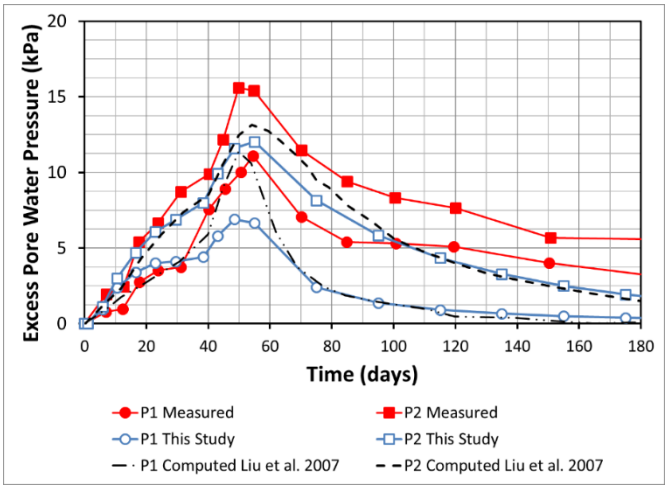


Figure 4.12. Excess pore water pressure vs. time for sensors P1 and P2.

#### 4.2.2.3. Vertical Stress

Figure 4.13 shows the vertical stress with time acting on earth pressure cells E4 and E9, which are located at the soft soil between the piles and at the pile head, respectively. Computed measurements have reasonable agreement with the measured values in the field. The 2D configuration used in this study overestimated the vertical stress acting on the pile head by 18.8% because of the continuous wall nature of the simulated piles as discussed above in the settlement and excess pore water pressure sections. It can also be noted that the vertical stress calculated at earth pressure cell E4 (at the soft soil between the piles) is almost 30 kPa which is only 29% of the embankment load (103 kPa), and this can be attributed to the arching effect where most of the load is transferred to the piles supporting the soil.

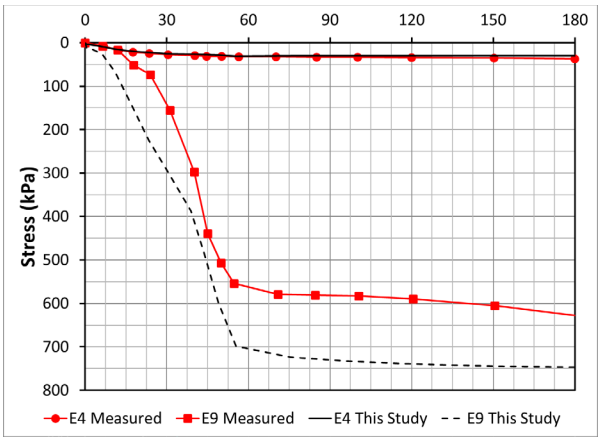


Figure 4.13. Vertical stress vs. time on earth pressure cells E4 and E9.

#### 4.2.2.4. Lateral Displacement

Figure 4.14 shows the lateral displacement profiles at 1.5 m from the toe of the embankment at embankment heights of 2.6 m and 5.6 m. Computed results captured the trend, but overestimated the lateral deformations at both embankment heights. However, results from this 2D FEM study were less than the values computed by Liu et al. (2007) through the 3D FEM study. On one hand, measured values in the field at 2.8 m and 5.6 m were 4 mm and 10 mm, respectively, at a depth of 4 m below the ground surface. On the other hand, computed results are 11 mm, and 25 mm, respectively, at the same depth. This overestimation might be from the reduced stiffness value of the pile material to account for the continuous plane strain piles in the 2D configuration.

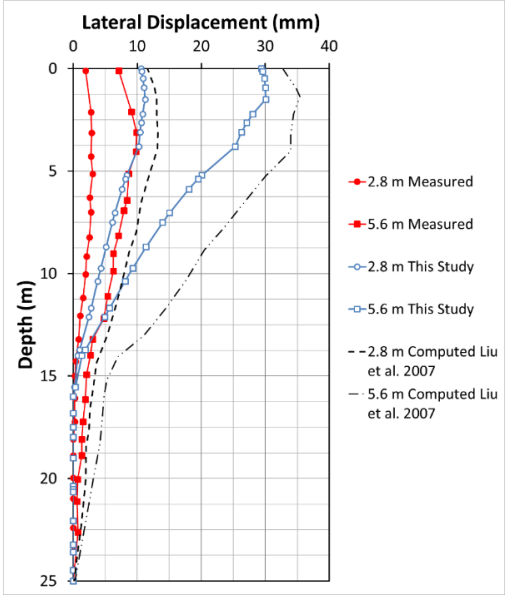


Figure 4.14. Lateral deformation profile vs. depth at 1.5 m away from the embankment toe with different embankment heights.

#### 4.2.2.5. Strain in the Geogrid Layer

Figure 4.15 shows the tensile strain percent at Pile A (Figure 4.10) at the end of construction. Computed results are only compared with the results published by Liu et al. (2007) as the tension was not measured in the field. Computed results from this 2D FEM study are in reasonable agreement with the computed results from the 3D FEM study by Liu et al. (2007). Both results show spikes at the pile edges with a strain percent of less than 2%. This observation indicates that the geogrid strains did not exceed the maximum allowable strain, which was reported to be 8%.

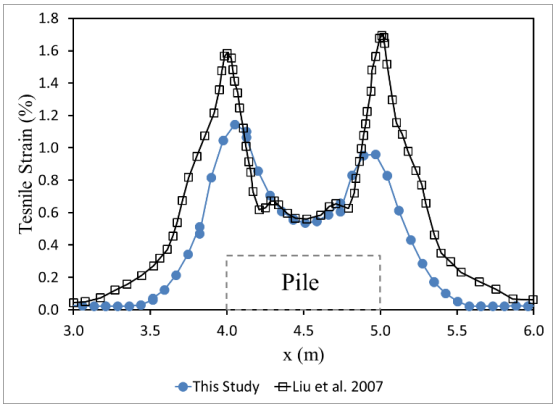


Figure 4.15. Strain in the geogrid layer at Pile A at the end of construction.

### 4.3. Japan Case Study

An embankment system built on soft clayey soil and supported by piles utilizing Deep Cement Mixing (DCM) technique is reported by Chai et al. (2015). The site was located in Saga, Japan, and the embankment was constructed in 2010. The road embankment varied from 5-8 m in height, and the clay layer with bad quality varied from 10-30 m in thickness. The soft clay layer is underlain by a sand layer, which was considered to be an aquifer. The soft clay layer was improved by floating soil-cement piles having a diameter of 1.2 m and a length of 8.5 m. Piles are set to be arranged in a square pattern with a center-to-center spacing of 1.9 m having an area replacement ratio of 31%. The embankment considered herein had a full height of 6.0 m with a crest of 12 m. The embankment side slope was 1 V to 1.8 H resulting in a total base length of 33.6 m. Decomposed granite was used as the filling material for the embankment. Sensors were installed in the test embankment to monitor the performance of the system with time. These include settlement sensors ($S_{s1}$ to $S_{s5}, S_0$ to $S_6$) to measure the settlement, inclinometers ($I_1, I_2$) to measure the lateral deformation near the embankment toe, and pore water pressure sensors ($P_1$, $P_2$, $P_3$) to measure excess pore water pressure induced with embankment loading. For the soil layering, the subsoil started with a 1.5 m thick surface layer followed by an 8 m thick mixed soft silty clay and sandy clay layer. These layers are followed by a 1.7 m thick stiff clay layer underlain by interchanging sand and stiff clay layers. The groundwater table varied from 0.5 m to 1.5 m from the ground surface. Figure 4.16 shows the geometry of the embankment demonstrating the pile configuration, subsoils, and the location of the monitoring points.

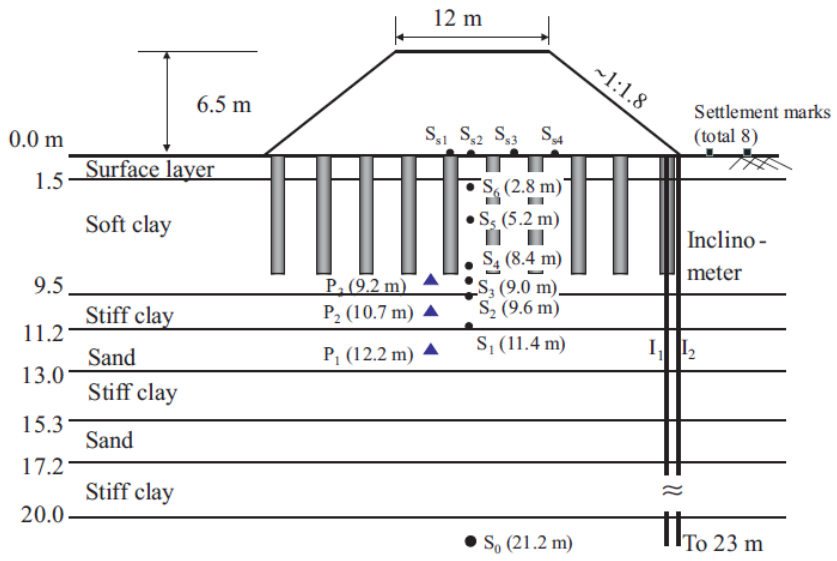


Figure 4.16. Instrumentation plan showing the embankment geometry, piles configuration, subsoil profile, and key instrumentation points (Chai et al., 2015).

### 4.3.1. Numerical Modeling

An equivalent 2D Finite Element Modeling (FEM) has been carried out using PLAXIS 2D (2021) software. Chai et al. (2015) simulated the same case study using equivalent 2D and 3D configurations. Consequently, the exact 2D numerical modeling procedure is adopted from Chai et al. (2015) and compared with the measured results in the field as well as the computed results from the 3D configuration by the same researcher. In this numerical simulation, columns (piles) are simulated as continuous plane strain walls with a reduced thickness of 0.59 m taking into account the actual axial stiffness (EA) into consideration maintaining the same area replacement ratio as suggested by Chai et al. (2015). The stiffness and center-to-center spacing of the piles are kept to be the same as the original case. For the constitutive modeling, the Modified Cam Clay model (MCC) was used to simulate the subsoil layers including the surface curst layer, the soft clay layer, and the stiff clay layers below the piles. The gravelly sand layers and the embankment fill were simulated using the Mohr-Coloumb model (MC). The piles were modeled using the linear elastic model adopting a value of the Young's modulus (E) to be 100 MPa, and the Poisson's ratio

is assumed to be 0.15. The hydraulic conductivity in the horizontal direction is set to be 1.5 times the values of the hydraulic conductivities in the vertical direction for the soft clay layers, whereas the vertical and horizontal hydraulic conductivities are set to be equal for the stiff clay and sand layers. Moreover, both hydraulic conductivities in the horizontal and vertical directions were allowed to decrease during with the variation of the void ratio ($e$) during the consolidation process as the following equation:

$$k = k_0 \times 10^{-(e_0 - e)/C_k} \tag{4.2}$$

The constant $C_k$ is assumed to be half of the initial void ratio for the clay layers ($0.5e_0$). In addition, the hydraulic conductivity of the DCM columns (piles) was assigned to be the same as the hydraulic conductivities of the surrounding soils as suggested by Chai et al. (2015). Table 4.6 shows the properties of the materials used in the numerical modeling study.

Due to symmetry of the geometry, only the right half of the embankment is modeled around the embankment centerline. The horizontal boundary of the model is extended to be approximately two and half times the embankment half-width resulting in a total width of 80 m, and the vertical boundary is set to be 35 m from the ground surface. Both horizontal and vertical movements were not allowed along the bottom boundary of the FEM model, whereas only vertical movement was allowed along the left (x=0) and right (x=80) boundaries. The hydrostatic pore pressure was applied by setting the groundwater table at 1 m depth from the ground surface. Due to embankment symmetry and the adequate horizontal distance of the model to the right, the left and right boundaries were closed drainage boundaries. In contrast, both the bottom boundary of the FEM model and the ground surface were set to be open drainage boundaries (fully permeable).

In this 2D FEM study, 15-noded triangular elements with excess pore water pressure degrees of freedom at all nodes were utilized to simulate the subsoil layers, meanwhile 15-noded triangular

elements without excess pore water pressure degrees of freedom at all nodes were utilized to model the embankment fill material.

The coefficient of at-rest earth pressure, $K_0$, was adopted to relate the initial horizontal and vertical effective stresses. The $K_0$ is assumed to be 0.6 for the subsoils up to 4 m depth from the ground surface having an overconsolidation ratio (OCR) of more than 1.5, whereas foundation soils below 4 m depth from the ground surface is set to 0.5 as adopted by Chai et al. (2015). For the construction sequence, the embankment is constructed in 12 steps for a 100 days construction period (filling rate of 0.06 m/day). Following the embankment construction, the FEM model is left to consolidate for a period of 459 days.

Table 4.6. Material properties used in the FEM study adopted from Chai et al. (2015).

| Soil Layer | Depth (m) | $\gamma$ (kN/m$^3$) | $\lambda$ (c kPa) | $\kappa$ ($\phi'°$) | $M$ | $e_0$ | $E$ (MPa) | $\nu$ | $k_v$x10$^{-4}$ (m/day) |
|---|---|---|---|---|---|---|---|---|---|
| Surface Crust | 0.0-1.5 | 16.0 | 0.25 | 0.025 | 1.2 | 1.50 | - | 0.15 | 6.0 |
| Soft clay 1 | 1.5-4.0 | 13.4 | 0.87 | 0.087 | 1.2 | 3.10 | - | 0.15 | 4.4 |
| Soft clay 2 | 4.0-6.0 | 14.0 | 0.87 | 0.087 | 1.2 | 2.81 | - | 0.15 | 5.3 |
| Soft clay 3 | 6.0-8.0 | 14.1 | 0.58 | 0.058 | 1.2 | 2.58 | - | 0.15 | 5.6 |
| Soft clay 4 | 8.0-9.5 | 14.3 | 0.43 | 0.043 | 1.2 | 2.49 | - | 0.15 | 4.6 |
| Stiff clay | 9.5-11.2 | 18.0 | 0.15 | 0.015 | 1.4 | 1.10 | - | 0.15 | 25 |
| Sand | 11.2-13.0 | 18.0 | (20) | (35) | - | 0.80 | 25 | 0.10 | 250 |
| Stiff clay | 13.0-15.3 | 18.0 | 0.12 | 0.012 | 1.4 | 0.80 | - | 0.15 | 25 |
| Sand | 15.3-17.2 | 19.0 | (20) | (35) | - | 0.80 | 25 | 0.10 | 250 |
| Stiff clay | 17.2-18.3 | 19.0 | 0.12 | 0.012 | 1.4 | 0.70 | - | 0.15 | 25 |
| Sand | 18.3-35.0 | 19.0 | (20) | (35) | - | 0.70 | 20 | 0.10 | 250 |
| Embankment | - | 19.0 | (20) | (35) | - | - | 1 | 0.4 | - |

### 4.3.2. Results

Computed results from this 2D FEM study are compared with the measured values from the field and with the 3D FEM calculated results published by Chai et al. (2015). Measurements include the settlement, excess pore water pressure, and the lateral displacement at the embankment toe.

#### 4.3.2.1. Settlement

Computed settlements are compared with measured settlements from the settlement sensors ($S_{s1}$, $S_{s2}$, $S_1$, and $S_4$). Figures 4.17a through 4.17d show the settlement vs. time for the four mentioned locations. Computed results in this 2D FEM study show a promising agreement with the measured values in the field. In contrast, results of the 3D FEM study by Chai et al. (2015) underestimated the settlement at all locations. For instance, the settlement on the soft soil between the piles at the ground surface (Figure 4.17a) is 57.8 cm and 59 cm for the field and computed results in this study, respectively, resulting in only 2% overestimation of the measured value. Other computed measurements for the rest of the sensors $S_{s1}$ (Figure 4.17b), $S_4$ (Figure 4.17c), and $S_1$ (Figure 4.17d) resulted in a difference of 2% (underestimation), 5% (overestimation), and 3% (overestimation), respectively. Underestimation of the settlements in 3D configuration for the simulated case may be attributed to the load reduction with depth being faster in the 3D compared to the 2D configuration as suggested by Chai et al. (2015).

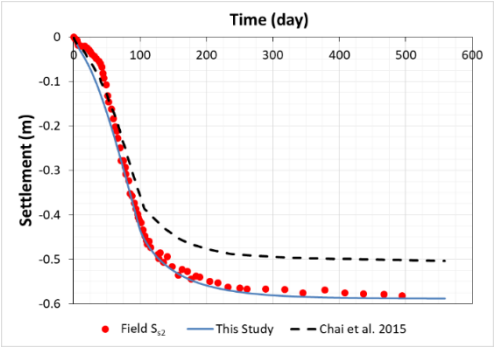


(a)

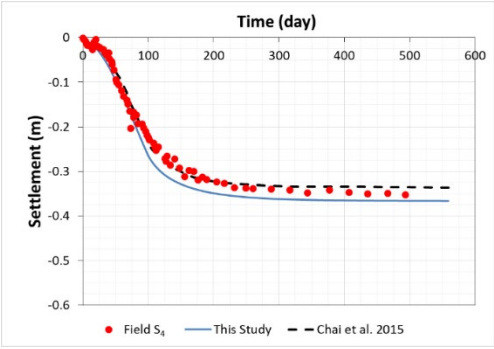


(c)

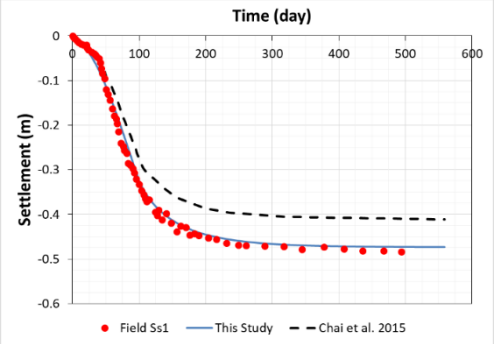


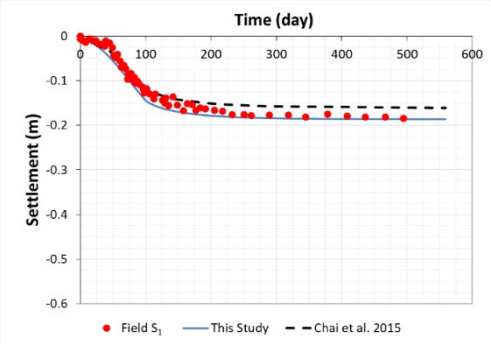


(b) (d)

Figure 4.17. Settlement vs. time at (a) $S_{s2}$: at the ground surface between piles; (b) $S_{s1}$: at the ground surface on the pile head; (c) $S_4$: -8.4 m depth between the piles; (d) $S_1$: -11.4 m depth between the piles.

#### 4.3.2.2. Excess Pore Water Pressure (PWP) Measurements

Figures 4.18a and 4.18b show the excess pore water pressure with time for sensors $P_3$ and $P_2$ measured at depths of -9.2 m and -10.7 m from the ground surface, respectively. Both computed results from this 2D FEM study and the 3D FEM study by Chai et al. (2015) are in good agreement and both simulated the embankment construction well. However, both studies underestimated the excess pore water pressure values for sensor $P_3$ at a depth of 9.2 m from the ground surface. Meanwhile, computed measurements for both studies are in good agreement with the excess pore water pressure observed in sensor $P_2$ at a depth of 11.4 from the ground surface. Furthermore, the slight difference between the results of this 2D FEM study with the 3D FEM study reported by Chai et al. (2015) is reflected in the excess pore water pressure values as the 3D results provided less settlements from the 2D results, thus, higher excess pore water pressure for the 2D results as explained in the settlement section above.

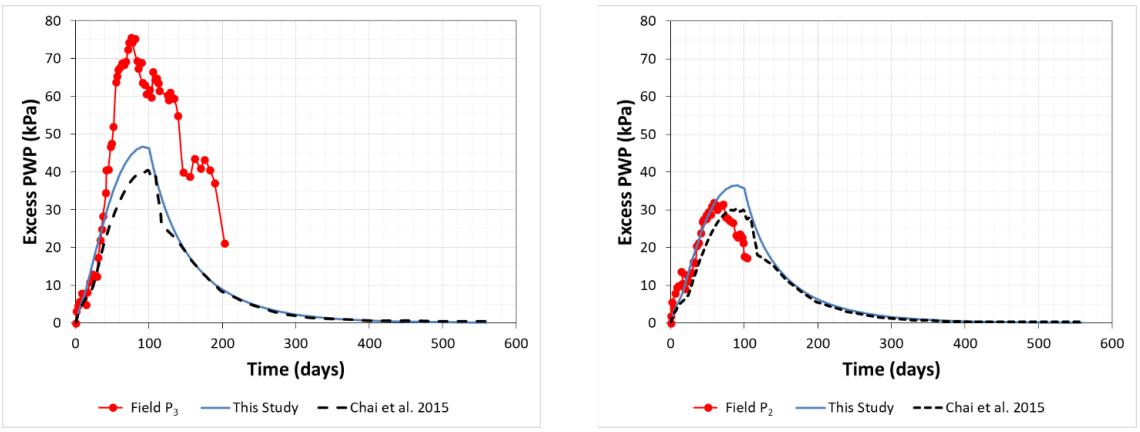


(a) (b)

Figure 4.18. Excess pore water pressure (PWP) vs. time for sensors (a) $P_3$ at a depth of 9.2 m; (b) $P_2$ at a depth of 11.4 m.

#### 4.3.2.3. Lateral Displacement

Figure 4.19 shows lateral displacement profiles for inclinometers $I_1$ (inside the pile near the toe) and I2 (at the embankment toe) at 559 days from the beginning of embankment construction. The inclinometers were installed up to a depth of 23 m from the ground surface, and the lateral displacement was assumed to be zero at that depth. The computed results from this 2D FEM study are in good agreement with the measured values in the field. It can also be noted that computed results from this study are higher than those predicted in the 3D FEM study by Chai et al. (2015), and this may be attributed to the reason that the piles had a reduced section to account for the 2D configuration that was used by Chai et al. (2015) in their 2D FEM procedure. Having the same cross-section may result in better agreement with the 3D results.

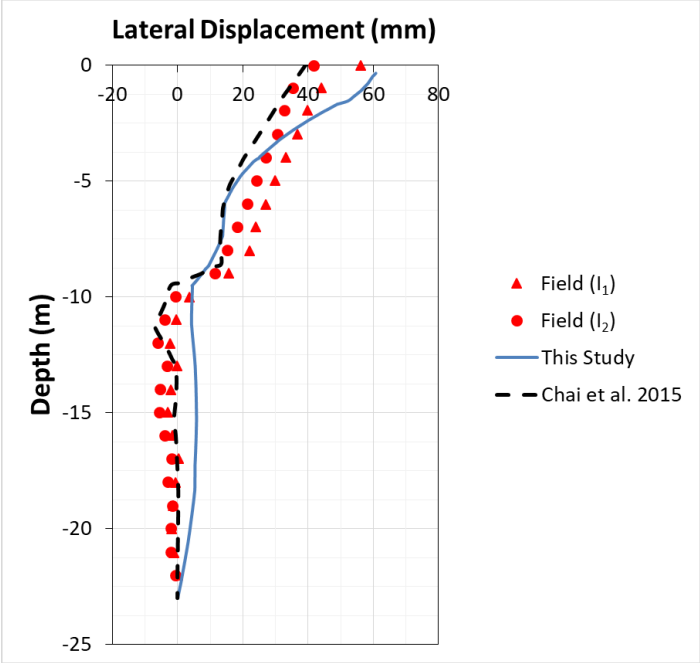


Figure 4.19. Lateral deformation profile for inclinometers $I_1$ and $I_2$ at 559 days.

# CHAPTER 5.
# AMITE RIVER PROJECT PERFORMANCE PREDICTION

An embankment built on soft soil proposed by the Louisiana Department of Transportation and Development (LA DOTD) in the state of Louisiana is improved by the pile-supported embankment system. The system utilizes a GRLTP to enhance the system performance by increasing the stresses on the rigid inclusions (piles) and reducing the part of the embankment load that is applied on the soft soil between the piles. Therefore, intolerable settlements and excessive differential settlements at the crest of the embankment are avoided. Moreover, the geosynthetic reinforcement in the LTP is used to help resist the lateral spreading effect at the sides of the embankment through the tensile forces developing in these geosynthetics. The project is located along Route LA 16 near French Settlement, and it involves replacing the old Amite River Bridge to meet the load requirements and to allow it to be opened for marine traffic. This replacement includes constructing new embankments before and after the new bridge to increase the height of the existing embankments. Figure 5.1 shows the location of the project with a closer look at the bridge being replaced.

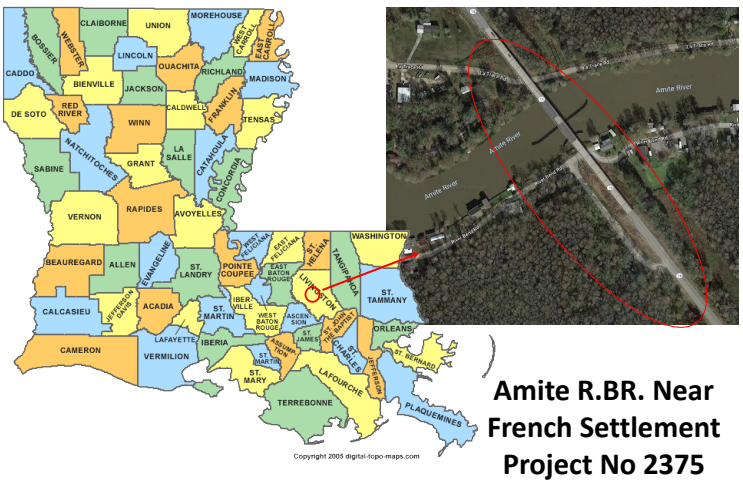


Figure 5.1. Location of the Amite River Project in Louisiana State.

A section of the new embankment is to be instrumented by the Louisiana Transportation Research Center (LTRC) and is to be monitored in the short term and long term to evaluate the performance

of the system. A total of 29 Boreholes (BH) were drilled for the geotechnical investigation. The boreholes demonstrate the soil classification, physical and mechanical properties of the soil, standard penetration test (SPT) number for cohesionless soils, unconsolidated undrained (UU) tests for cohesive soils, and finally, some soil samples are taken for consolidation testing. Information from the boreholes is used to come up with the subsoil profile conditions and properties. The proposed instrumented section lies between BH25 and BH26, but it was closer to BH26 as shown in Figure 5.2. Therefore, the information provided in BH26 is used through this FEM study to predict the system's performance, which includes the settlement, the lateral displacement, the excess pore water pressure, stress transfer, and strain in the geosynthetics.


Figure 5.2. Top view of the proposed project showing the boreholes and the field instrumentation locations.

The embankment base width, including the existing embankment, is approximately 39.3m (129 ft) with a crest width of 17.8 m (57.7 ft). The height of the embankment is 3.3 m (11 ft) including a GRLTP of 0.9 m (3 ft). The GRLTP consists of granular material that is reinforced with a total of 7 geosynthetic layers and are 0.15 m (6 inches) spaced: 3 layers of biaxial geogrid and 2 layers of uniaxial geogrid sandwiched between 2 layers of geotextile on top and bottom of the LTP. The geotextiles work as a separator between the LTP material and the subsoil at the bottom and the

embankment material at the top. Moreover, the geotextiles participate in the load transfer process by carrying tensile forces along them. The embankment is supported by timber piles arranged in a square pattern with a center-to-center spacing of 1.07 m (3.5 ft). The piles' diameter and length are 3.05m (1 ft) and 12.8m (42 ft), respectively.

For the soil layering, the top 5.5 m (18 ft) consists of a very soft clay layer with organics followed by a 0.6 m (2 ft) thick layer of silty sand underlain by another 0.6 m (2 ft) thick soft clay layer. The soft clay layer is followed by a 5 m (16.5 ft) thick layer of silty sand layer underlain by a 6.1 m (20 ft) thick sand layer. This layer overlies a 4.6 m (15 ft) thick silty sand layer. Below it is a 2.9 m (9.5 ft) thick stiff clay layer underlain by 1.5 m (5 ft) thick silty sand. Underneath this layer is another 1.5 (5 ft) m thick stiff clay layer followed by a 3.1 m (10 ft) thick sand layer. Moreover, the groundwater table was found at 0.75m (2.5 ft). Figure 4.3 shows the configuration of the site demonstrating the pile configuration, existing and new embankments, the subsurface soil condition, and the GRLTP.

(a)

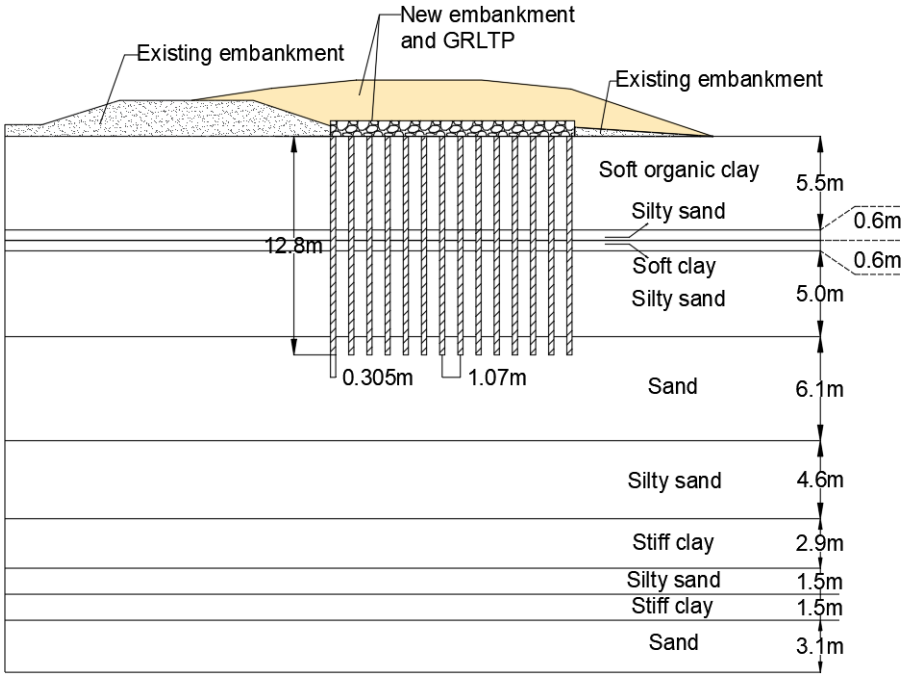

(b)

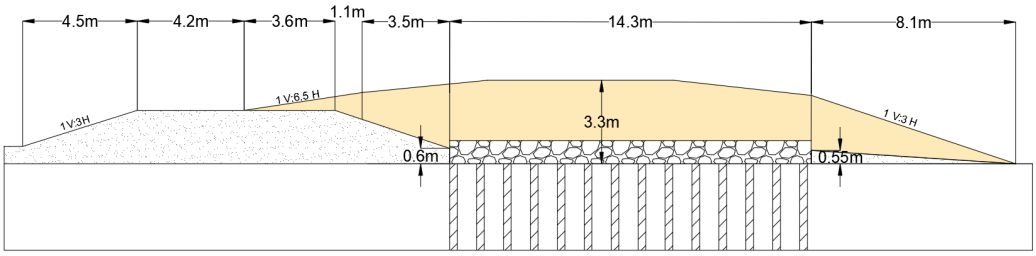


(c)

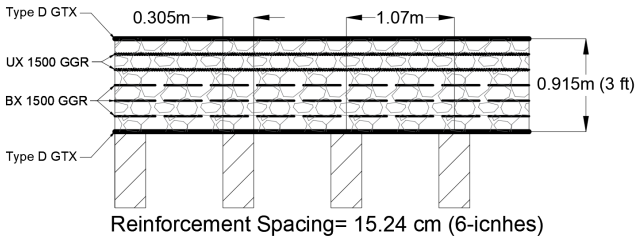


Figure 5.3. Proposed instrumentation plan showing the geometry, pile configuration, subsoil profile, and GRLTP detailing.

### 5.1. Parameters Determination

Soil properties are determined from the information provided in BH26 which includes the physical and mechanical properties of the soil layers such as the moisture content, liquid limit, plasticity index, unit weight, SPT number for cohesionless soils, and UU tests for cohesive soils, and some consolidation tests for the clay layers. Different empirical correlations are used to determine the soil properties which were calibrated by the data acquired from the lab tests. However, the soil properties determined in the lab were used as is. Figure 5.4 shows the moisture content, the SPT number, and the overconsolidation ratio (OCR) along depth as well as the adopted values in the FEM study.

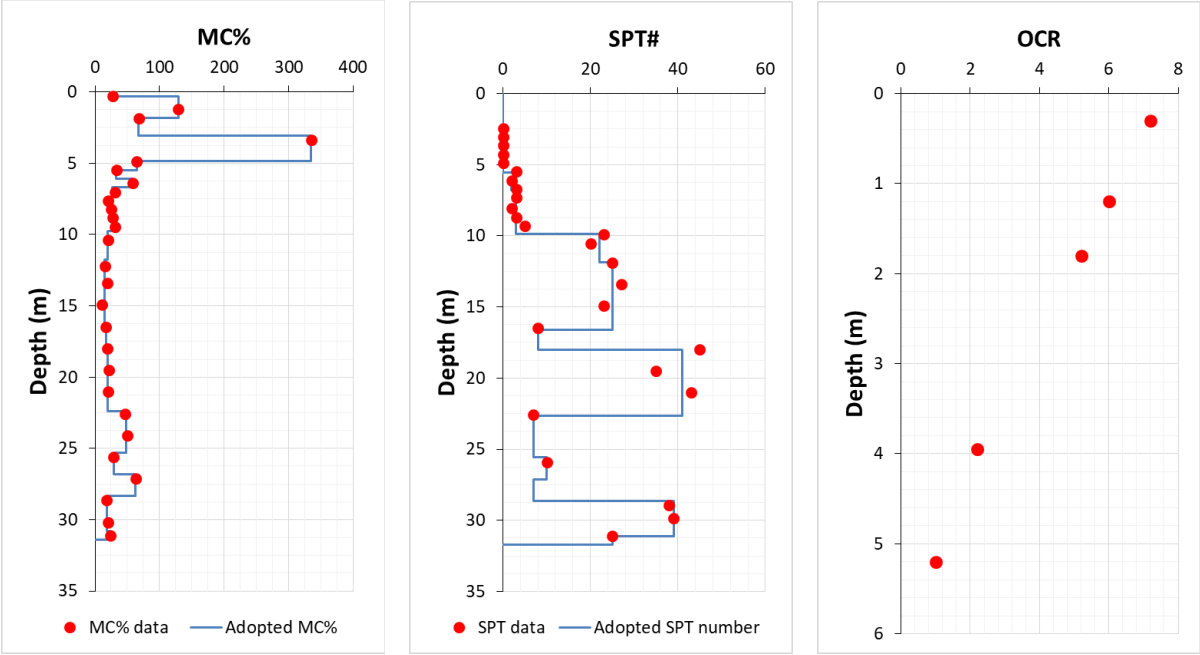


Figure 5.4. Moisture content (MC%), Standard Penetration test (SPT) number, and overconsolidation ratio (OCR) for borehole 26 (BH26).

### 5.1.1. Initial Void Ratio ($e_0$) and Unit Weight ($\gamma$)

The initial void ratio is calculated using the phase diagram relations as follows:

$$Se = wG_s \tag{5.1}$$

Where $S$ is the degree of saturation.

$e$ is the void ratio.

$w$ is the moisture content

$G_s$ is the specific gravity.

The groundwater table was found to be at a depth of 0.75 (2.5 ft) from the ground surface, and due to the capillary rise effect in the clayey soils, the whole layers are assumed to be fully saturated ($S = 100\%$). In addition, the specific gravity is assumed to be 2.7 and 2.65 for the cohesive soils and the cohesionless soils, respectively. The unit weight ($\gamma$) of the soil layers is determined as follows:

$$\gamma = \frac{(e+G_s)\,\gamma_w}{1+e} \tag{5.2}$$

Where $\gamma_w$ is the unit weight of water ($\gamma_w$ =9.81 kN/m$^3$).

### 5.1.2. Friction Angle ($\phi'$)

The friction angle of the cohesionless soils is computed using the SPT number determined at the site. First, the blow number ($N$) is corrected to an average efficiency of 60% ($N_{60}$) as follows:

$$N_{60} = \frac{N\eta_H\eta_B\eta_S\eta_R}{60} \tag{5.3}$$

Where $\eta_H$ is the hammer efficiency (%).

$\eta_B$ is the correction for borehole diameter.

$\eta_S$ is the sampler correction.

$\eta_R$ is the rod length correction.

The hammer efficacy is 97%, and the rest of the correction factors are 1. The friction angle of the cohesionless soils is determined through the graphical correlation between $N_{60}$ and the $\phi'$ provided by Peck et al. (1974), which was approximated by (Wolff, 1989) as follows:

$$\phi'(deg) = 27.1 + 0.3N_{60} - 0.00054[N_{60}]^2 \tag{5.4}$$

For the cohesive soils, Terzaghi et al. (1996) suggested that the typical values of the friction angle of clays range from 20° to 35°. Furthermore, Budhu (2010) suggested the range of the friction angle of clays is from 20° to 30°. Accordingly, the friction angle of soft clay is assumed in the range of 20° to 26°, medium stiff clay is assumed to be 30°, and the stiff clay is assumed to be 32°. The value, $M$, is calculated from equation (4.10).

### 5.1.3. Cohesion ($c'$)

The cohesion of the normally consolidated clay layers and the sand layers are assumed to be 0. However, the cohesion of the overconsolidated clay layers and the silty sand layers are assumed in the lower range of 0-10 kPa given by the Australian Standards for retaining walls (AS 4678).

### 5.1.4. Compression and Recompression Indices ($C_c$ and $C_r$)

The compression and recompression indices are determined for cohesive soil layers. All the consolidation test samples for all the boreholes in the site are used to find the best empirical correlation and to calibrate the computed results. First, the compression index is determined using the empirical correlation between the compression index ($C_c$) and the initial void ratio ($e_0$) suggested by Azzouz et al. (1976) as follows:

$$C_c = 0.4(e_0 - 0.25) \tag{5.5}$$

Second, the computed results are compared with all the compression index values determined in the lab. Lab test data for $C_c$ were divided by the values estimated by the above empirical correlation. It has been found that the estimated values from the empirical correlation overestimated the values determined in the lab by 1.9%. Accordingly, the empirical correlation is calibrated by multiplying the relation by 0.981 resulting in the following calibrated relation:

$$C_c = 0.392(e_0 - 0.25) \tag{5.6}$$

The recompression index ($C_r$) is assumed to be the same as the swelling index ($C_s$) which can be approximated as (Das and Sobhan, 2016):

$$C_s \approx \frac{1}{5} \text{ to } \frac{1}{10}\ C_c \tag{5.7}$$

An average value of $C_s (\approx C_r) = 0.15C_c$ is adopted. Accordingly, the slope of the consolidation line in e-ln p′ space in the modified cam clay model ($\lambda$) can be calculated as follows:

$$\lambda = \frac{C_c}{2.3} \tag{5.8}$$

Furthermore, the slope of rebound in e-ln p′ space in the modified cam clay model ($\kappa$) can be calculated as follows:

$$\kappa = \frac{C_r}{2.3} \tag{5.9}$$

### 5.1.5. Young's Modulus ($E$) and Poisson's ratio ($\nu$)

The Young's modulus ($E$) for cohesionless layers is correlated using the relation between $E$ and $N_{60}$ given by Kulhawy and Mayne (1990) as follows:

$$\frac{E_s}{p_a} = \alpha N_{60} \tag{5.10}$$

Where $p_a$ is the atmospheric pressure (same unit as $E_s$).

$\alpha$ is a dimensionless factor equal to 5 for sands with fines, 10 for clean normally consolidated sands, and 15 for clean overconsolidated sand.

Values of 7.5 and 10 for $\alpha$ are adopted for the silty sand layers and the sand layers, respectively. The Poisson's ratio of the whole foundation soils is assumed from the valid range of each corresponding layer given by Budhu (2010).

### 5.1.6. Hydraulic Conductivity ($k_v$)

The hydraulic conductivity of each corresponding layer is used from the values determined from the consolidation tests of BH26 when available. However, the hydraulic conductivity of the rest of the soil layers is chosen from the typical values provided by Budhu (2010). In addition, the hydraulic conductivity of the clay layers in the horizontal direction is assumed to be 1.5 times the values of the vertical hydraulic conductivity for each corresponding layer. In contrast, both the hydraulic conductivities in the horizontal and vertical directions are assumed to be equal for cohesionless soils.

## 5.2. Numerical Modeling

A 2D Finite Element Modeling (FEM) has been carried out using PLAXIS 2D software. The timber piles were simulated using plane strain walls of 0.305m (1 ft) thickness with an equivalent stiffness ($E_{eq}$) using the area replacement ratio (ARR) method using equation (3.11).

A sensitivity analysis of the ranging $E_{eq}$ from 642.5 MPa to 644.5 MPa showed no significant difference in the performance. Therefore, a value of 643.5 MPa is chosen as an average value. Meanwhile, the center to center spacing between two adjacent walls in this numerical simulation remains the same as the original center to center spacing between two adjacent timber piles of 1.07 m (3.5 ft).

Regarding the constitutive modeling of the materials, the embankment fill, silty sand layers, and sand layers were modeled as a linear elastic-perfectly plastic material using the Mohr-Coulomb (MC) model. Subsequently, the clay layers were represented by the Modified Cam Clay (MCC) model. Due to an increase in embankment load during the consolidation process, the hydraulic permeability was changed attributed to the relationship between the void ratio change and the corresponding embankment load; thus, the permeability change index $c_k = 0.5e_o$ is adopted in this prediction. The timber piles were simulated using a linear elastic model with an equivalent stiffness of $E_{eq}$= 643.5 MPa and ν=0.2.

For the LTP material, the hardening soil model was used to model the granular material. A minimum friction angle of 35° is suggested by Collin (2004) and Schaefer et al. (2017). Accordingly, the friction angle of the granular material is assumed to be 45° per as the requirements of the LA DOTD, and the dilation angle ($\psi$) is determined as suggested by Ameratunga et al. (2016) as follows:

$$\psi = \phi' - 30° \tag{5.11}$$

For the stiffness parameters, the same properties of granular material are adopted from Ardah (2018). Both the existing and new embankments material is assumed to be a compacted clayey silt material modeled with a friction angle of 30° and cohesion of 10 kPa as per the LA DOTD requirements for filling material. Furthermore, the geosynthetics were simulated using the linear

elastic geogrid elements. Interface elements were utilized between the geosynthetic layers and the LTP material with a strength reduction factor of 0.8 and 1.0 for geotextiles and geogrids, respectively. Regarding the interface between the pile material and the surrounding soil, an average strength reduction of 0.8 is adopted to account for the interaction at the interface between the pile material and the surrounding soil. Table 5.1, Table 5.2, and Table 5.3 show the properties of the subsoil and embankment materials, the LTP material, and the geosynthetics, respectively.

The whole embankment is modeled since it's asymmetric. In order to minimize the boundary effect, the modeled area is extended to 120m (390 ft) in the horizontal direction (approximately 3 times the width of the whole embankment base including the new and existing embankment) with a vertical thickness of 31.4m (103 ft) from the ground surface. Both the left and right boundaries were considered to be impermeable. Meanwhile, pore fluid flow was permitted from both the ground surface and the bottom boundary. The groundwater table was found at 0.75m (2.5 ft) depth in the borehole which was adopted in this FEM. In this analysis, for the 2D plane strain FEM model, the horizontal displacement at the left and right boundaries was not permitted, but the vertical movement was allowed, whereas both the vertical and horizontal displacements were prevented at the bottom boundary. In this modeling, fifteen-node triangular elements with excess pore water pressure degrees of freedom at all nodes were adopted to simulate all the materials below the groundwater table, while fifteen nodes triangular elements without excess pore water pressure degrees of freedom at all nodes were applied to model the embankment fill and LTP material. One on hand, the initial horizontal effective stresses for cohesive soils were set up assuming values of the coefficient of at-rest earth pressure, $K_0$, as suggested by Mayne and Kulhawy (1982) as follows:

$$K_o = (1 - sin\phi')\ OCR^{sin\phi'} \tag{5.12}$$

One the other hand, the initial horizontal effective stresses for cohesionless soils were set up assuming values of the coefficient of at-rest earth pressure, $K_0$, as suggested by (Jaky, 1944) as follows:

$$K_o \approx 1 - sin\phi' \tag{5.13}$$

To account for pile driving, the value of the lateral earth pressure coefficient is increased as the soil around the pile is remolded, which was estimated to be in the lower end of the range of $1K_o$ to $2K_o$ for the normally consolidated and moderately overconsolidated clay (Meyerhof, 1976; Coduto, 2001) and $3K_o$ for the heavily overconsolidated clay (O'Neill et al., 1981) for large displacement piles. The factors started from 1.5 to 1.0 for the soil surrounding the piles.

The construction sequence of the embankment is assumed to be in 2 weeks (14 days) with two rates of loading: 0.15 m/day (0.5 ft/day) for the LTP and 0.3 m/day (1.0 ft/day) for the rest of the embankment. Following the completion of embankment construction, a surcharge load of 12 kPa (250 psf) is utilized, and then the soil is left to consolidate for a period of 2 years. Finally, an updated mesh analysis was used to account for the membrane effect in the geosynthetic layers. Figure 5.5 shows the FEM mesh adopted in this study.

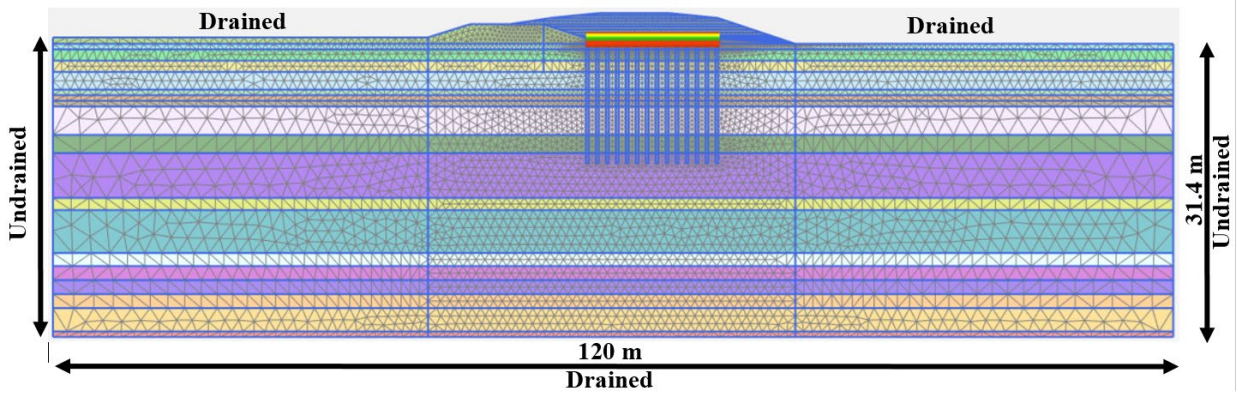


Figure 5.5. The FEM mesh adopted in this study.

Table 5.1. Subsoil materials and embankment properties.

| Soil Layer | Depth (m) | $\gamma$ (kN/m$^3$) | $e_0$ | $\lambda$ ($\phi'$°) | $\kappa$ ($c'$ kPa) | $M$ ($E'$ kPa) | $\nu$ | OCR | K$_o$ | $k_v \times 10^{-3}$ (m/day) |
|---|---|---|---|---|---|---|---|---|---|---|
| Soft clay | 0 | 19.5 | 0.729 | 0.082 | 0.012 | 0.856 | 0.33 | 7.2 | 1.334 | 1 |
| | 0.6 | | | | | | | | | |
| Very soft organic clay | 0.6 | 12.6 | 2.904 | 0.713 | 0.087 | 0.856 | 0.40 | 6 | 1.214 | 0.5 |
| | 1.8 | | | | | | | | | |
| Very soft clay | 1.8 | 15.5 | 1.569 | 0.24 | 0.048 | 0.856 | 0.35 | 4.3 | 1.080 | 0.7 |
| | 3 | | | | | | | | | |
| Very soft organic clay | 3 | 11.3 | 4.230 | 1.1 | 0.165 | 0.772 | 0.40 | 2.35 | 0.881 | 0.5 |
| | 4.9 | | | | | | | | | |
| Very soft clay | 4.9 | 15.9 | 1.755 | 0.26 | 0.04 | 0.772 | 0.35 | 1 | 0.625 | 0.7 |
| | 5.5 | | | | | | | | | |
| Silty sand | 5.5 | 18.4 | 0.875 | (28) | (3) | (3,650) | 0.20 | - | 0.531 | 8.64 |
| | 6.1 | | | | | | | | | |
| Very soft clay | 6.1 | 16.3 | 1.566 | 0.225 | 0.034 | 1.03 | 0.35 | 1 | 0.625 | 1 |
| | 6.7 | | | | | | | | | |
| Silty sand | 6.7 | 19.2 | 0.716 | (28) | (3) | (3,650) | 0.20 | - | 0.531 | 86.4 |
| | 9.75 | | | | | | | | | |
| Silty sand | 9.75 | 20.4 | 0.530 | (37) | (5) | (26,700) | 0.25 | - | 0.400 | 86.4 |
| | 11.7 | | | | | | | | | |
| Sand | 11.7 | 21.3 | 0.406 | (38) | (0) | (40,000) | 0.25 | - | 0.384 | 864 |
| | 16.5 | | | | | | | | | |
| Sand | 16.5 | 21 | 0.451 | (31) | (0) | (13,000) | 0.20 | - | 0.485 | 864 |
| | 17.8 | | | | | | | | | |
| Silty sand | 17.8 | 20.4 | 0.530 | (44) | (5) | (50,000) | 0.30 | - | 0.305 | 86.4 |
| | 22.4 | | | | | | | | | |
| Medium Stiff clay | 22.4 | 17.2 | 1.242 | 0.17 | 0.025 | 1.2 | 0.30 | 1 | 0.500 | 1 |
| | 23.8 | | | | | | | | | |

(table cond't.)

| Soil Layer | Depth (m) | $\gamma$ (kN/m$^3$) | $e_0$ | $\lambda$ ($\phi'$°) | $\kappa$ ($c'$ kPa) | $M$ ($E'$ kPa) | $\nu$ | OCR | K$_o$ | $k_v$ ×10$^{-3}$ (m/day) |
|---|---|---|---|---|---|---|---|---|---|---|
| Stiff clay | 23.8<br>25.3 | 17 | 1.350 | 0.19 | 0.028 | 1.3 | 0.20 | 1 | 0.470 | 1 |
| Silty sand | 25.3<br>26.8 | 19 | 0.7685 | (32) | (3) | (12,000) | 0.20 | - | 0.470 | 8.64 |
| Stiff clay | 26.8<br>28.3 | 15.7 | 1.701 | 0.25 | 0.037 | 1.3 | 0.20 | 1 | 0.470 | 1 |
| Silty sand | 28.3<br>30.8 | 20.6 | 0.5035 | (44) | (5) | (47,000) | 0.30 | - | 0.305 | 86.4 |
| Silty sand | 30.8<br>31.4 | 19.7 | 0.636 | (38) | (5) | (30,000) | 0.25 | - | 0.384 | 86.4 |
| Embankment Fill | - | 18.5 | - | (30) | (10) | (20,000) | 0.30 | - | - | - |

Table 5.2. LTP material properties.

| $\gamma$ (kN/m$^3$) | $c'$ (kPa) | $\phi'$ (°) | $\psi$ (°) | $E_{50}^{ref}$ (kPa) | $E_{oed}^{ref}$ (kPa) | $E_{ur}^{ref}$ (kPa) | $\nu$ | m power |
|---|---|---|---|---|---|---|---|---|
| 18.5 | 20 | 45 | 15 | 34,000 | 26,400 | 103,200 | 0.2 | 0.5 |

Table 5.3. Geosynthetic layers properties.

| Geosynthetic Type | Tensile strength @ 5% Strain (MD) (kN/m) | Axial stiffness (MD) (kN/m) | Tensile strength @ 5% Strain (XMD) (kN/m) | Axial stiffness (XMD) (kN/m) |
|---|---|---|---|---|
| UX1500 | 52 | 1040 | - | - |
| BX1500 | 17.5 | 350 | 20 | 400 |
| Type D Geotextile | - | 600 | - | 600 |

*MD: Machine direction; XMD: Cross machine direction.

## 5.3. Results

The FEM results of this study are presented demonstrating the performance of the system in terms of the settlement, the excess pore water pressure development, the stress transfer to the piles and the subsoil underneath the embankment, the lateral displacement, and the strain in the geosynthetics. Figure 5.6 shows the geometry and the key points that will be used to investigate the performance of the system. Point (A) is under the toe of the left existing embankment; Point (B) is at the interchange between the existing and new embankments on the left; Point (C) is at the location of the maximum settlement at the left of the LTP; Point (D) is at the left edge of the LTP; Point (E) is at the location of the maximum settlement observed at the pile head ($6^{th}$ pile); Point (F) is at the location of the maximum settlement observed between the piles ($6^{th}$ spacing); Point (G) is at the right edge of the LTP; Point (H) is at the location of the maximum settlement observed at the right of the LTP; Point (I) is at the right toe of the new embankment.

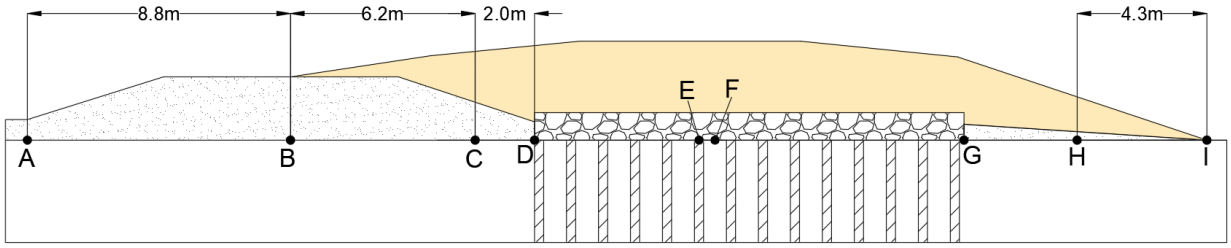


Figure 5.6. Key investigation points used to measure the performance of the system.

### 5.3.1. Settlement

Figure 5.7 shows the settlement along the base of embankment from Point (A) to Point I (Figure 5.6) at three different times: 1-month consolidation, 6-months of consolidation, and 2 years of consolidation after the end of construction (EOC). The settlement is characterized into 3 main zones: the left unsupported zone, the middle zone where the embankment is supported by timber piles and GRLTP, and the right unsupported zone. Maximum settlements observed after 2 years of consolidation are 8.7 cm, 6.8 cm, and 14.1 cm for the left unsupported zone (Point C), the zone

of piles and GRLTP (Point F), and the right unsupported zone (Point H), respectively. It can be noted that the settlement observed in the supported zone (piles and GRLTP) is way less than the settlements observed in the left and right unsupported zones, even though the maximum load (embankment and surcharge loads) is imposed in the middle at the supported zone. This confirms that the significance of this system in eliminating excessive settlements by reducing the loads on the soft soil by the arching effect. During the embankment loading, the soft soil experiences larger settlement compared to the settlement of the rigid inclusions (piles). This causes the embankment material to move downward in the location of the soft soil between the piles. This movement is counteracted by the shear resistance resulting between the stationary and moving embankment material. Therefore, the pressure imposed on the yielding support (soft soil) is reduced and the pressure imposed on the stationary support (piles) is increased (Terzaghi, 1943; Bosscher and Gray, 1985). This can be also noted by the differential settlement observed between the soft soil and the piles in the supported zone (Figure 5.7) which was almost 1 cm. Furthermore, the settlement observed in the left unsupported zone is less than the settlement observed under the right unsupported zone as the new embankment load above the right unsupported zone was higher than that of the left unsupported zone. For the time rate of consolidation, the fastest consolidation rate was in the supported zone as less stress is imposed at the soft soil between the piles followed by the left unsupported area and then the right unsupported area. This can be confirmed as shown in Figure 5.8 which demonstrates the settlement with time at the key points: Point (C), Point (E), Point (F), and Point (H). The settlement observed under Point (F) after in the supported zone after one month of consolidation is 6.35 cm which is 93% of the settlement observed after 2 years of consolidation. In contrast, the settlement observed under Point (C) and Point (H) in both the

unsupported zones after 1 month of consolidation is 7.32 cm and 11.63 cm, respectively, corresponding to only 84.3% and 82.5% of the settlements observed after 2 years of consolidation.

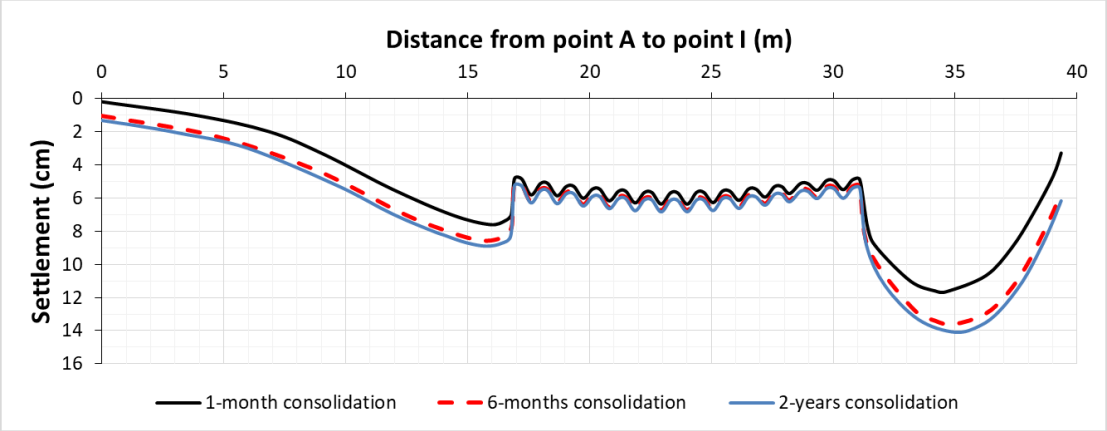


Figure 5.7. Settlement at different times along the base of embankment from Point (A) to Point (I).

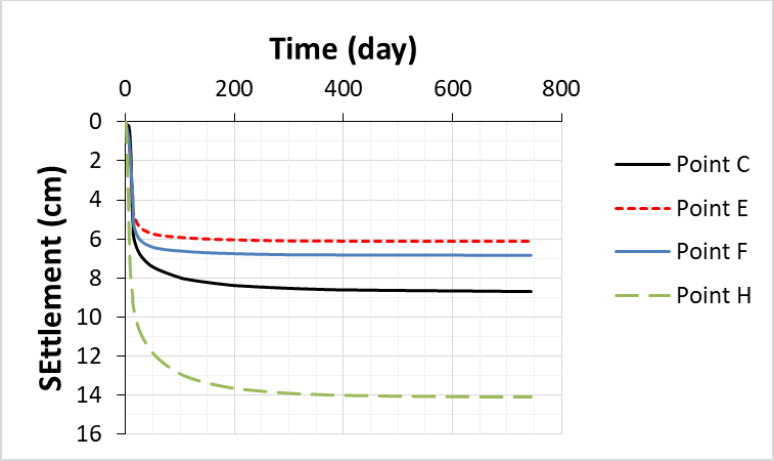


Figure 5.8. Settlement vs. time for the key points: Point (C), Point (F), and Point (H).

### 5.3.2. Excess Pore Water Pressure

Figure 5.9 shows the excess pore water pressure (PWP) with time for the key points of maximum settlements in the 3 main zones: Point (C), Point (F), and Point (H) at a depth of 3.7 m from the ground surface. This depth corresponds to the maximum PWP observed in the top 5.5 (m) soft clay layer. The maximum PWP values are 10.3 kPa, 8.1 kPa, and 11.6 kPa for Point (C), Point (F), and Point (H), respectively, and are observed at the end of construction. The maximum excess PWP is

observed in the very soft organic layer as it is the most compressible layer among all layers with the lowest hydraulic conductivity. The maximum values are sorted from the highest to the lowest in the right unsupported zone, the left unsupported zone, and the supported zone in the middle. This confirms the observation in the settlement above as the maximum settlements were observed in the same order. It can also be noted that the rate of consolidation is the fastest for the supported zone with piles and GRLTP. This implies that the pile-supported system utilizing the GRLTP not only eliminates intolerable settlement, but increases the time rate of consolidation as well which solves the problem of any time constraints for highway projects.

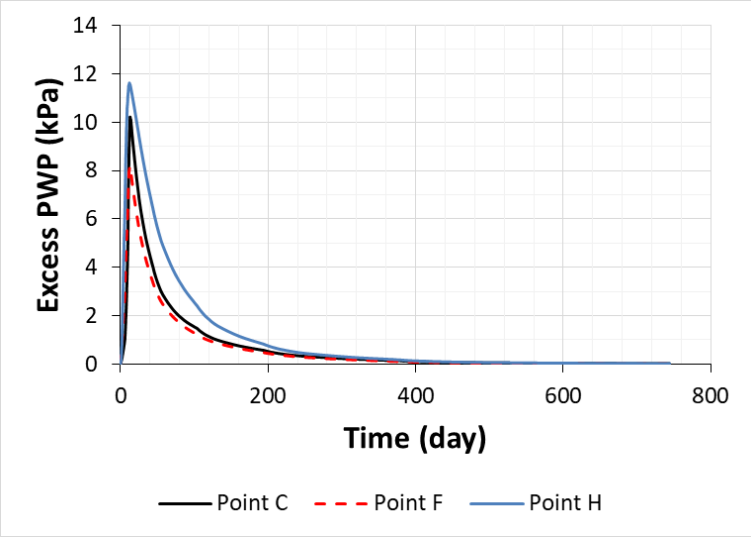


Figure 5.9. Excess Pore water Pressure (PWP) vs. time at a depth of 3.7 m from the ground surface for the key points: Point (C), Point (F), and Point (H).

### 5.3.3. Vertical Stress

As the embankment is constructed, more loads are subjected on the rigid inclusions (piles), while less load is imposed on the soft soil attributing to the arching effect. Figure 5.10 shows the principal stress direction demonstrating the arching effect. The intensity of the red lines represents the magnitude of vertical stresses imposed on the piles and soil between piles. Higher intensity of red lines is observed at the pile heads compared to the soft soil between the piles. In addition, the shape

of the arch can be observed between two adjacent piles and the soil between them (Figure 5.10). Figure 5.11 shows the vertical stress profile along the GRLTP on the piles and soil between piles at two different times: the EOC and long term vertical stresses after 2 years consolidation. Due to the arching effect, vertical stresses observed at the piles are way higher than those observed at the soft soil between the piles. Vertical stresses on piles tend to increase as the embankment center (highest load) is approached, and the vertical stresses on piles start to decrease again as the right edge of the GRLTP is approached with the decrease of the embankment height. However, the piles on the edges of the GRLTP had higher vertical stresses than the piles surrounding them. This observation may be attributed to the vertical stresses imposed on both those piles because of the sudden change in the settlements from the left and right unsupported zones. It can also be noted that vertical stresses on piles at the EOC are less than those after 2 years of consolidation. Conversely, vertical stresses on the soft soil between the piles at the EOC is higher than those after 2 years of consolidation. When the embankment is constructed, both the vertical stresses on the piles and the soft soil between the piles increases until the EOC, and as the soft soil settles more, the arching effect takes place by applying more load on the rigid inclusions and reducing the stresses on the yielding soils between the piles. This is demonstrated in Figure 5.12 which shows the vertical stresses on the pile head at Point (E) and the soft soil between the piles at Point (F). Both stresses on the piles and soft soil between the piles increased until the end of construction. Afterward, stresses are increased with time on the piles, whereas stresses on the soft soil between the piles decreased during the consolidation process. Furthermore, another way to express the arching effect is the stress concentration ratio (SCR), which is defined as the ratio between vertical stresses applied at the pile head to the vertical stresses applied on the soil between piles due to the arching effect. Han and Wayne (2000) reported a range of 10 to 30 of SCR for embankments

supported by timber piles utilizing a GRLTP. Predicted results of the SCR at the EOC and after 2 years of consolidation are 16 and 25, respectively, which lies in the same range above.

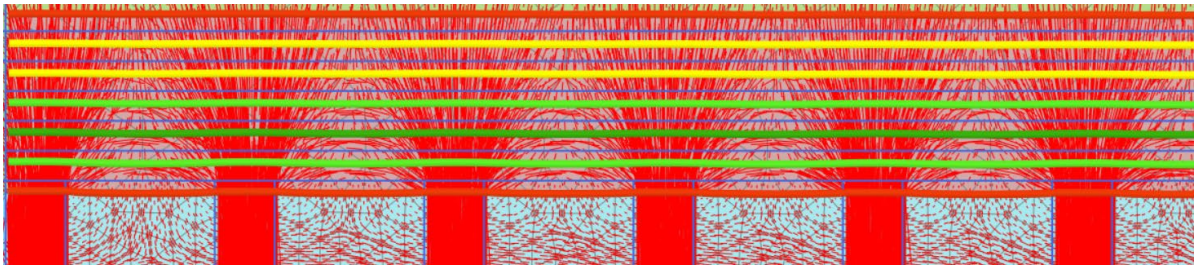

Figure 5.10. Principal stress direction at the GRLTP.

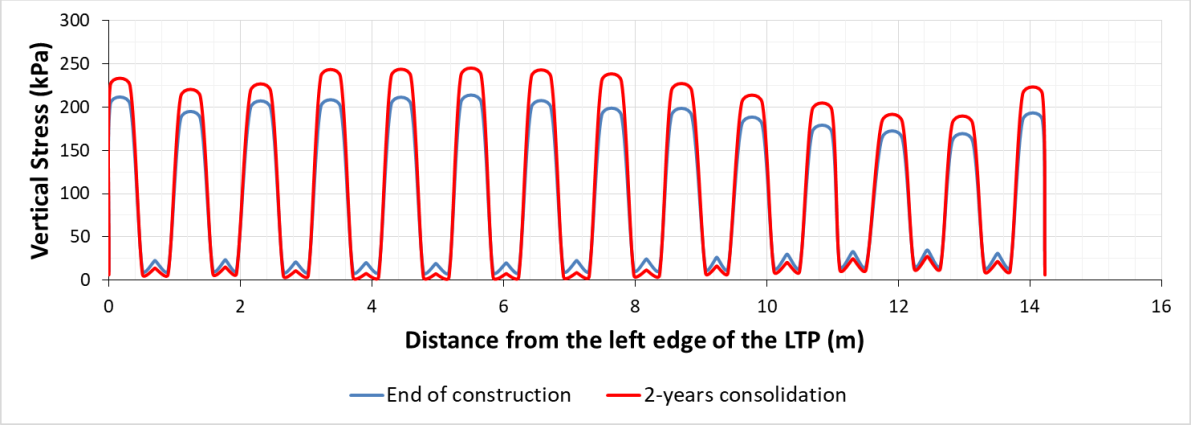


Figure 5.11. Vertical stress along the base of embankment under the LTP from point (D) to point (G) at two different times.

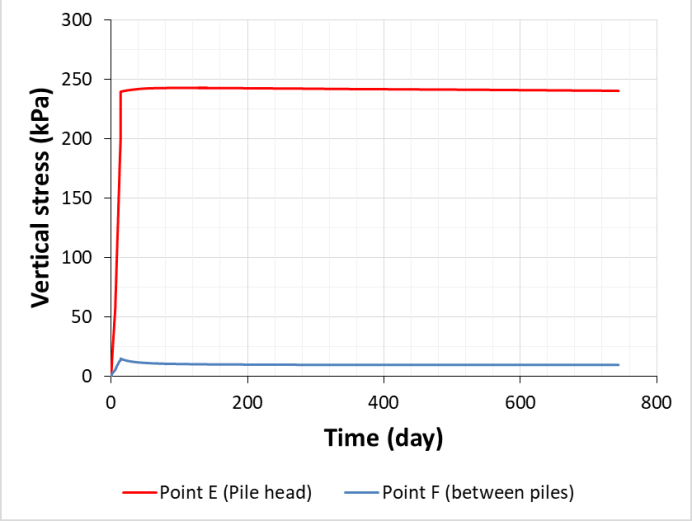


Figure 5.12. Vertical stress vs. time for Points (E) and Point (F).

### 5.3.4. Lateral Displacement

Figure 5.13 shows the lateral displacement profile along depth observed after 2 years of consolidation at the key points: Point (A), Point (B), Point (D), Point (G), and Point (I). For the lateral displacement at the left unsupported side, the soil is supposed to move to the left due to the lateral thrust on the embankment sides. Yet, the soil in this zone tend to move to the right as the soil settlement along the plane of Point (A) to Point (C) is increasing (Figure 5.7) as well as the sudden decrease in settlement along the plane of Point (C) to Point (D) because of the existence of the piles. Thus, the soil tends to move downward and to the right instead. Furthermore, the lateral thrust due to the new embankment load is not significant enough to counteract this effect and make the soil move to the left. Maximum lateral displacements to the right observed at the left unsupported area are 6.5 mm, 9.8 mm, and 18.8 mm for Point (A), Point (B), and Point (D), respectively, which increases by approaching the GRLTP. For the lateral displacement at the right unsupported area, the soil tends to move to the right because of the lateral thrust at the edges of the embankment. The maximum lateral displacement for Point (G) to Point (I) at the embankment toe are 18 mm and 43 mm, respectively, which demonstrate an increased value when the toe of the embankment is approached. This behavior is different from the one observed at the left unsupported side as the right unsupported area is not restrained by the piles in the supported zone (i.e., the settlement increased from Point (G) until reaching its maximum value at Point (H), and then decreased again towards Point (I)). It is also noted that maximum lateral displacement is observed in the most compressible layer, the top 5.5 m soft clay layer. However, the lateral displacement of the soil below the 5.5 m depth tends to move to the opposite side because of the piles in that area. Layers below a depth of 12.8 m (length of piles) started to move to the right side again after the pile effect is diminished in deeper depths.

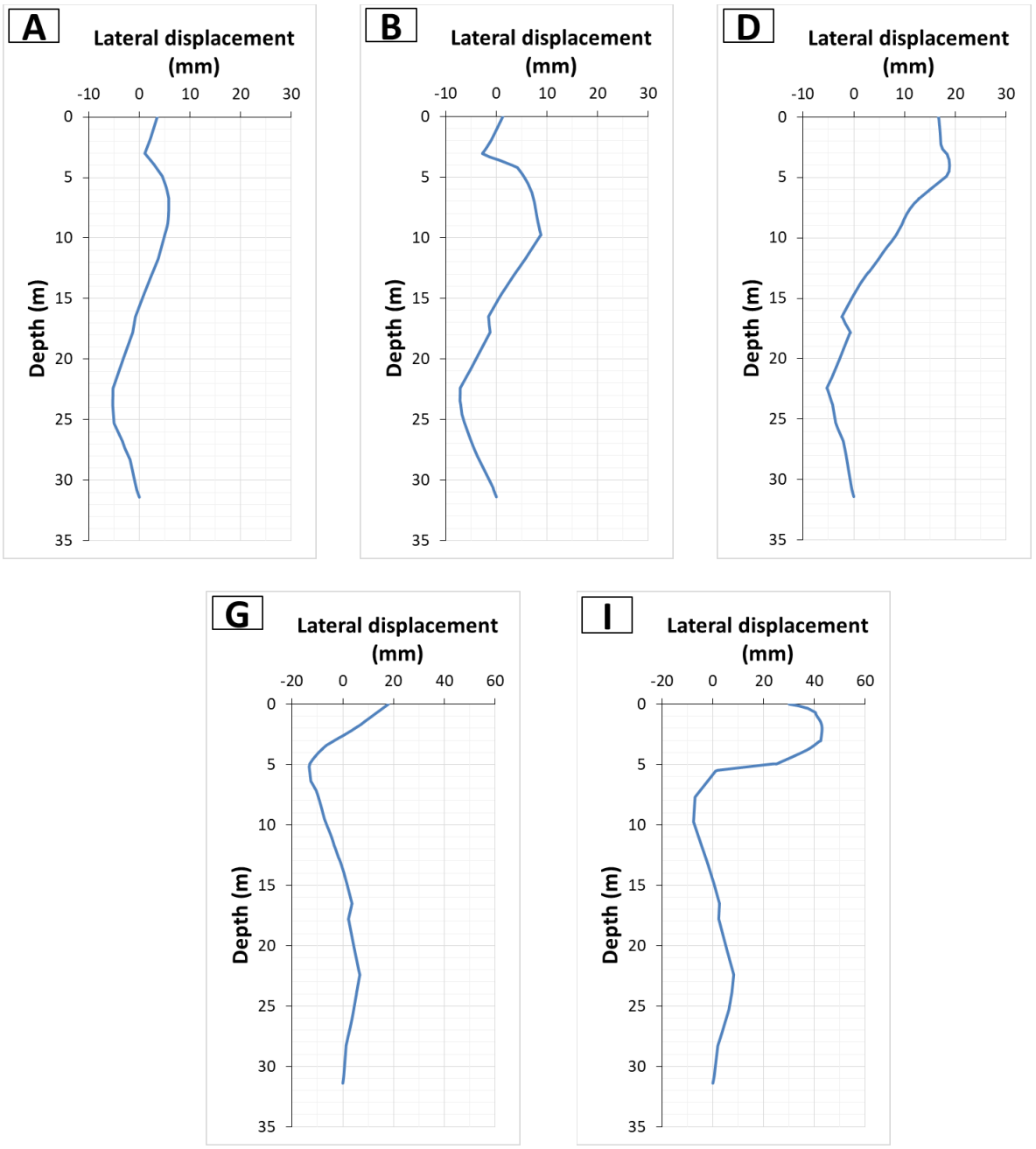


Figure 5.13. Lateral displacement after 2 years of consolidation for the key points: Point (A), Point (B), Point (D), Point (G), and Point (I).

### 5.3.5. Strain in Geosynthetics

Figure 5.14 shows the strain percentage profile in the geosynthetic layers along the GRLTP after 2 years of consolidation. The maximum strain percentage are 0.38%, 0.68%, 0.70%, 0.54%, 0.27%, 0.23%, and 0.27% for all the seven layers from the bottom to the top, respectively. Strain

values are way less than the maximum allowable strain in geosynthetics of 5%. Generally, the highest strain percentage was observed in the biaxial geogrid layers (2nd, 3rd, and 4th layers) with the lowest tensile stiffness (EA= 350 for MD and 400 for XMD). In contrast, uniaxial geogrids had the lowest strain percentage as they had the highest tensile stiffness (EA= 1040 kN/m). Top and bottom geotextiles had a lower strain percentage than the biaxial geogrids and a higher strain percentage than the uniaxial geogrids with an axial stiffness of 600 kN/m. It can also be noted that the strain profiles had a peak-trough behavior: the bottom geotextile layer placed directly on the pile head had the strain peaks on top of the soil between the piles and the troughs on top of the piles. This is attributed to the reason that the geotextile layer is supported by the pile head which restrains the reinforcement layer from deforming downward. Significant deformation occurring at the pile edge and moving towards the soil between piles where no rigid support exists under the reinforcement layer creates the strain peaks on top of the soil between the piles. Conversely, strain peaks occur on top of the pile heads and strain troughs on top of the soil between piles as no restraints exist on top of the pile forming an inverse triangular shape as reported by Eekelen et al. (2012a, 2012b). In addition, strains at the left and right edge of the GRLTP had higher values than those of the other locations in the GRLTP as higher stresses are imposed on these edges because of the abrupt change in the settlement between the supported zone and the unsupported zones as discussed in the vertical stress section.

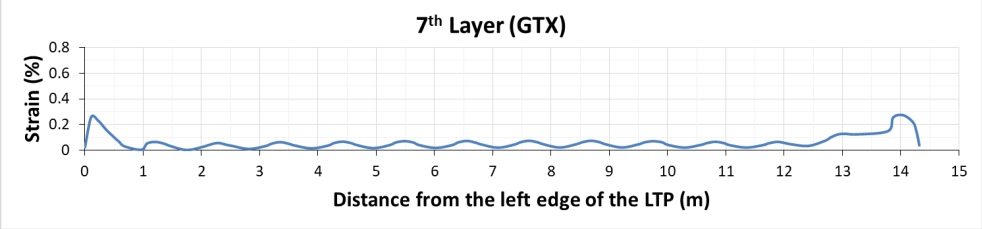

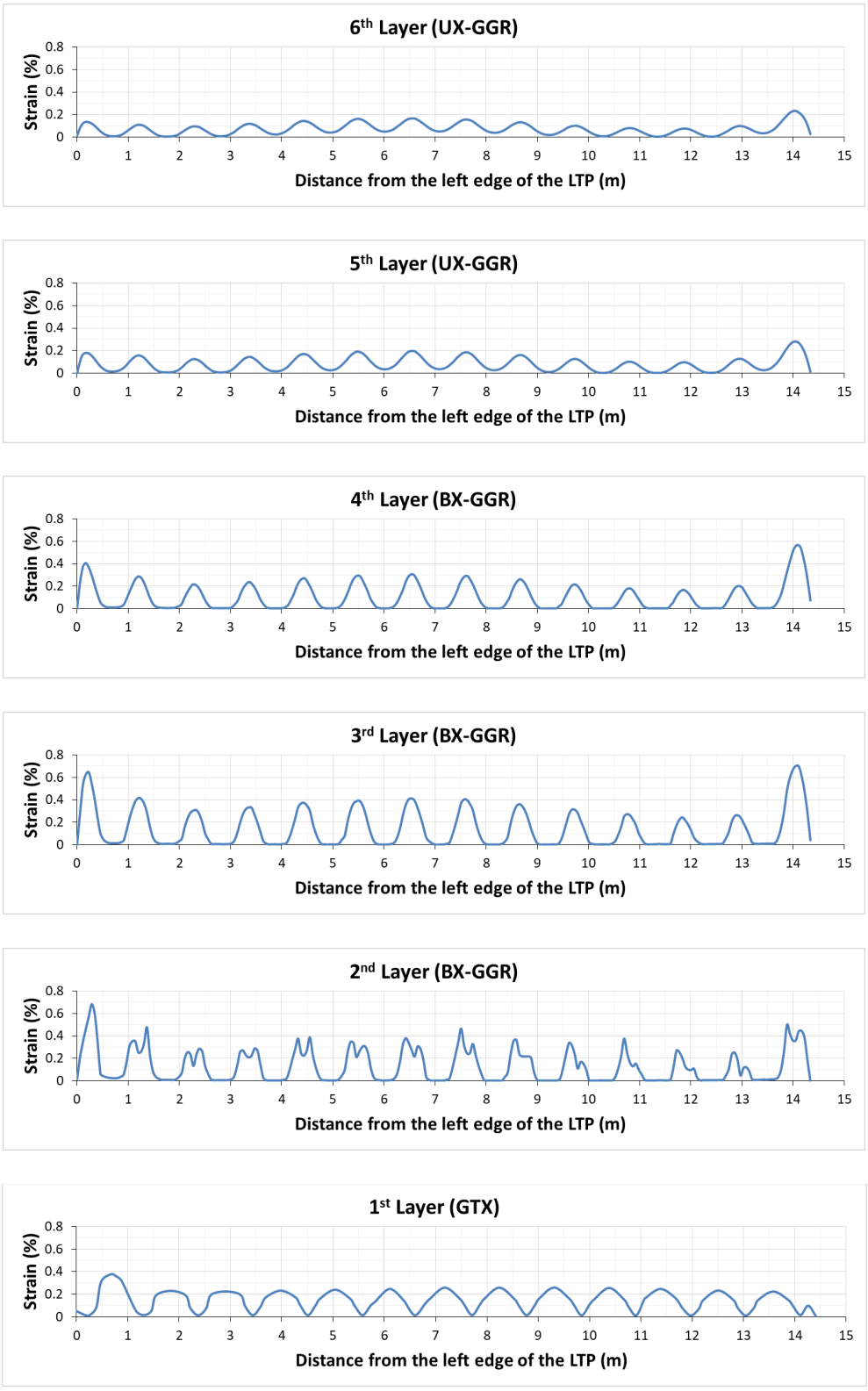


Figure 5.14. Strain percent profile in the geosynthetic layers from top to bottom after 2 years of consolidation.

# CHAPTER 6.
# FINITE ELEMENT MODELING PARAMETRIC STUDY

A FEM parametric study is conducted to investigate the performance of the pile-supported embankment system utilizing a GRLTP for the state of Louisiana. The purpose of the parametric study is to update the design recommendations and construction guidelines adopted for this system for the LA DOTD. End bearing timber piles are only considered in this study where piles tip on a dense sand layer or a stiff clay layer. The parametric study includes changing the subsoil profile, changing the piles and GRLTP extent under the embankment slope, changing the pile spacing starting from 3 times up to 6 times the pile diameter size (3D-6D), and changing the embankment height (H). Key performance measures include settlement, lateral displacement, heaving, stress transfer, excess pore water pressure, and geosynthetic reinforcement strain. The main parameters governing the design recommendations are the pile design (diameter and length), global stability of the system, settlement requirement, and strain in the reinforcement requirement.

## 6.1. Parameters and Concepts of the Finite Element Modeling Parametric Study

### 6.1.1. Subsoil Profiles

Four subsoil profiles are adopted for this study and are characterized into two main groups depending on the soil layer immediately underneath the embankment. Cases 1 and 2 represent group (1) where a very soft clay layer exists underneath the embankment. Cases 3 and 4 represent group (2) where the embankment is underlain by a very loose sand layer. Figure 6.1 shows the adopted subsurface conditions in the FEM parametric study. Case 1 soil profile (Figure 6.1a) consists of a 6.1 m (20 ft) thick very soft clay layer underlain by a 6.1 m (20 ft) thick dense sand layer. These layers are followed by a 3.05 m (10 ft) thick medium dense sand layer underlain by another extended dense sand layer. Similarly, Case 2 soil profile (Figure 6.1b) is composed of a 6.1 m (20 ft) thick very soft clay layer underlain by a 6.1 m (20 ft) thick dense sand layer.

Underneath these layers is a 3.05 m (10 ft) soft clay layer followed by an extended dense sand layer. Case 3 soil profile (Figure 6.1c) starts with a 6.1 m (20 ft) thick very loose sand layer followed by a 6.1 m (20 ft) thick medium stiff clay layer. This layer is underlain by a 3.05 m (10 ft) thick medium dense sand layer followed by an extended dense sand layer. Case 4 soil profile (Figure 6.1d) is composed of a 6.1 m (20 ft) thick very loose sand layer followed by a 6.1 m (20 ft) thick stiff clay layer. Beneath these layers is a 3.05 m (10 ft) soft clay layer followed by an extended dense sand layer.

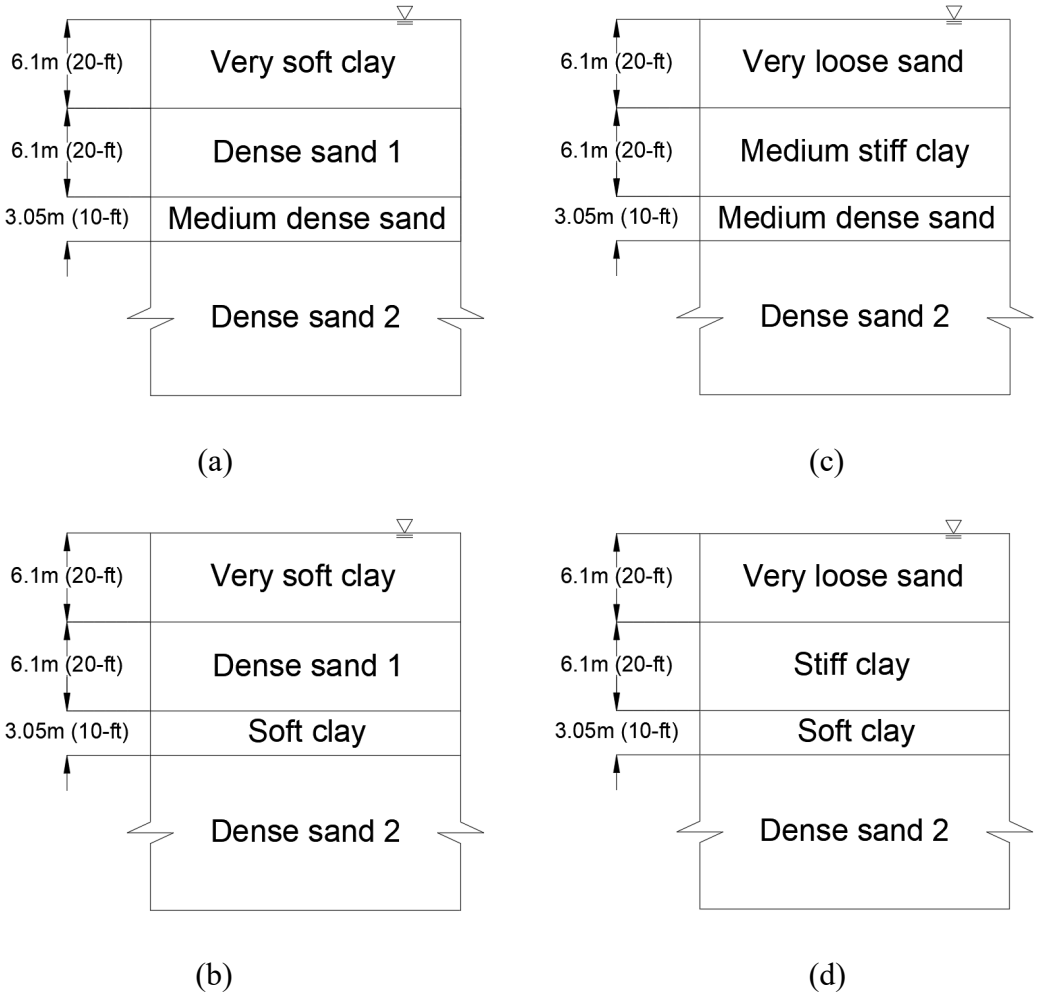


Figure 6.1. Soil profiles adopted in the FEM parametric study: (a) Case 1; (b) Case 2; (c) Case 3; (d) Case 4.

### 6.1.2. Material Parameters Determination

#### 6.1.2.1. Initial Void Ratio ($e_0$) and Unit Weight ($\gamma$)

The initial void ratio is calculated using the phase diagram relations from equation (5.1). All the soil layers are fully saturated ($S = 100\%$) as the groundwater table is assumed to be at the ground surface. For the moisture content values ($w\%$), values are assumed from the natural moisture content in a saturated state for typical soils suggested by Das and Sobhan (2016). Furthermore, the specific gravity is assumed to be 2.7 and 2.65 for the cohesive soils and the cohesionless soils, respectively, as assumed in the Amite River Project in Chapter 5. Accordingly, the unit weight ($\gamma$) of the soil layers is determined as in equation (5.2)

#### 6.1.2.2. Friction Angle ($\phi'$)

For the friction angle of the cohesionless soils, Gibbs and Holtz (1957) characterized the granular soils in terms of the relative density ($D_r$). Peck et al. (1974) followed the same characterization and provided typical values for friction angle of granular soils: the friction angle of the very loose sand is less than 28°, the loose sand friction angle ranges between 28° and 30°, the medium dense sand friction angle ranges between 30° and 36°, and the dense sand friction angle ranges between 36° and 41° (Peck et al., 1974). Accordingly, the friction angle is assumed to be 25°, 33°, and 38° for the very loose sand, medium dense sand, and dense sand layers, respectively.

For the cohesive soils, Terzaghi et al. (1996) suggested that the typical values of the friction angle of clays range from 20° to 35°. Furthermore, Budhu (2010) suggested the range of the friction angle of clays is from 20° to 30°. Accordingly, the friction angle is assumed to be 20° and 23° for the very soft clay and soft clay layers, respectively. Likewise, the friction is assumed to be 30° and 35° for the medium stiff clay and stiff clay layers, respectively. Accordingly, the $M$ value is computed from equation (3.10).

#### 6.1.2.3. Cohesion ($c'$)

The cohesion ($c'$) is assumed to be zero for all the layers as the cohesionless soils are all sands and the cohesive soils are clays that are considered to be normally consolidated.

#### 6.1.2.4. Undrained Shear Strength ($s_u$)

The undrained shear strength ($s_u$) used in the pile design for cohesive soils is assumed from the typical values published by Budhu (2010).

#### 6.1.2.5. Compression and Recompression Indices ($C_c$ and $C_r$)

The compression and recompression indices are determined for cohesive soil layers. The compression index is determined through the relationship with the initial void ratio ($e_0$) which was developed in Chapter 5 for the Amite river project as in equation (5.6). Computed compression index ($C_c$) values are then compared with the typical values of the compression index according to the compressibility level as suggested by Ameratunga et al. (2016). Computed values of $C_c$ are 0.4, 0.35, 0.3, and 0.19 for the very soft clay, soft clay, medium stiff clay, and stiff clay layers, respectively. These values correspond to compressibility levels of high compressibility, upper intermediate compressibility range, lower intermediate compressibility range, and low compressibility as reported by Ameratunga et al. (2016). Moreover, the recompression index ($C_r$) is assumed to be the same as adopted in the Amite River Project in Chapter 5 ($C_r = 0.15C_c$). Accordingly, $\lambda$ and $\kappa$ are computed from equations (5.8) and (5.9), respectively.

#### 6.1.2.6. Young's Modulus ($E$) and Poisson's ratio ($\nu$)

The Young's modulus ($E$) for cohesionless layers is assumed from the typical range from Bodhu (2010) as 5 MPa, 35 MPa, and 55 MPa for the very loose sand, medium dense sand, and dense sand layers, respectively. Similarly, the Poisson's ratio of cohesive and cohesionless soil layers is assumed from the valid range of each corresponding layer given by Budhu (2010). On one hand,

the very soft clay, soft clay, medium stiff clay, and stiff clay layers assumed values are 0.35, 0.35, 0.3, and 0.2, respectively. On the other hand, the very loose sand, medium dense sand, and dense sand layers assumed values are 0.2, 0.25, and 0.25, respectively.

#### 6.1.2.7. Hydraulic Conductivity ($k_v$)

The hydraulic conductivity of the soil layers is chosen from the typical values provided by Budhu (2010). Moreover, the horizontal hydraulic conductivity is assumed to be 1.5 times the $k_v$ for cohesive layers, whereas horizontal hydraulic conductivity for cohesionless layers is assumed to be equal to $k_v$ as adopted in the Amite River Project in Chapter 5. In addition, the change in hydraulic conductivities for cohesive soils during the consolidation process is considered in this study with an adopted value of the change index constant ($c_k$) to be $0.5e_0$.

### 6.1.3. Pile Design

The timber piles are assumed to carry the whole embankment load and the surcharge load to satisfy the strength limit state requirements. The geotechnical capacity of the piles is computed using the Nordlund method (Nordlund, 1963) and Alpha ($\alpha$)-method (Tomlinson, 1957) for cohesionless soils and cohesive soils, respectively. The Nordlund method uses the effective stress method to calculate the geotechnical capacity, while the alpha ($\alpha$)-method uses the total stress by considering the undrained shear strength ($s_u$) of cohesive soils. For more details, the reader is referred to Hannigan et al. (1997). Resistance factors for both methods are considered to be 0.5 as reported by Abu-Farsakh et al. (2009) which is adopted in the driven pile design guidelines of the LA DOTD. Piles are designed to satisfy the load requirements for each corresponding spacing and embankment height for all soil profiles. The geotechnical capacity is computed with depth, and the pile length is chosen accordingly to satisfy the loading requirement. For instance, Figure 6.2

shows the estimated geotechnical capacity with depth up to 18.3 m (60 ft) depth for the soil profile of Case 1.

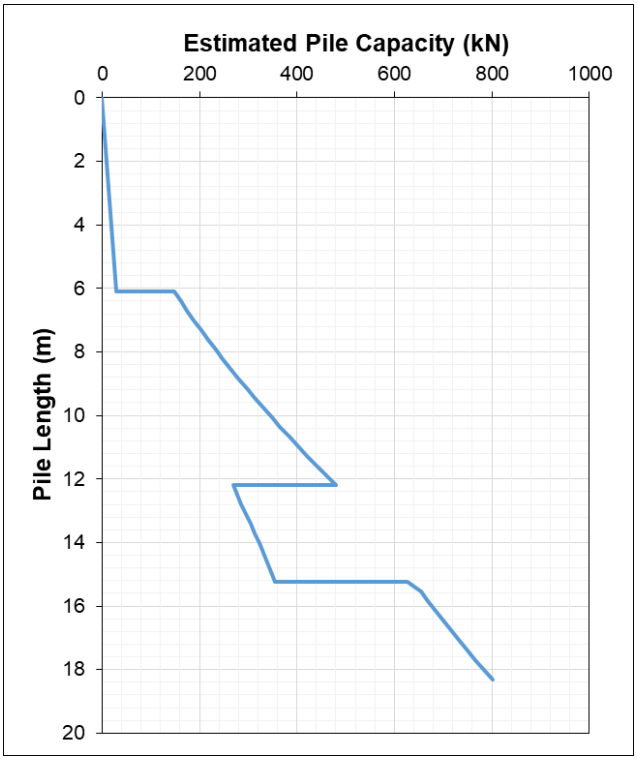


Figure 6.2. Estimated pile capacity vs. pile length for soil profile of Case 1.

### 6.1.4. Embankment Geometry and GRLTP Detailing

The embankment height in this FEM parametric is varied to be 3.05 m (10 ft), 6.1 m (20 ft), and 9.15 m (30 ft) with a crest of 18.3 m (60 ft). The embankment slope is 1V:2H resulting in a total base length of 30.5 m (100 ft), 42.7 m (140 ft), and 54.9 m (180 ft) for the three embankments heights from the least to the highest. The GRLTP consists of 5 layers of geosynthetic reinforcement: 2 geotextile layers at the top and bottom of the GRLTP, and 3 biaxial geogrid layers in the middle. The spacing between the geosynthetic layers is 15.24 cm (6 inches) resulting in a total thickness 0.61 m (2 ft) as the minimum required thickness of the GRLTP. Figure 6.3 shows the detailing of the GRLTP.

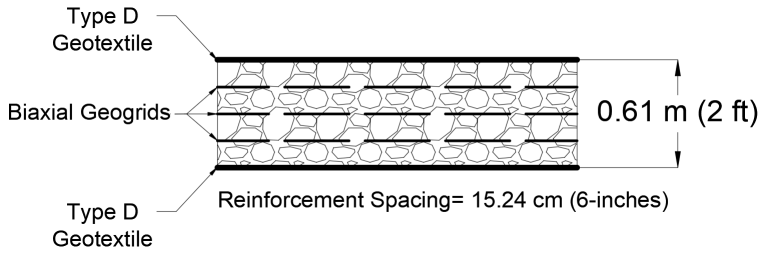


Figure 6.3. GRLTP detailing in the FEM parametric study.

### 6.1.5. GRLTP and Piles' Extent Under the Embankment Slope

The GRLTP and piles' extent under the embankment slope is investigated to maintain a stable system without any possible global or local failures due to the embankment and surcharge loading. The GRLTP and piles' extent is varied to be 0.0H (not extended under the embankment slope), 0.5H (extended up to one-quarter of the slope), 1.0H (extended up to the mid-slope), 1.5H (extended up to three-quarters of the slope), and 2.0H (extended up to the embankment toe). Figure 6.4 demonstrates the potential locations of the GRLTP and the piles' extent under the embankment slope. Stress history is considered for Cases 1 and 2 where a very soft clay layer underlies the embankment. Both normally consolidated clay (OCR= 1) and overconsolidated clay is considered to investigate the GRLTP and piles' extent under the slope. The assumed OCR value is the same adopted in the Amite River Project in Chapter 5 in which the OCR value starts with 7 at the top of the very soft clay layer and decreases with depth to reach a value of 1 at the bottom of the very soft clay layer. However, this is not considered for Cases 3 and 4 where a very loose sand layer underlies the embankment.

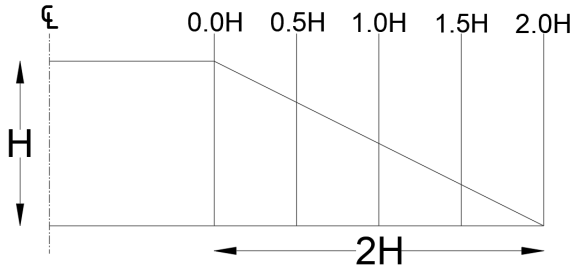


Figure 6.4. GRLTP and piles' extent under the embankment slope.

### 6.1.6. Pile Spacing

Piles' center-to-center spacing is varied to be 3 times the pile diameter up to 6 times the pile diameter (3D to 6D).

## 6.2. Design Requirements

### 6.2.1. Pile Length and Diameter Requirements

Performance of embankments supported by timber driven piles is investigated in this FEM parametric study for the state of Louisiana. Most common and available timber piles have a diameter of 0.305 m (1 ft) and a length ranging from 9.15 m (30 ft) to 18.3 (60 ft) as approved by the LA DOTD. Therefore, a diameter of 0.305 (1 ft) is adopted for the whole study with maintaining a minimum pile length of 9.15 m (30 ft) and a maximum pile length of 18.3 m (60 ft).

### 6.2.2. Stability of the System

A slope stability analysis of the pile-supported embankment system utilizing a GRLTP is conducted in the FEM parametric study to investigate any potential global or local failure in the system. A minimum required factor of safety of 1.5 is adopted in this study.

### 6.2.3. Settlement Requirement

Settlement observed underneath the embankment is one of the key performance measures considered in this study to satisfy the serviceability limit state requirements. A maximum required settlement of 15.24 cm (6 inches) is adopted in this FEM parametric study.

### 6.2.4. Reinforcement Strain Requirement

The strain in the reinforcement layers used in the GRLTP, as provided by the FHWA Ground Modification Methods – Reference Manual (Schaefer et al., 2017), must not exceed a maximum allowable value of 5% so that unacceptable differential settlement at the embankment crest is

avoided. Thus, a maximum strain in the geosynthetic layers of 5% is adopted in this FEM parametric study.

### 6.3. Numerical Modeling

The detailed numerical modeling procedure is adopted from Chapter 5. A 2D Finite Element Modeling (FEM) has been carried out using PLAXIS 2D software. The timber piles were simulated using plane strain walls of 0.305m (1 ft) thickness with an equivalent stiffness ($E_{eq}$) using the area replacement ratio (ARR) method as described by Huang et al. (2009). Young's modulus ($E$) of the timber pile and soil surrounding the piles considered in this study are 10 GPa and 5 MPa, respectively. The center-to-center spacing between the plane strain walls is kept the same as the original spacing. Regarding the constitutive modeling of the materials and soils, embankment fill material and all cohesionless soil layers (very loose sand, medium dense sand, and dense sand layers) are modeled using the Mohr-Coulomb (MC) model. On the other hand, all cohesive soil layers (very soft clay, soft clay, medium stiff clay, and stiff clay layers) are modeled using the Modified Cam Clay (MCC) model. Table 6.1 shows the material parameters adopted in this FEM parametric study for foundation soils and the embankment material. The GRLTP material is simulated using the Hardening Soil (HS) model with the same parameters adopted in Chapter 5 for the GRLTP material. The timber piles and the geosynthetic layers are simulated using the Linear Elastic model. The excess pore water pressure induced with embankment loading is expected to be overestimated because of the non-porous nature of the timber walls (piles). Accordingly, the pile material is assigned a hydraulic conductivity value taking into account the hydraulic conductivity of the surrounding soils as adopted in Chapter 5. Table 6.2 shows the plane strain walls $E_{eq}$ and the estimated hydraulic conductivities for each corresponding spacing in this FEM parametric study. For the geosynthetic reinforcement, tensile stiffness ($EA$) is assumed to be

600 kN/m and 375 kN/m for the geotextiles and geogrids, respectively. Interface elements are utilized between the geosynthetic layers and the GRLTP material, and between the pile material and the surrounding soils. Reduction factors of 1.0, 0.8, and 0.8 are adopted for the interface between the geogrids and GRLTP material, the interface between geotextiles and the GRLTP, and the interface between the timber piles and the surrounding soils.

Only half the embankment is modeled due to symmetry around the embankment centerline. The FEM model is extended in both the horizontal and vertical directions to minimize the boundary effect on the results. Thus, the model is extended in the horizontal direction a distance of 120 m (400 ft), 210 m (700 ft), and 300 m (1000 ft) for embankment heights of 3.05 m (10 ft), 6.1 m (20 ft), and 9.15 m (30 ft), respectively, which is almost ten times the embankment half-width. Likewise, the vertical distance of the FEM model is extended a distance of 27 m (90 ft), 36 m (120 ft), and 45 m (150 ft) for embankment heights of 3.05 m (10 ft), 6.1 m (20 ft), and 9.15 m (30 ft), respectively, which corresponds to a value of less than 0.05q (embankment and surcharge load) stress increase at the bottom boundary of the FEM model.

For the mechanical boundary conditions of the FEM model, the right and left extreme boundaries are prevented from being displaced in the horizontal direction, while displacement in the vertical direction is allowed. Conversely, the extreme bottom boundary of the FEM model is prevented from moving in both the horizontal and vertical directions (fixed in both directions). For the hydraulic and drainage boundary conditions, the ground water table is assumed to coincide with the ground surface. Furthermore, the extreme right and left boundaries are not allowed to dissipate excess PWP, while the bottom and top boundaries of the FEM model are considered to be permeable. During the consolidation process, the hydraulic permeability was changed attributed to the relationship between the void ratio change and the corresponding embankment load. Thus,

the permeability change index $c_k = 0.5e_o$ is adopted in this FEM parametric study. On one hand, all the materials below the ground water table are modeled using 15-nodded triangular elements with excess pore water pressure degrees of freedom at all nodes. On the other hand, all materials above the ground water table are modeled using 15-nodded triangular elements without excess pore water pressure degrees of freedom at all nodes. Initial horizontal effective stresses are evaluated by assuming the coefficient earth pressure of the foundation soils to be the at-rest earth pressure coefficient ($K_0$) using the same relations from Chapter 5 as in equations (5.12) and (5.13). The construction sequence of the embankment is assumed to be at a rate of 0.305 m/day (1 ft/day). The foundation soils are then left to consolidate a period of 30 days after the end of construction (EOC). Subsequently, a surcharge load of 12 kPa (250 psf) is utilized, and finally, the foundation soil is left to consolidate again for 700 days to reach a period of 2 years for consolidation. Updated mesh analysis option on PLAXIS is adopted in this study to account for the membrane effect in the geosynthetic reinforcement as well as the arching effect. Figure 6.5 shows the FEM mesh adopted in this study for the investigated embankment heights 3.05 m (10 ft), 6.1 m (20 ft), and 9.15 m (30 ft). For simplicity, the spacing of the piles is reported herein as 3-ft, 4-ft, 5-ft, and 6-ft for the FEM parametric study.

Table 6.1. Subsoil materials and embankment properties adopted in the FEM parametric study.

| Soil Layer | $\gamma$ (kN/m$^3$) | $e_0$ | $\lambda$ ($\phi'$°) | $\kappa$ ($c'$ kPa) | $M$ ($E'$ kPa) | $\nu$ | $K_o$ | $k_v \times 10^{-4}$ (m/day) |
|---|---|---|---|---|---|---|---|---|
| Very soft clay | 17.4 | 1.20 | 0.174 | 0.026 | 0.77 | 0.35 | 0.658 | 4.32 |
| Soft clay | 17.83 | 1.08 | 0.150 | 0.023 | 0.90 | 0.35 | 0.609 | 4.32 |
| Medium stiff clay | 18.4 | 0.95 | 0.130 | 0.020 | 1.20 | 0.30 | 0.500 | 4.32 |
| Stiff clay | 19.6 | 0.70 | 0.083 | 0.012 | 1.40 | 0.20 | 0.426 | 4.32 |
| Very loose sand | 18.3 | 0.90 | (25) | (0) | (5,000) | 0.20 | 0.577 | 10000 |
| Medium dense sand | 19.1 | 0.74 | (33) | (0) | (35,000) | 0.25 | 0.455 | 10000 |
| Dense sand 1 | 20.4 | 0.53 | (38) | (0) | (55,000) | 0.25 | 0.384 | 10000 |
| Dense sand 2 | 20.6 | 0.50 | (38) | (0) | (55,000) | 0.25 | 0.384 | 10000 |
| Embankment | 18.5 | - | (30) | (10) | (20,000) | 0.3 | - | - |

Table 6.2. Subsoil materials and embankment properties adopted in the FEM parametric study.

| Spacing (m) | $E_{eq}$ (MPa) | Poisson's ratio | $k_v$ in clay $\times 10^{-4}$ (m/day) | $k_v$ in sand $\times 10^{-4}$ (m/day) |
|---|---|---|---|---|
| 0.915 (3 ft) | 875 | 0.15 | 3.2 | 7400 |
| 1.220 (4 ft) | 495 | 0.15 | 3.5 | 8000 |
| 1.525 (5 ft) | 319 | 0.15 | 3.6 | 8400 |
| 1.830 (6 ft) | 223 | 0.15 | 3.8 | 8700 |

(a)

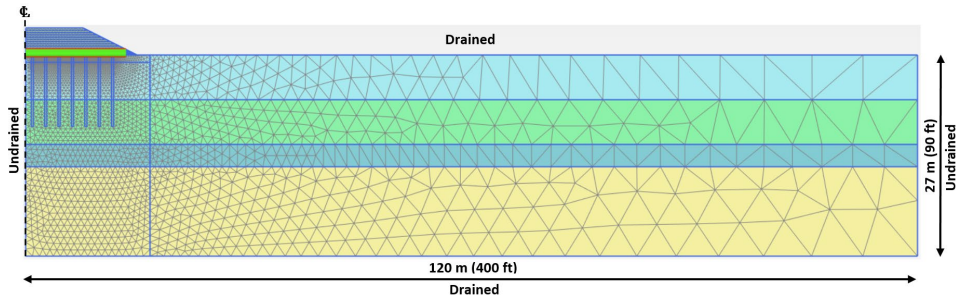


(b)

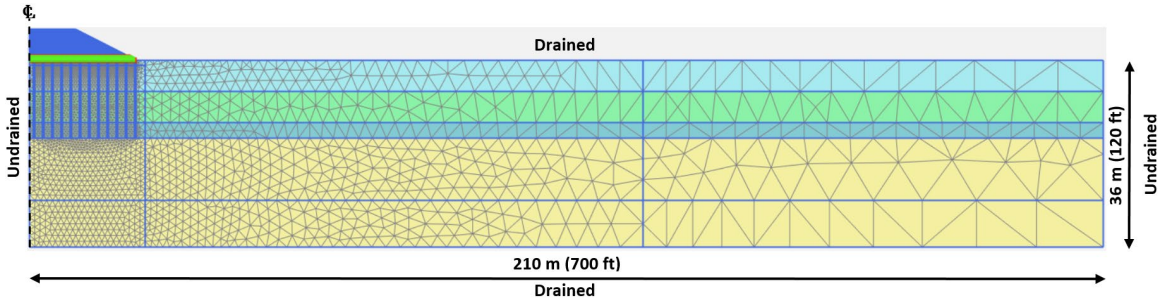


(c)

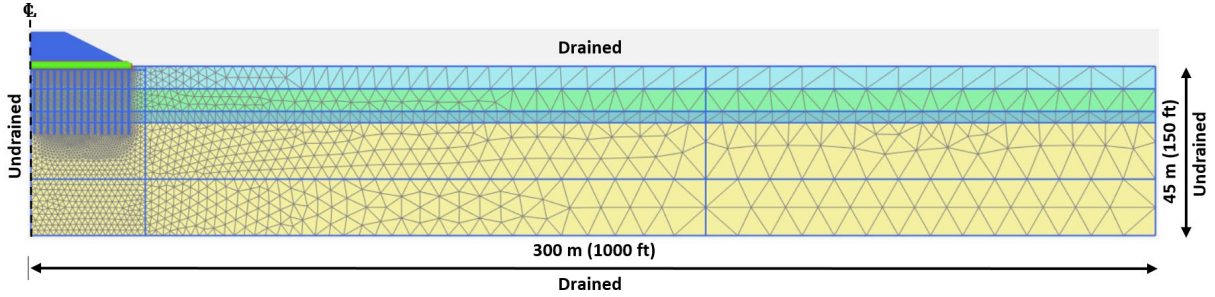


Figure 6.5. FEM mesh adopted in this study: (a) H= 3.05 m (10 ft); (b) H= 6.1 m (20 ft); (c) H= 9.15 m (30 ft).

### 6.4. Case (1) Soil Profile

This section discusses the FEM parametric study for the soil profile of Case 1 (Figure 6.1a). The proposed three embankment heights (3.05 m (10 ft), 6.1 m (20 ft), and 9.15 m (30 ft)) will be analyzed in terms of the required pile length design, GRLTP and piles' extent under the embankment slope, and performance of the system by changing the center-to-center pile spacing.

#### 6.4.1. Embankment Height (H)= 3.05 m (10 ft)

##### 6.4.1.1. Pile Design

Piles are designed to carry the whole embankment load plus the surcharge load for each corresponding pile spacing. Estimated factored loads are 77 kN, 137 kN, 214 kN, and 308 kN for 0.915 m (3 ft), 1.22 m (4 ft), 1.525 m (5 ft), and 1.83 m (6 ft) pile spacing, respectively. Table 6.3 shows the pile design information including the pile diameter (D) and pile length (L) for each corresponding pile spacing. Similar pile length is adopted for the "3-ft", "4-ft", and "5-ft" pile spacing as the minimum required timber pile length is 9.15 m (30 ft) which satisfies both the geotechnical capacity requirement and the minimum length requirement of this study.

Table 6.3. Pile Design for Case 1, H= 3.05 m (10 ft).

| Spacing | Pile Diameter (D) | Pile Length (L) |
|---|---|---|
| 0.915 m (3 ft) | 0.305 m (1 ft) | 9.15 m (30 ft) |
| 1.220 m (4 ft) | 0.305 m (1 ft) | 9.15 m (30 ft) |
| 1.525 m (5 ft) | 0.305 m (1 ft) | 9.15 m (30 ft) |
| 1.830 m (6 ft) | 0.305 m (1 ft) | 9.76 m (32 ft) |

##### 6.4.1.2. Stability Analysis

A stability analysis is conducted using PLAXIS 2D FEM software to investigate the stability of the system as well as investigating potential local and global failures with changing the GRLTP

and piles' extent under the slope. A case of 4D pile spacing, 1.22 m (4 ft), with 5 layers of GRLTP is considered a base case for the stability analysis. Meanwhile, the piles and GRLTP extent under the slope is varied as 0.0H, 0.5H, 1.0H, 1.5H, and 2.0H. Both soil conditions of normally consolidated (NC) soil and overconsolidated (OC) soil are investigated. Slope stability factor of safety is computed at the end of construction (EOC) and after 2 years of consolidation. It should be noted that the GRLTP edge will coincide with the exact computed distance, and the piles will be distributed on the computed distance (i.e., the distance between the GRLTP edge and the last pile edge will be governed by the pile spacing). Figure 6.6 through Figure 6.10 show the total displacement ($|u|$) observed in the embankment after two years of consolidation for cases of NC soil and OC soil with all proposed GRLTP and piles' extent.

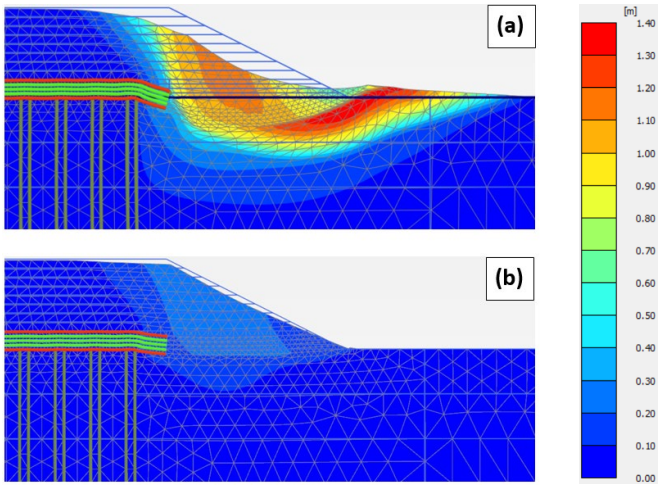


Figure 6.6. Total Displacement (m) after 2 years of consolidation for (a) NC soil; (b) OC soil for the case of 0.0H extension.

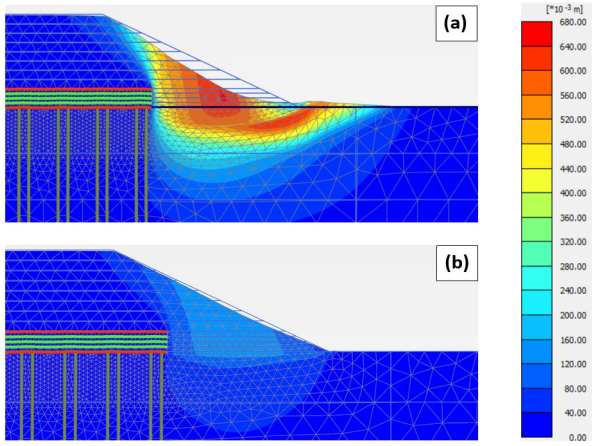


Figure 6.7. Total Displacement (m) after 2 years of consolidation for (a) NC soil; (b) OC soil for the case of 0.5H extension.

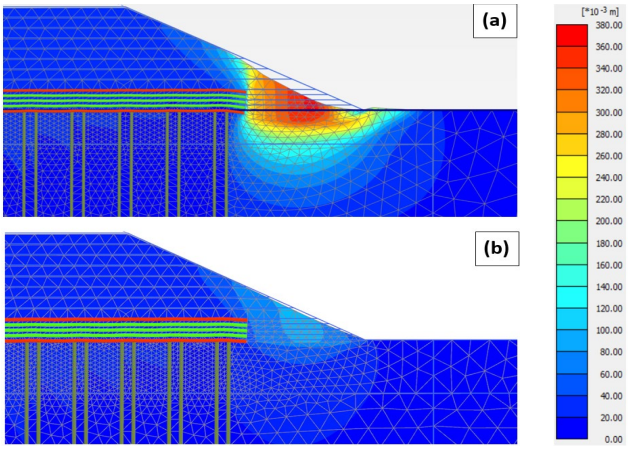


Figure 6.8. Total Displacement (m) after 2 years of consolidation for (a) NC soil; (b) OC soil for the case of 1.0H extension.

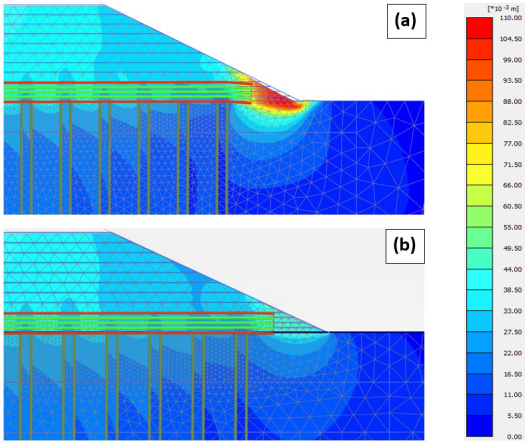


Figure 6.9. Total Displacement (m) after 2 years of consolidation for (a) NC soil; (b) OC soil for the case of 1.5H extension.

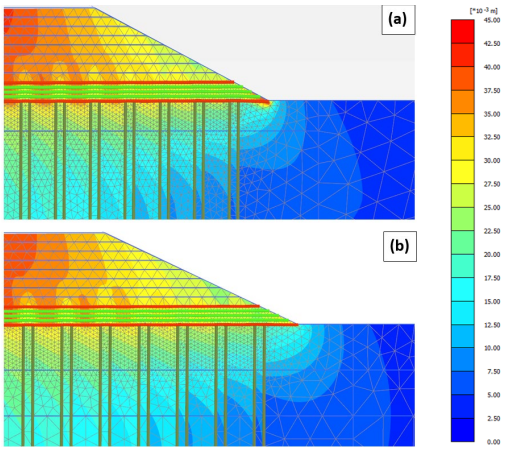


Figure 6.10. Total Displacement (m) after 2 years of consolidation for (a) NC soil; (b) OC soil for the case of 2.0H extension.

Figure 6.6 through Figure 6.10 are summarized in Figure 6.11, showing the maximum observed total displacement comparison between the NC and OC soils after 2 years of consolidation. The maximum total displacement observed in the slope decreases significantly with increasing the supported distance with GRLTP and piles under the slope. Results also show a significant difference between the NC and OC soil cases. For instance, the maximum total displacement for a GRLTP and piles' extent of 0.0H is 138 cm and 25 cm, respectively. Thus, a larger proportion of H is needed for the GRLTP and piles to be extended under the slope for the case of NC soil compared to the OC soil case. Furthermore, slope stability factor of safety is evaluated for the system at two different times: at the end of construction (EOC) representing short term analysis, and after 2 years of consolidation representing long term analysis. The foundation soil is expected to have the highest excess pore water pressure at the end of construction due to the embankment load resulting in minimum effective stress component at that time. In addition, the system needs to maintain stability requirements for the long term condition for a consolidation period of 2 years. Table 6.4 shows the slope stability factor of safety for NC and OC soil cases with changing the GRLTP and piles' extent under the embankment slope at two different times: at the end of construction (EOC) and after 2 years of consolidation. Results show that the slope is expected to

fail for the NC soil case with an extent of 0.0H, 0.5H, and 1.0H, whereas no slope failure is predicted for the OC soil case with all the GRLTP and piles' extent. Results also show that the factor of safety increases with time (from the EOC to after 2 years of consolidation) for cases where failure planes develop in the very soft clay layer. This is attributed to the shear strength gain with time due to the consolidation process. However, other cases where the slope failure plane is only initiated in the embankment material are expected to have close safety factors at the EOC and after 2 years of consolidation. This can be observed in the NC soil case with an extent of 2.0H, and the OC soil case with an extent of 1.5H and 2.0H. On one hand, slope stability analysis shows that the system is expected to fail when the GRLTP and piles are extended up to mid-slope (1.0H) for the NC soil case. However, an extent of 1.5H (three-quarters of the slope) and 2.0H (full length under the slope) for the NC would maintain the stability of the system with safety factors of more than 1.5 for the short-term and long-term analyses. On the other hand, the system would maintain stability if the GRLTP and piles are extended up to one-quarter of the slope (0.5H) with safety factors of more than 1.5 for the short-term and long-term analyses. Therefore, the extent of the GRLTP and the piles is chosen to be 1.5H (three-quarters of the slope) and 0.5H (one-quarter of the slope) for the cases of NC soil and OC soil, respectively. Figure 6.12 shows the failure planes for the NC and OC soil cases with an extent of 1.5H, and 0.5H, respectively. Accordingly, the required number of piles per row for the NC soil case is 30, 22, 18, and 15 for the 0.95 m, 1.22 m, 1.525 m, and 1.83 m pile spacing, respectively.

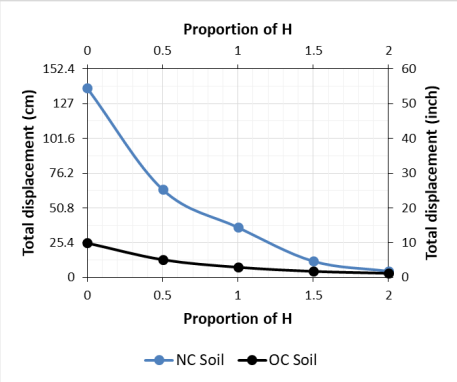


Figure 6.11. Maximum total displacement in the slope observed after 2 years of consolidation for the NC and OC soils.

Table 6.4. Factor of safety for different GRLTP and piles' extent at different times.

| Soil Condition | Proportion of H | End of construction (EOC) | After 2 years of consolidation |
|---|---|---|---|
| Normally Consolidated (NC) | 0.0H | Fails | |
| | 0.5H | Fails | |
| | 1.0H | Fails | |
| | 1.5H | 2.16 | 3.02 |
| | 2.0H | 3.25 | 3.26 |
| Overconsolidated (OC) | 0.0H | 1.21 | 1.88 |
| | 0.5H | 1.56 | 1.9 |
| | 1.0H | 2.39 | 2.65 |
| | 1.5H | 3.25 | 3.27 |
| | 2.0H | 3.18 | 3.19 |

### 6.4.1.3. Spacing Parametric Study

The performance of the system is investigated with changing the center-to-center pile spacing with the GRLTP and the piles extended up to three-quarters of the slope (1.5H). Further analysis will only be conducted on the NC soil case. Pile spacing will be ranged from 3D to 6D as follows: 0.915 m (3 ft), 1.22 m (4 ft), 1.525 m (5 ft), and 1.83 m (6 ft). The designed pile length for each

corresponding pile spacing, from the smallest to the largest, is 9.15 m (30 ft), 9.15 m (30 ft), 9.15 m (30 ft), and 9.76 m (32 ft).

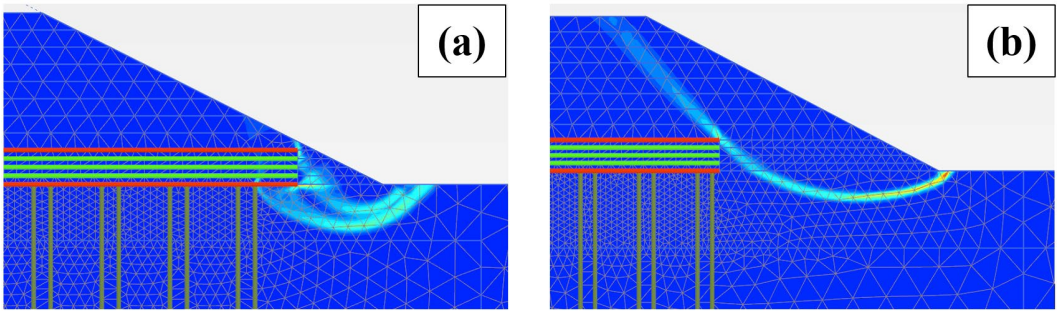


Figure 6.12. Failure planes after 2 years of consolidation for: (a) the NC soil case (1.5H extent); (b) the OC soil case (0.5H extent).

#### 6.4.1.3.1. Settlement

Figure 6.13 shows the settlement at the base of embankment after 2 years of consolidation for the pile spacing 0.915 m (3 ft), 1.22 m (4 ft), 1.525 m (5 ft), and 1.83 m (6 ft). The maximum observed settlement under the centerline of the embankment is 2.72 cm, 3.88 cm, 5.45 cm, and 7.64 cm for each corresponding spacing from the smallest to the largest. It can be observed that the settlement at the soft soil between the piles tends to increase with increasing the pile spacing. However, the unsupported zone under the slope experiences larger settlement than that of the supported area. This is attributed to the improvement of the system due to the existence of the GRLTP and the pile foundation. The maximum settlement observed under the unsupported zone is 8.26 cm, 11.43 cm, 10.16 cm, and 12.45 cm for each corresponding spacing from the smallest to the largest. Settlement in this area depends primarily on the distance of the last pile from the GRLTP edge, which coincides with a distance of three-quarters of the slope (1.5H). The distance between the edge of the GRLTP and the far edge of the last pile, $x$, is 0.305 m, 0.762 m, 0.61 m, and 0.762 m for each corresponding spacing from the smallest to the largest (Figure 6.14). This explains the larger settlement observed in the unsupported zone for the “4-ft” than the “5-ft” pile spacing. Figure 6.15

shows the settlement along the base of the embankment comparison for a "6-ft" pile spacing with 14 and 15 piles per row. Only one pile is added to the 14 pile model under the embankment centerline to result in 15 piles per row. It can be noted that the maximum settlement decreased significantly from 24.8 cm to 12.45 cm as the $x$ distance (Figure 6.14) is reduced from 1.68 m to 0.762 m. Thus, the 15 piles per row for the "6-ft" pile spacing was adopted in the analysis.

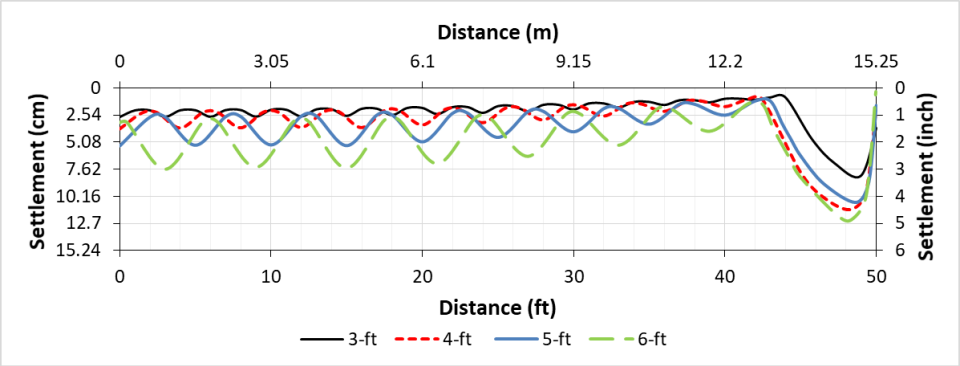


Figure 6.13. Settlement along the base of embankment after 2 years of consolidation for each pile spacing.

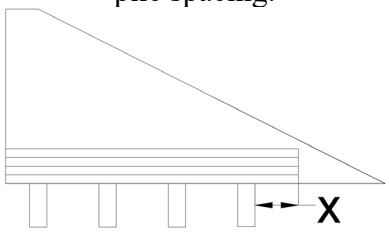


Figure 6.14. Distance, $x$, between the GRLTP edge and the far edge of the last pile.

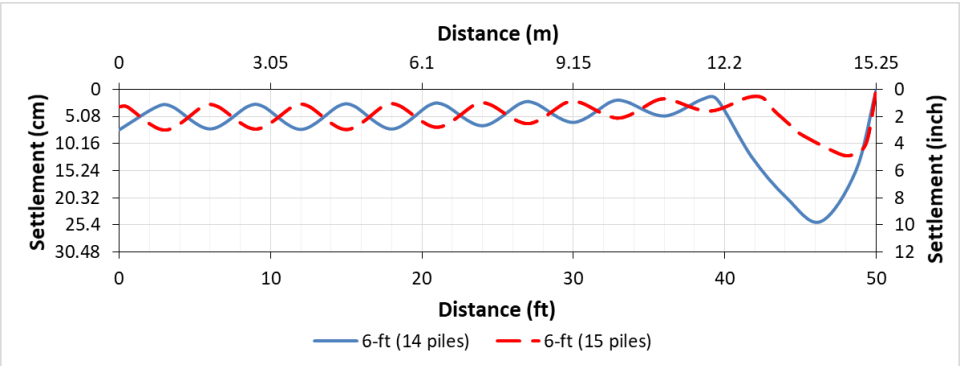


Figure 6.15. Settlement comparison between 14 and 15 piles per row for the "6-ft" pile spacing.

Figure 6.16 shows the settlement with time for each pile spacing at the soft soil between the piles under the embankment centerline, at the pile head under the embankment centerline, and at the location of the maximum settlement observed in the unsupported zone. Both Figure 6.16a and Figure 6.16b show a fast consolidation settlement rate compared to the unsupported zone (Figure 6.16c). This is attributed to the inclusion of the GRLTP and the pile foundation in which the settlement is improved, and a faster consolidation rate is achieved. In addition, the fast dissipation of excess pore water pressure is the cause of the high hydraulic conductivities of the sand layers existing under the very soft clay layer. This results in a double drainage boundary for the very soft clay layer, at the top and the bottom of the layer. For instance, 99% of the maximum settlement observed in the very soft clay layer is achieved after 40 days and 500 days from the project start for the supported zone and the unsupported zone, respectively.

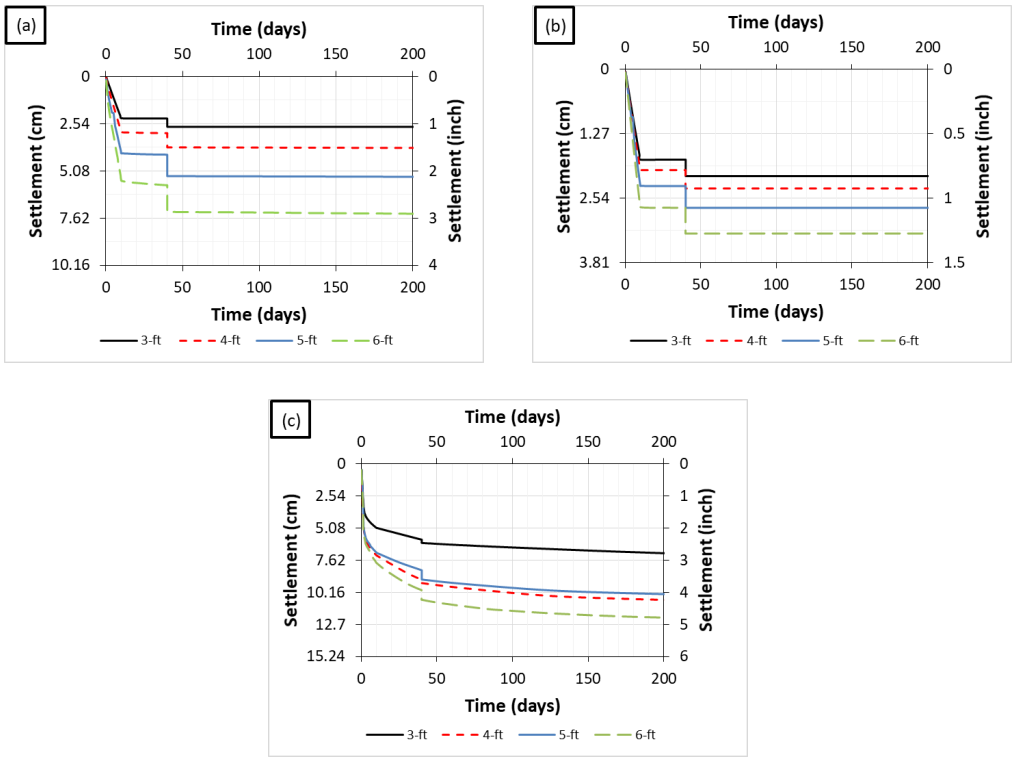


Figure 6.16. Settlement vs. time for each pile spacing at (a) the soft soil between the piles at the embankment centerline; (b) the pile head under the embankment centerline; (c) the maximum settlement in the unsupported area.

### 6.4.1.3.2. Excess Pore Water Pressure

Figure 6.17. shows the maximum excess pore water pressure induced due to embankment loading at two different locations: under the embankment centerline and under the unsupported area near the embankment toe at a depth of 0.5 m, and 1 m, respectively. These values are observed at the end of construction (EOC). Results show that the excess pore water pressure values increase with the pile spacing increase under the supported area (where the foundation soil is supported by piles and the GRLTP). In contrast, the excess pore water pressure in the unsupported area depends on the distance $x$ (Figure 6.14), in which the "4-ft" spacing is having a larger $x$ distance resulting in higher excess pore water pressure as discussed in the settlement section above. This confirms the larger settlement observed for the "4-ft" spacing than the "5-ft" spacing. Furthermore, it can be noted that the induced pore water pressure at the centerline of the embankment due to the stress increase is lower than that in the unsupported area. This is attributed to the existence of the GRLTP and the pile foundation.

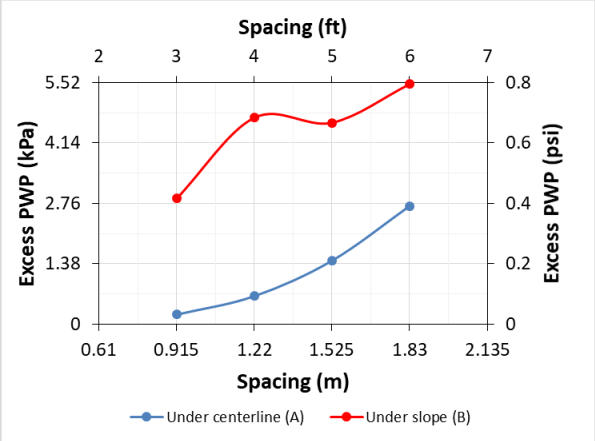


(a)

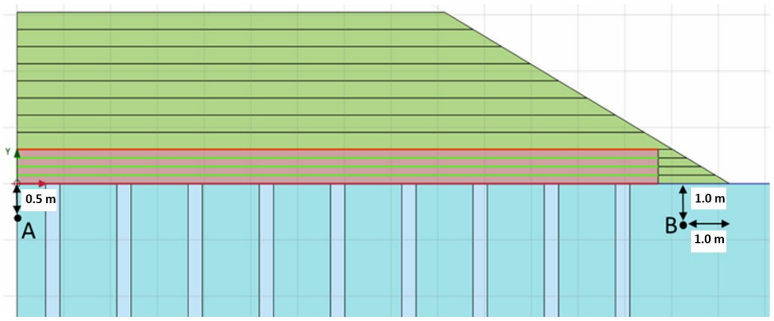


(b)

Figure 6.17. (a) Maximum excess pore water pressure at the end of construction observed under the centerline of the embankment (Point A), and the unsupported area (Point B); and (b) its location.

#### 6.4.1.3.3. Vertical Stress

Figure 6.18 shows vertical stress observed at the base of the embankment for the 1.83 m (6 ft) pile spacing at two different times: the end of construction (EOC), and after 2 years of consolidation. Results show higher vertical stress observed on the pile heads compared to the soft soil between piles. It can also be noted that vertical stress on top of piles is higher after 2 years of consolidation compared to vertical stresses observed at the EOC. Conversely, vertical stress on the soft soil between the piles is higher at the EOC than those after 2 years of consolidation. This is attributed to the arching effect as the load tends to be imposed on the rigid inclusions with the soil between the piles settling. This mechanism forms due to the shear resistance in the embankment material to resist movement downward. The stress concentration ratio (SCR) is found to be 12 and 53 at the EOC and after 2 years of consolidation. Pile-supported embankments with timber piles and a GRLTP are expected to have a SCR of 10 to 30 (Han and Wayne, 2000). This range was exceeded by the SCR value observed after 2 years of consolidation. This may be explained because the very soft clay layer underneath the embankment lost contact with the GRLTP for this embankment load resulting in very minimal stresses on the soft soil between the piles with almost all the embankment load carried by the piles.

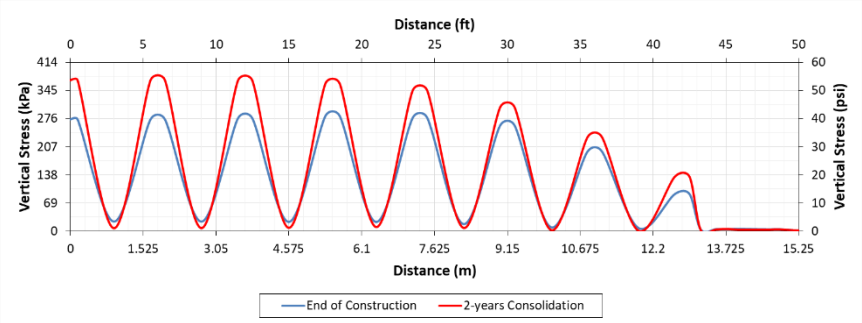


Figure 6.18. Vertical Stress along the base of the embankment at the end of construction (EOC) and after 2 years of consolidation.

### 6.4.1.3.4. Lateral Displacement

Figure 6.19 shows the lateral displacement profile along depth at the toe of the embankment after 2 years of consolidation. The maximum observed lateral displacement in all the pile spacing is in the very soft soil layer at the ground surface. Lateral displacement tends to become zero since the rest of the foundation soils are medium dense sand and dense sand layers with higher stiffness compared to the very soft clay layer. It can also be noted that the lateral displacement increased with increasing the pile spacing. Maximum observed lateral displacements are 10.16 mm, 15.24 mm, 17.78 mm, and 22.86 mm for the pile spacing from the smallest to the largest.

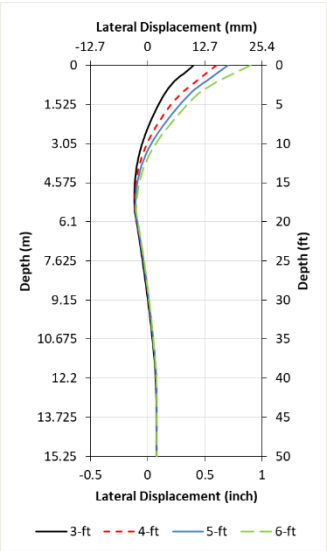


Figure 6.19. Lateral displacement profile along depth at the embankment toe after 2 years of consolidation.

### 6.4.1.3.5. Strain in Geosynthetics

Figure 6.20 shows the strain profile along the base of the embankment for the 1.83 m (6 ft) pile spacing after 2 years of consolidation for the 5 geosynthetic layers. Results show a peak-trough profile for all the geosynthetic layers. The peak is observed on top of the soft soil between the piles for the bottom geotextile layer (Haring et al., 2008), whereas the peak is found on top of the pile heads for the rest of the geosynthetic layers. This is attributed to the rigid support under the first geosynthetic layer in which the reinforcement layer is restrained from going downward with the embankment and GRLTP materials settling downward resulting in less deformation to the geosynthetic layer with minimal tension forces at these locations. However, the same geosynthetic layer would have a large curvature at the pile edge due to the lack of support at that location resulting in maximum strain at the pile edges (Shen et al., 2018), which is extended to be on top of the soft soil between the piles. This behavior is different from the rest of the geosynthetic layers as no rigid support restrains them from deformation with higher vertical stresses at the pile head due to the arching effect. Thus, maximum strain is expected to occur at the pile head. It can also be noted that the maximum strain percentage along each geosynthetic layer is observed under the embankment centerline where the maximum load exists. Figure 6.21 shows a closer look of the strain profile for the 1.83 m (6 ft) pile spacing in the 1$^{st}$ and 2$^{nd}$ geosynthetic layers.

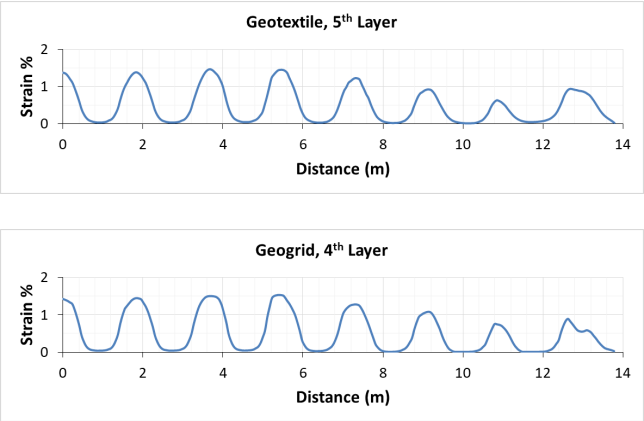

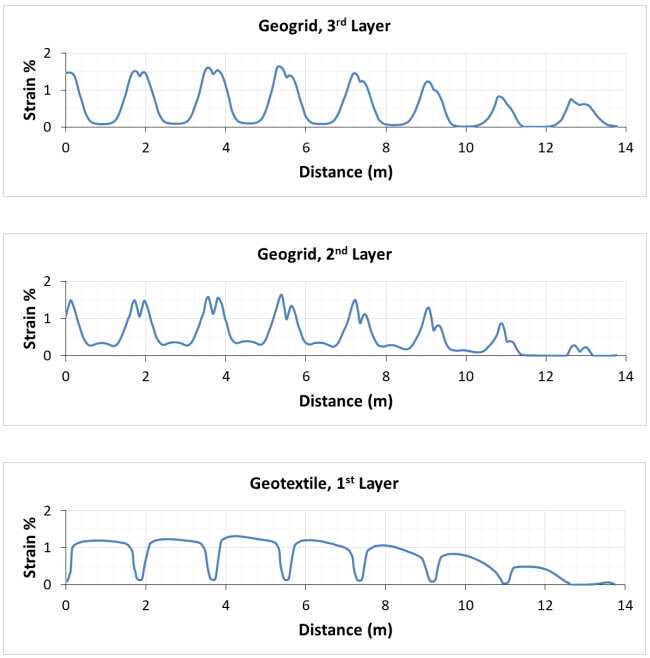


Figure 6.20. Strain profile along the base of embankment in the geosynthetic layers after 2 years of consolidation for the "6-ft" pile spacing.

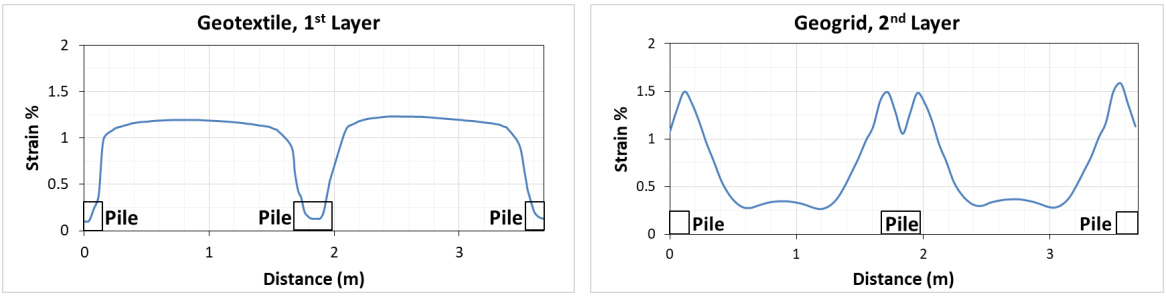


Figure 6.21. Closer look of the strain profile in the 1st and 2nd geosynthetic layers after 2 years of consolidation for the "6-ft" pile spacing.

Figure 6.22 shows the maximum strain observed in the geosynthetic layers after 2 years of consolidation for each pile spacing. All the layers have an almost linear relationship between the strain in each layer and the corresponding pile spacing. Moreover, maximum strain of 1.65% is computed in the 2nd geosynthetic layer for the 1.83 m (6 ft) pile spacing.

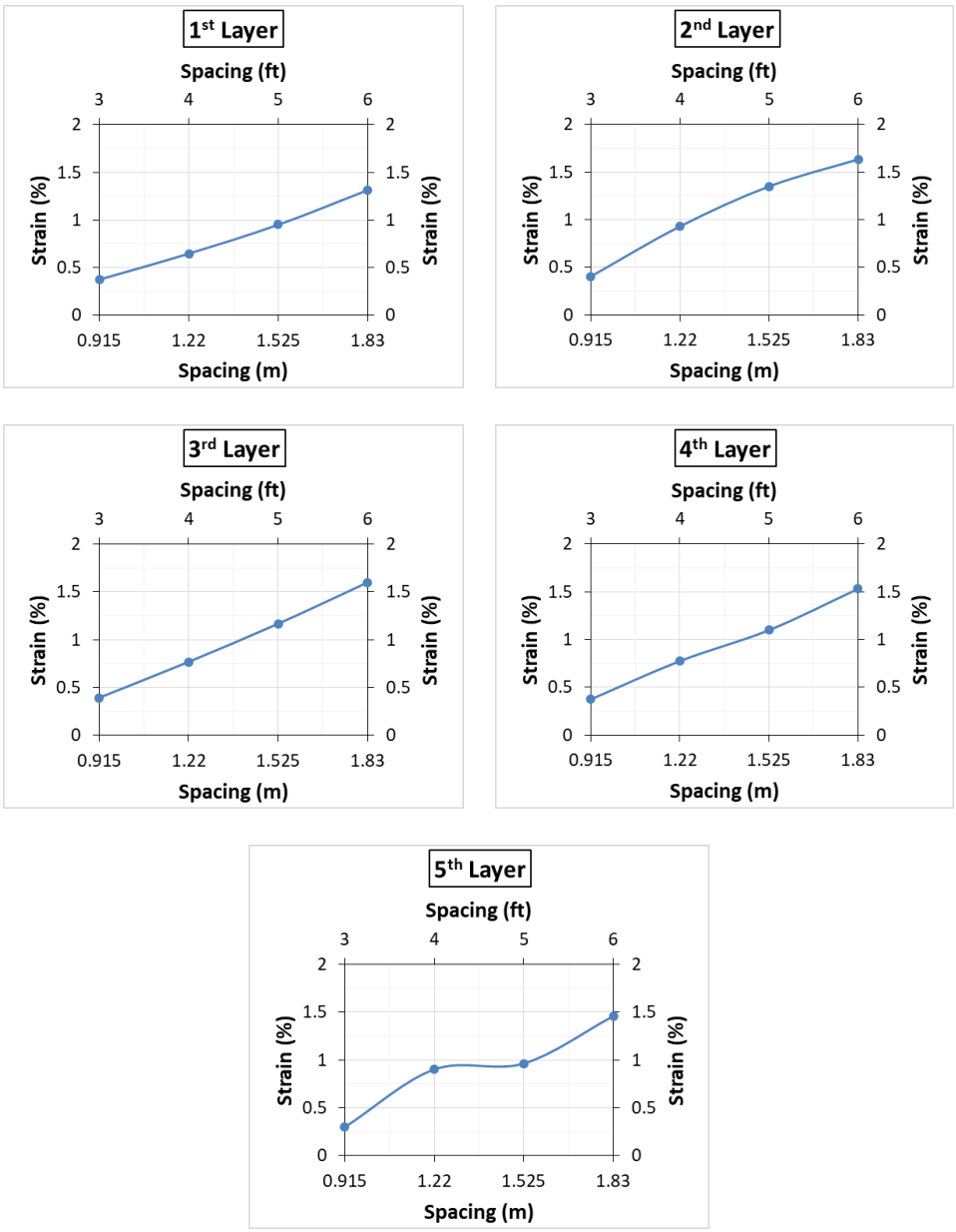


Figure 6.22. Maximum strain in geosynthetic layers for each pile spacing after 2 years of consolidation.

### 6.4.2. Embankment Height (H)= 6.10 m (20 ft)

#### 6.4.2.1. Pile Design

Piles are designed to carry the whole embankment load plus the surcharge load for each corresponding pile spacing. Estimated factored loads are 138 kN, 246 kN, 384 kN, and 552 kN for 0.915 m (3 ft), 1.22 m (4 ft), 1.525 m (5 ft), and 1.83 m (6 ft) pile spacing, respectively. Table 6.5

shows the pile design information including the pile diameter (D) and pile length (L) for each corresponding pile spacing. Similar pile length is adopted for the "3-ft", and "4-ft" pile spacing as the minimum required timber pile length is 9.15 m (30 ft) which satisfies both the geotechnical capacity requirement and the minimum length requirement of this study.

Table 6.5. Pile Design for Case 1, H= 6.1 m (20 ft).

| Spacing | Pile Diameter (D) | Pile Length (L) |
|---|---|---|
| 0.915 m (3 ft) | 0.305 m (1 ft) | 9.15 m (30 ft) |
| 1.220 m (4 ft) | 0.305 m (1 ft) | 9.15 m (30 ft) |
| 1.525 m (5 ft) | 0.305 m (1 ft) | 10.67 m (35 ft) |
| 1.830 m (6 ft) | 0.305 m (1 ft) | 15.25 m (50 ft) |

#### 6.4.2.2. Stability Analysis

A stability analysis is conducted to investigate the stability of the system as well as investigating potential local and global failures with changing the GRLTP and piles' extent under the slope. A case of 4D pile spacing, 1.22 m (4 ft), with 5 layers of GRLTP is considered as a base case for the stability analysis. Meanwhile, the piles and GRLTP extent under the slope is varied as 0.5H, 1.0H, 1.5H, and 2.0H. The case of 0.0H is excluded as the system fails in both the NC and OC soil cases. In addition, the system fails for cases of 0.5H and 1.0H for the NC soil case but they are included here for the purpose of comparison with the OC soil case. Slope stability factor of safety is computed at the end of construction (EOC) and after 2 years of consolidation. It should be noted that the GRLTP edge will coincide with the exact computed distance, and the piles will be distributed on the computed distance (i.e., the distance between the GRLTP edge and the last pile edge will be governed by the pile spacing). Figure 6.23 through Figure 6.26 show the total

displacement ($|u|$) observed in the embankment after two years of consolidation for cases of NC soil and OC soil.

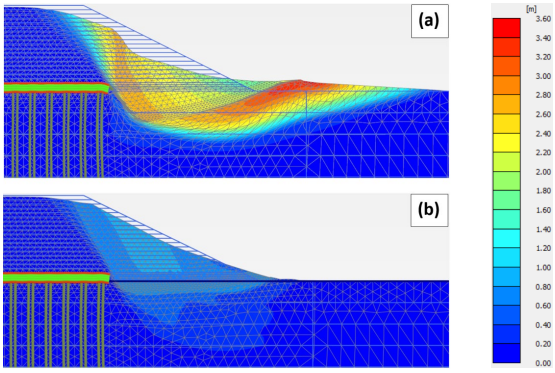


Figure 6.23. Total Displacement (m) after 2 years of consolidation for (a) NC soil; (b) OC soil for the case of 0.5H extension.

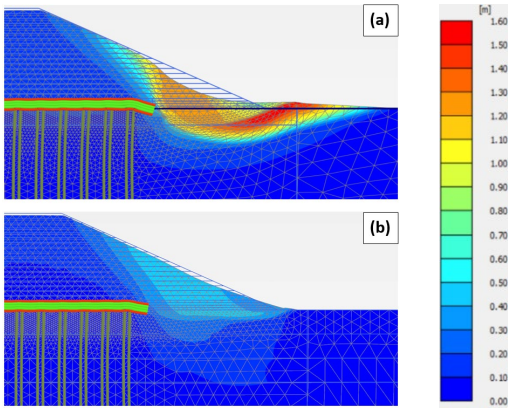


Figure 6.24. Total Displacement (m) after 2 years of consolidation for (a) NC soil; (b) OC soil for the case of 1.0H extension.

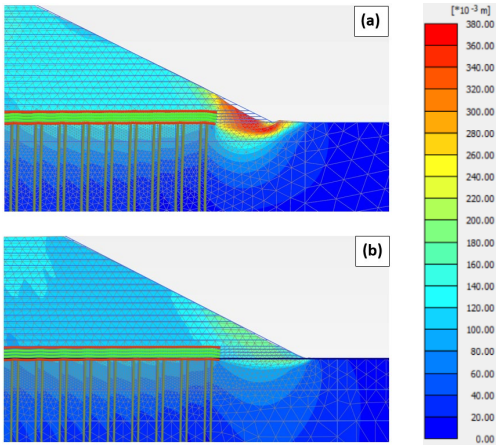


Figure 6.25. Total Displacement (m) after 2 years of consolidation for (a) NC soil; (b) OC soil for the case of 1.5H extension.

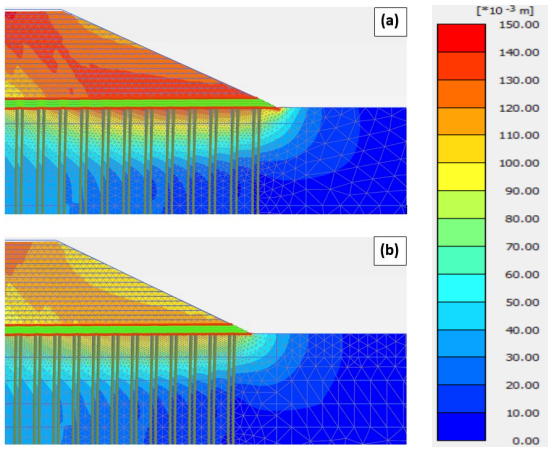


Figure 6.26. Total Displacement (m) after 2 years of consolidation for (a) NC soil; (b) OC soil for the case of 2.0H extension.

Figure 6.23 through Figure 6.26 are summarized in Figure 6.27, showing the maximum observed total displacement comparison between the NC and OC soils after 2 years of consolidation. The maximum total displacement observed in the slope decreases significantly with increasing the supported distance with GRLTP and piles under the slope. Results also show a significant difference between the NC and OC soil cases especially at small proportions of H. Total displacements tend to be so close at larger proportion of H such as 2.0H. For instance, the maximum total displacement for a GRLTP and piles' extent of 0.5H is 348 cm and 85 cm, respectively, whereas the maximum total displacement for a GRLTP and piles' extent of 2.0H is 15 cm and 11 cm for the same order. Thus, larger proportion of H is needed for the GRLTP and piles to be extended under the slope for the case of NC soil compared to the OC soil case. Furthermore, slope stability factor of safety is evaluated for the system at two different times: at the end of construction (EOC) representing short term analysis, and after 2 years of consolidation representing long term analysis. Table 6.6 shows the slope stability factor of safety for NC and OC soil cases with changing the GRLTP and piles' extent under the embankment slope at two different times: at the end of construction (EOC) and after 2 years of consolidation. Results show that the slope is expected to fail for the NC soil case with an extent of 0.0H, 0.5H, and 1.0H, whereas slope

failure is predicted for the OC soil case with 0.0H and 0.5H extent. Results also show that the factor of safety increases with time (from the EOC to after 2 years of consolidation) for cases where failure planes develop in the very soft clay layer such as the 1.5H for the NC soil case, and the 1.0H, 1.5H of the OC soil case. This is attributed to the shear strength gain with time due to the consolidation process. However, other cases where the slope failure plane is only initiated in the embankment material are expected to have close safety factors at the EOC and after 2 years of consolidation. This can be observed in both the NC and OC soil cases with an extent of 2.0H. On one hand, an extent of 2.0H (full length up to the embankment toe) for the NC soil case would maintain stability of the system with safety factors of more than 1.5 for the short-term and long-term analyses. On the other hand, the system would maintain stability on the short and long term if the GRLTP and piles are extended up to three-quarters of the slope (1.5H) with safety factors of more than 1.5. Therefore, the extent of the GRLTP and the piles is chosen to be 2.0H and 1.5H for the cases of NC soil and OC soil, respectively. Figure 6.28 shows the failure planes for the NC and OC soil cases with an extent of 2.0H, and 1.5H, respectively. Accordingly, the required number of piles per row for the NC soil case is 46, 34, 28, and 24 for the 0.915 m, 1.22 m, 1.525 m, and 1.83 m pile spacing, respectively.

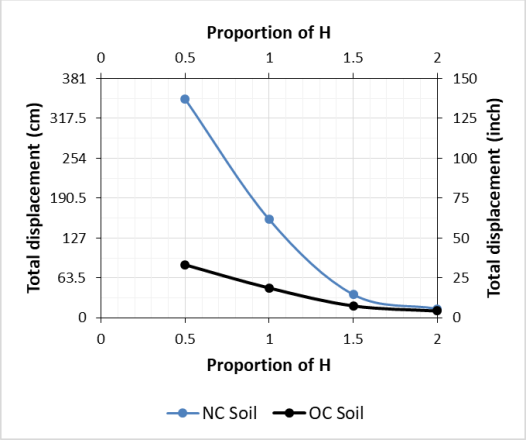


Figure 6.27. Maximum total displacement in the slope observed after 2 years of consolidation for the NC and OC soils.

Table 6.6. Factor of safety for different GRLTP and piles' extent at different times.

| Soil Condition | Proportion of H | End of construction (EOC) | After 2 years of consolidation |
|---|---|---|---|
| Normally Consolidated (NC) | 0.5H | Fails | |
| | 1.0H | Fails | |
| | 1.5H | 1.01 | 1.81 |
| | 2.0H | 2.21 | 2.26 |
| Overconsolidated (OC) | 0.5H | Fails | |
| | 1.0H | 1.07 | 1.38 |
| | 1.5H | 1.83 | 2.03 |
| | 2.0H | 2.20 | 2.23 |

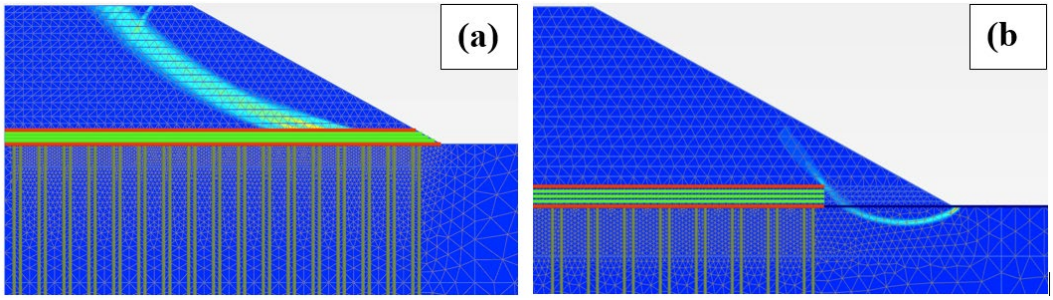


Figure 6.28. Failure planes after 2 years of consolidation for (a) the NC soil case (2.0H extent); (b) the OC soil case (1.5H extent).

### 6.4.2.3. Spacing Parametric Study

The performance of the system is investigated with changing the center-to-center pile spacing with the GRLTP and the piles extended up to the toe of the embankment (2.0H extent). Further analysis will only be conducted on the NC soil case. Pile spacing will be ranged from 3D to 6D as follows: 0.915 m (3 ft), 1.22 m (4 ft), 1.525 m (5 ft), and 1.83 m (6 ft). The designed pile length for each corresponding pile spacing, from the smallest to the largest, is 9.15 m (30 ft), 9.15 m (30 ft), 10.76 m (35 ft), and 15.25m (50 ft).

#### 6.4.2.3.1. Settlement

Figure 6.29 shows the settlement at the base of the embankment after 2 years of consolidation for the pile spacing 0.915 m (3 ft), 1.22 m (4 ft), 1.525 m (5 ft), and 1.83 m (6 ft). The maximum observed settlement under the centerline of the embankment is 5.30 cm, 7.80 cm, 9.90 cm, and 14.15 cm for each corresponding spacing from the smallest to the largest. It can be observed that with increasing the pile length, the settlement at the soft soil between the piles tends to increase as observed in the lower embankment height (H) of 3.05 (10 ft). There was no difference in behavior since all the piles in each pile spacing model were tipping on a dense sand layer. Figure 6.30 shows the settlement with time for each pile spacing at the soft soil between the piles under the embankment centerline, and at the pile head under the embankment centerline. Both Figure 6.30a and Figure 6.30b show a fast consolidation settlement rate due to the inclusion of the GRLTP and the pile foundation in which the settlement is improved, and a faster consolidation rate is achieved. This is also attributed to the high hydraulic conductivities of the sand layers existing under the very soft clay layer. This results in a double drainage boundary for the very soft clay layer, at the top and the bottom of the layer. For instance, 99% of the maximum settlement observed in the very soft clay layer is achieved after 50 days.

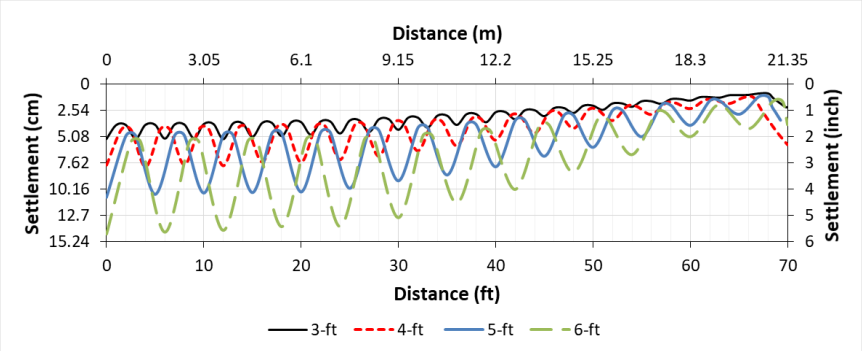


Figure 6.29. Settlement along the base of embankment after 2 years of consolidation for each pile spacing.

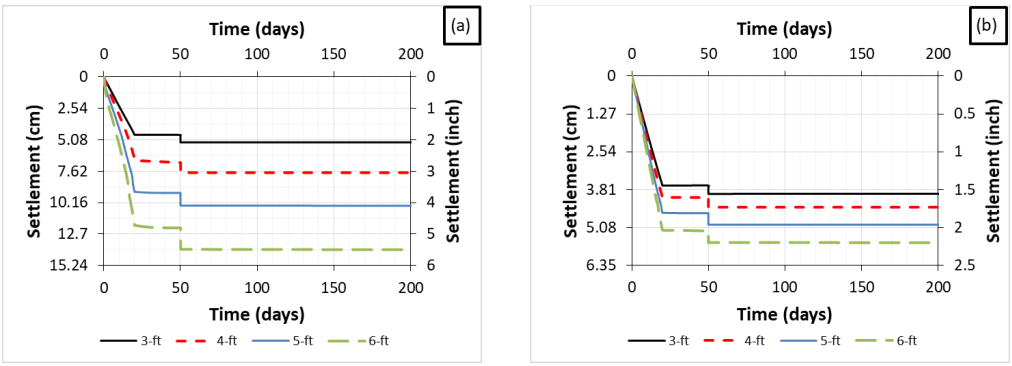


Figure 6.30. Settlement vs. time for each pile spacing at (a) the soft soil between the piles at the embankment centerline; (b) the pile head under the embankment centerline.

### 6.4.2.3.2. Excess Pore Water Pressure

Figure 6.31 shows the maximum excess pore water pressure developed due to embankment loading at two different locations: under the embankment centerline and under the embankment toe at depths of 0.5 m, and 1.5 m, respectively. These values are observed at the end of construction (EOC). Results show that the excess pore water pressure values increase with the pile spacing increase under the centerline of the embankment and under the embankment toe. The higher induced excess pore water pressure value may be due to the loading of the soil from the lateral movement of the piles near the toe.

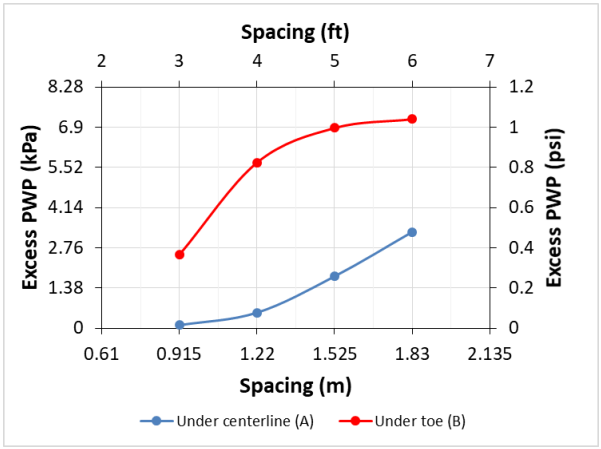


(a)

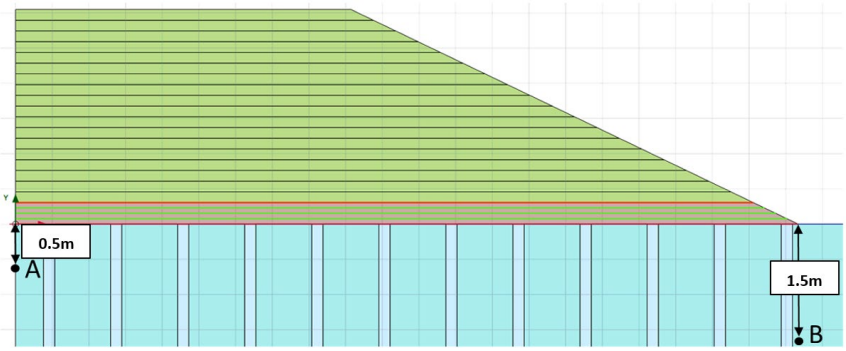


(b)

Figure 6.31. (a) Maximum excess pore water pressure at the end of construction observed under the centerline of the embankment (Point A), and under the embankment toe (Point B); and (b) its location.

#### 6.4.2.3.3. Vertical Stress

Figure 6.32 shows vertical stress observed at the base of the embankment for the 1.83 m (6 ft) pile spacing at two different times: the end of construction (EOC), and after 2 years of consolidation. Higher vertical stress is observed on top of piles compared to the soft soil between piles. It can also be noted that vertical stress on top of piles are higher after 2 years of consolidation compared to vertical stresses observed at the EOC. Conversely, vertical stresses on the soft soil between the piles is higher at the EOC than those after 2 years of consolidation. This is attributed to the arching effect in which vertical stresses are transferred to pile heads leaving the soil with less imposed loads. The stress concentration ratio (SCR) is found to be 20 and 36 at the EOC and after 2 years of consolidation, which almost fall between the range of 10 to 30 reported by Han and Wayne (2000). Compared to H= 3.05 m (10 ft) in which the SCR is 12 and 53, the SCR values are closer to each other implying a faster consolidation settlement occurred for H= 6.1 m (20 ft).

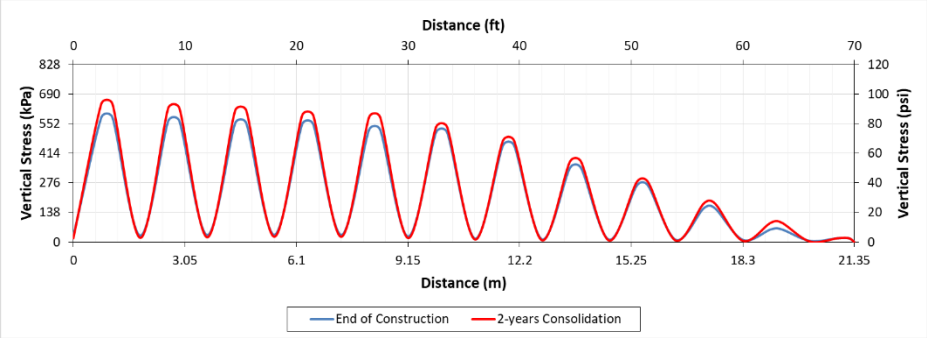


Figure 6.32. Vertical Stress along the base of the embankment at the end of construction (EOC) and after 2 years of consolidation.

### 6.4.2.3.4. Lateral Displacement

Figure 6.32 shows the lateral displacement profile along depth at the toe of the embankment after 2 years of consolidation. The maximum observed lateral displacement in all the pile spacing is in the very soft soil layer at the ground surface. Lateral displacement tends to become zero at deeper depths where medium and dense sand layers exist. It can also be noted that the lateral displacement increased as the pile spacing is increased. Maximum observed lateral displacements are 32.51 mm, 73.91 mm, 121.92 mm, and 153.01 mm for the pile spacing from the smallest to the largest. Higher lateral displacement is observed for the H= 6.1 m (20 ft) compared to H= 3.05 m (10 ft) as the lateral thrust at the edges of the embankment increases by a factor of almost 3.5 from the increase of embankment loading.

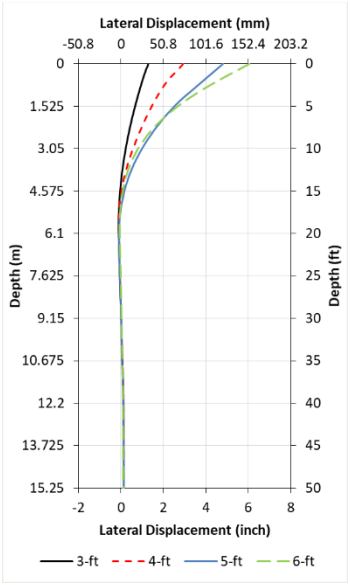


Figure 6.32. Lateral displacement profile along depth at the embankment toe after 2 years of consolidation.

### 6.4.2.3.5. Strain in Geosynthetics

Figure 6.33 shows the strain profile along the base of the embankment for the 1.83 m (6 ft) pile spacing after 2 years of consolidation for the 5 geosynthetic layers. Results confirm the peak-trough profile for all the geosynthetic layers as observed before. The peak is observed on top of the soft soil between the piles for the bottom geotextile layer (1$^{st}$ layer), whereas the peak is found on top of the pile heads for the rest of the geosynthetic layers. It can also be noted that the maximum strain percentage along each geosynthetic layer is observed almost under the centerline where the maximum load exists. Figure 6.34 shows a closer look of the strain profile for the 1.83 m (6 ft) pile spacing in the 1$^{st}$ and 2$^{nd}$ geosynthetic layers.

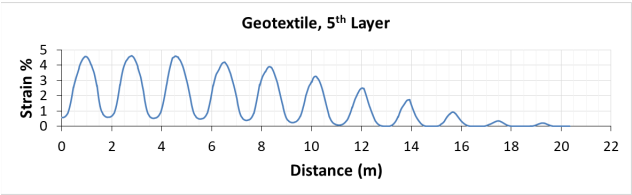

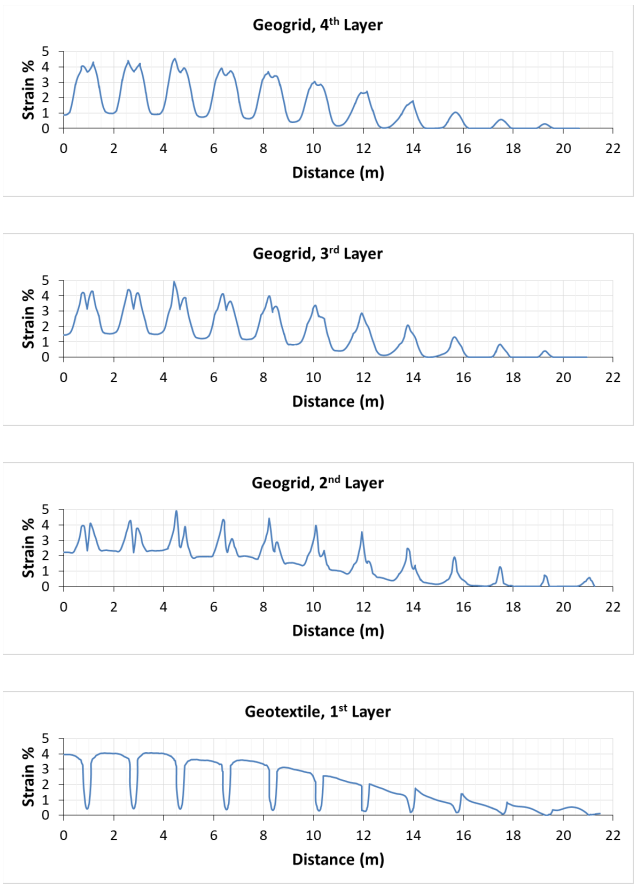


Figure 6.33. Strain profile along the base of embankment in the geosynthetic layers after 2 years of consolidation for the "6-ft" pile spacing.

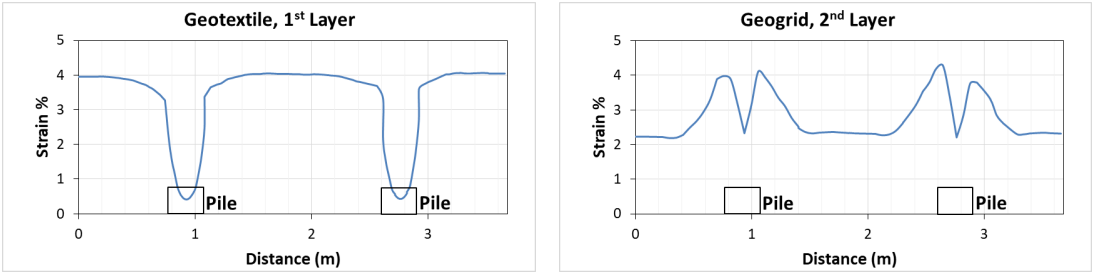


Figure 6.34. Closer look of the strain profile in the 1st and 2nd geosynthetic layers after 2 years of consolidation for the "6-ft" pile spacing.

Figure 6.35 shows the maximum strain observed in the geosynthetic layers after 2 years of consolidation for each pile spacing. All the layers have an almost linear relationship between the strain in each layer and the corresponding pile spacing. Moreover, maximum observed strain is computed in the 2nd and 3rd geosynthetic layers for the 1.83 m (6 ft) pile spacing which almost 5%.

It can also be noted that the strain values for each pile spacing are increased from H=3.05 m (10 ft) to H= 6.1 m (20 ft) until they almost reached the maximum allowable value which is 5%.

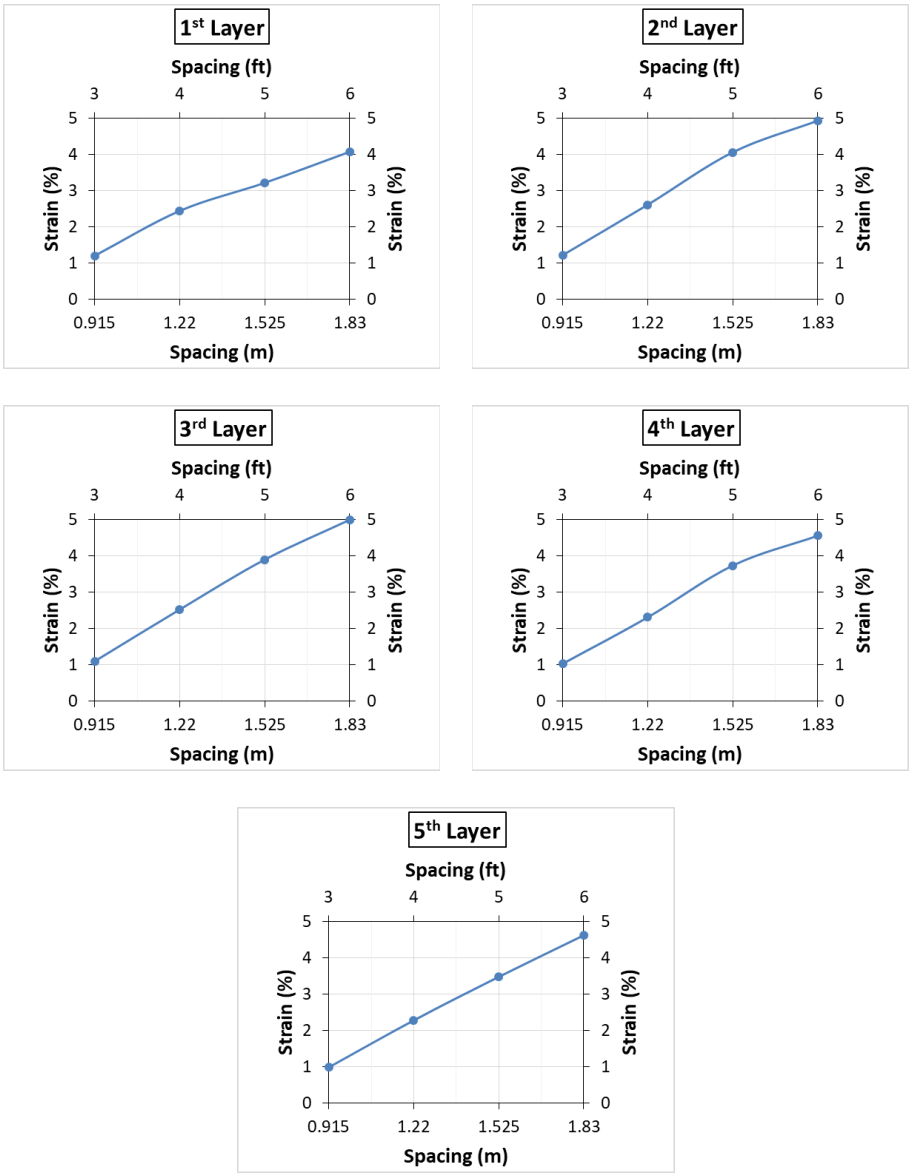


Figure 6.35. Maximum strain in geosynthetic layers for each pile spacing after 2 years of consolidation.

### 6.4.3. Embankment Height (H)= 9.15 m (30 ft)

#### 6.4.3.1. Pile Design

Piles are designed to carry the whole embankment load plus the surcharge load for each corresponding pile spacing. Estimated factored loads are 196 kN, 348 kN, 543 kN, and 782 kN for

0.915 m (3 ft), 1.22 m (4 ft), 1.525 m (5 ft), and 1.83 m (6 ft) pile spacing, respectively. Table 6.7 shows the pile design information including the pile diameter (D) and pile length (L) for each corresponding pile spacing. The pile lengths ranged from the minimum required pile length (9.15 m) to the maximum required pile length (18.3 m) for the highest embankment load (H= 9.15 m).

Table 6.7. Pile Design for Case 1, H= 9.15 m (30 ft).

| Spacing | Pile Diameter (D) | Pile Length (L) |
|---|---|---|
| 0.915 m (3 ft) | 0.305 m (1 ft) | 9.15 m (30 ft) |
| 1.220 m (4 ft) | 0.305 m (1 ft) | 10.67 m (35 ft) |
| 1.525 m (5 ft) | 0.305 m (1 ft) | 15.25 m (50 ft) |
| 1.830 m (6 ft) | 0.305 m (1 ft) | 18.30 m (60 ft) |

#### 6.4.3.2. Stability Analysis

A case of 4D pile spacing, 1.22 m (4 ft), with 5 layers of GRLTP is considered a base case for the stability analysis. Meanwhile, the piles and GRLTP extent under the slope is varied as 1.5H and 2.0H. Cases of 0.0H, 0.5H, and 1.0H did not meet the stability requirements for both NC and OC soil cases for the intermediate embankment load (H= 6.1 m). Thus, they were excluded from the analysis. The NC soil case with an extent of 1.5H is only included for comparison purposes with the OC soil case. Slope stability factor of safety is computed at the end of construction (EOC) and after 2 years of consolidation. It should be noted that the GRLTP edge will coincide with the exact computed distance, and the piles will be distributed on the computed distance (i.e., the distance between the GRLTP edge and the last pile edge will be governed by the pile spacing). Figure 6.36 and Figure 6.37 show the total displacement ($|u|$) observed in the embankment after two years of consolidation for cases of NC soil and OC soil for 1.5H and 2.0H GRLTP and piles' extent, respectively.

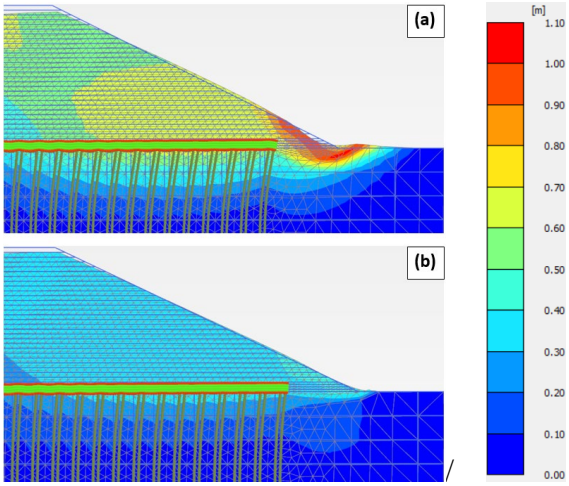


Figure 6.36. Total Displacement (m) after 2 years of consolidation for (a) NC soil; (b) OC soil for the case of 1.5H extension.

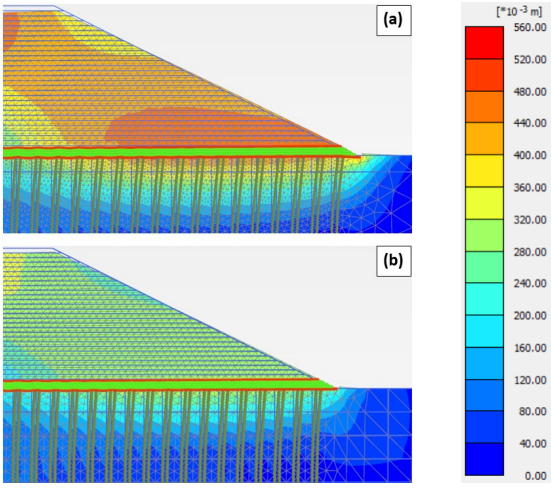


Figure 6.37. Total Displacement (m) after 2 years of consolidation for (a) NC soil; (b) OC soil for the case of 2.0H extension.

Figure 6.36 and Figure 6.37 are summarized in Figure 6.38, showing the maximum observed total displacement comparison between the NC and OC soils after 2 years of consolidation. The maximum total displacement observed in the slope decreases significantly with increasing the supported distance with GRLTP and piles under the slope especially for the NC case. Furthermore, results show a significant difference between the NC and OC soil cases for the 1.5H extent, whereas this difference is reduced at 2.0H extent. For instance, the maximum total displacement

for a GRLTP and piles' extent of 1.5H is 105 cm and 47 cm for the NC and soil cases, respectively, while the maximum total displacement for a GRLTP and piles' extent of 2.0H is 46 cm and 32 cm for the same order. Therefore, larger proportion of H is needed for the GRLTP and piles to be extended under the slope for the case of NC soil compared to the OC soil case. Moreover, slope stability factor of safety is evaluated for the system at two different times: at the end of construction (EOC) representing short term analysis, and after 2 years of consolidation representing long term analysis. Table 6.8 shows the slope stability factor of safety for NC and OC soil cases with changing the GRLTP and piles' extent under the embankment slope at two different times: at the end of construction (EOC) and after 2 years of consolidation with 1.5H and 2.0H extent. Results show that the slope is expected to fail for the NC soil case with an extent of 0.0H, 0.5H, 1.0H, and 1.5H, whereas slope failure is predicted for the OC soil case with 0.0H, 0.5H, and 1.0H extent. Results also show that the factor of safety increases with time (from the EOC to after 2 years of consolidation) for cases where failure planes develop in the very soft clay layer such as the 1.5H for the OC soil case. This is attributed to the shear strength gain with time due to the consolidation process. However, other cases where the slope failure plane is only initiated in the embankment material are expected to have close safety factors at the EOC and after 2 years of consolidation. This can be observed in both the NC and OC soil cases with an extent of 2.0H. On one hand, an extent of 2.0H (full length up to the embankment toe) for the NC soil case would maintain stability of the system with safety factors of more than 1.5 for the short-term and long-term analyses. On the other hand, the system would maintain stability on the short and long term if the GRLTP and piles are extended up to three-quarters of the slope (1.5H) with safety factors of more than 1.5. Therefore, the extent of the GRLTP and the piles is chosen to be 2.0H and 1.5H for the cases of NC soil and OC soil, respectively. Figure 6.39 shows the failure planes for the NC and OC soil

cases with an extent of 2.0H, and 1.5H, respectively. Accordingly, the required number of piles per row for the NC soil case is 60, 44, 36, and 30 for the 0.915 m, 1.22 m, 1.525 m, and 1.83 m pile spacing, respectively.

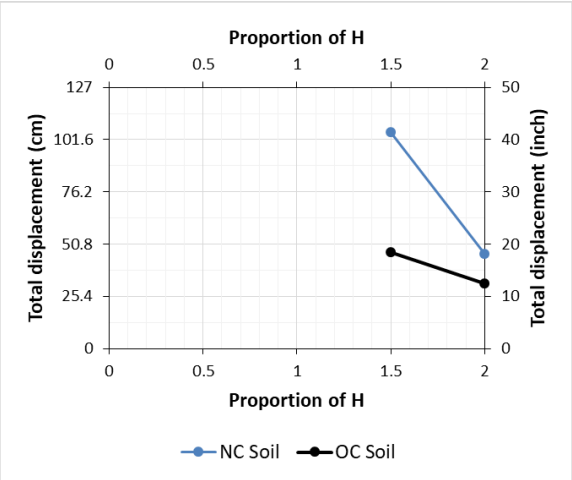


Figure 6.38. Maximum total displacement in the slope observed after 2 years of consolidation for the NC and OC soils.

Table 6.8. Factor of safety for different GRLTP and piles' extent at different times.

| Soil Condition | Proportion of H | End of construction (EOC) | After 2 years of consolidation |
|---|---|---|---|
| Normally Consolidated (NC) | 1.5H | Fails | |
| | 2.0H | 1.91 | 1.92 |
| Overconsolidated (OC) | 1.5H | 1.88 | 1.92 |
| | 2.0H | 1.92 | 1.93 |

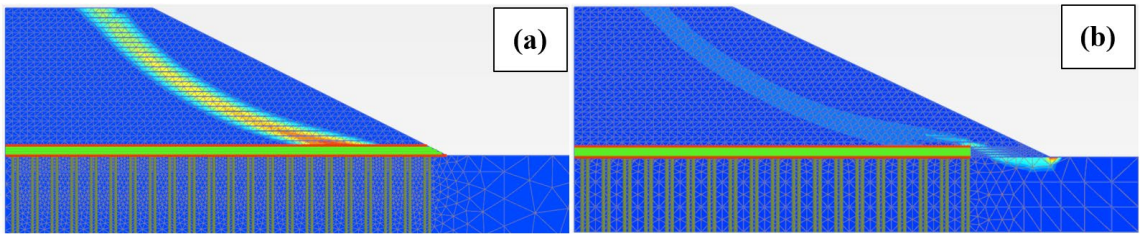


Figure 6.39. Failure planes after 2 years of consolidation for (a) the NC soil case (2.0H extent); (b) the OC soil case (1.5H extent).

#### 6.4.3.3. Spacing Parametric Study

The performance of the system is investigated with changing the center-to-center pile spacing with the GRLTP and the piles extended up to the toe of the embankment (2.0H extent). Further analysis will only be conducted on the NC soil case. Pile spacing will be ranged from 3D to 6D as follows: 0.915 m (3 ft), 1.22 m (4 ft), 1.525 m (5 ft), and 1.83 m (6 ft). The designed pile length for each corresponding pile spacing, from the smallest to the largest, is 9.15 m (30 ft), 10.67 m (35 ft), 15.25 m (50 ft), and 18.30 m (60 ft).

##### 6.4.3.3.1. Settlement

Figure 6.40 shows the settlement at the base of the embankment after 2 years of consolidation for the pile spacing 0.915 m (3 ft), 1.22 m (4 ft), 1.525 m (5 ft), and 1.83 m (6 ft). Maximum settlement is observed under the embankment centerline, where exists the maximum load, for the 0.915 (3 ft) and 1.22 (4 ft) pile spacing which is 12.0 cm and 15.3 cm, respectively. In contrast, the maximum settlement for the 1.525 (5 ft) and 1.83 m (6 ft) is 25.5 cm and 26.2 cm, respectively. In both cases, this settlement is observed at the soft soil between piles near the centerline at the 5$^{th}$ space between piles. The settlement for these pile spacing increased from the embankment centerline up to the 5$^{th}$ space between piles and then started to decrease up to the embankment toe with decreasing the load. This may be attributed to the excessive lateral displacement experienced by the piles due to the very high embankment load with these pile spacing in which the piles are not completely straight underneath the embankment. Consequently, the ability of the piles to resist vertical loads is reduced resulting in higher settlement with the direction to the right up to the point that the settlement starts to decrease along with the decreasing embankment load. It can also be noted that the settlement increases with increasing pile spacing the same as observed for the lower two embankment heights. Figure 6.41 shows the settlement with time for each pile spacing at the soft

soil between the piles under the embankment centerline, and at the pile head under the embankment centerline. The settlement increased with time with the embankment construction which ends at 30 days. This is followed by a consolidation period of 30 days in which no significant settlement has occurred which means that almost all the settlement occurs with the embankment construction for this soil profile. This fast consolidation settlement is attributed to the use of the pile-supported system utilizing a GRLTP within it. Also, the double drainage condition for the very soft clay layer plays a role in the fast consolidation settlement observed. For instance, an increase in the settlement at the soft soil between the piles of only 2.3% is observed between the settlement at the end of construction (EOC) and the settlement at 60 days (after 30 days of consolidation) for the 1.83m (6 ft) pile spacing. Then, the settlement increased by 22% before and after applying the surcharge load. This is followed by an increase of only 0.4% in the settlement between the time after applying the surcharge load and the end of the consolidation period.

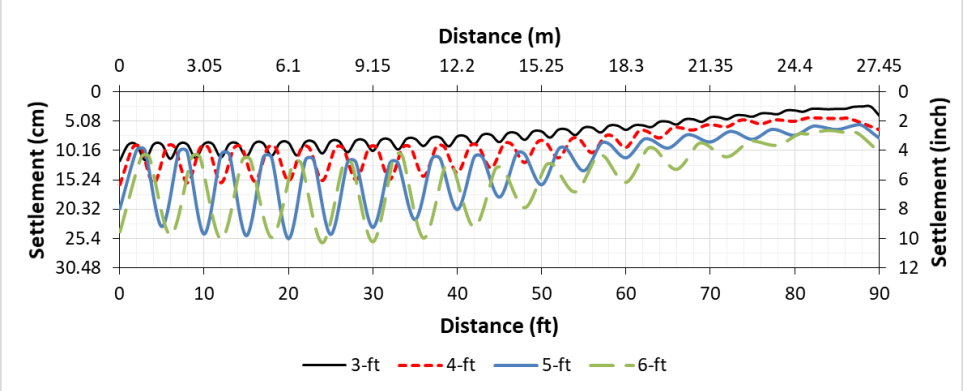


Figure 6.40. Settlement along the base of embankment after 2 years of consolidation for each pile spacing.

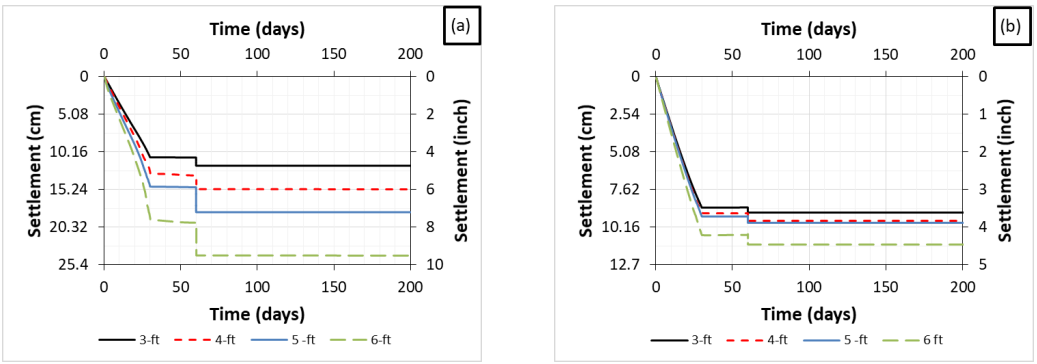


Figure 6.41. Settlement vs. time for each pile spacing at (a) the soft soil between the piles at the embankment centerline; (b) the pile head under the embankment centerline.

#### 6.4.3.3.2. Excess Pore Water Pressure

Figure 6.42 shows the maximum excess pore water pressure developed due to embankment loading at two different locations: under the embankment centerline and under the embankment toe at depths of 0.5 m, and 2.3 m, respectively. These values are observed at the end of construction (EOC). Results show that the excess pore water pressure values increase with the pile spacing increase under the centerline of the embankment and under the embankment toe. Higher excess pore water is observed near the toe of the embankment due to the horizontal loading of the foundation soil from the lateral displacement of the piles at the top compared to the excess pore water pressure observed under the centerline of the embankment due to the stress increase (stresses on the soft soil between piles). For example, the excess pore water pressure values for the 1.83 m (6 ft) pile spacing are 6 kPa and 20 kPa under the centerline of the embankment and the embankment toe, respectively.

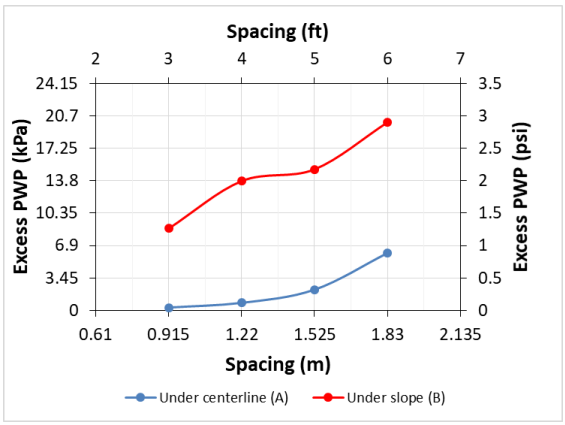


(a)

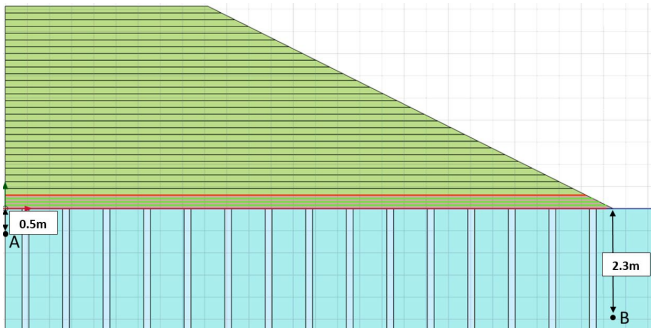


(b)

Figure 6.42. (a) Maximum excess pore water pressure at the end of construction observed under the centerline of the embankment (Point A), and under the embankment toe (Point B); and (b) its location.

### 6.4.3.3.3. Vertical Stress

Figure 6.43 shows vertical stress observed at the base of the embankment for the 1.83 m (6 ft) pile spacing at two different times: the end of construction (EOC), and after 2 years of consolidation. Results show that the pile head carries most of the total load due to the arching effect. In addition, the vertical stress on top of piles is higher after 2 years of consolidation compared to vertical stresses observed at the EOC, whereas the opposite behavior is observed on the soft soil between the piles. The stress concentration ratio (SCR) is found to be 8 and 23 at the EOC and after 2 years of consolidation, respectively, both of which almost fall between the range of 10 to 30 as reported

by Han and Wayne (2000). Compared to H= 6.1 m (20 ft) in which the SCR is 20 and 36, the SCR values at the two times decreased with increasing the embankment load.

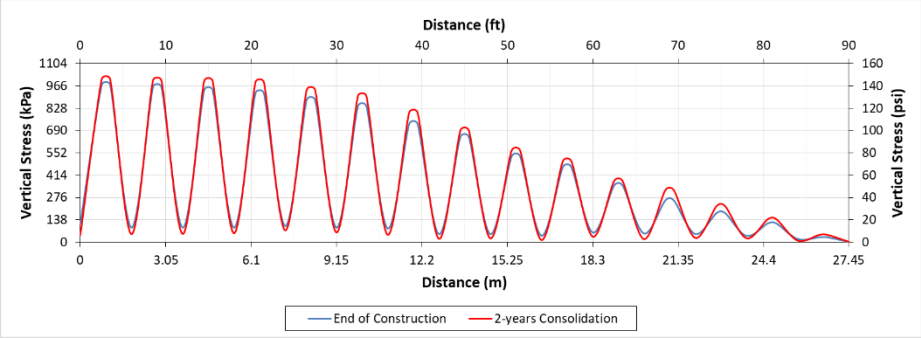


Figure 6.43. Vertical Stress along the base of the embankment at the end of construction (EOC) and after 2 years of consolidation.

### 6.4.3.3.4. Lateral Displacement

Figure 6.44 shows the lateral displacement profile along depth at the toe of the embankment after 2 years of consolidation. The maximum observed lateral displacement in all the pile spacing is in the very soft soil layer at the ground surface which is the weakest layer among all the foundation soils. Lateral displacement tends to become zero at deeper depths where medium and dense sand layers exist. It can also be noted that the lateral displacement increased with increasing the pile spacing. Maximum observed lateral displacements are 119.6 mm, 188.5 mm, 254 mm, and 330.2 mm for the pile spacing from the smallest to the largest. Higher lateral displacement is observed when comparing the highest embankment height (H= 9.15 m) with the lower embankment heights (H= 3.05 m and 6.1 m) as the lateral thrust at the edges of the embankment increases by a factor of almost 7.2 and 2.1, respectively, because of the increase of embankment loading.

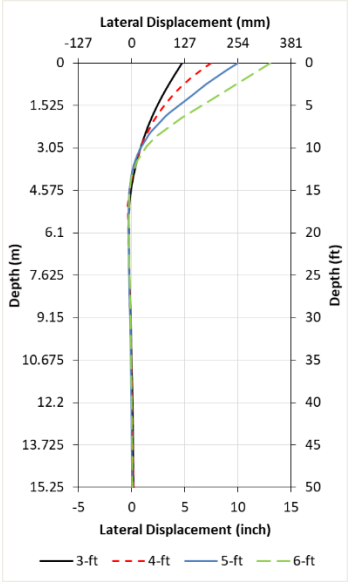


Figure 6.44. Lateral displacement profile along depth at the embankment toe after 2 years of consolidation.

### 6.4.3.3.5. Strain in Geosynthetics

Figure 6.45 shows the strain profile along the base of the embankment for the 1.83 m (6 ft) pile spacing after 2 years of consolidation for the 5 geosynthetic layers. Results confirm the peak-trough profile for all the geosynthetic layers as observed before. The peak occurs on top of the soft soil between the piles for the bottom geotextile layer (1$^{st}$ layer), and the peak is found on top of the pile heads for the rest of the geosynthetic layers. It can also be noted that the maximum strain percentage along each geosynthetic layer is observed almost under the centerline where the maximum load exists. Figure 6.46 shows a closer look of the strain profile for the 1.83 m (6 ft) pile spacing in the 1$^{st}$ and 2$^{nd}$ geosynthetic layers.

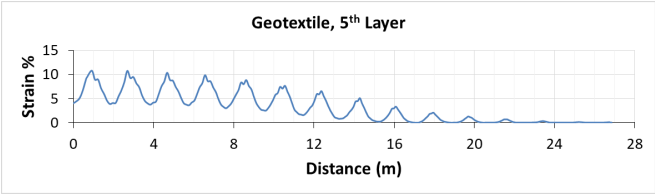

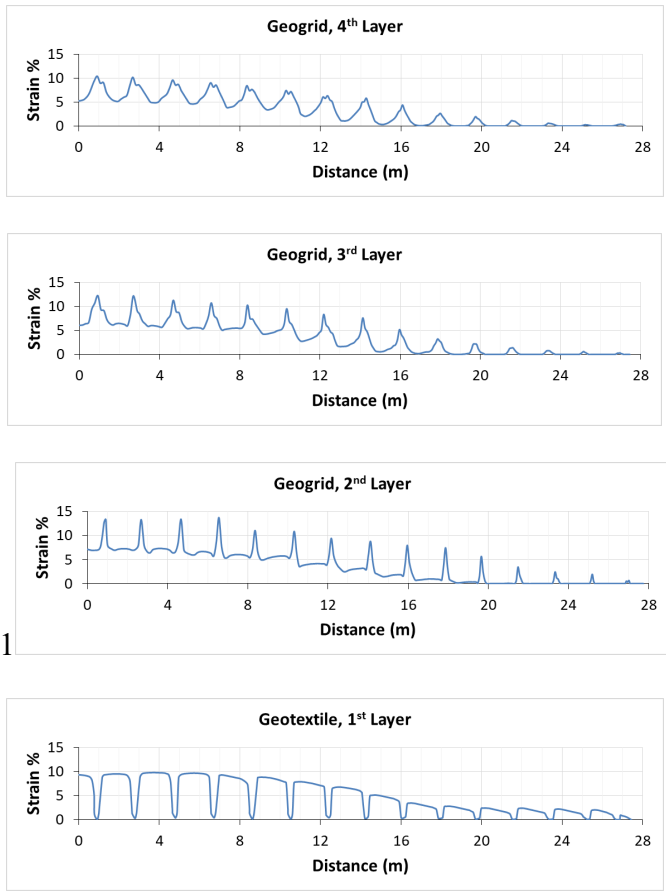


Figure 6.45. Strain profile along the base of embankment in the geosynthetic layers after 2 years of consolidation for the "6-ft" pile spacing.

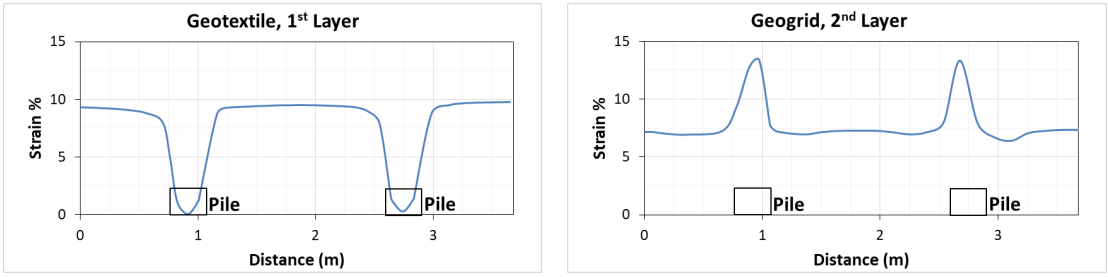


Figure 6.46. Closer look of the strain profile in the 1st and 2nd geosynthetic layers after 2 years of consolidation for the "6-ft" pile spacing.

Figure 6.47 shows the maximum strain observed in the geosynthetic layers after 2 years of consolidation for each pile spacing. Strain in the geosynthetic layers has an almost linear increasing relationship with increasing the pile spacing. Moreover, maximum observed strain is computed in the 2nd geosynthetic layer for the 1.83 m (6 ft) pile spacing which is almost 13.5%. It can also be

noted that strain in the geosynthetic layers exceeded the maximum allowable limit (5%) except for geosynthetics in the 0.915 m (3 ft) pile spacing.

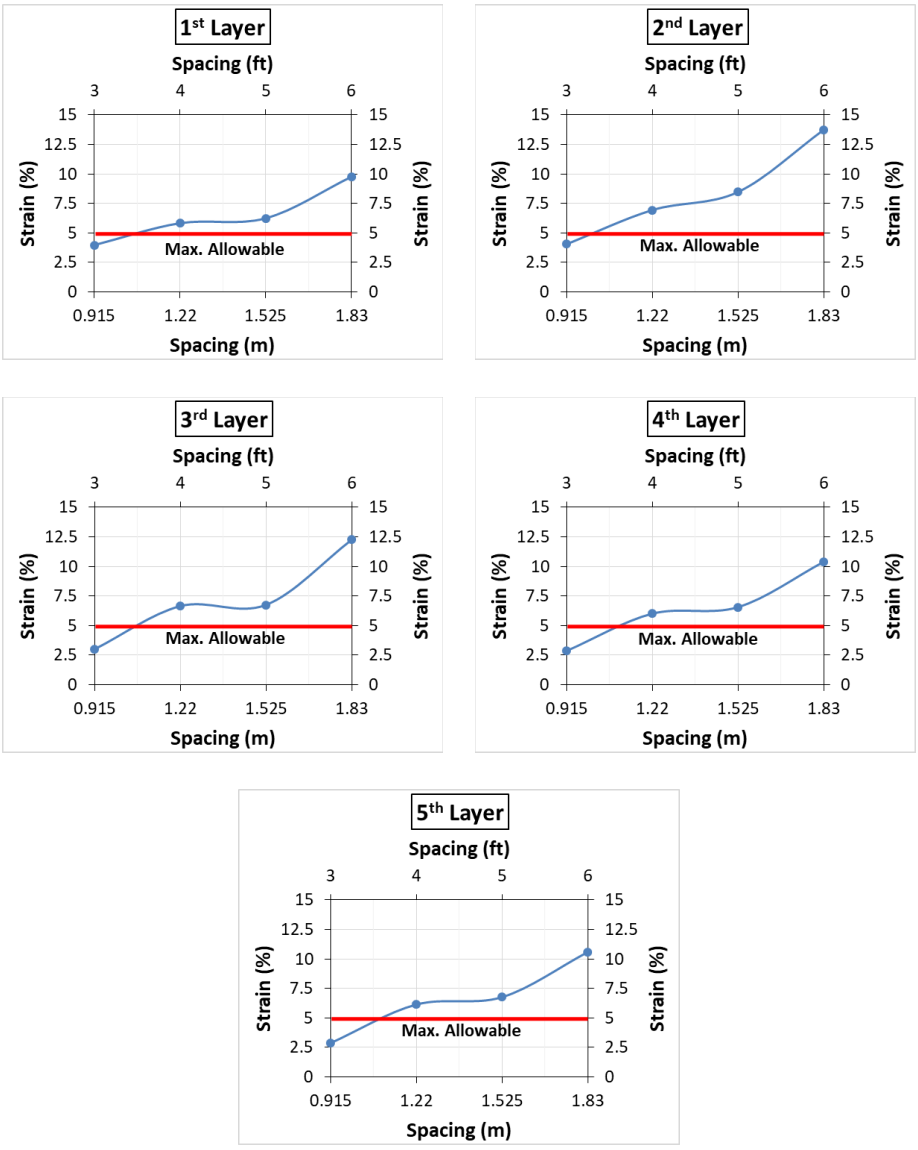


Figure 6.47. Maximum strain in geosynthetic layers for each pile spacing after 2 years of consolidation.

### 6.4.4. Discussion

The performance of the pile-supported system must satisfy both the strength and serviceability limit state requirements. For the strength limit state, the geotechnical capacity of the piles is maintained through the design with taking into consideration the pile length requirement. All the

designed pile lengths with changing the embankment load (H= 3.05 m, 6.1 m, and 9.15 m) for each pile spacing (0.915 m, 1.22 m, 1.525 m, and 1.83 m) satisfy the minimum and maximum timber pile length requirement as all the pile lengths fall within the range of 9.15-18.30 m (30-60 ft). Furthermore, the global stability of the system is maintained on the short-term and long-term the GRLTP and piles are extended up to three-quarters of the slope (1.5H) at the lowest embankment load (H=3.05 m), and up to the embankment toe (2.0H) at the intermediate and highest embankment loads (H=6.1 m and 9.15 m). The calculated factor of safety at all embankment loads with each pile spacing is more than 1.5 for the short-term and long-term analyses. For the serviceability limit state, the foundation settlement must not exceed a maximum upper limit which is defined as 15.24 cm (6 inches) in this study. The settlement of the foundation soil requirement is maintained at the lowest and intermediate embankment heights for each pile spacing. However, only the 0.915 m (3 ft) and 1.22 m (4 ft) pile spacing satisfied the settlement requirement at the highest embankment load. Therefore, the 1.525 m (5 ft) and 1.83 m (6 ft) pile spacing are excluded from the recommendations at this embankment load. Moreover, the strain of the geosynthetic reinforcement must be less than or equal to a maximum upper limit of 5%. On one hand, the strain percentage requirement is maintained for each pile spacing at the lowest and intermediate embankment load. On the other hand, the strain in the geosynthetic layers did exceed the maximum allowable limit at the maximum embankment load for all the proposed pile spacing except for the 0.915 m (3 ft) pile spacing. It should be noted that the 1.22 m (4 ft) pile spacing almost satisfies the strain requirement (maximum strain in all layers is 6.94%). Accordingly, the 1.22 m (4 ft) pile spacing is re-analyzed with three scenarios. First, the tensile stiffness of the biaxial geogrids is increased from 375 kN/m to 420 kN/m while maintaining the same number of geosynthetic layers (i.e., 5 layers). Second, two biaxial geogrid layers are added to the GRLTP to create a GRLTP of

7 layers (2 geotextiles and 5 geogrids) while maintaining the same axial stiffness of the geogrids as the original case (i.e., 375 kN/m). The geosynthetic layers are 15.24 cm (6 inches) spaced resulting in a GRLTP of a total thickness of 0.915 m. Third, both the number of layers and the tensile stiffness of the geogrids are increased to 7 layers and 420 kN/m, respectively. Table 6.9 shows the strain in the geosynthetic layers for the original and the proposed cases for comparison. Maintaining the same number of geosynthetic layers while increasing the axial stiffness of the geogrid layers reduced the strain percentage by an average reduction of 5.5% for all the layers. However, the maximum allowable strain limit is still exceeded for this configuration. In contrast, increasing the number of reinforcement layers to 7 while maintaining the same axial stiffness improved the performance of the strain values, but the strain in the first three layers from the bottom did exceed the maximum allowable limit. Similarly, increasing the number of geosynthetics to 7 layers with increasing the tensile stiffness to 420 kN/m solved the problem in which all strain in all the geosynthetic layers is less than 5%.

It should be noted that no requirement is set on the lateral displacements near the toe of the embankment as the movement is in the foundation soil and does not appear on the ground surface. Meanwhile, excessive lateral displacements are not allowed provided these movements cause a problem in the global stability of the system, which was checked in the stability analysis. Table 6.10 shows the cost evaluation depending mainly on the required timber pile length per row to maintain a stable system with all requirements being satisfied. All the proposed pile spacing are included for the lowest and intermediate embankment loads, whereas only the 0.915 m (3 ft) and 1.22 m (4 ft) pile spacing are included for the highest embankment load as only these two satisfy the serviceability limit state requirements. For the 3.05 m (10 ft) embankment height, the 1.83 m (6 ft) resulted in the most economical design for Case 1 soil profile. Furthermore, the 1.525 m (5

ft) pile spacing is chosen as a design recommendation for this soil profile of Case 1 for the intermediate embankment load (H= 6.1 m). The same GRLTP configuration with the original tensile stiffness is adopted for the above-mentioned cases. In contrast, the 9.15 m (30 ft) embankment load is suggested to be used with the 1.22 m (4 ft) pile spacing while increasing both the number of reinforcement layers and the axial stiffness to 7 layers and to 420 kN/m, respectively.

Table 6.9. Strain level comparison between different GRLTP configurations.

| H= 9.15 m (30 ft), Spacing= 1.22 m (4 ft), No. Layers= 5, GRLTP thickness= 0.61m | | | H= 9.15 m (30 ft), Spacing= 1.22 m (4 ft), No. Layers= 7, GRLTP thickness= 0.915m | | |
|---|---|---|---|---|---|
| Layer No. | EA (Geogrids)= 375 kN/m | EA (Geogrids)= 420 kN/m | Layer No. | EA (Geogrids)= 375 kN/m | EA (Geogrids)= 420 kN/m |
| 1st Layer (GTX) | 5.83 | 5.48 | 1st Layer (GTX) | 5.19 | 4.87 |
| 2nd Layer (GGR) | 6.94 | 6.55 | 2nd Layer (GGR) | 5.55 | 4.89 |
| 3rd Layer (GGR) | 6.65 | 6.20 | 3rd Layer (GGR) | 5.20 | 4.86 |
| 4th Layer (GGR) | 6.01 | 5.54 | 4th Layer (GGR) | 4.53 | 4.20 |
| 5th Layer (GTX) | 6.14 | 6.06 | 5th Layer (GGR) | 4.00 | 3.70 |
| - | - | - | 6th Layer (GGR) | 3.82 | 3.56 |
| - | - | - | 7th Layer (GTX) | 4.01 | 3.88 |

Table 6.10. Cost evaluation for Case 1 soil profile.

| H (m) | Valid Pile Spacing (m) | Pile Length (m) | Number of Piles per Row | Total Required Pile length per Row (m) |
|---|---|---|---|---|
| 3.05 (10 ft) | 0.915 (3 ft) | 9.15 (30 ft) | 30 | 275 |
| | 1.220 (4 ft) | 9.15 (30 ft) | 22 | 202 |
| | 1.525 (5 ft) | 9.15 (30 ft) | 18 | 165 |
| | 1.830 (6 ft) | 9.76 (32 ft) | 15 | 147 |
| 6.10 (20 ft) | 0.915 (3 ft) | 9.15 (30 ft) | 46 | 421 |
| | 1.220 (4 ft) | 9.15 (30 ft) | 34 | 312 |
| | 1.525 (5 ft) | 10.67 (35 ft) | 28 | 299 |
| | 1.830 (6 ft) | 15.25 (50 ft) | 24 | 366 |
| 9.15 (30 ft) | 0.915 (3 ft) | 9.15 (30 ft) | 60 | 549 |
| | 1.220 (4 ft) | 10.67 (35 ft) | 44 | 470 |

## 6.5. Case (2) Soil Profile

This section discusses the FEM parametric study for the soil profile of Case 2 (Figure 6.1b). The proposed three embankment heights (3.05 m (10 ft), 6.1 m (20 ft), and 9.15 m (30 ft)) will be analyzed in terms of the required pile length design, the GRLTP and piles' extent under the embankment slope, and performance of the system by changing the center-to-center pile spacing.

### 6.5.1. Embankment Height (H)= 3.05 m (10 ft)

#### 6.5.1.1. Pile Design

Piles are designed to carry the whole embankment load plus the surcharge load for each corresponding pile spacing. Estimated factored loads are 77 kN, 137 kN, 214 kN, and 308 kN for 0.915 m (3 ft), 1.22 m (4 ft), 1.525 m (5 ft), and 1.83 m (6 ft) pile spacing, respectively. Table 6.11 shows the pile design information including the pile diameter (D) and pile length (L) for each corresponding pile spacing. Similar pile length is adopted for the "3-ft", "4-ft", and "5-ft" pile

spacing as the minimum required timber pile length is 9.15 m (30 ft) which satisfies both the geotechnical capacity requirement and the minimum length requirement of this study.

Table 6.11. Pile Design for Case 2, H= 3.05 m (10 ft).

| Spacing | Pile Diameter (D) | Pile Length (L) |
|---|---|---|
| 0.915 m (3 ft) | 0.305 m (1 ft) | 9.15 m (30 ft) |
| 1.220 m (4 ft) | 0.305 m (1 ft) | 9.15 m (30 ft) |
| 1.525 m (5 ft) | 0.305 m (1 ft) | 9.15 m (30 ft) |
| 1.830 m (6 ft) | 0.305 m (1 ft) | 9.76 m (32 ft) |

#### 6.5.1.2. Stability Analysis

The GRLTP and piles' extent under the embankment slope is adopted from the stability analysis of Case 1 as the subsoil condition underneath the embankment is exactly the same as Case 1. However, the factor of safety is determined for each pile spacing to ensure that the safety factor for the short and long term is more than the minimum required factor of safety of 1.5. Accordingly, the GRLTP and pile are extended up to three-quarters of the slope (1.5H) and one-quarter of the slope (0.5H) for the NC soil case and OC soil case, respectively. The average factor of safety for the NC soil case of all the pile spacing with the adopted GRLTP and piles' extent is 2.1 and 3.0 for the short-term and long-term analyses, respectively. Therefore, the extent of the GRLTP and the piles is chosen to be 1.5H (three-quarters of the slope) and 0.5H (one-quarter of the slope) for the cases of NC soil and OC soil, respectively. Accordingly, the required number of piles per row for the NC soil case is 30, 22, 18, and 15 for the 0.915 m, 1.22 m, 1.525 m, and 1.83 m pile spacing, respectively.

#### 6.5.1.3. Spacing Parametric Study

The performance of the system is investigated with changing the center-to-center pile spacing with the GRLTP and the piles extended up to three-quarters of the slope (1.5H). Further analysis will only be conducted on the NC soil case. Pile spacing will be ranged from 3D to 6D as follows: 0.915 m (3 ft), 1.22 m (4 ft), 1.525 m (5 ft), and 1.83 m (6 ft). The designed pile length for each corresponding pile spacing, from the smallest to the largest, is 9.15 m (30 ft), 9.15 m (30 ft), 9.15 m (30 ft), and 9.76 m (32 ft).

##### 6.5.1.3.1. Settlement

Figure 6.48 shows the settlement at the base of embankment after 2 years of consolidation for the pile spacing 0.915 m (3 ft), 1.22 m (4 ft), 1.525 m (5 ft), and 1.83 m (6 ft). The maximum observed settlement under the centerline of the embankment is 6.40 cm, 8.54 cm, 10.67 cm, and 12.8 cm for each corresponding spacing from the smallest to the largest. It can be observed that with increasing the pile length the settlement at the soft soil between the piles tends to increase. However, the unsupported zone under the slope experiences larger settlement compared to the supported area. This is attributed to the improvement of the system due to the existence of the GRLTP and the pile foundation. The maximum settlement observed under the unsupported zone is 9.82 cm, 13.20 cm, 12.51 cm, and 15.02 cm for each corresponding spacing from the smallest to the largest. Settlement in this area depends primarily on the distance of the last pile from the GRLTP edge, which coincides with a distance of three-quarters of the slope (1.5H). Distance between the edge of the GRLTP and the far edge of the last pile, $x$, is 0.305 m, 0.762 m, 0.61 m, and 0.762 m for each corresponding spacing from the smallest to the largest (Figure 6.14). This explains the larger settlement observed in the unsupported zone for the “4-ft” than the “5-ft” pile spacing.

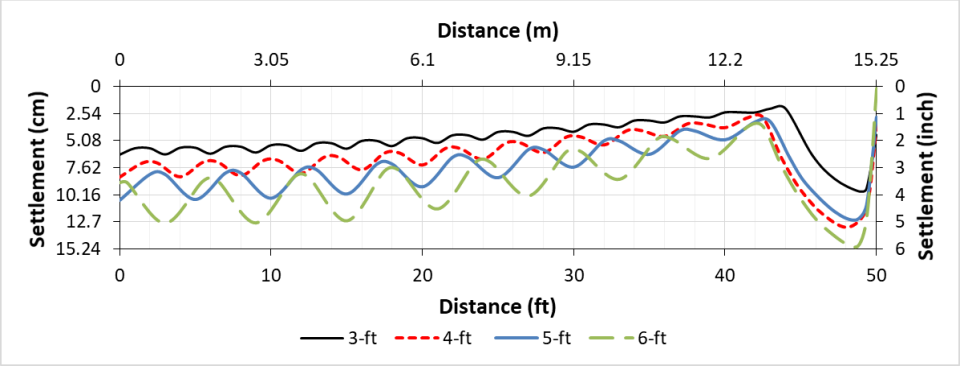


Figure 6.48. Settlement along the base of embankment after 2 years of consolidation for each pile spacing.

Figure 6.49 shows the settlement with time for each pile spacing at the soft soil between the piles under the embankment centerline, at the pile head under the embankment centerline, and at the location of the maximum settlement observed in the unsupported zone. Both Figure 6.49a and Figure 6.49b show a fast consolidation settlement rate compared to the unsupported zone (Figure 6.49c). This is attributed to the inclusion of the GRLTP and the pile foundation in which the settlement is improved, and a faster consolidation rate is achieved. In addition, the fast dissipation of excess pore water pressure is the cause of the high hydraulic conductivities of the sand layers existing under the very soft clay layer. This results in a double drainage boundary for the very soft clay layer, at the top and the bottom of the layer. For instance, 99% of the maximum settlement observed in the very soft clay layer is achieved after 40 days and 500 days from the project start for the supported zone and the unsupported zone, respectively.

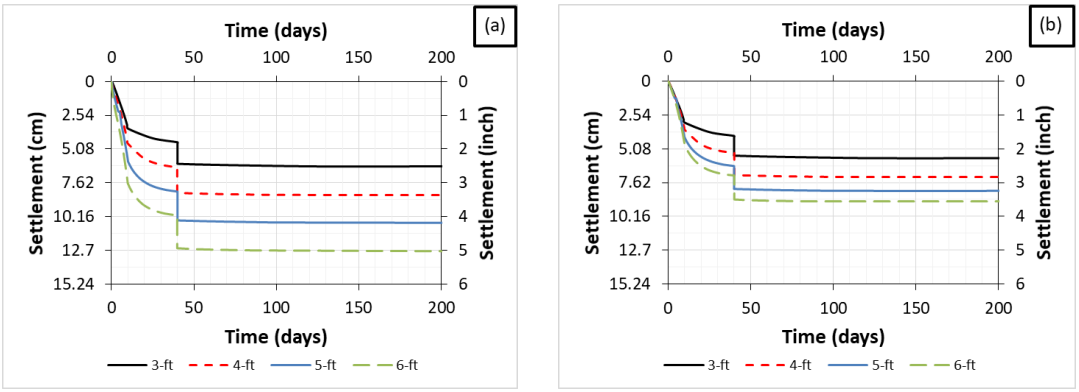

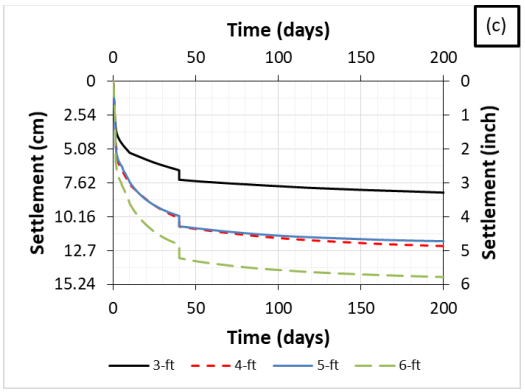


Figure 6.49. Settlement vs. time for each pile spacing at (a) the soft soil between the piles at the embankment centerline; (b) the pile head under the embankment centerline; (c) the maximum settlement in the unsupported area.

#### 6.5.1.3.2. Excess Pore Water Pressure

Figure 6.50 shows the maximum excess pore water pressure induced due to embankment loading at three different locations: under the embankment centerline, under the unsupported area near the embankment toe, and at the middle of the soft clay layer under the embankment centerline at depths of 0.3 m, 0.5 m, and 13.72 m, respectively. These values are observed at the end of construction (EOC). Results show that the excess pore water pressure values increase as the pile spacing increases under the supported area (Point A). In contrast, the excess pore water pressure in the unsupported area depends on the distance $x$ (Figure 6.14), in which the "4-ft" spacing has a larger $x$ distance resulting in a little higher excess pore water pressure as discussed in the settlement section above. This confirms the larger settlement observed for the "4-ft" spacing than the "5-ft" spacing. Furthermore, the excess pore water pressure observed in the middle of the soft clay layer (Point C) is the highest value observed in all locations. Piles are tipping on the dense sand layer in which a considerable stress increase from the embankment load is transferred through the piles to the dense sand and the soft clay layer which exists underneath it. The value of the excess pore water pressure at Point C increased with increasing the pile spacing. In addition, it can be noted that the induced pore water pressure at the centerline of the embankment due to the stress increase

is lower than that in the unsupported area. This is attributed to the existence of the GRLTP and the pile foundation.

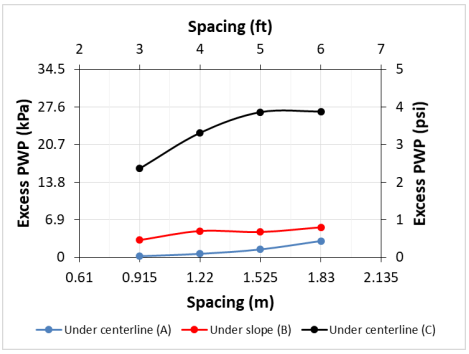


(a)

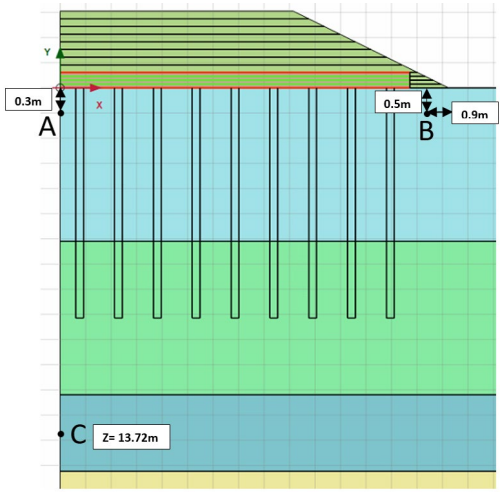


(b)

Figure 6.50. (a) Maximum excess pore water pressure at the end of construction observed under the centerline of the embankment (Point A), the unsupported area (Point B), and at the mid of the soft clay layer; and (b) its location.

### 6.5.1.3.3. Vertical Stress

Figure 6.51 shows vertical stress observed at the embankment base for the 1.83 m (6 ft) pile spacing at two different times: the end of construction (EOC), and after 2 years of consolidation. Results show higher vertical stress observed on the pile heads compared to the soft soil between piles. It can also be noted that vertical stress on top of piles is higher after 2 years of consolidation than vertical stresses observed at the EOC. Conversely, vertical stresses on the soft soil between

the piles are higher at the EOC than those after 2 years of consolidation. This is attributed to the arching effect as the load tends to be imposed on the rigid inclusions with the soil between the piles settling. The stress concentration ratio (SCR) is found to be 13 and 45 at the EOC and after 2 years of consolidation. Pile-supported embankments with timber piles and a GRLTP are expected to have a SCR of 10 to 30 (Han and Wayne, 2000). This range was exceeded by the SCR value observed after 2 years of consolidation as observed in the same embankment load in Case 1. This may be attributed to the very soft clay layer underneath the embankment losing contact with the GRLTP for this embankment load resulting in very minimal stresses on the soft soil between the piles with almost all the embankment load carried by the piles.

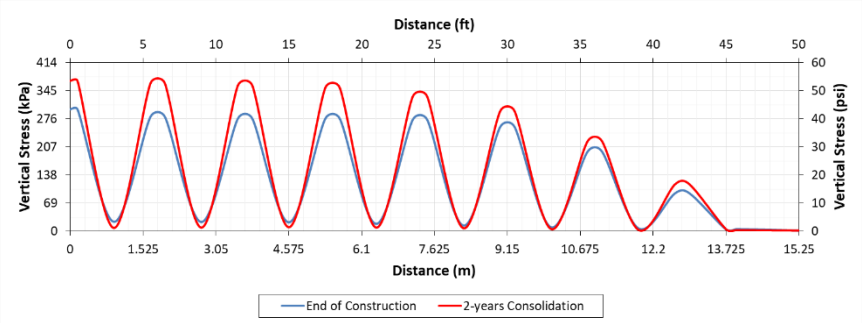


Figure 6.51. Vertical Stress along the base of the embankment at the end of construction (EOC) and after 2 years of consolidation.

### 6.5.1.3.4. Lateral Displacement

Figure 6.52 shows the lateral displacement profile along depth at the toe of the embankment after 2 years of consolidation. The maximum observed lateral displacement in all the pile spacing is in the very soft clay layer at the ground surface. Lateral displacement tends to change direction at deeper depths because of the dense sand layer underneath the very soft clay layer. The lateral displacements then increase again at the soft clay layer (3$^{rd}$ layer), then the lateral displacements are diminished because of the second dense sand layer at the end of the soil profile.

It can also be noted that the lateral displacement increased with increasing the pile spacing, whereas the maximum lateral displacement is the same for the "4-ft" and "5-ft". This may be attributed to the larger distance between the GRLTP edge and the far end of the last pile of the "4-ft" than the "5-ft". Maximum observed lateral displacements are 12.7 mm, 25.4 mm, 25.4 mm, and 40.64 mm for the pile spacing from the smallest to the largest.

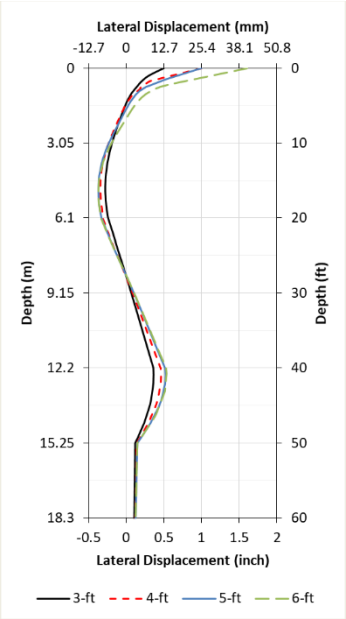


Figure 6.52. Lateral displacement profile along depth at the embankment toe after 2 years of consolidation.

### 6.5.1.3.5. Strain in Geosynthetics

Figure 6.53 shows the strain profile along the base of the embankment for the 1.83 m (6 ft) pile spacing after 2 years of consolidation for the 5 geosynthetic layers. Results show a peak-trough profile for all the geosynthetic layers. The peak is observed on top of the soft soil between the piles for the bottom geotextile layer (Haring et al., 2008), whereas the peak is found on top of the pile heads for the rest of the geosynthetic layers. This may be attributed to the rigid support under the first geosynthetic layer. The reinforcement layer is restrained from going downward with the embankment and GRLTP materials settling downward, resulting in less deformation to the

geosynthetic layer with minimal tension forces at these locations. However, the same geosynthetic layer would have a large curvature at the pile edge due to the lack of support at that location resulting in the maximum strain at the pile edges (Shen et al., 2018), which is extended to be on top of the soft soil between the piles. This behavior is different from the rest of the geosynthetic layers as no rigid support restrains them from deformation with higher vertical stresses at the pile head due to the arching effect. Thus, maximum strain is expected to occur at the pile head, exactly at the edges. The maximum observed strain values along the geosynthetic profiles lie in the area of the full embankment load with a decrease in value towards the embankment toe. Figure 6.54 shows a closer look of the strain profile for the 1.83 m (6 ft) pile spacing in the 1st and 2nd geosynthetic layers.

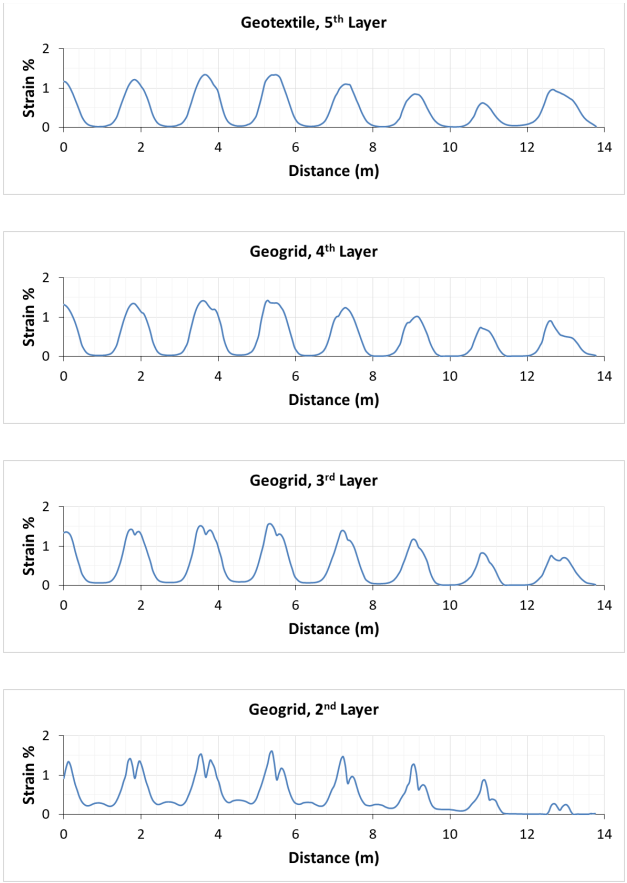

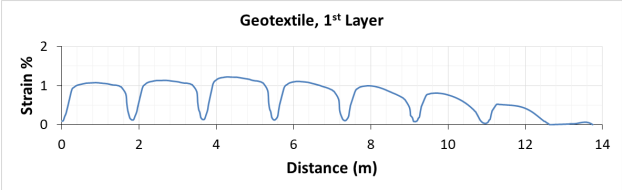


Figure 6.53. Strain profile along the base of embankment in the geosynthetic layers after 2 years of consolidation for the "6-ft" pile spacing.

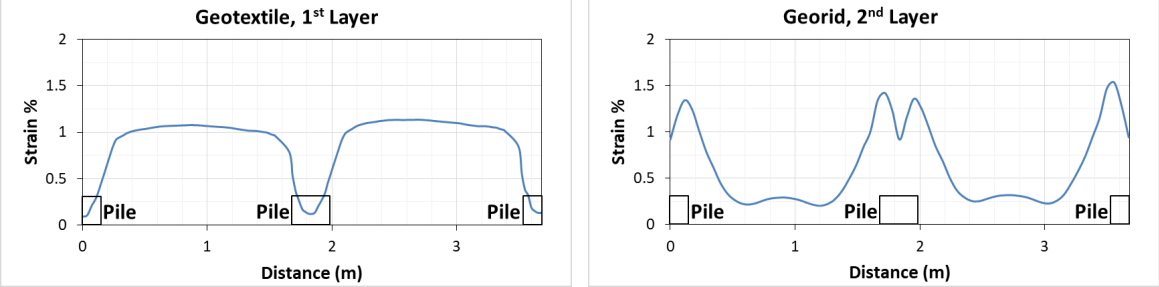


Figure 6.54. Closer look of the strain profile in the 1st and 2nd geosynthetic layers after 2 years of consolidation for the "6-ft" pile spacing.

Figure 6.55 shows the maximum strain observed in the geosynthetic layers after 2 years of consolidation for each pile spacing. All the layers have an almost linear relationship between the strain in each layer and the corresponding pile spacing. Moreover, maximum observed strain is computed in the 2nd geosynthetic layer for the 1.83 m (6 ft) pile spacing which is 1.6%.

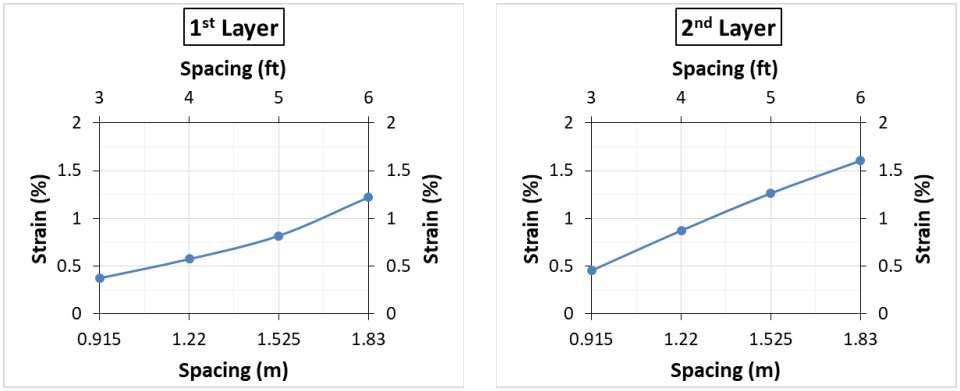

2

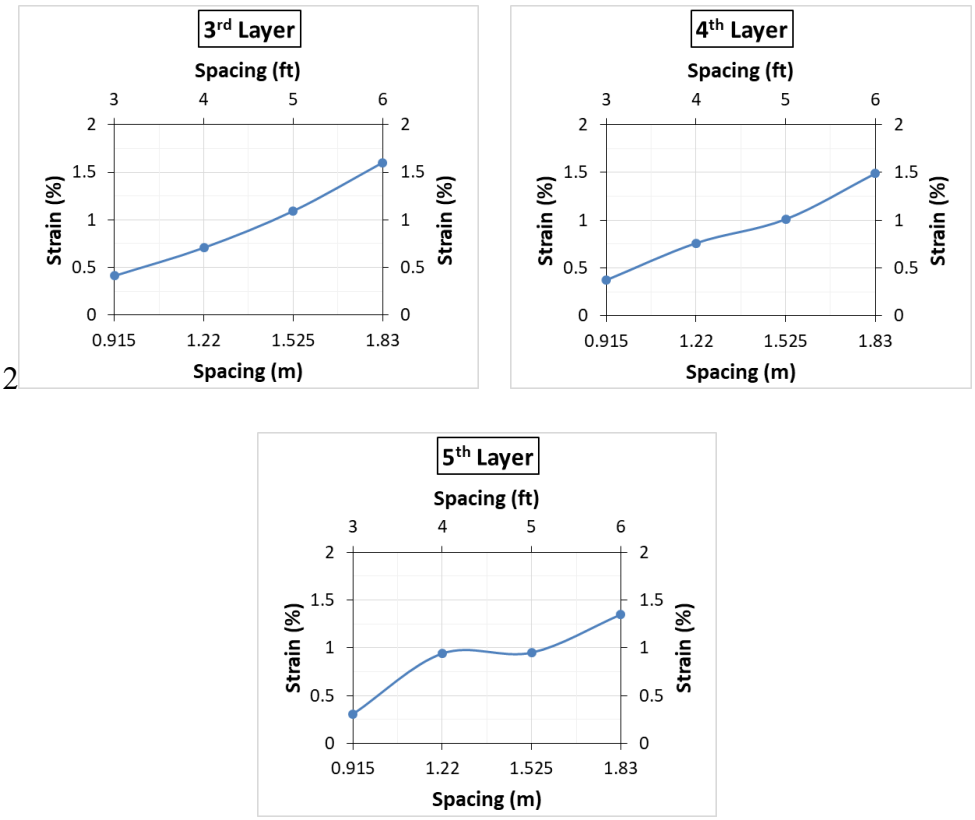


Figure 6.55. Maximum strain in geosynthetic layers for each pile spacing after 2 years of consolidation.

### 6.5.2. Embankment Height (H)= 6.10 m (20 ft)

#### 6.5.2.1. Pile Design

Piles are designed to carry the whole embankment load plus the surcharge load for each corresponding pile spacing. Estimated factored loads are 138 kN, 246 kN, 384 kN, and 552 kN for 0.915 m (3 ft), 1.22 m (4 ft), 1.525 m (5 ft), and 1.83 m (6 ft) pile spacing, respectively. Table 6.12 shows the pile design information including the pile diameter (D) and pile length (L) for each corresponding pile spacing. Similar pile length is adopted for the "3-ft" and "4-ft" pile spacing as the minimum required timber pile length is 9.15 m (30 ft) which satisfies both the geotechnical capacity requirement and the minimum length requirement of this study. Furthermore, the "6-ft" pile spacing satisfy the geotechnical capacity requirement at a length of 15.25 m (50 ft) where the piles are tipping on the second dense sand layer, but it was extended a distance of two times the

pile diameter (2D) resulting in a length of 15.86 m (52 ft) to make sure that the piles tip on the dense sand layer not on the soft clay layer on top of it. The top and bottom boundaries of the soil layers in reality are not completely straight (i.e., the soil layer thickness might change from one location to another). Therefore, an extended distance of two times the pile diameter (2D) is adopted in this study for the cases where a bad quality soil layer exists on the layer that the piles are tipping on.

Table 6.12. Pile Design for Case 2, H= 6.1 m (20 ft).

| Spacing | Pile Diameter (D) | Pile Length (L) |
|---|---|---|
| 0.915 m (3 ft) | 0.305 m (1 ft) | 9.15 m (30 ft) |
| 1.220 m (4 ft) | 0.305 m (1 ft) | 9.15 m (30 ft) |
| 1.525 m (5 ft) | 0.305 m (1 ft) | 10.76 m (35 ft) |
| 1.830 m (6 ft) | 0.305 m (1 ft) | 15.86 m (52 ft) |

**6.5.2.2. Stability Analysis**

The GRLTP and piles' extent under the embankment slope is adopted from the stability analysis of Case 1 as the subsoil condition underneath the embankment is exactly the same as Case 1. However, the factor of safety is determined for each pile spacing to ensure that the safety factor for the short and long term is more than the minimum required factor of safety of 1.5. Accordingly, the GRLTP and pile are extended up to the embankment toe (2.0H) and three-quarters of the slope (1.5H) for the NC soil case and OC soil case, respectively. An average factor of safety for the NC soil case of all the pile spacing with the adopted GRLTP and piles' extent is 2.15 and 2.20 for the short-term and long-term analyses, respectively. Therefore, the extent of the GRLTP and the piles is chosen to be 2.0H (full length up to the embankment toe) and 1.5H (three-quarters of the slope) for the cases of NC soil and OC soil, respectively. Accordingly, the required number of piles per

row for the NC soil case is 46, 34, 28, and 24 for the 0.915 m, 1.22 m, 1.525 m, and 1.83 m pile spacing, respectively.

#### 6.5.2.3. Spacing Parametric Study

The performance of the system is investigated with changing the center-to-center pile spacing with the GRLTP and the piles extended up to the embankment toe (2.0H). Further analysis will only be conducted on the NC soil case. Pile spacing will be ranged from 3D to 6D as follows: 0.915 m (3 ft), 1.22 m (4 ft), 1.525 m (5 ft), and 1.83 m (6 ft). The designed pile length for each corresponding pile spacing, from the smallest to the largest, is 9.15 m (30 ft), 9.15 m (30 ft), 10.67 m (35 ft), and 15.86 m (52 ft).

##### 6.5.2.3.1. Settlement

Figure 6.56 shows the settlement at the base of the embankment after 2 years of consolidation for the pile spacing 0.915 m (3 ft), 1.22 m (4 ft), 1.525 m (5 ft), and 1.83 m (6 ft). The maximum observed settlement under the centerline of the embankment is 10.05 cm, 19.57 cm, 22.28 cm, and 14.86 cm for each corresponding spacing from the smallest to the largest. The maximum settlement among all the pile spacing is observed for the 1.525 m (5 ft) followed by the 1.22 m (4 ft), and the best settlement performance is observed for the 0.915 m (3 ft) pile spacing. The piles do not penetrate the soft clay layer (3rd layer), so significant stresses are transferred to this soft clay layer resulting in a high settlement. In contrast, the piles in the 1.83 m (6 ft) pile spacing penetrate the soft clay layer and tip on the dense sand layer, which significantly improved the system's performance. A comparison between the 1.525 m (5 ft) pile spacing is made between a pile length of 10.67 (35 ft) and 15.86 m (52 ft) as shown in Figure 6.56. The maximum settlement observed under the embankment centerline for the 15.86 m (52 ft) pile length is 10.72 cm which represents a reduction in settlement of 52% from the original length. Therefore, further analysis will be

considered for the newly adopted pile length for the 1.525 m (5 ft) pile spacing as the originally designed pile length exceeds the settlement requirement of 15.24 cm (6 inches).

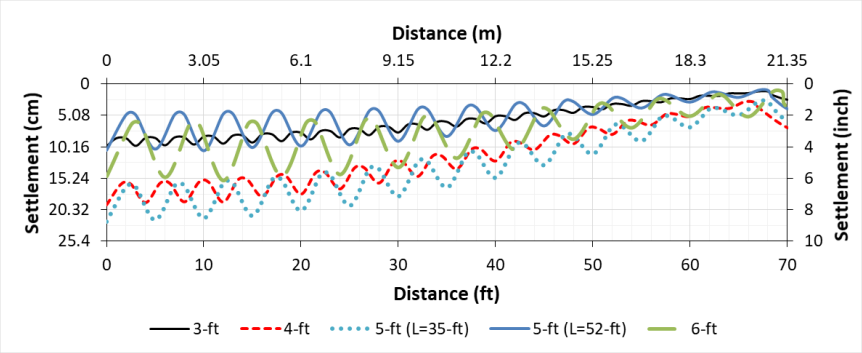


Figure 6.56. Settlement along the base of embankment after 2 years of consolidation for each pile spacing.

Figure 6.57 shows the settlement with time for each pile spacing at the soft soil between the piles under the embankment centerline, and at the pile head under the embankment centerline. Both Figure 6.57a and Figure 6.57b show a fast consolidation settlement rate even for the 1.22 m (4 ft) pile spacing in which significant stress increase is transferred to the soft clay layer (3$^{rd}$ layer) as explained before. This is attributed to the inclusion of the GRLTP and the pile foundation in which the settlement is improved, and a faster consolidation rate is achieved. In addition, the fast dissipation of excess pore water pressure is the cause of the high hydraulic conductivities of the sand layers existing under the very soft clay layer. This results in a double drainage boundary for the very soft clay layer, at the top and the bottom of the layer. For instance, 99% of the maximum settlement observed in the very soft clay layer is achieved after 50 days (Figure 6.57a). Moreover, the settlement at the pile head (Figure 6.57b) of 1.525 m (5 ft) and 1.83 m (6 ft) pile spacing is less than those of the lower proposed spacing as the piles are penetrating through the soft clay layer and tipping on the second dense sand layer leaving the piles with much less settlement.

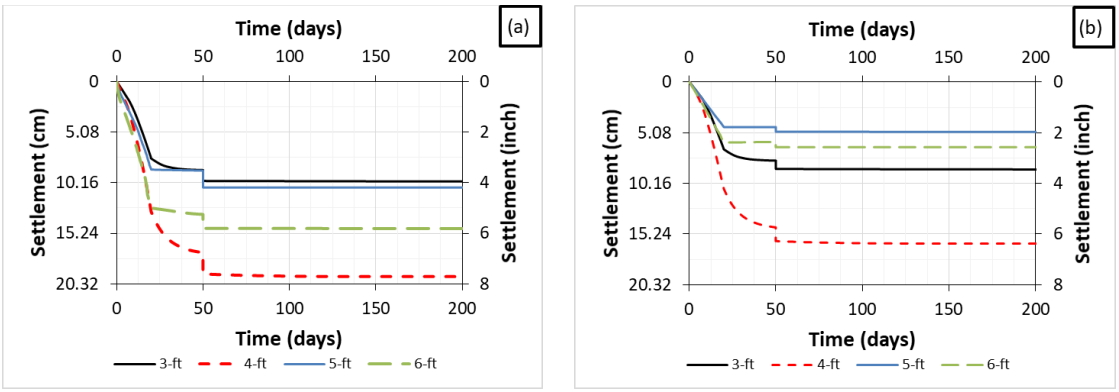


Figure 6.57. Settlement vs. time for each pile spacing at (a) the soft soil between the piles at the embankment centerline; (b) the pile head under the embankment centerline.

#### 6.5.2.3.2. Excess Pore Water Pressure

Figure 6.58 shows the maximum excess pore water pressure induced due to embankment loading at three different locations: under the embankment centerline, under the unsupported area near the embankment toe, and at the middle of the soft clay layer under the embankment centerline at a depth of 0.3 m, 1.8 m, and 13.72 m, respectively. These values are observed at the end of construction (EOC). Results show that the excess pore water pressure values increase with the pile spacing increase under the supported area (Point A) and near the embankment toe (Point B). Larger excess pore water pressure is observed near the embankment than that under the centerline of the embankment because of the horizontal loading of the soil mass with the lateral displacement of the piles to the right. However, significant excess pore water pressure is observed for the 0.915 m (3 ft) and 1.22 m (4 ft) pile spacing at Point C. The piles are tipping on the dense sand layer on top of the soft clay resulting in significant stresses transferred to this layer. Excess pore water pressure is almost zero for the 1.525 m (5 ft) and the 1.83 m (6 ft) pile spacing as the piles are penetrating the soft clay layer, so no significant stresses are transferred to it.

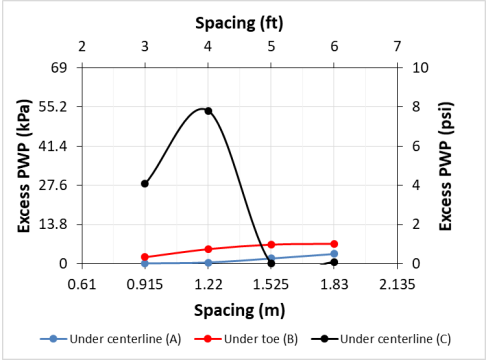


(a)

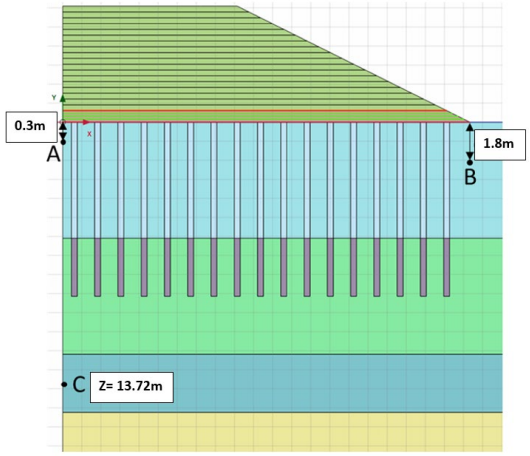


(b)

Figure 6.58. (a) Maximum excess pore water pressure at the end of construction observed under the centerline of the embankment (Point A), the unsupported area (Point B), and at the mid of the soft clay layer; and (b) its location.

### 6.5.2.3.3. Vertical Stress

Figure 6.59 shows vertical stress observed at the base of the embankment for the 1.83 m (6 ft) pile spacing at two different times: the end of construction (EOC), and after 2 years of consolidation. Results show higher vertical stress observed on the pile heads compared to the soft soil between piles. It can also be noted that vertical stress on top of piles is higher after 2 years of consolidation than vertical stresses observed at the EOC. Conversely, vertical stresses on the soft soil between the piles is higher at the EOC than those after 2 years of consolidation. This is attributed to the arching effect as the load tends to be imposed on the rigid inclusions with the soil settling between

the piles. Moreover, the difference between the vertical stress on the pile heads at the end of construction and after 2 years of consolidation is not significant. This is attributed to the fast consolidation settlement for the 1.83 m (6-ft) pile spacing where the piles are tipped on the deepest dense sand layer. The stress concentration ratio (SCR) is found to be 21 and 30 at the EOC and after 2 years of consolidation, respectively, which almost fall between the range of 10 to 30 reported by Han and Wayne (2000).

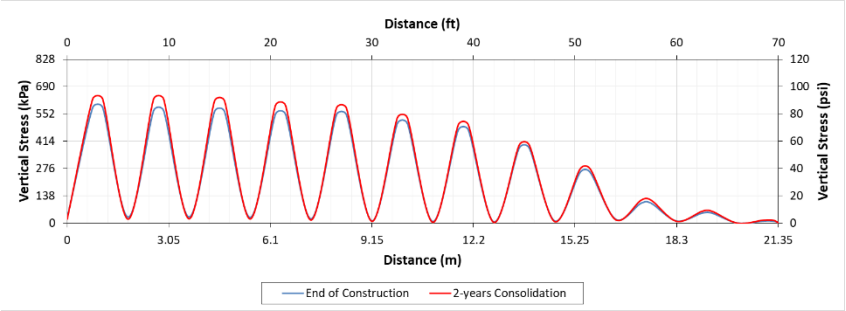


Figure 6.59. Vertical Stress along the base of the embankment at the end of construction (EOC) and after 2 years of consolidation.

### 6.5.2.3.4. Lateral Displacement

Figure 6.60 shows the lateral displacement profile along depth at the toe of the embankment after 2 years of consolidation. The maximum observed lateral displacement in all the pile spacing is in the very soft clay layer at the ground surface. Lateral displacement tends to change direction with going to deeper depths because of the dense sand layer underneath the very soft clay layer. The lateral displacements then increases again at the soft clay layer ($3^{rd}$ layer) then the lateral displacements is diminished because of the second dense sand layer at the end of the soil profile. It can also be noted that the lateral displacement increased with increasing the pile spacing. Maximum observed lateral displacements are 29.21 mm, 83.82 mm, 133.35 mm, and 172.72 mm for the pile spacing from the smallest to the largest.

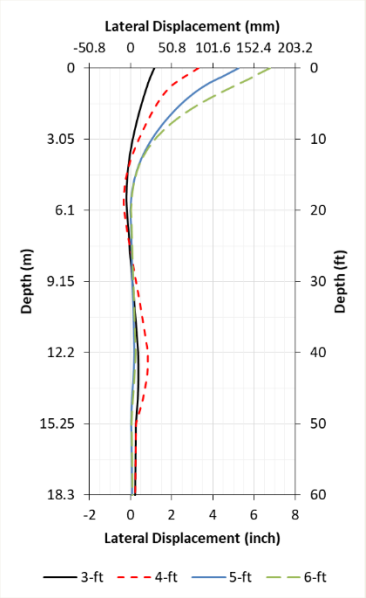


Figure 6.60. Lateral displacement profile along depth at the embankment toe after 2 years of consolidation.

### 6.5.2.3.5. Strain in Geosynthetics

Figure 6.61 shows the strain profile along the base of the embankment for the 1.83 m (6 ft) pile spacing after 2 years of consolidation for the 5 geosynthetic layers. Results show a peak-trough profile for all the geosynthetic layers. The peak is observed on top of the soft soil between the piles for the bottom geotextile layer (1$^{st}$ layer), whereas the peak is found on top of the pile heads for the rest of the geosynthetic layers. For the 1$^{st}$ geosynthetic layer, the strain at the edges increased rapidly with lack of support between the piles resulting in maximum strain at pile edges. This is also observed for the rest of the reinforcement layers in which peaks are on top of piles and the maximum strain occurs exactly at the pile edges (Shen et al., 2018). The maximum observed strain values along the geosynthetic profiles lie all in the area of the full embankment load with a decrease in value towards the embankment toe. Figure 6.62 shows a closer look of the strain profile for the 1.83 m (6 ft) pile spacing in the 1$^{st}$ and 2$^{nd}$ geosynthetic layers.

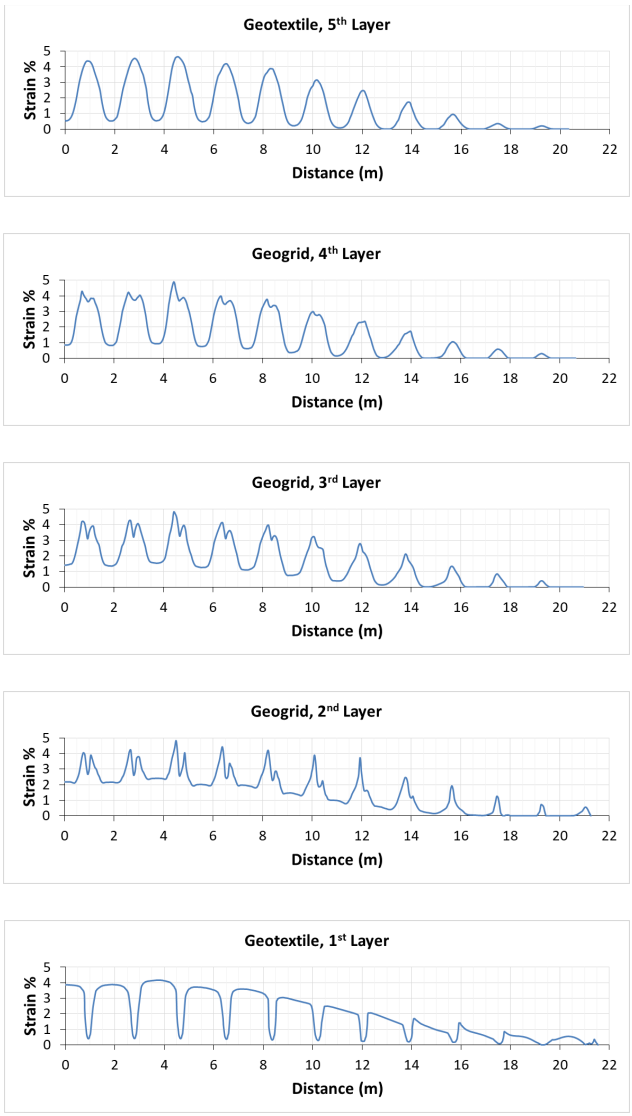


Figure 6.61. Strain profile along the base of embankment in the geosynthetic layers after 2 years of consolidation for the "6-ft" pile spacing.

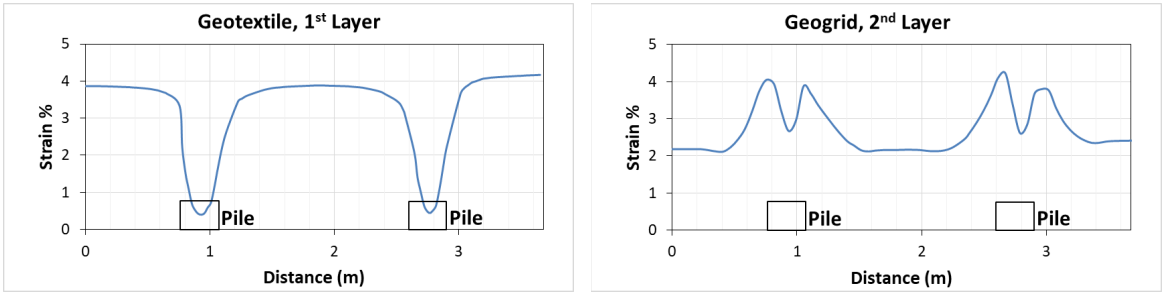


Figure 6.62. Closer look of the strain profile in the 1st and 2nd geosynthetic layers after 2 years of consolidation for the "6-ft" pile spacing.

Figure 6.63 shows the maximum strain observed in the geosynthetic layers after 2 years of consolidation for each pile spacing. All the layers have an almost linear relationship between the strain in each layer and the corresponding pile spacing. Maximum strain values almost reached the maximum allowable value as observed in the same embankment load (H=6.1 m) in Case 1. Moreover, maximum observed strain is computed in the 2nd geosynthetic layer for the 1.83 m (6 ft) pile spacing which is 4.82%.

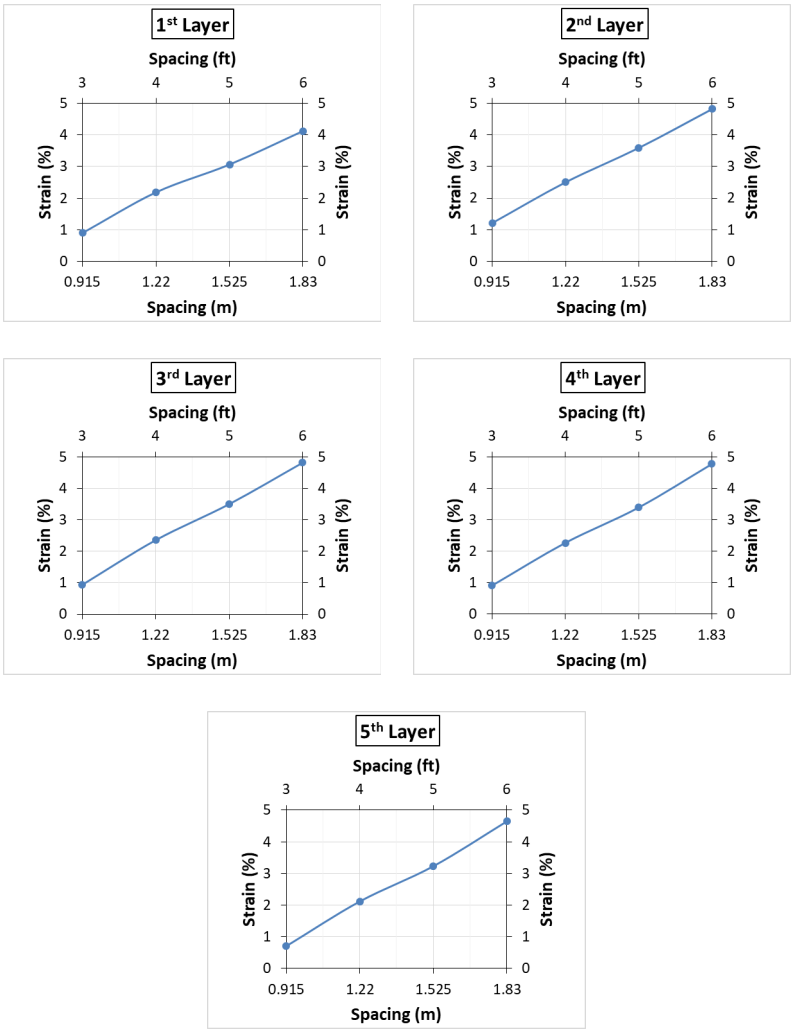


Figure 6.63. Maximum strain in geosynthetic layers for each pile spacing after 2 years of consolidation.

### 6.5.3. Embankment Height (H)= 9.15 m (30 ft)

#### 6.5.3.1. Pile Design

Piles are designed to carry the whole embankment load plus the surcharge load for each corresponding pile spacing. Estimated factored loads are 196 kN, 348 kN, 543 kN, and 782 kN for 0.915 m (3 ft), 1.22 m (4 ft), 1.525 m (5 ft), and 1.83 m (6 ft) pile spacing, respectively. Table 6.13 shows the pile design information including the pile diameter (D) and pile length (L) for each corresponding pile spacing. The pile lengths ranged from the minimum required pile length (9.15 m) to the maximum required pile length (18.3 m) for the highest embankment load (H= 9.15 m). It should be noted that the piles of 1.22 m (4 ft) and 1.525 m (5 ft) pile spacing are extended to penetrate the soft clay layer (3$^{rd}$ layer) as a result of the large settlement values obtained from an embankment height of 6.1 m (20 ft). Moreover, the piles are extended a distance of twice the pile diameter to ensure that the piles are tipping on the dense sand layer as adopted before.

Table 6.13. Pile Design for Case 2, H= 9.15 m (30 ft).

| Spacing | Pile Diameter (D) | Pile Length (L) |
|---|---|---|
| 0.915 m (3 ft) | 0.305 m (1 ft) | 9.15 m (30 ft) |
| 1.220 m (4 ft) | 0.305 m (1 ft) | 15.86 m (52 ft) |
| 1.525 m (5 ft) | 0.305 m (1 ft) | 15.86 m (52 ft) |
| 1.830 m (6 ft) | 0.305 m (1 ft) | 18.30 m (60 ft) |

#### 6.5.3.2. Stability Analysis

The GRLTP and piles' extent under the embankment slope is adopted from the stability analysis of Case 1 as the subsoil condition underneath the embankment is exactly the same as Case 1. However, the factor of safety is determined for each pile spacing to make sure that the factor of safety for the short and long term is more than the minimum required factor of safety of 1.5.

Accordingly, the GRLTP and pile are extended up to the embankment toe (2.0H) and three-quarters of the slope (1.5H) for the NC soil case and OC soil case, respectively. The average factor of safety for the NC soil case of all the pile spacing with the adopted GRLTP and piles' extent is 1.8 for both the short-term and long-term analyses. Therefore, the extent of the GRLTP and the piles is chosen to be 2.0H (full length up to the embankment toe) and 1.5H (three-quarters of the slope) for the cases of NC soil and OC soil, respectively. Accordingly, the required number of piles per row for the NC soil case is 60, 44, 36, and 30 for the 0.915 m, 1.22 m, 1.525 m, and 1.83 m pile spacing, respectively.

#### 6.5.3.3. Spacing Parametric Study

The performance of the system is investigated with changing the center-to-center pile spacing with the GRLTP and the piles extended up to the toe of the embankment (2.0H extent). Further analysis will only be conducted on the NC soil case. Pile spacing will be ranged from 3D to 6D as follows: 0.915 m (3 ft), 1.22 m (4 ft), 1.525 m (5 ft), and 1.83 m (6 ft). The designed pile length for each corresponding pile spacing, from the smallest to the largest, is 9.15 m (30 ft), 15.86 m (52 ft), 15.86 m (52 ft), and 18.30 m (60 ft).

##### 6.5.3.3.1. Settlement

Figure 6.64 shows the settlement at the base of the embankment after 2 years of consolidation for the pile spacing 0.915 m (3 ft), 1.22 m (4 ft), 1.525 m (5 ft), and 1.83 m (6 ft). Maximum settlement is observed under the embankment centerline, where exists the maximum load, for the 0.915 (3 ft), 1.22 (4 ft), and 1.525 m (5 ft) pile spacing which is 28.01 cm, 15.21 cm, and 19.67 cm, respectively. In contrast, the maximum settlement is observed at the soft soil between piles near the centerline at the 5$^{th}$ space between piles for the 1.83 m (6 ft) pile spacing which is 25.67 cm. The settlement for this pile spacing increased from the embankment centerline up to the 5$^{th}$ space

between piles and then started to decrease up to the embankment toe with decreasing the load. This may be attributed to the excessive lateral displacement experienced by the piles due to the very high embankment load with this pile spacing in which the piles are not completely straight underneath the embankment. Consequently, the ability of the piles to resist vertical loads is reduced resulting in higher settlement with the direction to the right up to the point that the settlement starts to decrease where the embankment load is decreasing as well. The maximum settlement among all the pile spacing is observed for the 0.915 m (3 ft). The piles do not penetrate the soft clay layer (3rd layer), so significant stresses are transferred to this soft clay layer resulting in a high settlement. In contrast, the piles in the 1.22 m (4 ft), 1.525 m (5 ft), and 1.83 m (6 ft) pile spacing penetrate the soft clay layer and tip on the dense sand layer which improved the performance of the system significantly even with increasing the load with increasing the pile spacing. A comparison between the 0.915 m (3 ft) pile spacing is made between a pile length of 9.15 m (30 ft) and 15.86 m (52 ft) as shown in Figure 6.64. The maximum settlement observed under the embankment centerline for the 15.86 m (52 ft) pile length is 11.40 cm which represents a reduction in settlement of 59% from the original length. Therefore, further analysis will be considered for the newly adopted pile length for the 0.915 m (3 ft) pile spacing as the originally designed pile length leads to exceeding the settlement requirement of 15.24 cm (6 inches). Figure 6.65 shows the settlement with time for each pile spacing at the soft soil between the piles under the embankment centerline, and at the pile head under the embankment centerline. The settlement increased over time with the embankment construction which ends at 30 days. This is followed by a consolidation period of 30 days in which no significant settlement has occurred meaning that almost all the settlements occurred with the embankment construction for this soil profile. This fast consolidation settlement is attributed to the use of the pile-supported system utilizing a GRLTP

within it. Also, the double drainage condition for the very soft clay layer plays a role in the fast consolidation settlement observed. For instance, an increase in the settlement at the soft soil between the piles of only 1.03% is observed between the settlement at the end of construction (EOC) and the settlement at 60 days (after 30 days of consolidation) for the 1.83m (6 ft) pile spacing. Then a 20.31% increase in the settlement between the settlement before and after applying the surcharge load. This is followed by an increase of only 0.2% in the settlement between the time after applying the surcharge load and the end of the consolidation period.

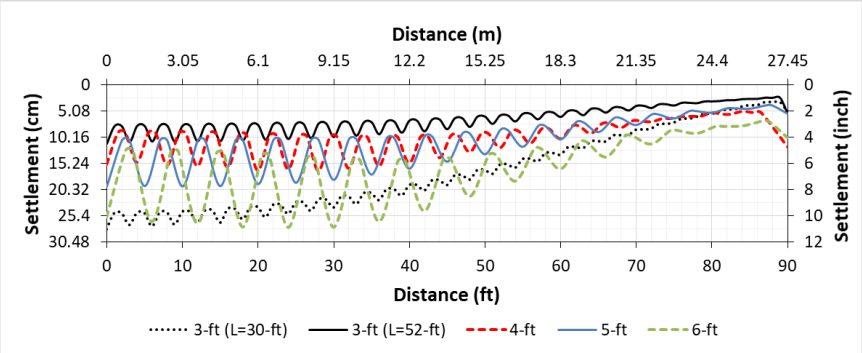


Figure 6.64. Settlement along the base of embankment after 2 years of consolidation for each pile spacing.

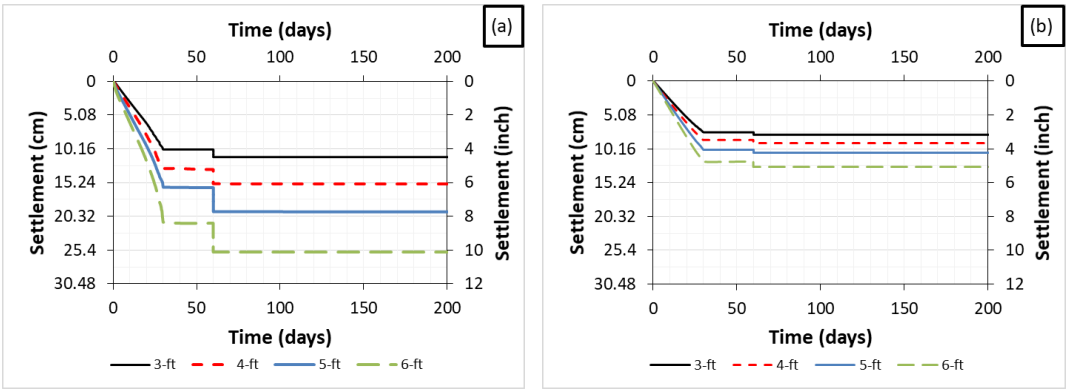


Figure 6.65. Settlement vs. time for each pile spacing at (a) the soft soil between the piles at the embankment centerline; (b) the pile head under the embankment centerline.

### 6.5.3.3.2. Excess Pore Water Pressure

Figure 6.66 shows the maximum excess pore water pressure induced due to embankment loading at three different locations: under the embankment centerline, under the unsupported area near the

embankment toe, and at the middle of the soft clay layer under the embankment centerline at depths of 0.3 m, 2.5 m, and 13.72 m, respectively. These values are observed at the end of construction (EOC). Results show that the excess pore water pressure values increase with the pile spacing increase under the supported area (Point A). However, for excess pore water pressure under the embankment toe, the values depend on the distance between the far edge of the pile and the embankment toe. The maximum unsupported distance is 1.07 m for the 1.22 m (4 ft) pile spacing which confirms the maximum observed value for this pile spacing (Figure 6.66a).

Larger excess pore water pressure is observed near the embankment than that under the centerline of the embankment because of the horizontal loading of the soil mass with the lateral displacement of the piles to the right. However, minor excess pore water pressure is observed for all the proposed pile spacing at Point C as the piles are penetrating the soft clay layer (3rd layer) and tipping on the dense layer.

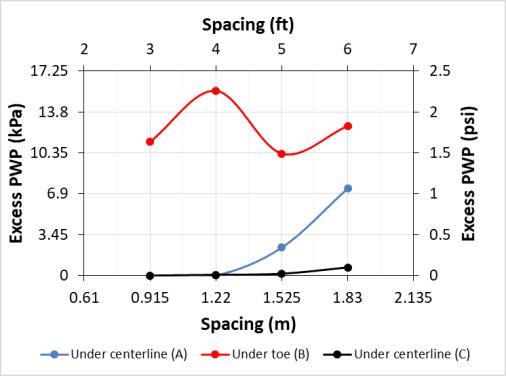


(a)

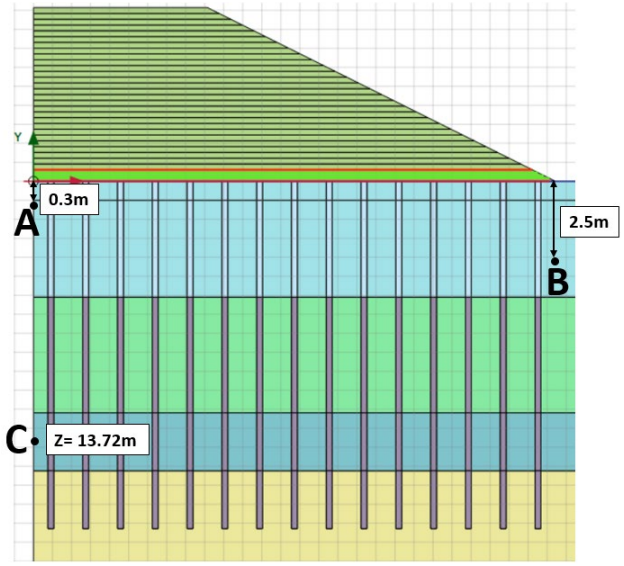


(b)

Figure 6.66. (a) Maximum excess pore water pressure at the end of construction observed under the centerline of the embankment (Point A), and under the embankment toe (Point B); and (b) its location.

#### 6.5.3.3.3. Vertical Stress

Figure 6.67 shows vertical stress observed at the base of the embankment for the 1.83 m (6 ft) pile spacing at two different times: the end of construction (EOC), and after 2 years of consolidation. Results show that the pile head carries most of the total load due to the arching effect. In addition, the vertical stress on top of piles is higher after 2 years of consolidation compared to vertical stresses observed at the EOC, whereas the opposite behavior is observed on the soft soil between the piles. The stress concentration ratio (SCR) is found to be 13 and 29 at the EOC and after 2 years of consolidation, respectively, which fall between the range of 10 to 30 reported by Han and Wayne (2000). Compared to H= 6.1 m (20 ft) in which the SCR is 21 and 30, the SCR values at the two times decreased with increasing the embankment load.

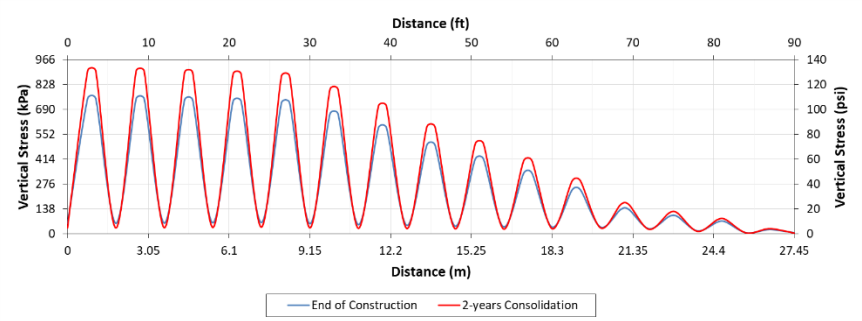


Figure 6.67. Vertical Stress along the base of the embankment at the end of construction (EOC) and after 2 years of consolidation.

### 6.5.3.3.4. Lateral Displacement

Figure 6.68 shows the lateral displacement profile along depth at the toe of the embankment after 2 years of consolidation. The maximum observed lateral displacement in all the pile spacing is in the very soft soil layer at the ground surface which is the weakest layer among all the foundation soils. Lateral displacement tends to become zero at deeper depths as the piles are extended to penetrate the soft clay layer (3$^{rd}$ layer). It can also be noted that the lateral displacement increased with increasing the pile spacing. Maximum observed lateral displacements are 172.7 mm, 215.9 mm, 304.8 mm, and 444.5 mm for the pile spacing from the smallest to the largest. Higher lateral displacement is observed comparing the highest embankment height (H= 9.15 m) with the lower embankment heights (H= 3.05 m and 6.1 m) as the lateral thrust at the edges of the embankment increases by a factor of almost 7.2 and 2.1, respectively.

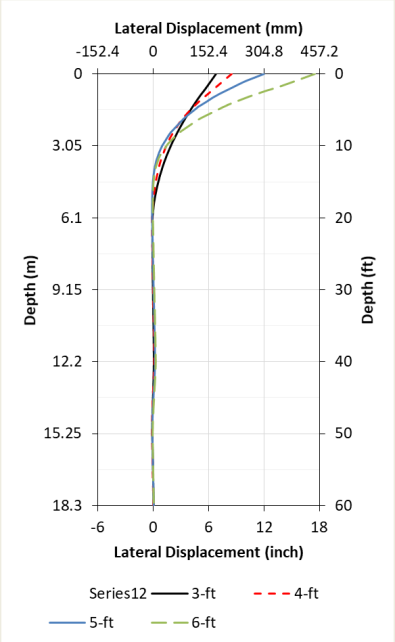


Figure 6.68. Lateral displacement profile along depth at the embankment toe after 2 years of consolidation.

### 6.5.3.3.5. Strain in Geosynthetics

Figure 6.69 shows the strain profile along the base of the embankment for the 1.83 m (6 ft) pile spacing after 2 years of consolidation for the 5 geosynthetic layers. Results confirm the peak-trough profile for all the geosynthetic layers as observed before. On one hand, the peak occurs on top of the soft soil between the piles for the bottom geotextile layer (1$^{st}$ layer) with a significant increase at the pile edge due to the lack of support. On the other hand, peaks are found on top of the pile heads for the rest of the geosynthetic layers. It can also be noted that the maximum strain percentage along each geosynthetic layer is observed almost under the centerline where the maximum load exists. Figure 6.70 shows a closer look of the strain profile for the 1.83 m (6 ft) pile spacing in the 1$^{st}$ and 2$^{nd}$ geosynthetic layers.

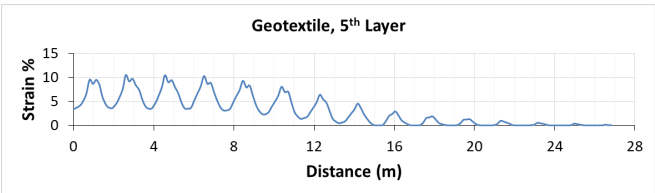

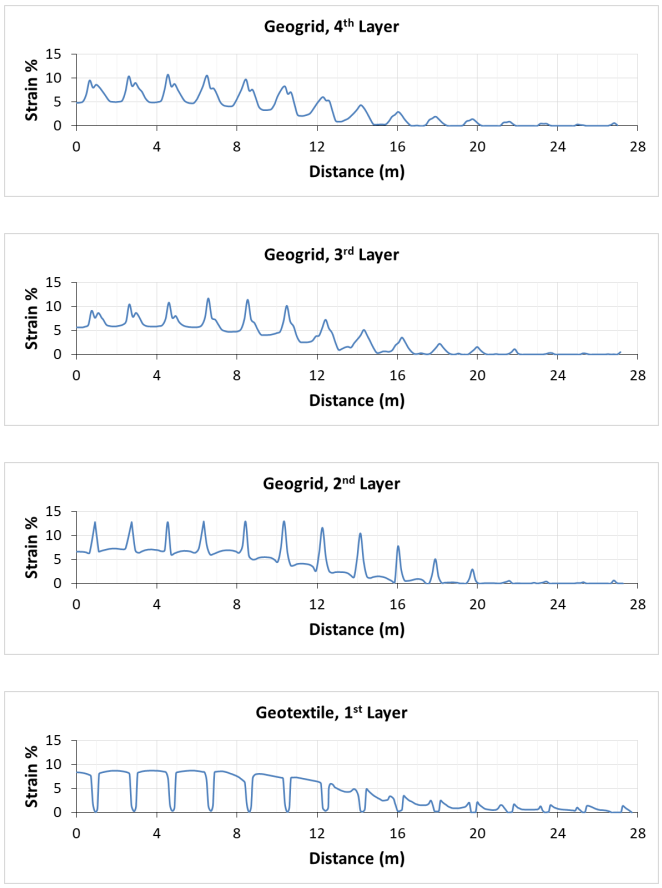


Figure 6.69. Strain profile along the base of the embankment in the geosynthetic layers after 2 years of consolidation for the "6-ft" pile spacing.

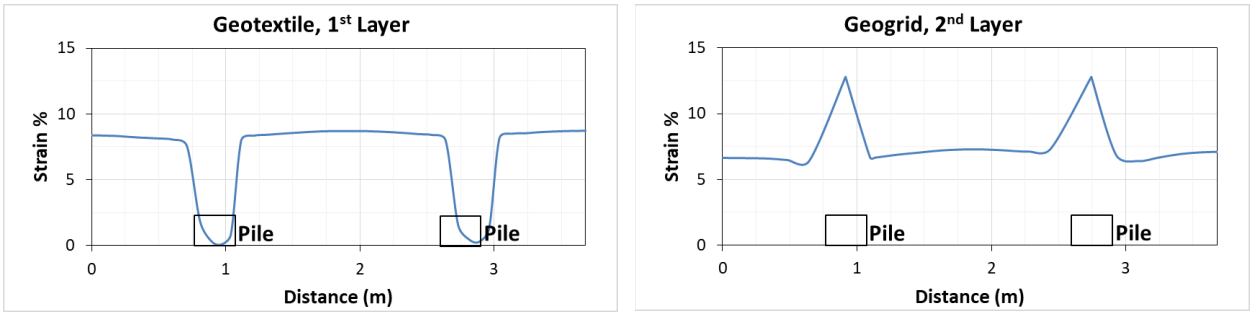


Figure 6.70. Closer look of the strain profile in the 1st and 2nd geosynthetic layers after 2 years of consolidation for the "6-ft" pile spacing.

Figure 6.71 shows the maximum strain observed in the geosynthetic layers after 2 years of consolidation for each pile spacing. Strain in the geosynthetic layers has an almost linear increasing relationship with increasing the pile spacing. Moreover, maximum observed strain is computed in

the 3rd geosynthetic layer for the 1.83 m (6 ft) pile spacing, almost 11.7%. It can also be noted that strain in the geosynthetic layers exceeded the maximum allowable limit (5%) except for geosynthetics in the 0.915 m (3 ft) pile spacing.

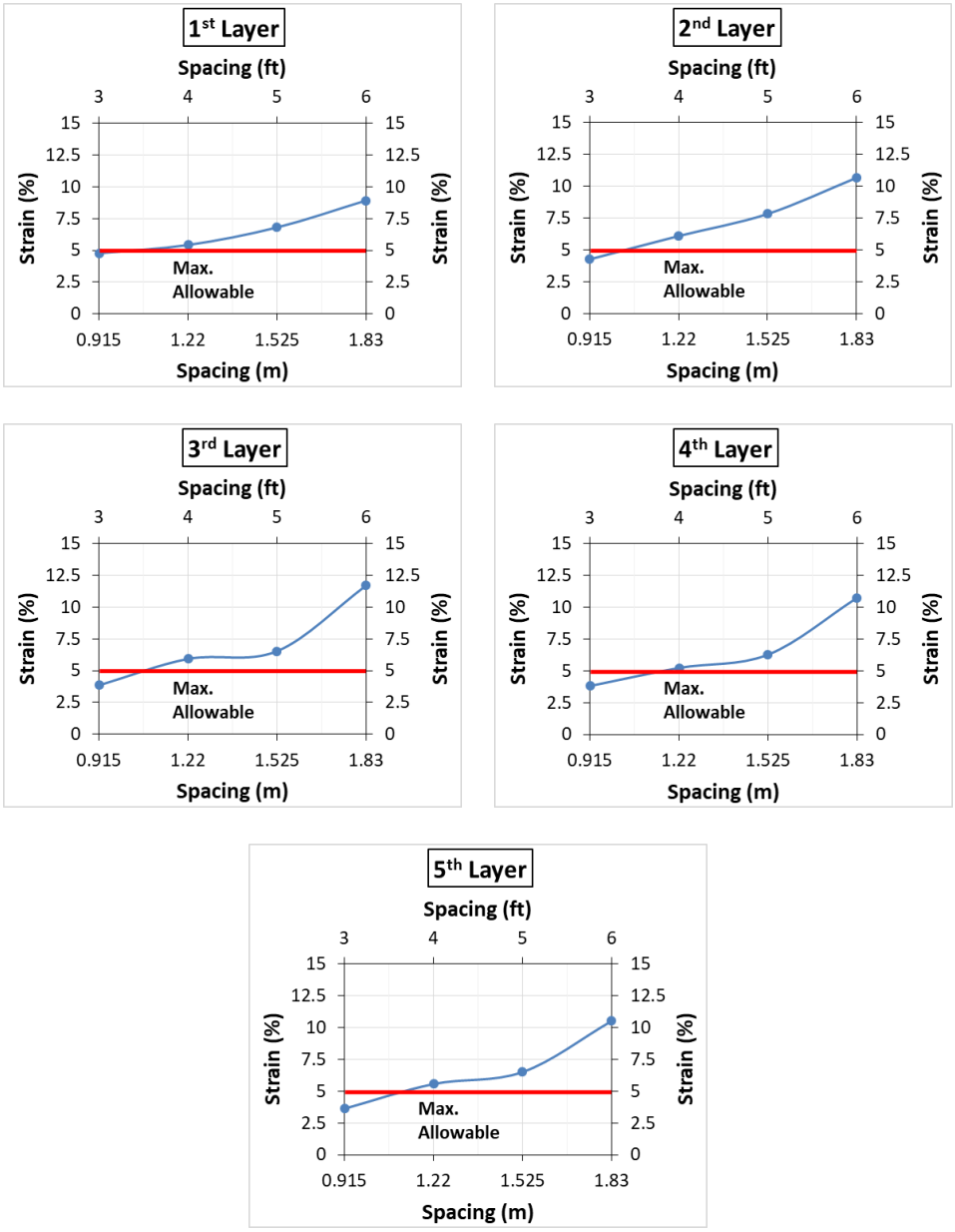


Figure 6.71. Maximum strain in geosynthetic layers for each pile spacing after 2 years of consolidation.

### 6.5.4. Discussion

The performance of the pile-supported system must satisfy both the strength and serviceability limit state requirements. For the strength limit state, the geotechnical capacity of the piles are maintained through the design with taking into consideration the pile length requirement. All the designed pile lengths with changing the embankment load (H= 3.05 m, 6.1 m, and 9.15 m) for each pile spacing (0.915 m, 1.22 m, 1.525 m, and 1.83 m) satisfy the minimum and maximum timber pile length requirement as all the pile lengths fall within the range of 9.15-18.30 m (30-60 ft). Furthermore, the global stability of the system is maintained on the short-term and long-term provided that the GRLTP and piles are extended up to three-quarters of the slope (1.5H) at the lowest embankment load (H=3.05 m), and up to the embankment toe (2.0H) at the intermediate and highest embankment loads (H=6.1 m and 9.15 m). The calculated factor of safety at all embankment loads with each pile spacing is more than 1.5 for the short term and long term analyses. For the serviceability limit state, the foundation settlement must not exceed a maximum upper limit which is defined as 15.24 cm (6 inches) in this study. The settlement of the foundation soil requirement is maintained at the lowest embankment height for each pile spacing. Furthermore, the settlement requirement is satisfied for an embankment height of 6.1 m (20 ft) for all the pile spacing except for the 1.22 m (4 ft) pile spacing. Thus, this pile spacing will be excluded from the design recommendations. Finally, only the 0.915 m (3 ft) and the 1.22 m (4 ft) did satisfy the settlement requirement for an embankment height of 9.15 m (30 ft). Therefore, the 1.525 m (5 ft) and 1.83 m (6 ft) pile spacing are excluded from the design recommendations at this embankment load. Moreover, the strain of the geosynthetic reinforcement must be less than or equal to a maximum upper limit of 5%. On one hand, the strain percentage requirement is maintained for each pile spacing at the lowest and intermediate embankment load. On the other

hand, the strain in the geosynthetic layers did exceed the maximum allowable limit at the maximum embankment load for all the proposed pile spacing except for the 0.915 m (3 ft) pile spacing. It should be noted that the 1.22 m (4 ft) pile spacing almost satisfies the strain requirement (maximum strain in all layers is 6.09%). Accordingly, the 1.22 m (4 ft) pile spacing is re-analyzed with three scenarios. First, the tensile stiffness of the biaxial geogrids is increased from 375 kN/m to 420 kN/m while maintaining the same number of geosynthetic layers (i.e., 5 layers). Second, two biaxial geogrid layers are added to the GRLTP to create a GRLTP of 7 layers (2 geotextiles and 5 geogrids) while maintaining the same axial stiffness of the geogrids as the original case (i.e., 375 kN/m). The geosynthetic layers are 15.24 cm (6 inches) spaced resulting in a GRLTP which is 0.915 m thick. Third, the number of layers and the tensile stiffness of the geogrids are increased to 7 layers and 420 kN/m, respectively. Table 6.14 shows the strain in the geosynthetic layers for the original and the proposed cases for comparison. Maintaining the same number of geosynthetic layers with increasing the axial stiffness of the geogrid layers reduced the strain percentage by an average reduction of 4.5% for all the layers. However, the maximum allowable strain limit is still exceeded for this configuration. In contrast, increasing the number of reinforcement layers to 7 while maintaining the same axial stiffness of the improved the performance of the strain values, but the strain in the 2$^{nd}$ and 3$^{rd}$ layers did exceed the maximum allowable limit. Similarly, increasing the number of geosynthetics to 7 layers while increasing the tensile stiffness to 420 kN/m solved the problem in which all strain in all the geosynthetic layers is less than 5%.

Table 6.14. Strain level comparison between different GRLTP configurations.

| H= 9.15 m (30 ft), Spacing= 1.22 m (4 ft), No. Layers= 5, GRLTP thickness= 0.61m | | | H= 9.15 m (30 ft), Spacing= 1.22 m (4 ft), No. Layers= 7, GRLTP thickness= 0.915m | | |
|---|---|---|---|---|---|
| Layer No. | EA (Geogrids)= 375 kN/m | EA (Geogrids)= 420 kN/m | Layer No. | EA (Geogrids)= 375 kN/m | EA (Geogrids)= 420 kN/m |
| 1st Layer (GTX) | 5.42 | 5.25 | 1st Layer (GTX) | 4.65 | 4.45 |
| 2nd Layer (GGR) | 6.09 | 5.74 | 2nd Layer (GGR) | 5.55 | 4.95 |
| 3rd Layer (GGR) | 5.91 | 5.60 | 3rd Layer (GGR) | 5.12 | 4.76 |
| 4th Layer (GGR) | 5.23 | 5.01 | 4th Layer (GGR) | 4.42 | 4.12 |
| 5th Layer (GTX) | 5.56 | 5.35 | 5th Layer (GGR) | 3.95 | 3.67 |
| - | - | - | 6th Layer (GGR) | 3.87 | 3.58 |
| - | - | - | 7th Layer (GTX) | 4.16 | 3.76 |

It should be noted that no requirement is set on the lateral displacements near the toe of the embankment as the movement is in the foundation soil and does not appear on the ground surface. Meanwhile, excessive lateral displacements are not allowed if these movements cause a problem in the global stability of the system which was checked in the stability analysis. Table 6.15 shows the cost evaluation depending mainly on the required timber pile length per row to maintain a stable system with all requirements being satisfied. All the proposed pile spacing is included for the lowest embankment load (H= 3.05 m). For an embankment height of 6.1 m (20 ft), only the 1.22 m (4 ft) pile spacing is excluded as this pile spacing violated the settlement requirement. For the highest embankment load (H= 9.15m), only the 0.915 m (3 ft), and 1.22 m (4 ft) pile spacing are included as these two only satisfy the serviceability limit state requirements. For the 3.05 m (10 ft) and 6.10 m (20 ft) embankment heights, the 1.83 m (6 ft) resulted in the most economical

design for Case 2 soil profile. The same GRLTP configuration with the original tensile stiffness is adopted for the above-mentioned cases. Furthermore, the 9.15 m (30 ft) embankment load is suggested to be used with the 1.22 m (4 ft) pile spacing with increasing both the number of reinforcement layers and the axial stiffness to 7 layers, and to 420 kN/m, respectively.

Table 6.15. Cost evaluation for Case 2 soil profile.

| H (m) | Valid Pile Spacing (m) | Pile Length (m) | Number of Piles per Row | Total Required Pile length per Row (m) |
|---|---|---|---|---|
| 3.05 (10 ft) | 0.915 (3 ft) | 9.15 (30 ft) | 30 | 275 |
| | 1.220 (4 ft) | 9.15 (30 ft) | 22 | 202 |
| | 1.525 (5 ft) | 9.15 (30 ft) | 18 | 165 |
| | 1.830 (6 ft) | 9.76 (32 ft) | 15 | 147 |
| 6.10 (20 ft) | 0.915 (3 ft) | 9.15 (30 ft) | 46 | 421 |
| | 1.525 (5 ft) | 15.86 (52 ft) | 28 | 445 |
| | 1.830 (6 ft) | 15.86 (52 ft) | 24 | 381 |
| 9.15 (30 ft) | 0.915 (3 ft) | 15.86 (52 ft) | 60 | 952 |
| | 1.220 (4 ft) | 15.86 (52ft) | 44 | 698 |

It should also be noted that better performance is expected in the field than the performance predicted in this study. The timber piles will be installed in the very soft clay layer producing disturbance in the surrounding soil. Excess pore water pressure is induced due to pile driving (Hwang et al., 2001; Hunt et al., 2002; Orrje and Broms, 1967), depending on the distance between the piles and the soil type. Consolidation settlement will occur with the dissipation of excess pore water pressure, which is accompanied by the shear strength gain of the soft soil resulting in better performance than that of the original soil condition. In this study, the excess pore water pressure induced due to pile driving is assumed to be all dissipated, then the embankment is being constructed without taking into account the shear strength gain into the analysis. Furthermore, the lateral earth pressure coefficient of the soil is expected to increase due to pile driving. This increase

is expected to be in the range between one to twice the at-rest earth pressure coefficient for the NC soil case as reported by Meyerhof (1976) and Coduto (2001). An assumed value of $1.5K_0$, which is approximately equal to 1.0, is assumed to be evaluated for the very soft clay layer in Case 1 and Case 2. Results show no significant effect observed in the settlements, while the lateral displacement observed at the embankment toe is improved. Figure 6.72 shows the lateral displacement at the toe of embankment after 2 years of consolidation for the $K_0$ condition and the condition of $K_s$=1 for the 1.22 m (4 ft) pile spacing at the intermediate embankment load for both Case 1 and Case 2. Results show a significant reduction in the lateral displacement of 20.3 mm and 27.9 mm for Case 1 (Figure 6.72a) and Case 2 (Figure 6.72b), respectively. Lateral displacements observed at the highest embankment load (H= 9.15 m) are reported with $K_s$=1 for Case 1 and Case 2 due to the excessive lateral displacements observed in the FEM models.

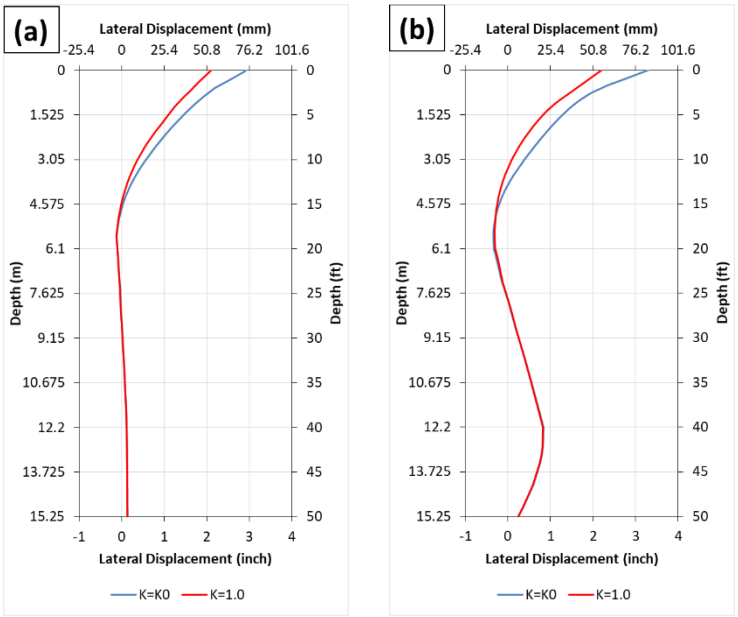


Figure 6.72. Lateral displacement at the embankment toe after 2 years of consolidation with an embankment height of 6.1 m and a pile spacing of 1.22 m for (a) Case 1; and (b) Case 2.

Moreover, heaving of the very soft clay layer near the embankment toe was observed in Cases 1 and 2 for all embankment heights and pile spacings. This is attributed to the movement of the slope

during the embankment construction and during the long-term life of the embankment. Figure 6.73 shows a comparison between the heave observed near the embankment toe after 2 years of consolidation for an embankment height of 3.05 m (10 ft) for both Cases 1 and 2 as they both have the same pile lengths for each pile spacing. Results show an increase in the soil heave with increasing the pile length for both cases (almost linear relationship with the pile spacing). In addition, heaving was larger in Case 1 than in Case 2 as the soil profile of Case consisted of another soft clay layer that was underneath the piles. Thus, the larger settlement experienced by all the pile spacing in Case 2 reduced the heaving compared to Case 1. However, no significant heaving is observed in each case (the maximum observed heaving is only 4.4 cm).

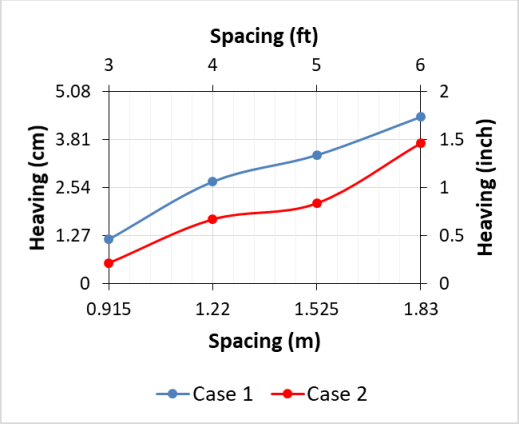


Figure 6.73. Heaving near the embankment toe after 2 years of consolidation vs. pile spacing comparison for an embankment height of 3.05 m for both Cases 1 and 2.

## 6.6. Case (3) Soil Profile

This section discusses the FEM parametric study for the soil profile of Case 3 (Figure 6.1c). The proposed three embankment heights (3.05 m (10 ft), 6.1 m (20 ft), and 9.15 m (30 ft)) will be analyzed in terms of the required pile length design, GRLTP and piles' extent under the embankment slope, and performance of the system by changing the center-to-center pile spacing.

### 6.6.1. Embankment Height (H)= 3.05 m (10 ft)

#### 6.6.1.1. Pile Design

Piles are designed to carry the whole embankment load plus the surcharge load for each corresponding pile spacing. Estimated factored loads are 77 kN, 137 kN, 214 kN, and 308 kN for 0.915 m (3 ft), 1.22 m (4 ft), 1.525 m (5 ft), and 1.83 m (6 ft) pile spacing, respectively. Table 6.16 shows the pile design information including the pile diameter (D) and pile length (L) for each corresponding pile spacing. The 0.915 m (3 ft) pile spacing satisfies the geotechnical capacity with a length of 10.07 m (33 ft), meaning that the pile penetrates the very loose sand layer and tips on the medium stiff clay. This is considered a floating pile as most of the capacity comes from the shaft resistance. Furthermore, the geotechnical capacity of the 1.22 m (4 ft) pile spacing is satisfied with a pile length of 11.59 m (38 ft), but it is suggested to increase the length so the pile will be tipped on the medium dense sand layer. The extra 0.61 m (twice the pile diameter) extension into the medium dense sand layer is to account for the irregularity of the soil layers in the field. For the rest of the proposed pile spacing, the piles are tipping on the middle of the medium dense sand layer and the dense sand layer for the 1.525 m (5 ft) and 1.83 m (6 ft), respectively.

Table 6.16. Pile Design for Case 3, H= 3.05 m (10 ft).

| Spacing | Pile Diameter (D) | Pile Length (L) |
|---|---|---|
| 0.915 m (3 ft) | 0.305 m (1 ft) | 10.07 m (33 ft) |
| 1.220 m (4 ft) | 0.305 m (1 ft) | 12.81 m (42 ft) |
| 1.525 m (5 ft) | 0.305 m (1 ft) | 13.73 m (45 ft) |
| 1.830 m (6 ft) | 0.305 m (1 ft) | 15.25 m (50 ft) |

#### 6.6.1.2. Stability Analysis

A stability analysis is conducted using PLAXIS 2D FEM software to investigate the stability of the system as well as investigating potential local and global failures with changing the GRLTP and piles' extent under the slope. A case of 4D pile spacing, 1.22 m (4 ft), with 5 layers of GRLTP is considered as a base case for the stability analysis. Meanwhile, the piles and GRLTP extent under the slope is varied as 0.0H, 0.5H, 1.0H, 1.5H, and 2.0H. Slope stability factor of safety is computed at the end of construction (EOC) and after 2 years of consolidation. Since the subsoil layer underneath the embankment is a very loose sand layer, there was no significant difference in the factor of safety for the short-term and long-term analyses (the difference is only $\pm 0.03$). Therefore, only the factor of safety for the long-term analysis is reported. It should be noted that the GRLTP edge will coincide with the exact computed distance, and the piles will be distributed on the computed distance (i.e., the distance between the GRLTP edge and the last pile edge will be governed by the pile spacing). Figure 6.74 through Figure 6.78 show the total displacement ($|u|$) observed in the embankment after two years of consolidation with all proposed GRLTP and piles' extent.

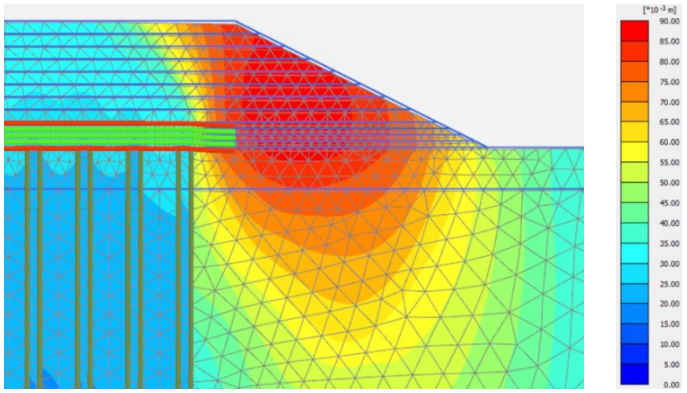


Figure 6.74. Total Displacement (m) after 2 years of consolidation for the case of 0.0H extension.

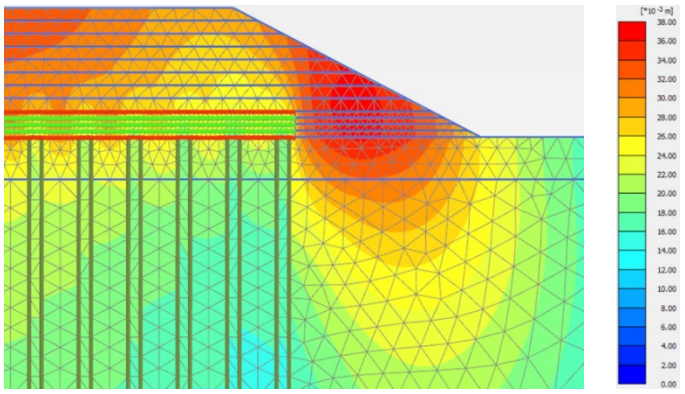


Figure 6.75. Total Displacement (m) after 2 years of consolidation for the case of 0.5H extension.

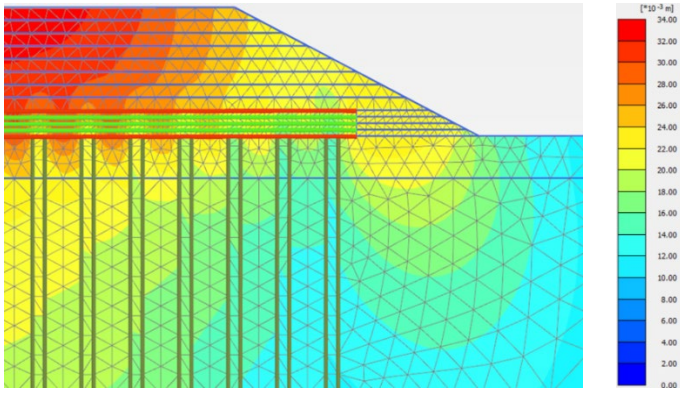


Figure 6.76. Total Displacement (m) after 2 years of consolidation for the case of 1.0H extension.

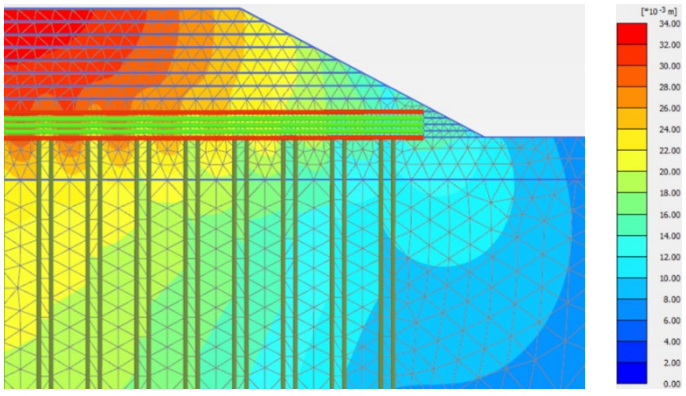


Figure 6.77. Total Displacement (m) after 2 years of consolidation for the case of 1.5H extension.

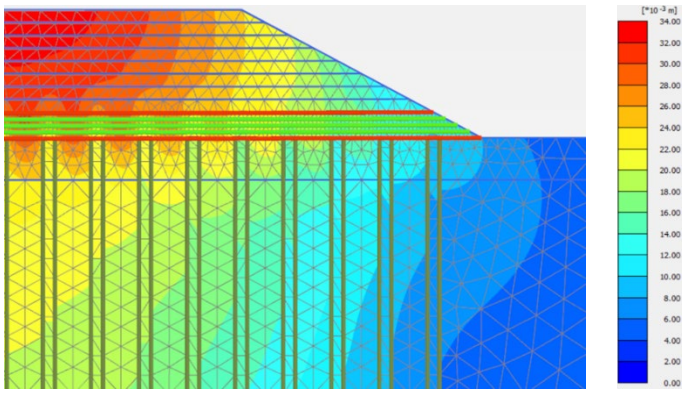


Figure 6.78. Total Displacement (m) after 2 years of consolidation for the case of 2.0H extension.

Figure 6.74 through Figure 6.78 are summarized in Figure 6.79, showing the maximum observed total displacement comparison after 2 years of consolidation. The maximum total displacement observed in the slope decreases significantly with increasing the supported distance with GRLTP and piles under the slope. For instance, the maximum observed total displacement at 0.0H and 2.0H are 8.9 cm and 1.2 cm, respectively. Furthermore, the slope stability factor of safety is evaluated for the system and is reported for the long-term condition (after 2 years of consolidation) in Table 6.17. No slope failure is observed for all the GRLTP and piles' extent (factor of safety $>$1.0). The minimum and maximum safety factors are 1.72 and 3.32 for an extent of 0.0H and 2.0H, respectively. Therefore, the extent of the GRLTP and the piles is chosen to be 0.0H (no support under the slope). Figure 6.80 shows the failure plane with an extent of 0.0H. Accordingly, the required number of piles per row is 20, 14, 12, and 10 for the 0.915 m, 1.22 m, 1.525 m, and 1.83 m pile spacing, respectively. It can also be noted that the existence of the very loose sand underneath the embankment has maintained a stable system with a smaller GRLTP and piles' extent than that of the very soft clay layer in Case 1 and 2 (GRLTP and piles' extent is 1.5H) under the same embankment height (H= 3.05 m).

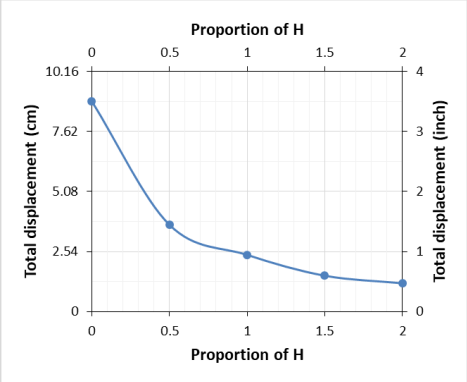


Figure 6.79. Maximum total displacement in the slope observed after 2 years of consolidation for the proposed GRLTP and piles' extent.

Table 6.17. Factor of safety for different GRLTP and piles' extent.

| GRLTP and Piles' Extent | Factor of Safety |
|---|---|
| 0.0H | 1.72 |
| 0.5H | 1.83 |
| 1.0H | 2.24 |
| 1.5H | 3.20 |
| 2.0H | 3.32 |

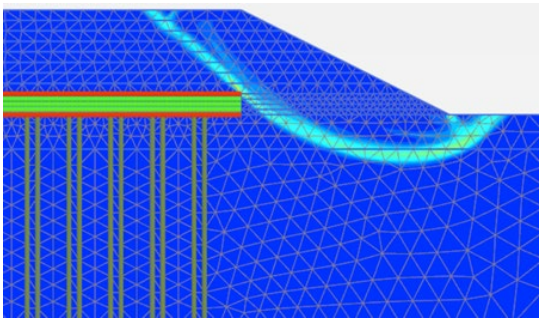

Figure 6.80. Failure plane after 2 years of consolidation for the adopted GRLTP and piles' extent of 0.0H extent

### 6.6.1.3. Spacing Parametric Study

The performance of the system is investigated with changing the center-to-center pile spacing with the GRLTP and the piles extended up to the crest of the embankment (no support under the slope).

Pile spacing will be ranged from 3D to 6D as follows: 0.915 m (3 ft), 1.22 m (4 ft), 1.525 m (5 ft), and 1.83 m (6 ft). The designed pile length for each corresponding pile spacing, from the smallest to the largest, is 10.07 m (33 ft), 12.81 m (42 ft), 13.73 m (45 ft), and 15.25 m (50 ft).

#### 6.6.1.3.1. Settlement

Figure 6.81 shows the settlement at the base of the embankment after 2 years of consolidation when the embankment is not supported by the piles and the GRLTP. Maximum settlement is observed under the embankment centerline of 38 cm which is way more than the settlement requirement of 15.24 cm. This confirms that a very loose sand layer underneath the embankment is problematic as 13 cm of the settlement is experienced by the very loose sand only with the lowest embankment load. Thus, the performance of the system will be investigated with the use of the pile foundation and the GRLTP. Figure 6.82 shows the settlement at the base of the embankment after 2 years of consolidation for the pile spacing 0.915 m (3 ft), 1.22 m (4 ft), 1.525 m (5 ft), and 1.83 m (6 ft) utilizing the GRLTP. The maximum observed settlement under the centerline of the embankment is 6.94 cm, 2.90 cm, 3.64 cm, and 4.52 cm for each corresponding spacing from the smallest to the largest. It can be observed that with increasing the pile length, the settlement at the very loose sand between the piles tends to increase except for the 0.915 m (3 ft), which experiences the maximum settlement among all pile spacing. This is attributed to the use of floating piles for the smallest pile spacing, whereas the piles of the rest of the proposed pile spacing are tipping on the medium dense sand and dense sand layers, so better performance is observed for these pile spacing. However, the unsupported zone under the slope experiences larger settlement compared to the supported area. This difference in performance is attributed to the improvement of the system due to the existence of the GRLTP and the pile foundation. The maximum settlement observed under the unsupported zone is 9.82 cm, 8.71 cm, 7.61 cm, and 8.03 cm for each corresponding

spacing from the smallest to the largest. Settlement in this area depends primarily on the distance of the last pile from the GRLTP edge, which coincides with the embankment crest. The distance between the edge of the GRLTP and the far edge of the last pile, $x$, is 0.305 m, 1.07 m, 0.61 m, and 0.762 m for each corresponding spacing from the smallest to the largest (Figure 6.83). This explains the larger settlement observed in the unsupported zone for the "4-ft" than the "5-ft", and "6-ft" pile spacing. Meanwhile, the 0.915 m (3 ft) pile spacing has the worst performance under the unsupported zone because of the floating piles existence.

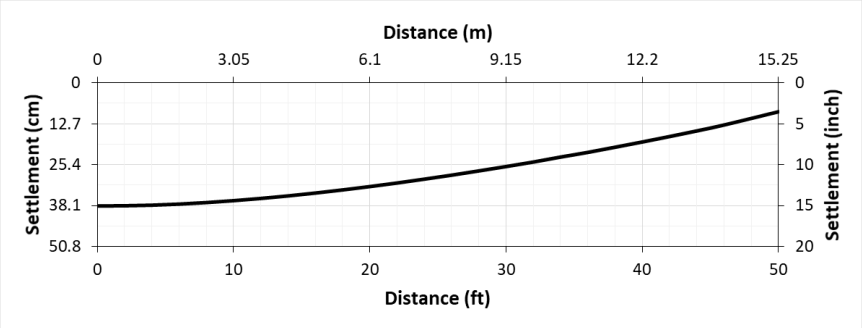


Figure 6.81. Settlement along the base of the embankment after 2 years of consolidation with no support under the embankment.

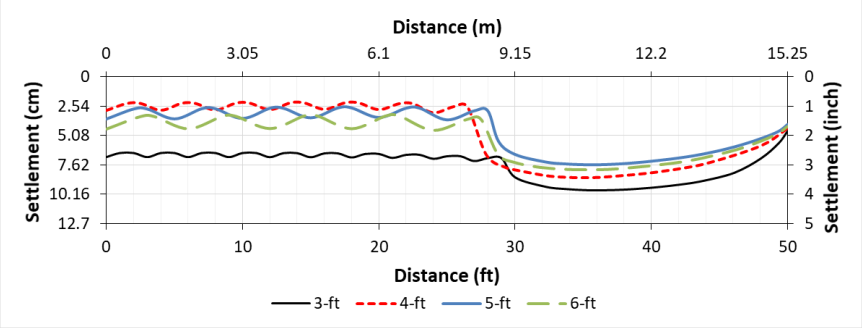


Figure 6.82. Settlement along the base of the embankment after 2 years of consolidation for each pile spacing.

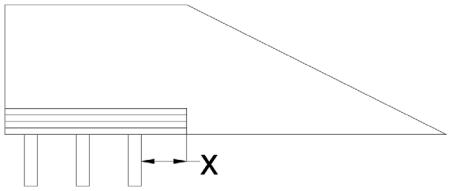


Figure 6.83. Distance, $x$, between the GRLTP edge and the far edge of the last pile.

Figure 6.84 shows the settlement with time for each pile spacing at the very loose sand between the piles under the embankment centerline, and at the pile head under the embankment centerline. Figure 6.84a and Figure 6.84b show a fast consolidation settlement rate. This is attributed to the inclusion of the GRLTP and the pile foundation in which the settlement is improved, and a faster consolidation rate is achieved. In addition, the fast dissipation of excess pore water pressure is the cause of the high hydraulic conductivities of the sand layers existing underneath the embankment and at the bottom of the model (i.e., the only source of the excess pore water pressure is the medium stiff clay layer). It can be noted that almost all excess pore water pressure is dissipated during the embankment construction for the 1.22 m (4 ft), 1.525 m (5 ft), and 1.83 m (6 ft) pile spacing as the average increase in the settlement between the end of construction (EOC) and the settlement observed at 40 days is only 0.6%. However, the 0.915 m (3 ft) pile spacing shows an increase in the settlement between the end of construction (EOC) and the settlement observed at 40 days of 35.5%. This may be attributed to the high excess pore water pressure for this pile spacing due to the use of floating piles.

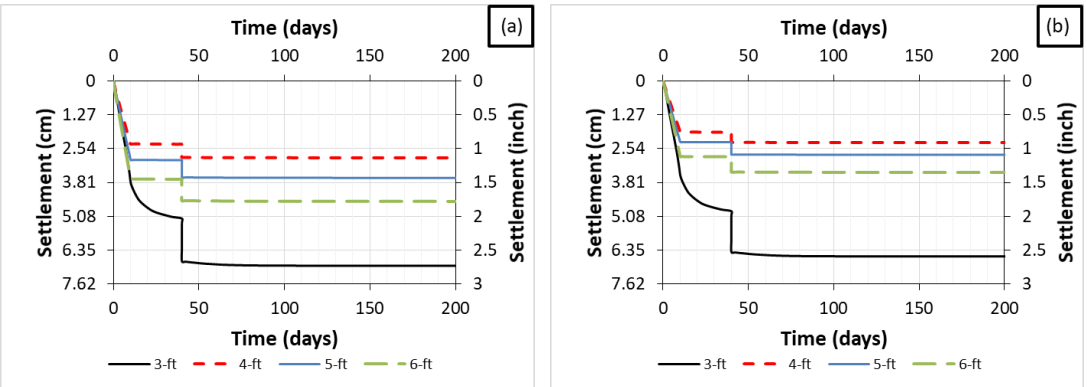


Figure 6.84. Settlement vs. time for each pile spacing at (a) the very loose sand between the piles at the embankment centerline; (b) the pile head under the embankment centerline.

#### 6.6.1.3.2. Excess Pore Water Pressure

Figure 6.85. shows the maximum excess pore water pressure induced due to embankment loading at two different locations: under the embankment centerline and under the unsupported zone at the middle of slope, both in the middle of the medium stiff clay layer. These values are observed at the end of construction (EOC). Results show that the excess pore water pressure values increase with the pile spacing increase under the supported area (where the foundation soil is supported by piles and the GRLTP) except for the 0.915 m (3 ft) pile spacing where piles are tipping on the medium stiff clay layer. In contrast, the excess pore water pressure in the unsupported area depends on the distance $x$ (Figure 6.83), in which the "4-ft" spacing has a larger $x$ distance resulting in higher excess pore water pressure as discussed in the settlement section above. Furthermore, the 0.915 m (3 ft) pile spacing has a higher value under the unsupported area due to the existence of the floating piles. Moreover, it can be noted that the induced pore water pressure at the centerline of the embankment due to the stress increase is lower than that in the unsupported area. This is attributed to the existence of the GRLTP and the pile foundation.

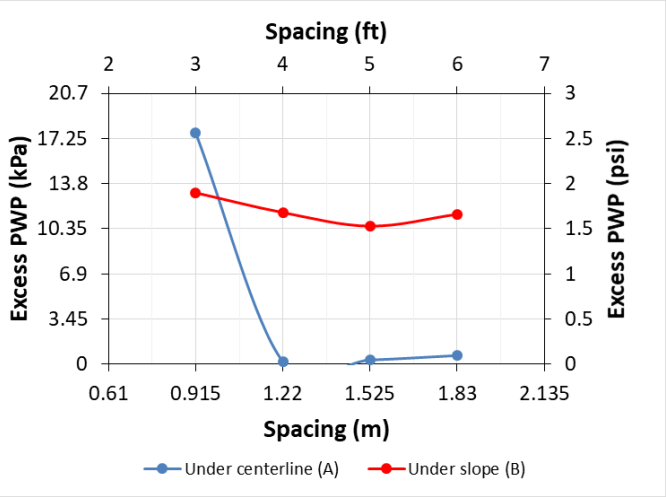


(a)

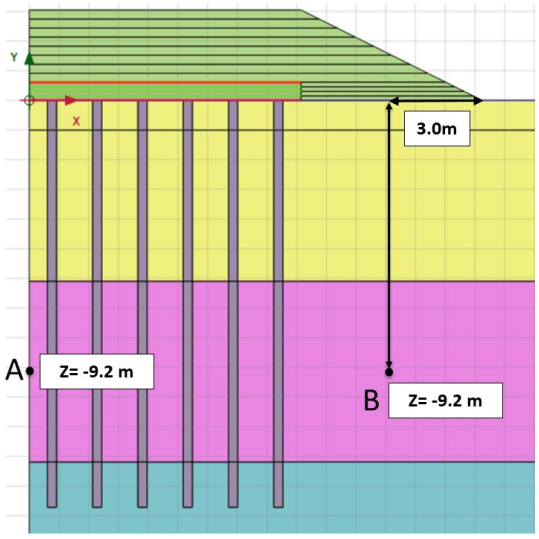


(b)

Figure 6.85. (a) Maximum excess pore water pressure observed at the end of construction under the centerline of the embankment (Point A), and the unsupported area (Point B); and (b) its location.

#### 6.6.1.3.3. Vertical Stress

Figure 6.86 shows vertical stress observed at the base of the embankment for the 1.83 m (6 ft) pile spacing at two different times: the end of construction (EOC), and after 2 years of consolidation. Results show higher vertical stress observed on the pile heads compared to the very loose sand between piles. It can also be noted that vertical stresses on top of piles are higher after 2 years of consolidation compared to vertical stresses observed at the EOC. Conversely, vertical stresses on the very loose sand between the piles are a little higher at the EOC than those after 2 years of consolidation. This is attributed to the arching effect as the load tends to be imposed on the rigid inclusions with the soil between the piles settling. This mechanism forms due to the shear resistance in the embankment material to resist movement downward. The SCR is found to be 8 and 12 at the end of construction and after 2 years of consolidation, respectively. These values almost fall within the lower range of the SCR reported by Han and Wayne (2000) of 10 to 30 for pile-supported embankments with timber piles and a GRLTP. Comparing the values determined

in Case 1 and 2 for the same embankment height and pile spacing (12 and 53 for Case 1, and 13 and 45 for Case 2), cohesionless soils show less arching effect than those of the soft cohesive soils.

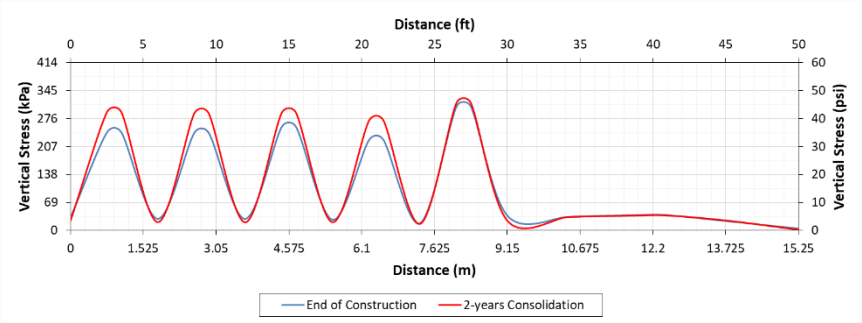


Figure 6.86. Vertical Stress along the base of the embankment at the end of construction (EOC) and after 2 years of consolidation.

### 6.6.1.3.4. Lateral Displacement

Figure 6.87 shows the lateral displacement profile along depth at the toe of the embankment after 2 years of consolidation. The maximum lateral displacement in all the pile spacing is observed at the beginning of the medium clay layer, whereas minor lateral displacements are observed in the cohesionless soils. Lateral displacement tends to become zero since the rest of the foundation soils are medium dense sand and dense sand layers with higher stiffness than the very loose sand and medium stiff clay layers. Furthermore, the soil mass near the ground surface for the 0.915 m (3 ft) pile spacing tends to move to the left due to the floating piles' configuration. The settlement experienced by the medium stiff clay layer under the supported zone is more than that under the unsupported area because piles transmitted more stresses to the medium stiff clay layer. Consequently, the soil mass tends to move downward and to the left because of the differential settlement between the supported and the unsupported zones. However, this is not observed for the rest of the proposed pile spacing as all piles are end bearing piles. Maximum observed lateral displacements are 12.15 mm, 13.48 mm, 11.10 mm, and 12.68 mm for the pile spacing from the smallest to the largest. The higher lateral displacement of the 1.22 (4 ft) pile spacing among all the

pile spacing with end bearing piles configuration is caused by the larger distance between the far edge of the last pile and the GRLTP edge for that pile spacing.

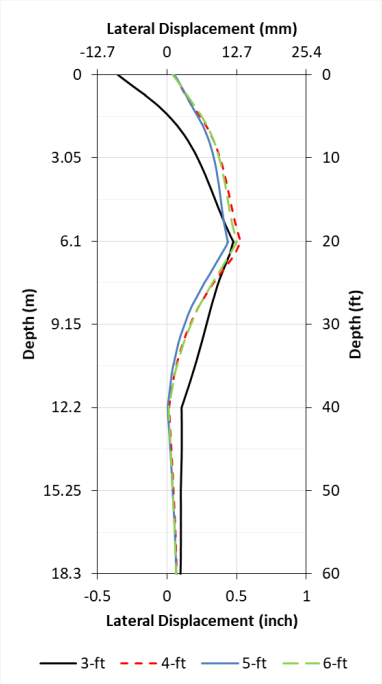


Figure 6.87. Lateral displacement profile along depth at the embankment toe after 2 years of consolidation.

### 6.6.1.3.5. Strain in Geosynthetics

Figure 6.88 shows the strain profile along the base of the embankment for the 1.83 m (6 ft) pile spacing after 2 years of consolidation for the 5 geosynthetic layers. Results show a peak-trough profile for all the geosynthetic layers. The peak is observed on top of the very loose sand between the piles for the bottom geotextile layer (Haring et al., 2008), whereas the peak is found on top of the pile heads for the rest of the geosynthetic layers. This may be attributed to the rigid support under the first geosynthetic layer in which the reinforcement layer is restrained from going downward with the embankment and GRLTP materials settling downward resulting in less deformation to the geosynthetic layer with minimal tension forces at these locations. However, the same geosynthetic layer would have a large curvature at the pile edge due to the lack of support at

that location resulting in maximum strain at the pile edges (Shen et al., 2018), which is extended to be on top of the very loose sand between the piles. This behavior is different from the rest of the geosynthetic layers as no rigid support restrains them from deformation with higher vertical stresses at the pile head due to the arching effect. Thus, maximum strain is expected to occur at the pile head. It can also be noted that the maximum strain percentage along each geosynthetic layer is observed near the end of the GRLTP because of the higher stresses experienced by the GRLTP due to differential settlement between the supported and unsupported zone. Figure 6.89 shows a closer look of the strain profile for the 1.83 m (6 ft) pile spacing in the 1st and 2nd geosynthetic layers.

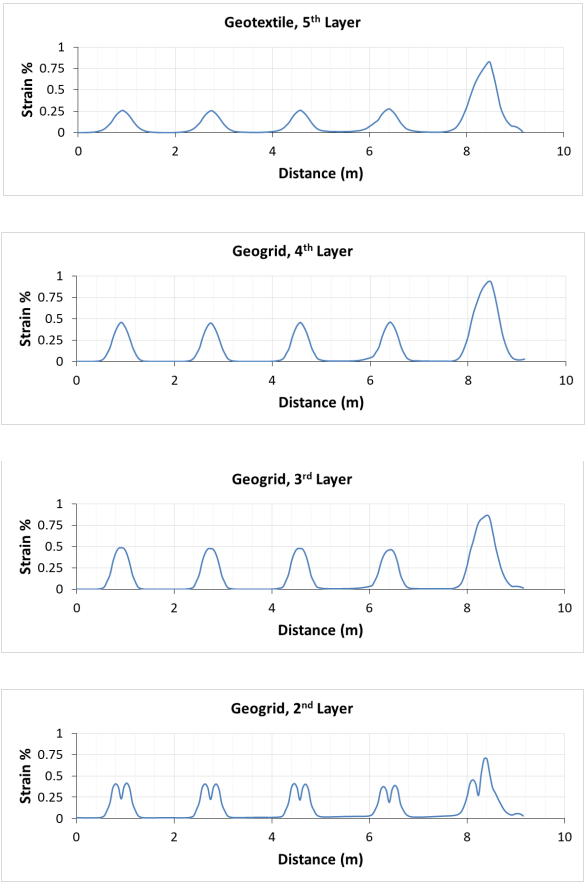

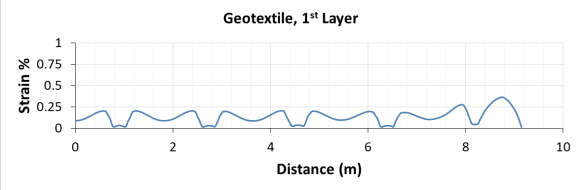


Figure 6.88. Strain profile along the base of embankment in the geosynthetic layers after 2 years of consolidation for the "6-ft" pile spacing.

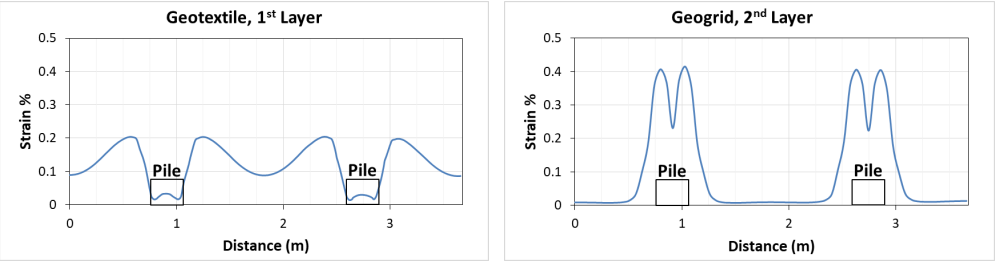


Figure 6.89. Closer look of the strain profile in the 1st and 2nd geosynthetic layers after 2 years of consolidation for the "6-ft" pile spacing.

Figure 6.90 shows the maximum strain observed in the geosynthetic layers after 2 years of consolidation for each pile spacing. The maximum strain among all the pile spacing is observed in the 1.22 m (4 ft) pile spacing because of the larger distance between the far edge of the last pile and the GRLTP edge for that pile spacing. However, almost a linear relationship between the strain in each layer and the corresponding pile spacing is expected if we exclude the 1.22 m (4 ft) pile spacing, meaning that the strain increases with increasing the pile spacing if all the last piles ended in the same location. Moreover, maximum observed strain is computed in the 3rd geosynthetic layer for the 1.22 m (4 ft) pile spacing which is 1.29%.

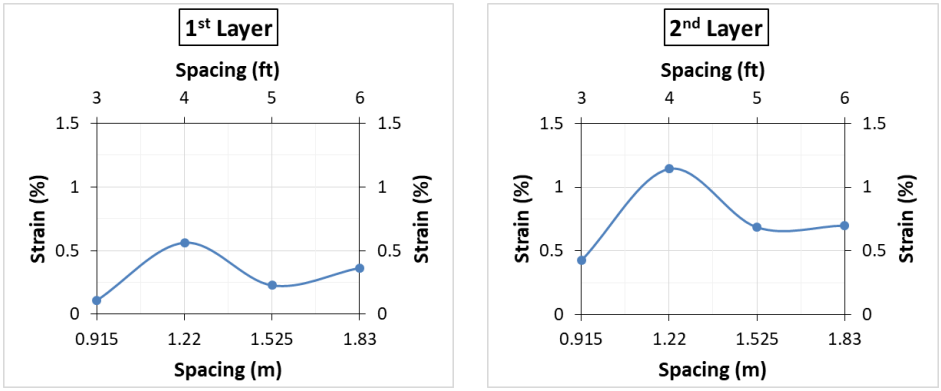

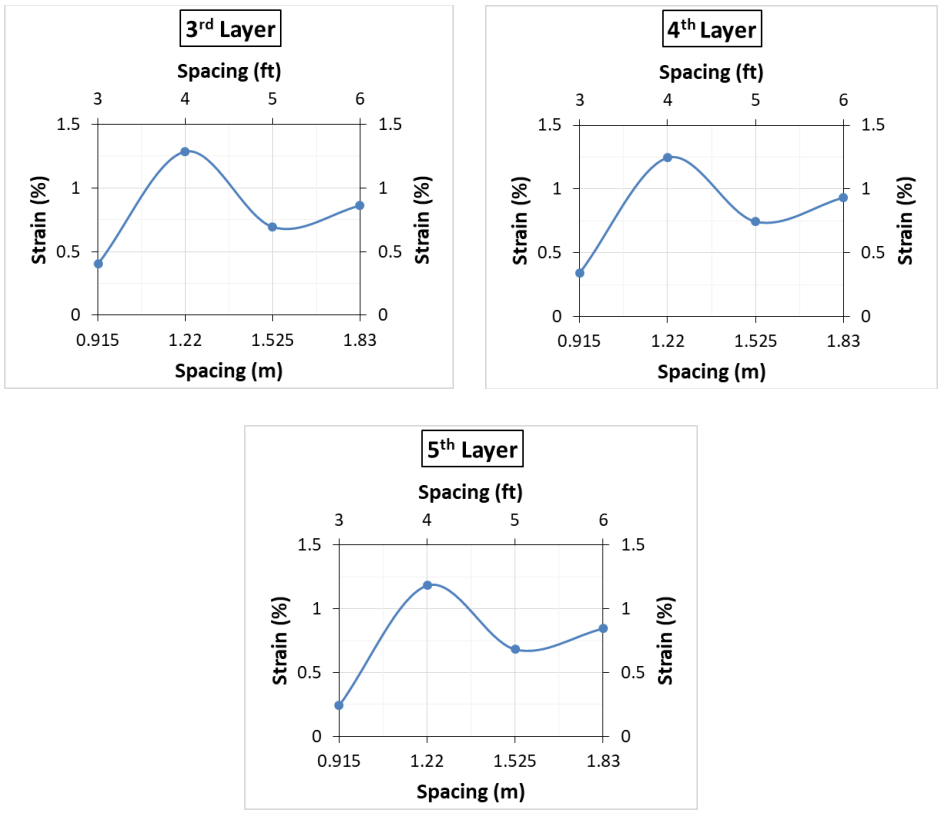


Figure 6.90. Maximum strain in geosynthetic layers for each pile spacing after 2 years of consolidation.

### 6.6.2. Embankment Height (H)= 6.10 m (20 ft)

#### 6.6.2.1. Pile Design

Piles are designed to carry the whole embankment load plus the surcharge load for each corresponding pile spacing. Estimated factored loads are 138 kN, 246 kN, 384 kN, and 552 kN for 0.915 m (3 ft), 1.22 m (4 ft), 1.525 m (5 ft), and 1.83 m (6 ft) pile spacing, respectively. Table 6.18 shows the pile design information including the pile diameter (D) and pile length (L) for each corresponding pile spacing. The 0.915 m (3 ft) pile spacing satisfies the geotechnical capacity at a length of 12.2 m (40 ft), but it is extended a distance of twice the diameter of the pile to account for the irregularity of the soil layers in the field. However, the 1.525 m (5 ft) pile spacing is not extended the same way as the overlaying layer is a medium dense sand layer. For this embankment

height, all the piles are end bearing piles tipping on either the medium dense sand or the dense sand layer.

Table 6.18. Pile Design for Case 3, H= 6.10 m (20 ft).

| Spacing | Pile Diameter (D) | Pile Length (L) |
|---|---|---|
| 0.915 m (3 ft) | 0.305 m (1 ft) | 12.81 m (42 ft) |
| 1.220 m (4 ft) | 0.305 m (1 ft) | 14.64 m (48 ft) |
| 1.525 m (5 ft) | 0.305 m (1 ft) | 15.25 m (50 ft) |
| 1.830 m (6 ft) | 0.305 m (1 ft) | 15.86 m (52 ft) |

**6.6.2.2. Stability Analysis**

A stability analysis is conducted to investigate the stability of the system as well as investigating potential local and global failures with changing the GRLTP and piles' extent under the slope. A case of 4D pile spacing, 1.22 m (4 ft), with 5 layers of GRLTP is considered a base case for the stability analysis. Meanwhile, the piles and GRLTP extent under the slope is varied as 0.0H, 0.5H, 1.0H, 1.5H, and 2.0H. The slope stability factor of safety is computed at the end of construction (EOC) and after 2 years of consolidation. Since the subsoil layer underneath the embankment is a very loose sand layer, there was no significant difference in the factor of safety for the short-term and long-term analyses (the difference is only $\pm 0.03$). Therefore, only the factor of safety for the long-term analysis is reported. Figure 6.91 through Figure 6.95 show the total displacement ($|u|$) observed in the embankment after two years of consolidation with all proposed GRLTP and piles' extent.

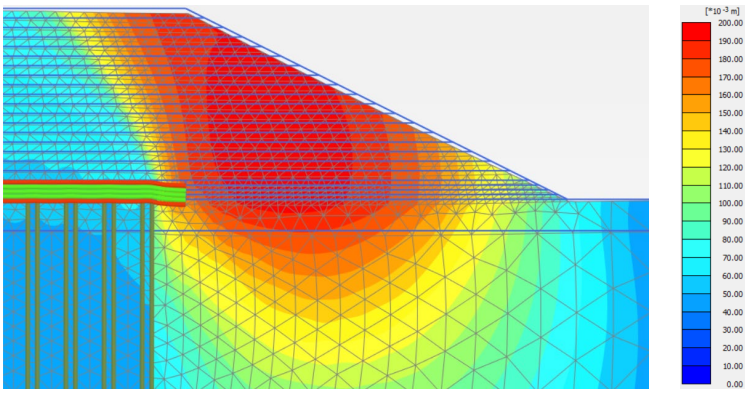


Figure 6.91. Total Displacement (m) after 2 years of consolidation for the case of 0.0H extension.

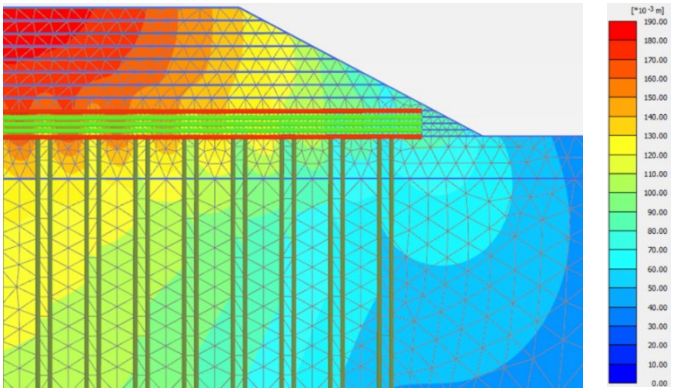


Figure 6.92. Total Displacement (m) after 2 years of consolidation for the case of 0.5H extension.

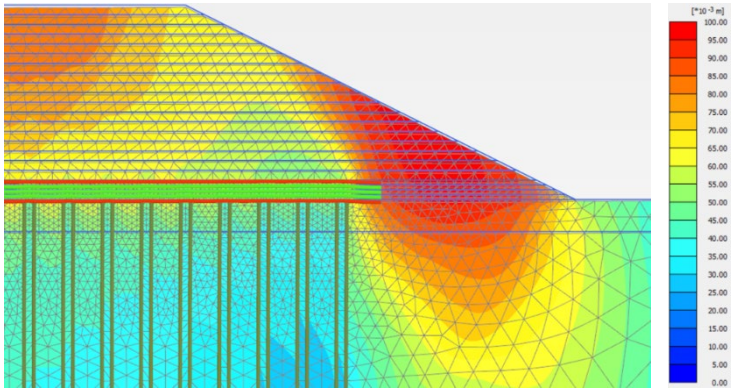


Figure 6.93. Total Displacement (m) after 2 years of consolidation for the case of 1.0H extension.

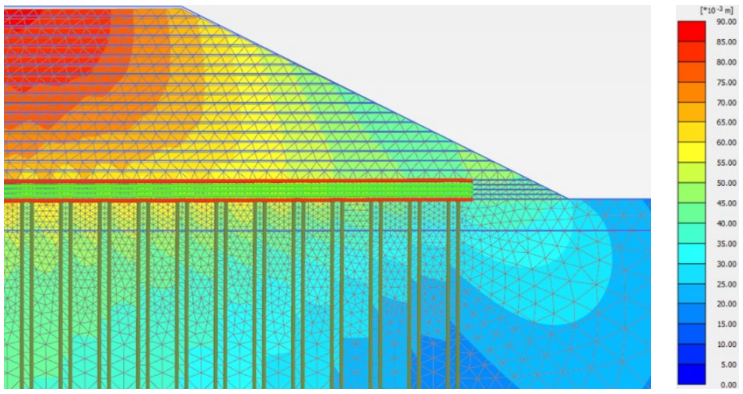

Figure 6.94. Total Displacement (m) after 2 years of consolidation for the case of 1.5H extension.

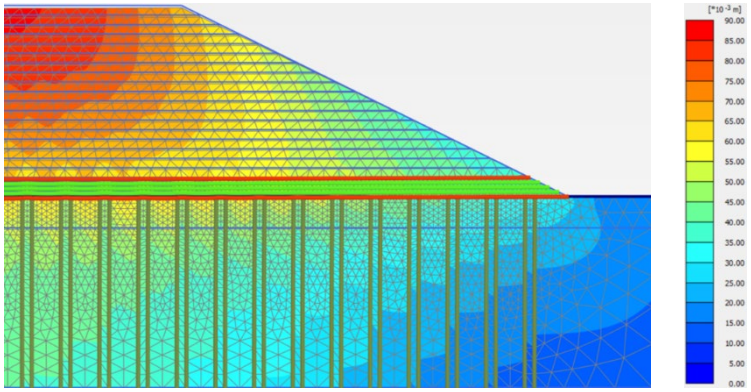

Figure 6.95. Total Displacement (m) after 2 years of consolidation for the case of 2.0H extension.

Figure 6.91 through Figure 6.95 are summarized in Figure 6.96, showing the maximum observed total displacement comparison after 2 years of consolidation. The maximum total displacement observed in the slope decreases significantly with increasing the supported distance with GRLTP and piles under the slope. For instance, the maximum observed total displacement at 0.0H and 2.0H are 20 cm and 4 cm, respectively. Furthermore, the slope stability factor of safety is evaluated for the system and is reported for the long-term condition (after 2 years of consolidation) in Table 6.19. No slope failure is observed for all the GRLTP and piles' extent (factor of safety >1.0). The minimum and maximum safety factors are 1.22 and 2.24 for an extent of 0.0H and 2.0H, respectively. Both the 0.0H and the 0.5H GRLTP and piles' extent violate the stability analysis

requirement (factor of safety > 1.5). Therefore, the extent of the GRLTP and the piles is chosen to be 1.0H (mid-slope). Figure 6.97 shows the failure plane with an extent of 1.0H. Accordingly, the required number of piles per row is 34, 24, 20, and 17 for the 0.915 m, 1.22 m, 1.525 m, and 1.83 m pile spacing, respectively. It can be also noted that the existence of the very loose sand underneath the embankment has maintained a stable system with less GRLTP and piles' extent than that of the very soft clay layer in Case 1 and 2 (GRLTP and piles' extent is 2.0H) under the same embankment height (H= 6.1 m).

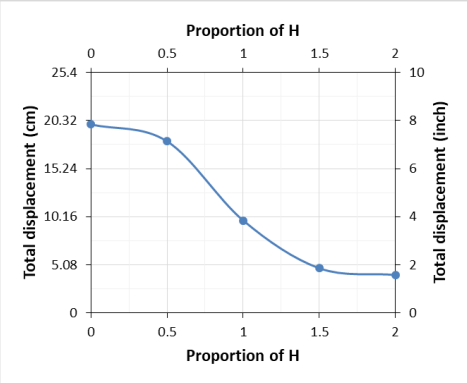


Figure 6.96. Maximum total displacement in the slope observed after 2 years of consolidation for the proposed GRLTP and piles' extent.

Table 6.19. Factor of safety for different GRLTP and piles' extent.

| GRLTP and Piles' Extent | Factor of Safety |
|---|---|
| 0.0H | 1.22 |
| 0.5H | 1.48 |
| 1.0H | 1.65 |
| 1.5H | 2.14 |
| 2.0H | 2.24 |

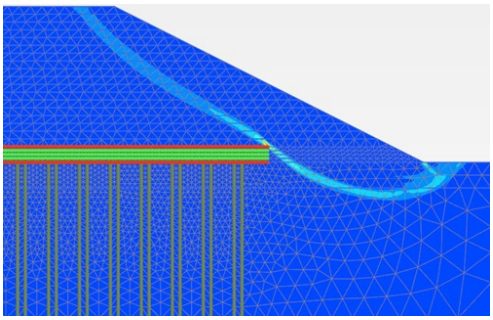

Figure 6.97. Failure plane after 2 years of consolidation for the adopted GRLTP and piles' extent of 0.0H extent

#### 6.6.2.3. Spacing Parametric Study

The performance of the system is investigated with changing the center-to-center pile spacing with the GRLTP and the piles extended up mid-slope area (1.0H). Pile spacing will be ranged from 3D to 6D as follows: 0.915 m (3 ft), 1.22 m (4 ft), 1.525 m (5 ft), and 1.83 m (6 ft). The designed pile length for each corresponding pile spacing, from the smallest to the largest, is 12.81 m (42 ft), 14.64 m (48 ft), 15.25 m (50 ft), and 15.86 m (52 ft).

##### 6.6.2.3.1. Settlement

Figure 6.98 shows the settlement at the base of the embankment after 2 years of consolidation for the pile spacing 0.915 m (3 ft), 1.22 m (4 ft), 1.525 m (5 ft), and 1.83 m (6 ft) utilizing the GRLTP. The maximum observed settlement under the centerline of the embankment is 5.25 cm, 6.10 cm, 8.02 cm, and 10.29 cm for each corresponding spacing from the smallest to the largest. It can be observed that with increasing the pile length, the settlement at the very loose sand between the piles tends to increase as well. Less settlement is observed under the unsupported zone than the supported area as the stress increase under the GRLTP is more significant than that under the slope with an extent of 1.0H of GRLTP and piles (i.e., the unsupported area carries a small embankment load). The maximum settlement observed under the unsupported zone is 2.67 cm, 3.59 cm, 3.25 cm, and 3.28 cm for each corresponding spacing from the smallest to the largest. Settlement in this

area depends primarily on the distance of the last pile from the GRLTP edge, which coincides with the middle of the slope. The distance between the edge of the GRLTP and the far edge of the last pile, $x$, is 0.0 m, 1.07 m, 0.61 m, and 0.46 m for each corresponding spacing from the smallest to the largest (Figure 6.99). This explains the larger settlement observed in the unsupported zone for the "4-ft" than the "5-ft", and "6-ft" pile spacing. Meanwhile, the "5-ft", and "6-ft" pile spacing have almost the same settlement.

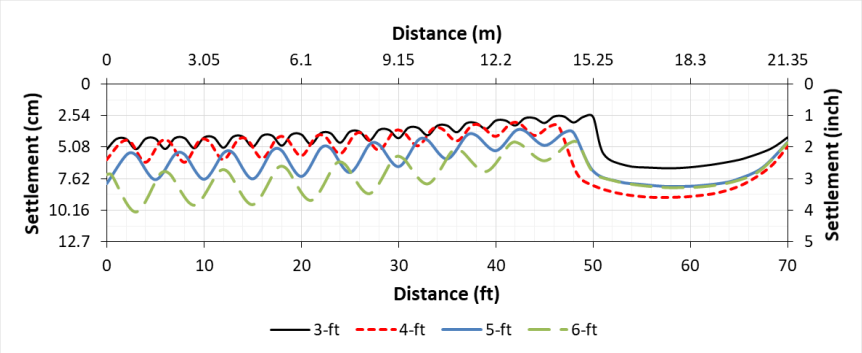


Figure 6.98. Settlement along the base of embankment after 2 years of consolidation for each pile spacing.

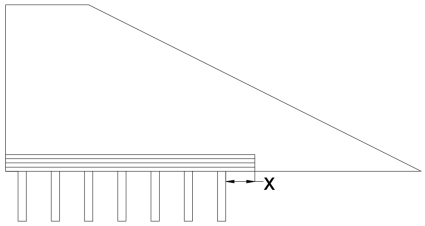


Figure 6.99. Distance, $x$, between the GRLTP edge and the far edge of the last pile.

Figure 6.100 shows the settlement with time for each pile spacing at the very loose sand between the piles under the embankment centerline, and at the pile head under the embankment centerline. Both Figure 6.100a and Figure 6.100b show a fast consolidation settlement rate. This is attributed to the inclusion of the GRLTP and the pile foundation in which the settlement is improved, and a faster consolidation rate is achieved. In addition, the fast dissipation of excess pore water pressure is the cause of the high hydraulic conductivities of the sand layers existing underneath the

embankment and at the bottom of the model (i.e., the only source of the excess pore water pressure is the medium stiff clay layer). For instance, 99% of the maximum settlement observed in the very loose sand layer is achieved after 50 days.

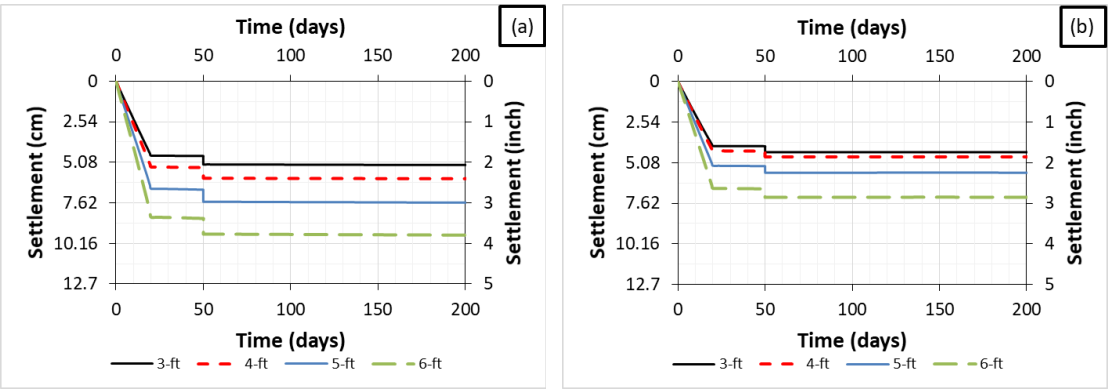


Figure 6.100. Settlement vs. time for each pile spacing at (a) the very loose sand between the piles at the embankment centerline; (b) the pile head under the embankment centerline.

### 6.6.2.3.2. Excess Pore Water Pressure

Figure 6.101. shows the maximum excess pore water pressure induced due to embankment loading at two different locations: under the embankment centerline and under the unsupported zone at the middle of slope, both in the middle of the medium stiff clay layer. These values are observed at the end of construction (EOC). Results show that the excess pore water pressure values increase with the pile spacing increase under the supported area (where the foundation soil is supported by piles and the GRLTP). In contrast, the excess pore water pressure in the unsupported area depends on the distance $x$ (Figure 6.99) resulting in very close results for the "4-ft", "5-ft", and "6-ft" pile spacing with the smallest for the "3-ft" pile spacing as the $x$ distance is zero. Moreover, it can be noted that the induced pore water pressure at the centerline of the embankment due to the stress increase is lower than that in the unsupported area. This is attributed to the existence of the GRLTP and the pile foundation.

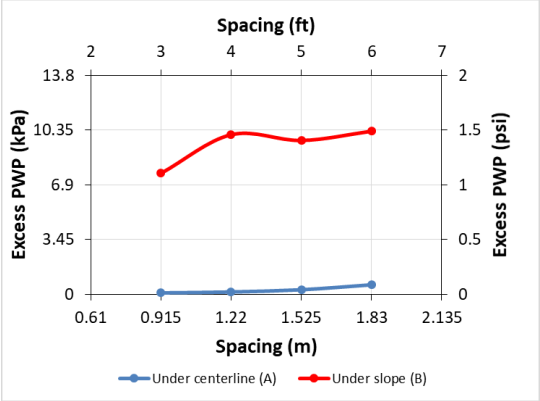


(a)

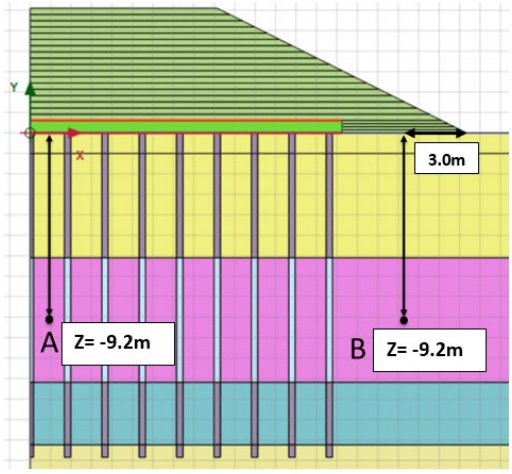


(b)

Figure 6.101. (a) Maximum excess pore water pressure observed at the end of construction under the centerline of the embankment (Point A), and the unsupported area (Point B); and (b) its location.

### 6.6.2.3.3. Vertical Stress

Figure 6.102 shows vertical stress observed at the base of the embankment for the 1.83 m (6 ft) pile spacing at two different times: the end of construction (EOC), and after 2 years of consolidation. Results show higher vertical stress observed on the pile heads compared to the very loose sand between piles. It can also be noted that vertical stresses on top of piles are higher after 2 years of consolidation than those observed at the EOC. Conversely, vertical stresses on the very loose sand between the piles are almost the same at the EOC and after 2 years of consolidation.

The SCR is found to be 11 and 12 at the end of construction and after 2 years of consolidation, respectively. These values fall within the lower range of the SCR reported by Han and Wayne (2000) of 10 to 30 for pile-supported embankments with timber piles and a GRLTP. Comparing the values determined in Case 1 and 2 for the same embankment height and pile spacing (20 and 36 for Case 1, and 21 and 30 for Case 2), cohesionless soils show less arching effect than those of the soft cohesive soils with no significant arching occurring after the EOC (i.e., the SCR is so close between the EOC and after 2 years of consolidation).

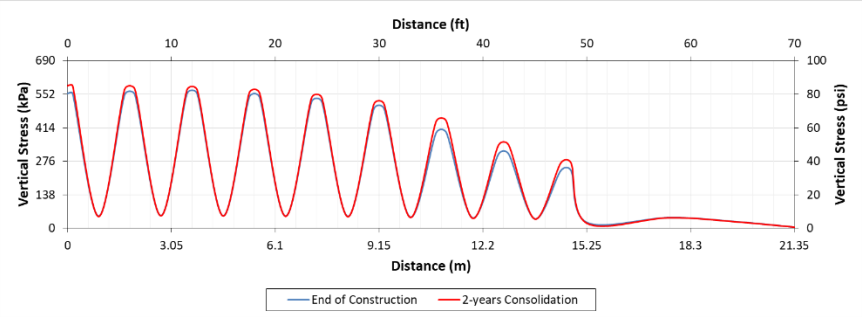


Figure 6.102. Vertical Stress along the base of the embankment at the end of construction (EOC) and after 2 years of consolidation.

#### 6.6.2.3.4. Lateral Displacement

Figure 6.103 shows the lateral displacement profile along depth at the toe of the embankment after 2 years of consolidation. The lateral displacement is at its greatest at the middle of the very loose sand layer and starts to decrease with increasing depth, starting with the medium stiff clay layer. Then the lateral displacement decreases rapidly at the location of the medium dense sand and dense sand layers where the lateral displacement is almost zero. Maximum observed lateral displacements are 9.78 mm, 16.43 mm, 17.47 mm, and 20.60 mm for the pile spacing from the smallest to the largest.

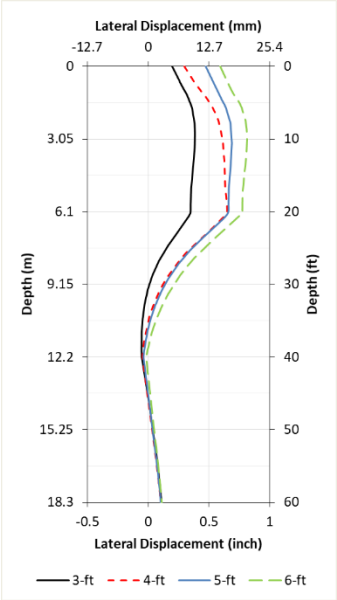


Figure 6.103. Lateral displacement profile along depth at the embankment toe after 2 years of consolidation.

### 6.6.2.3.5. Strain in Geosynthetics

Figure 6.104 shows the strain profile along the base of the embankment for the 1.83 m (6 ft) pile spacing after 2 years of consolidation for the 5 geosynthetic layers. Results show a peak-trough profile for all the geosynthetic layers. The peak is observed on top of the very loose sand between the piles for the bottom geotextile layer (1$^{st}$ layer), whereas the peak is found on top of the pile heads for the rest of the geosynthetic layers as observed before. All layers show an abrupt change in the strain at the pile edges. It can also be noted that the maximum strain percentage along each geosynthetic layer is observed almost at the middle of the embankment where the maximum load exists. Figure 6.105 shows a closer look of the strain profile for the 1.83 m (6 ft) pile spacing in the 1$^{st}$ and 2$^{nd}$ geosynthetic layers.

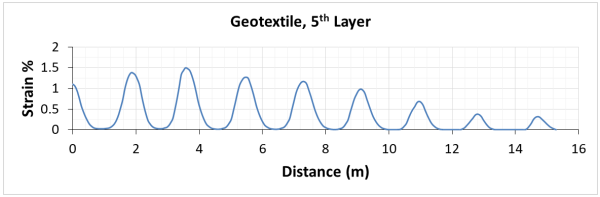

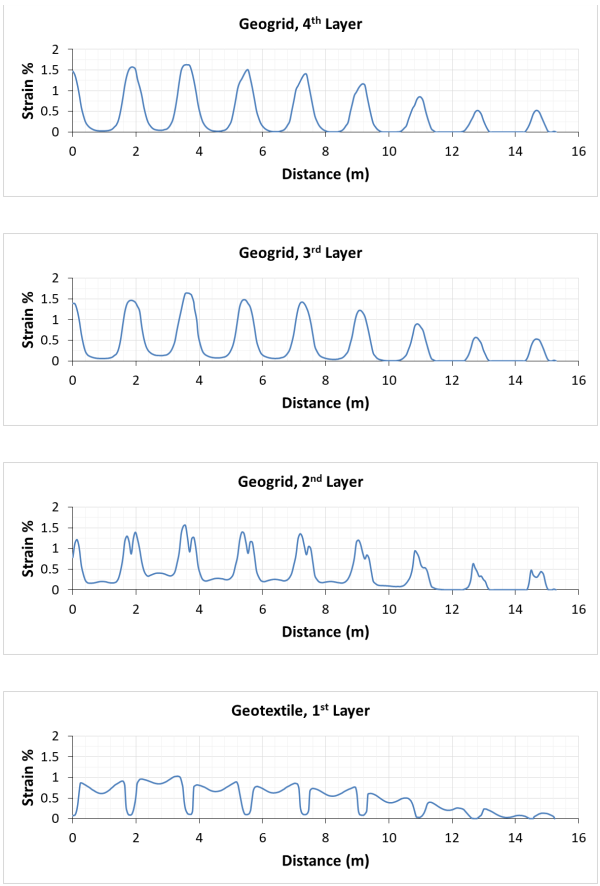


Figure 6.104. Strain profile along the base of embankment in the geosynthetic layers after 2 years of consolidation for the "6-ft" pile spacing.

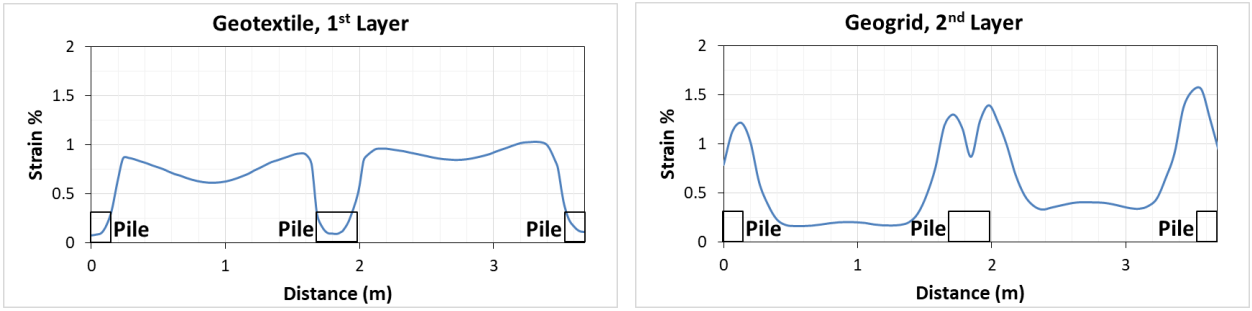


Figure 6.105. Closer look of the strain profile in the 1st and 2nd geosynthetic layers after 2 years of consolidation for the "6-ft" pile spacing.

Figure 6.106 shows the maximum strain observed in the geosynthetic layers after 2 years of consolidation for each pile spacing. All the layers have a nearly linear relationship between the strain in each layer and the corresponding pile spacing. Strain levels are way less than the maximum allowable limit (5%) compared to the same embankment load in Cases 1 and 2 in which

the strain almost reached the maximum allowable limit. Maximum observed strain is computed in the 4th geosynthetic layer for the 1.83 m (6 ft) pile spacing which is 1.64%.

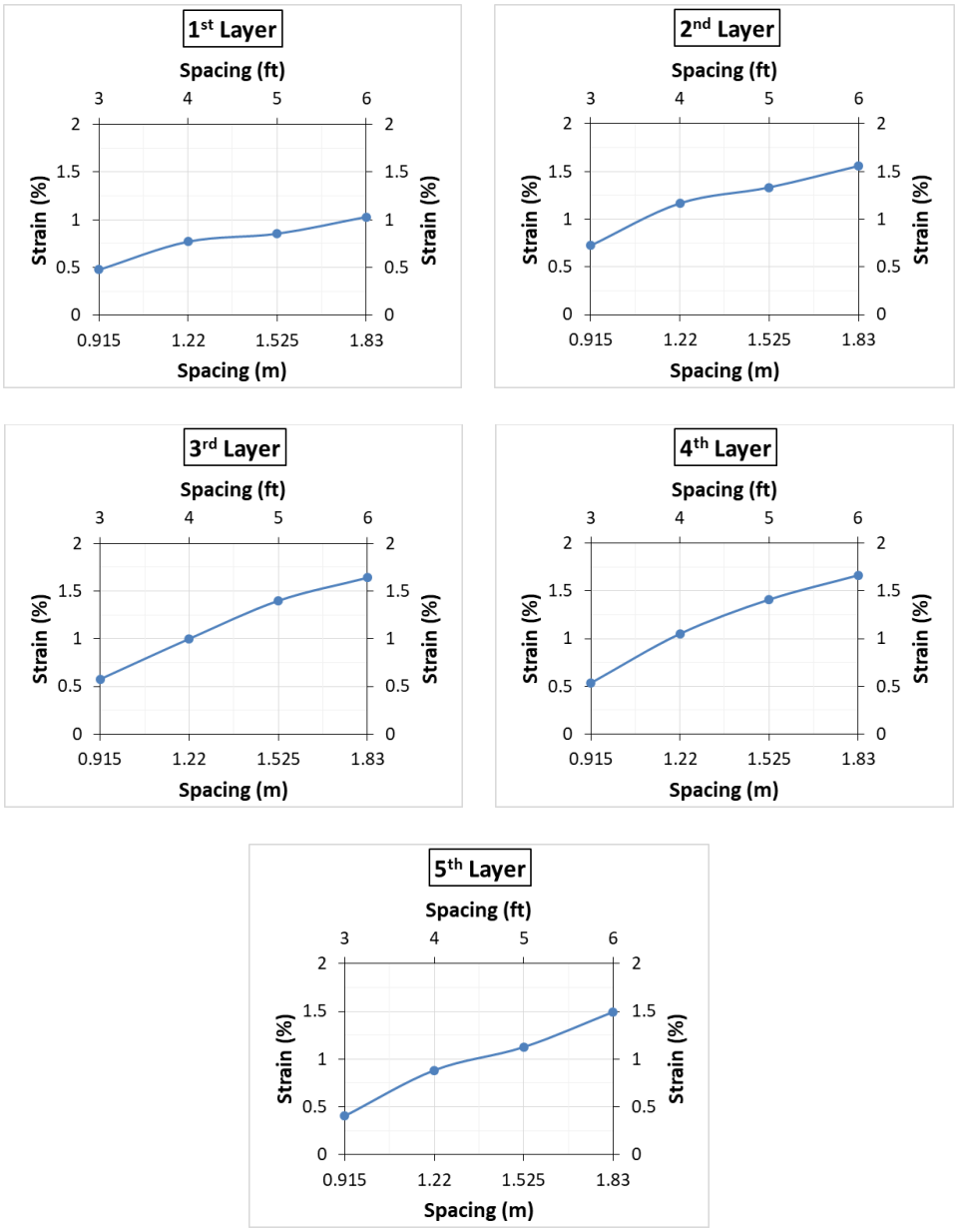


Figure 6.106. Maximum strain in geosynthetic layers for each pile spacing after 2 years of consolidation.

### 6.6.3. Embankment Height (H)= 9.15 m (30 ft)

#### 6.6.3.1. Pile Design

Piles are designed to carry the whole embankment load plus the surcharge load for each corresponding pile spacing. Estimated factored loads are 196 kN, 348 kN, 543 kN, and 782 kN for 0.915 m (3 ft), 1.22 m (4 ft), 1.525 m (5 ft), and 1.83 m (6 ft) pile spacing, respectively. Table 6.20 shows the pile design information including the pile diameter (D) and pile length (L) for each corresponding pile spacing. For this embankment height, all the piles are end bearing piles tipping on either the medium dense sand or the dense sand layer.

Table 6.20. Pile Design for Case 3, H= 9.15 m (30 ft).

| Spacing | Pile Diameter (D) | Pile Length (L) |
|---|---|---|
| 0.915 m (3 ft) | 0.305 m (1 ft) | 13.16 m (43 ft) |
| 1.220 m (4 ft) | 0.305 m (1 ft) | 15.25 m (50 ft) |
| 1.525 m (5 ft) | 0.305 m (1 ft) | 15.86 m (52 ft) |
| 1.830 m (6 ft) | 0.305 m (1 ft) | 18.91 m (62 ft) |

#### 6.6.3.2. Stability Analysis

A stability analysis is conducted to investigate the stability of the system as well as investigating potential local and global failures with changing the GRLTP and piles' extent under the slope. A case of 4D pile spacing, 1.22 m (4 ft), with 5 layers of GRLTP is considered a base case for the stability analysis. Meanwhile, the piles and GRLTP extent under the slope is varied as 1.0H, 1.5H, and 2.0H. An extent of 0.0H and 0.5H are excluded as they do not satisfy the stability requirement for the lower embankment height. Figure 6.107 through Figure 6.109 show the total displacement ($|u|$) observed in the embankment after two years of consolidation with all proposed GRLTP and piles' extent.

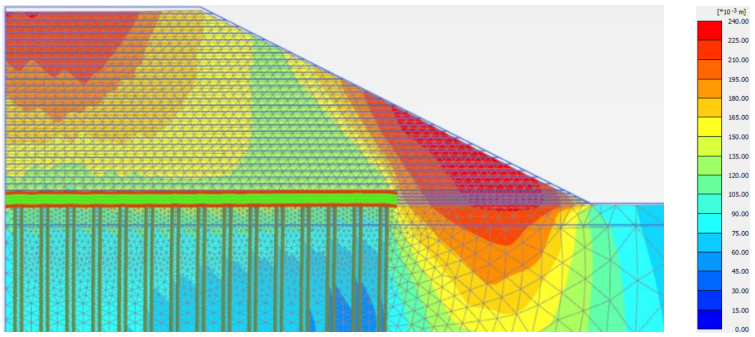

Figure 6.107. Total Displacement (m) after 2 years of consolidation for the case of 1.0H extension.

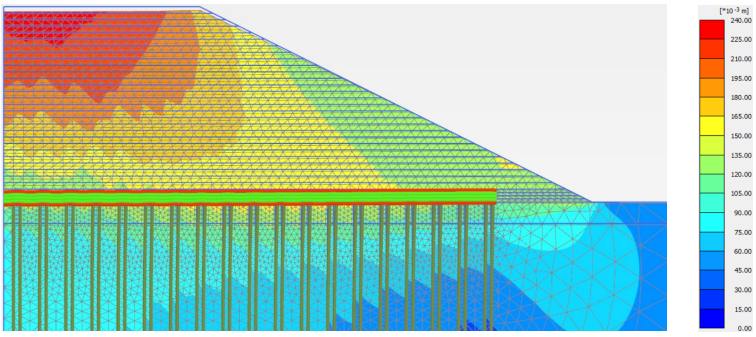

Figure 6.108. Total Displacement (m) after 2 years of consolidation for the case of 1.5H extension.

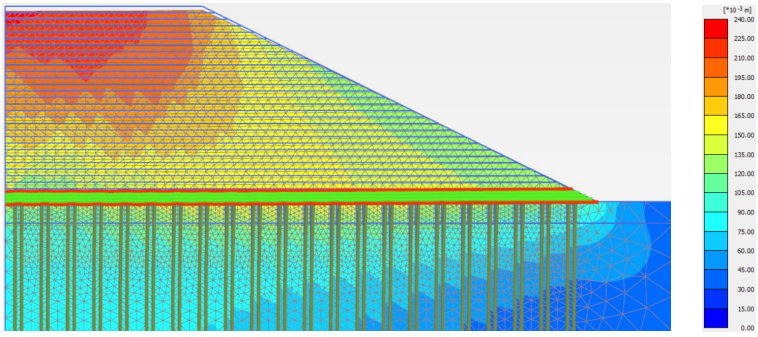

Figure 6.109. Total Displacement (m) after 2 years of consolidation for the case of 2.0H extension.

Figure 6.107 through Figure 6.109 are summarized in Figure 6.110, showing the maximum observed total displacement comparison after 2 years of consolidation. The maximum total displacement observed in the slope decreases significantly with increasing the supported distance with GRLTP and piles under the slope. For instance, the maximum observed total displacement at

1.0H and 2.0H is 23 cm and 13 cm, respectively. Furthermore, slope stability factor of safety is evaluated for the system and is reported for the long-term condition (after 2 years of consolidation) in Table 6.21. No slope failure is observed for all the GRLTP and piles' extent (factor of safety >1.0). The minimum and maximum safety factors are 1.43 and 1.96 for an extent of 1.0H and 2.0H, respectively. The 1.0H GRLTP and piles' extent violates the stability analysis requirement (factor of safety > 1.5). Therefore, the extent of the GRLTP and the piles is chosen to be 1.5H (three-quarters of the slope). Figure 6.111 shows the failure plane with an extent of 1.5H. Accordingly, the required number of piles per row is 50, 38, 30, and 25 for the 0.915 m, 1.22 m, 1.525 m, and 1.83 m pile spacing, respectively. It can also be noted that the existence of the very loose sand underneath the embankment has maintained a stable system with less GRLTP and piles' extent than that of the very soft clay layer in Case 1 and 2 (GRLTP and piles' extent is 2.0H) under the same embankment height (H= 9.15 m).

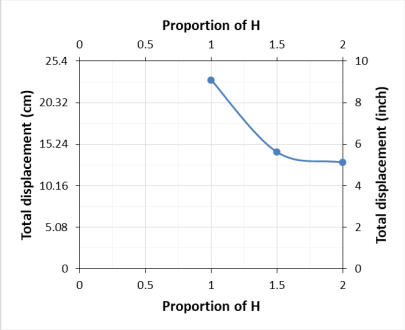


Figure 6.110. Maximum total displacement in the slope observed after 2 years of consolidation for the proposed GRLTP and piles' extent.

Table 6.21. Factor of safety for different GRLTP and piles' extent.

| GRLTP and Piles' Extent | Factor of Safety |
|---|---|
| 1.0H | 1.43 |
| 1.5H | 1.80 |
| 2.0H | 1.96 |

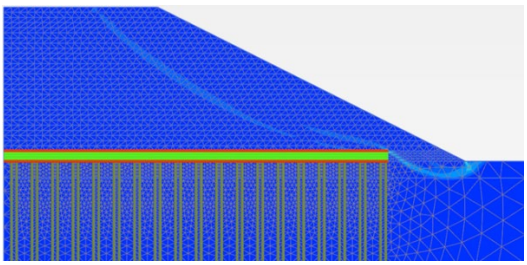

Figure 6.111. Failure plane after 2 years of consolidation for the adopted GRLTP and piles' extent of 0.0H extent

#### 6.6.3.3. Spacing Parametric Study

The performance of the system is investigated with changing the center-to-center pile spacing where the GRLTP and the piles extended up mid-slope area (1.0H). Pile spacing will be ranged from 3D to 6D as follows: 0.915 m (3 ft), 1.22 m (4 ft), 1.525 m (5 ft), and 1.83 m (6 ft). The designed pile length for each corresponding pile spacing, from the smallest to the largest, is 13.16 m (43 ft), 15.25 m (50 ft), 15.86 m (52 ft), and 18.91 m (62 ft).

##### 6.6.3.3.1. Settlement

Figure 6.112 shows the settlement at the base of the embankment after 2 years of consolidation for the pile spacing 0.915 m (3 ft), 1.22 m (4 ft), 1.525 m (5 ft), and 1.83 m (6 ft) utilizing the GRLTP. The maximum observed settlement under the centerline of the embankment is 11.08 cm, 12.84 cm, 15.20 cm, and 19.29 cm for each corresponding spacing from the smallest to the largest. It can be observed that with increasing the pile length, the settlement at the very loose sand between the piles tends to increase as well. Less settlement is observed under the unsupported zone compared to the supported area as the stress increase under the GRLTP is more significant than that under the slope with an extent of 1.5H of GRLTP and piles (i.e., the unsupported area carry a small embankment load). The maximum settlement observed under the unsupported zone is 6.76 cm, 6.87 cm, 8.02 cm, and 8.50 cm for each corresponding spacing from the smallest to the largest. Settlement in this area depends primarily on the distance of the last pile from the GRLTP edge,

which coincides with three-quarters of the slope. Distance between the edge of the GRLTP and the far edge of the last pile, $x$, is 0.305 m, 0.152 m, 0.61 m, and 0.762 m for each corresponding spacing from the smallest to the largest (Figure 6.113). However, the settlement in the unsupported zone for each pile spacing is almost the same.

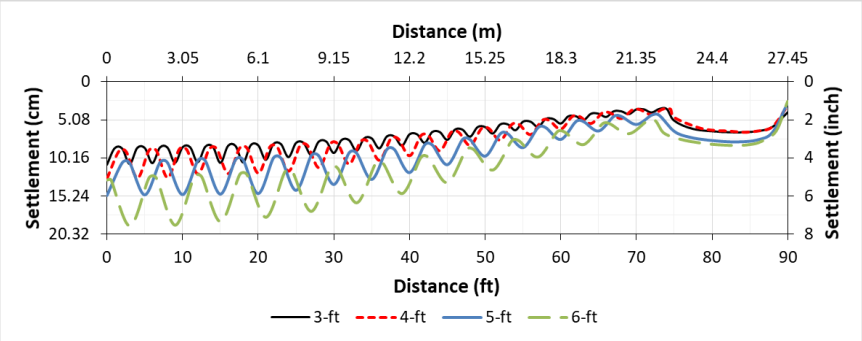


Figure 6.112. Settlement along the base of embankment after 2 years of consolidation for each pile spacing.

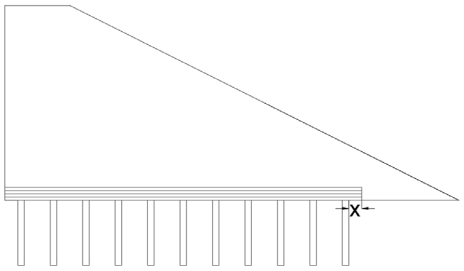


Figure 6.113. Distance, $x$, between the GRLTP edge and the far edge of the last pile.

Figure 6.114 shows the settlement with time for each pile spacing at the very loose sand between the piles under the embankment centerline, and at the pile head under the embankment centerline. Both Figure 6.114a and Figure 6.114b show a fast consolidation settlement rate as observed in the previous cases. For instance, 99% of the maximum settlement observed in the very loose sand layer is achieved after 60 days.

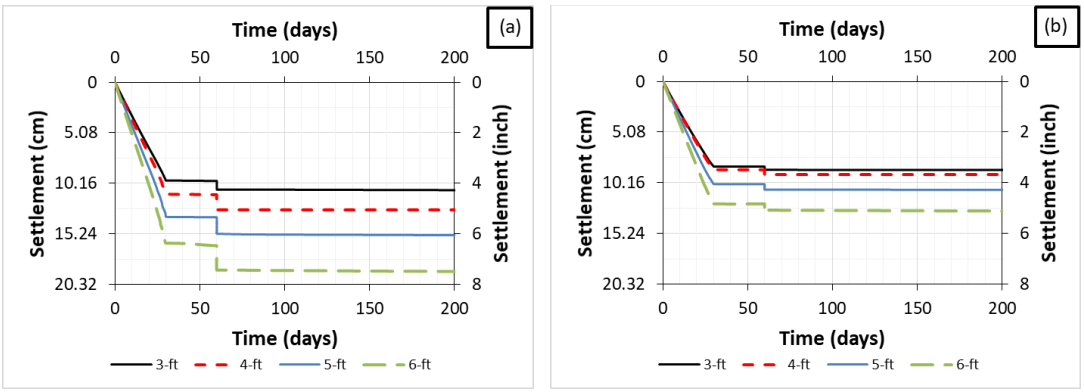


Figure 6.114. Settlement vs. time for each pile spacing at (a) the very loose sand between the piles at the embankment centerline; (b) the pile head under the embankment centerline.

### 6.6.3.3.2. Excess Pore Water Pressure

Figure 6.115. shows the maximum excess pore water pressure induced due to embankment loading at two different locations: under the embankment centerline and under the unsupported zone at the middle of slope, both in the middle of the medium stiff clay layer. These values are observed at the end of construction (EOC). Results show that the excess pore water pressure values increase with the pile spacing increase under the supported area and under the unsupported area as well. Moreover, it can be noted that the induced pore water pressure at the centerline of the embankment due to the stress increase is lower than that in the unsupported area. This is attributed to the existence of the GRLTP and the pile foundation.

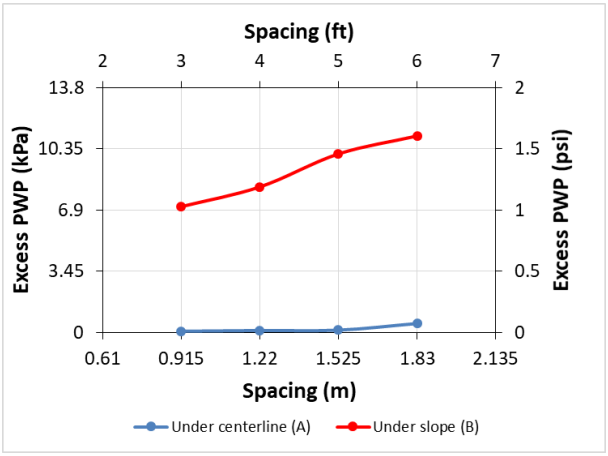


(a)

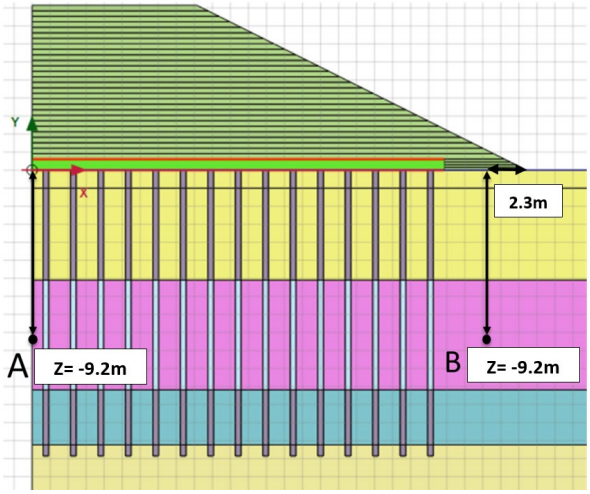


(b)

Figure 6.115. (a) Maximum excess pore water pressure observed at the end of construction under the centerline of the embankment (Point A), and the unsupported area (Point B); and (b) its location.

#### 6.6.3.3.3. Vertical Stress

Figure 6.116 shows vertical stress observed at the base of the embankment for the 1.83 m (6 ft) pile spacing at two different times: the end of construction (EOC), and after 2 years of consolidation. Results show higher vertical stress observed on the pile heads compared to the very loose sand between piles. It can also be noted that vertical stresses on top of piles are higher after 2 years of consolidation than vertical stresses observed at the EOC. Conversely, vertical stresses on the very loose sand between the piles are almost the same at the EOC and after 2 years of consolidation. The SCR is found to be 11 and 13 at the end of construction and after 2 years of consolidation, respectively. These values fall within the lower range of the SCR reported by Han and Wayne (2000) of 10 to 30 for pile-supported embankments with timber piles and a GRLTP, and are almost the same as observed in the lower embankment height (H= 6.1 m). Comparing the values determined in Case 1 and 2 for the same embankment height and pile spacing (8 and 23 for Case 1, and 13 and 29 for Case 2), cohesionless soils show less arching effect than those of the

soft cohesive soils with no significant arching occurring after the EOC (i.e., the SCR is so close between the EOC and after 2 years of consolidation).

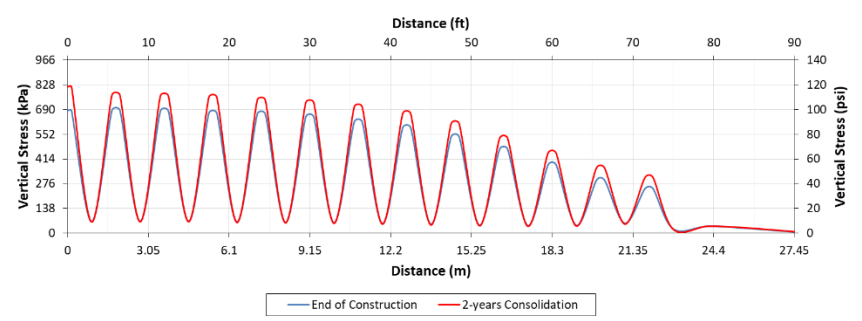


Figure 6.116. Vertical Stress along the base of the embankment at the end of construction (EOC) and after 2 years of consolidation.

### 6.6.3.3.4. Lateral Displacement

Figure 6.117 shows the lateral displacement profile along depth at the toe of the embankment after 2 years of consolidation. The lateral displacement is at its greatest at the ground surface in the very loose sand layer, and then it starts to decrease with depth up to the point where it changes direction to the left near the end of the medium stiff clay layer. Then the lateral displacement changes direction again to the right and starts to decrease again in which values are almost zero in the medium dense and dense sand layers. Maximum observed lateral displacements are 33.02 mm, 44.45 mm, 49.53 mm, and 55.88 mm for the pile spacing from the smallest to the largest, showing an increase with increasing the pile spacing.

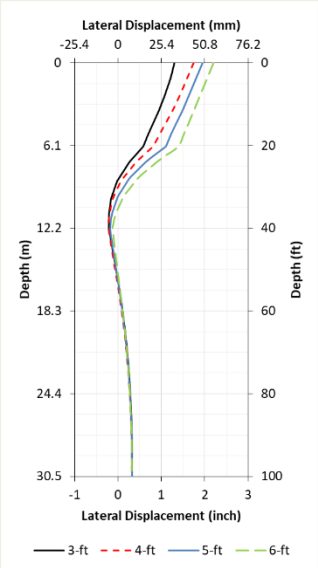


Figure 6.117. Lateral displacement profile along depth at the embankment toe after 2 years of consolidation.

### 6.6.3.3.5. Strain in Geosynthetics

Figure 6.118 shows the strain profile along the base of the embankment for the 1.83 m (6 ft) pile spacing after 2 years of consolidation for the 5 geosynthetic layers. Results show a peak-trough profile for all the geosynthetic layers. The peak is observed on top of the very loose sand between the piles for the bottom geotextile layer (1$^{st}$ layer), whereas the peak is found on top of the pile heads for the rest of the geosynthetic layers as observed before. All layers show a rapid change in the strain at the pile edges. It can also be noted that the maximum strain percentage along each geosynthetic layer is observed almost at the middle of the embankment where the maximum load exists. Figure 6.119 shows a closer look of the strain profile for the 1.83 m (6 ft) pile spacing in the 1$^{st}$ and 2$^{nd}$ geosynthetic layers.

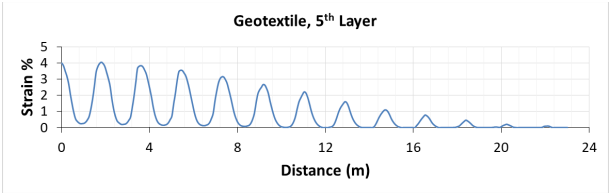

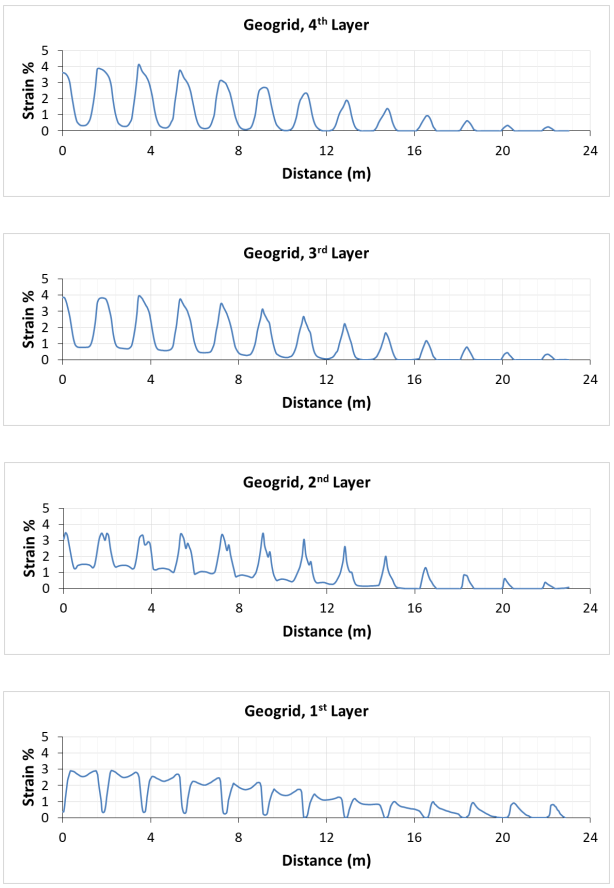


Figure 6.118. Strain profile along the base of embankment in the geosynthetic layers after 2 years of consolidation for the "6-ft" pile spacing.

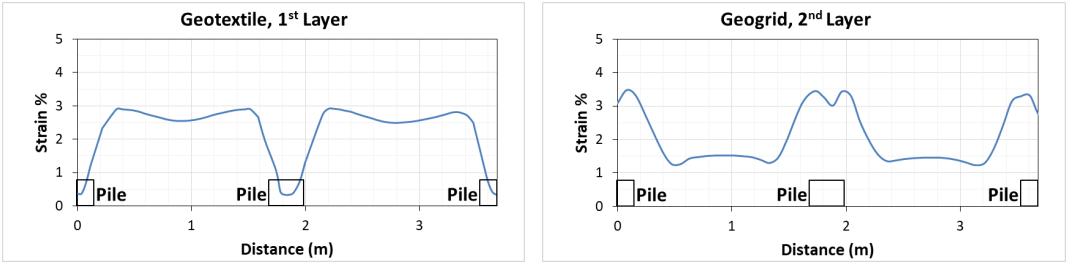


Figure 6.119. Closer look of the strain profile in the 1st and 2nd geosynthetic layers after 2 years of consolidation for the "6-ft" pile spacing.

Figure 6.120 shows the maximum strain observed in the geosynthetic layers after 2 years of consolidation for each pile spacing. All the layers have an almost linear relationship between the strain in each layer and the corresponding pile spacing. Strain levels are less than the maximum allowable limit (5%) compared to the same embankment load in Cases 1 and 2, in which the strain

exceeded the maximum allowable limit for the majority of the cases. The maximum observed strain is computed in the 4th geosynthetic layer for the 1.83 m (6 ft) pile spacing which is 4.13%.

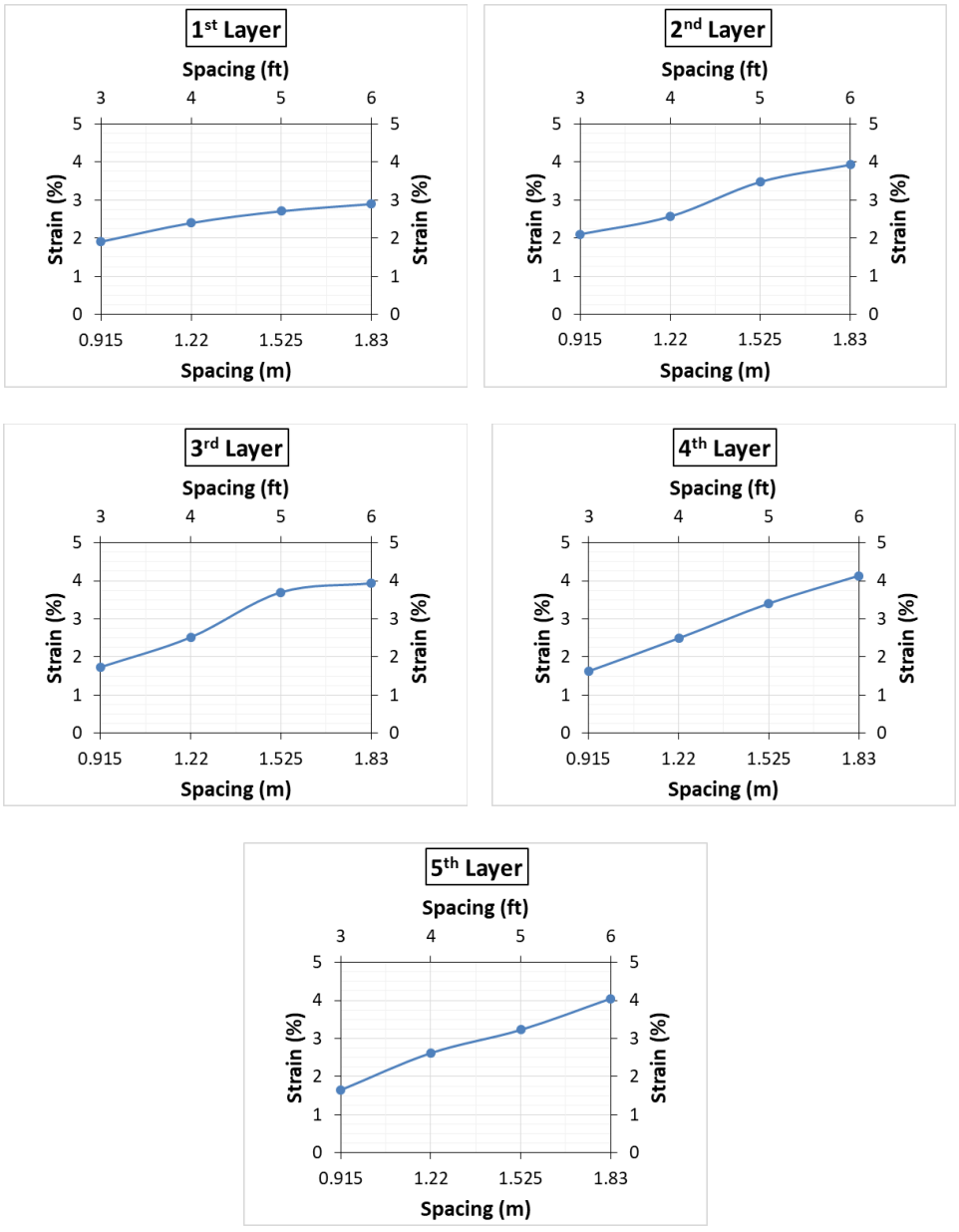


Figure 6.120. Maximum strain in geosynthetic layers for each pile spacing after 2 years of consolidation.

### 6.6.4. Discussion

The performance of the pile-supported system must satisfy both the strength and serviceability limit state requirements. For the strength limit state, the geotechnical capacity of the piles is maintained through the design with taking into consideration the pile length requirement. All the designed pile lengths with changing the embankment load (H= 3.05 m, 6.1 m, and 9.15 m) for each pile spacing (0.915 m, 1.22 m, 1.525 m, and 1.83 m) satisfy the minimum and maximum timber pile length requirement as all the pile lengths fall within the range of 9.15-18.30m (30-60 ft). However, only the case of the highest embankment height with the largest pile spacing (H= 9.15 m, and spacing= 1.83 m) is excluded from the design recommendations as the length of the pile exceeded the maximum timber pile length of 18.3 m (60 ft). Furthermore, the global stability of the system is maintained on the short-term and long-term provided that the GRLTP and piles are extended up to the embankment crest (0.0H), up to mid-slope (1.0H), and up to three-quarters of the slope (1.5H) for the lowest, intermediate, and highest embankment loads (H= 3.05 m, 6.10 m, and 9.15m), respectively. The calculated factor of safety at all embankment loads with each pile spacing is more than 1.5 for the short-term and long-term analyses.

For the serviceability limit state, the foundation settlement must not exceed a maximum upper limit which is defined as 15.24 cm (6 inches) in this study. The settlement of the foundation soil requirement is maintained at the lowest and intermediate embankment heights for each pile spacing. In addition, the settlement requirement is satisfied for an embankment height of 9.15 m (30 ft) for all the pile spacing except for the 1.83 m (6 ft) pile spacing, which was previously excluded because of the pile length requirement.

Moreover, the strain of the geosynthetic reinforcement must be less than or equal a maximum upper limit of 5%. The strain percentage requirement is maintained for each pile spacing at all

embankment heights. This confirms the low values of the SCR observed in the vertical stress sections. The arching mechanism is not fully developed for the condition where there is a very loose sand layer underneath the embankment. This may be attributed to the lesser settlement experienced by the very loose sand, so no significant differential settlement occurs between the rigid inclusions (piles) and the very loose sand layer preventing the arching mechanism from being fully developed. As a result, the very loose sand does provide support for the embankment load leaving the GRLTP and the piles with less loads than that observed in Cases 1 and 2, where a very soft clay layer exists underneath the embankment. It should also be noted that no requirement is set on the lateral displacements near the toe of the embankment as the movement is in the foundation soil and does not appear on the ground surface. Meanwhile, excessive lateral displacements are not allowed if these movements cause a problem in the global stability of the system which was checked in the stability analysis. Table 6.22 shows the cost evaluation depending mainly on the required timber pile length per row to maintain a stable system with all requirements being satisfied. All the proposed pile spacings are included for the lowest and intermediate embankment loads (H= 3.05 m, and 6.10 m). For an embankment height of 9.15 m (30 ft), only the 1.83 m (6 ft) pile spacing is excluded from the evaluation. For the 3.05 m (10 ft) and 6.10 m (20 ft) embankment heights, the 1.83 m (6 ft) resulted in the most economical design for Case 3 soil profile. For the highest embankment height (H= 9.15 m), the 1.525 m (5 ft) is suggested to be used for Case 3 soil profile. Same GRLTP configuration with the original tensile stiffness is adopted for all cases.

Table 6.22. Cost evaluation for Case 3 soil profile.

| H (m) | Valid Pile Spacing (m) | Pile Length (m) | Number of Piles per Row | Total Required Pile length per Row (m) |
|---|---|---|---|---|
| 3.05 (10 ft) | 0.915 (3 ft) | 10.07 m (33 ft) | 20 | 202 |
| | 1.220 (4 ft) | 12.81 m (42 ft) | 14 | 180 |
| | 1.525 (5 ft) | 13.73 m (45 ft) | 12 | 165 |
| | 1.830 (6 ft) | 15.25 m (50 ft) | 10 | 153 |
| 6.10 (20 ft) | 0.915 (3 ft) | 12.81 m (42 ft) | 34 | 436 |
| | 1.220 (4 ft) | 14.64 m (48 ft) | 24 | 352 |
| | 1.525 (5 ft) | 15.25 m (50 ft) | 20 | 305 |
| | 1.830 (6 ft) | 15.86 m (52 ft) | 17 | 270 |
| 9.15 (30 ft) | 0.915 (3 ft) | 13.16 m (43 ft) | 50 | 658 |
| | 1.220 (4 ft) | 15.25 m (50 ft) | 38 | 580 |
| | 1.525 (5 ft) | 15.86 m (52 ft) | 30 | 476 |

## 6.7. Case (4) Soil Profile

This section discusses the FEM parametric study for the soil profile of Case 3 (Figure 6.1d). The proposed three embankment heights (3.05 m (10 ft), 6.1 m (20 ft), and 9.15 m (30 ft)) will be analyzed in terms of the required pile length design, GRLTP and piles' extent under the embankment slope, and performance of the system by changing the center-to-center pile spacing.

### 6.7.1. Embankment Height (H)= 3.05 m (10 ft)

#### 6.7.1.1. Pile Design

Piles are designed to carry the whole embankment load plus the surcharge load for each corresponding pile spacing. Estimated factored loads are 77 kN, 137 kN, 214 kN, and 308 kN for 0.915 m (3 ft), 1.22 m (4 ft), 1.525 m (5 ft), and 1.83 m (6 ft) pile spacing, respectively. Table 6.23 shows the pile design information including the pile diameter (D) and pile length (L) for each corresponding pile spacing. The first three proposed pile spacings are designed to be tipped on the

stiff clay layer, while the largest pile spacing is designed to be tipped on the dense sand layer. Furthermore, the geotechnical capacity of the 1.83 m (6 ft) pile spacing is satisfied with a pile length of 15.25 m (50 ft). The extra 0.61 m (twice the pile diameter) extension into the dense sand layer is to account for the irregularity of the soil layers in the field.

Table 6.23. Pile Design for Case 4, H= 3.05 m (10 ft).

| Spacing | Pile Diameter (D) | Pile Length (L) |
|---|---|---|
| 0.915 m (3 ft) | 0.305 m (1 ft) | 9.15 m (30 ft) |
| 1.220 m (4 ft) | 0.305 m (1 ft) | 9.76 m (32 ft) |
| 1.525 m (5 ft) | 0.305 m (1 ft) | 11.59 m (38 ft) |
| 1.830 m (6 ft) | 0.305 m (1 ft) | 15.86 m (52 ft) |

#### 6.7.1.2. Stability Analysis

The GRLTP and piles' extent under the embankment slope is adopted from the stability analysis of Case 3 as the subsoil condition underneath the embankment is exactly the same as Case 3. However, the factor of safety is determined for each pile spacing to ensure that the safety factor for the short and long term is more than the minimum required factor of safety of 1.5. Accordingly, the GRLTP and pile are extended up to the embankment crest (0.0H). The average factor of safety of all the pile spacing with the adopted GRLTP and piles' extent is 1.7. Therefore, the extent of the GRLTP and the piles is chosen to be 0.0H. Accordingly, the required number of piles per row for the NC soil case is 20, 14, 12, and 10 for the 0.915 m, 1.22 m, 1.525 m, and 1.83 m pile spacing, respectively.

#### 6.7.1.3. Spacing Parametric Study

The system's performance is investigated with changing the center-to-center pile spacing with the GRLTP and the piles extended up to the crest of the embankment (no support under the slope).

Pile spacing will be ranged from 3D to 6D as follows: 0.915 m (3 ft), 1.22 m (4 ft), 1.525 m (5 ft), and 1.83 m (6 ft). The designed pile length for each corresponding pile spacing, from the smallest to the largest, is 9.15 m (30 ft), 9.76 m (32 ft), 11.59 m (38 ft), and 15.86 m (52 ft).

#### 6.7.1.3.1. Settlement

Figure 6.121shows the settlement at the base of the embankment after 2 years of consolidation for the pile spacing 0.915 m (3 ft), 1.22 m (4 ft), 1.525 m (5 ft), and 1.83 m (6 ft) utilizing the GRLTP. The maximum observed settlement under the centerline of the embankment is 10.61 cm, 11.98 cm, 9.87 cm, and 4.73 cm for each corresponding spacing from the smallest to the largest. It can be observed that the computed settlement values are uneven. This is attributed to the differences in the soil layer where the piles are tipping onto. On one hand, the piles are tipping on the stiff clay layer for the first three proposed pile spacing leaving the soft clay layer ($3^{rd}$ layer) with a high stress increase. The "4-ft" had the highest settlement, followed by the "3-ft" pile spacing. Less settlement is observed for the "5-ft" spacing as piles are almost penetrating the whole stiff clay layer. On the other hand, the piles are tipping on the dense sand layer for the largest pile spacing. As a result, the largest pile spacing had the lowest settlement. However, the unsupported zone under the slope experiences larger settlement compared to the supported area. This difference in performance is attributed to the improvement of the system due to the existence of the GRLTP and the pile foundation. The maximum settlement observed under the unsupported zone is 11.81 cm, 13.85 cm, 11.00 cm, and 7.316 cm for each corresponding spacing from the smallest to the largest. Settlement in this area depends primarily on the distance of the last pile from the GRLTP edge, which coincides with the embankment crest. The distance between the edge of the GRLTP and the far edge of the last pile, $x$, is 0.305 m, 1.07 m, 0.61 m, and 0.762 m for each corresponding spacing from the smallest to the largest (Figure 6.83). In addition, the settlement in this area is affected by

the location of the pile tip. This explains the fact that the best performance is for the "6-ft" pile spacing as piles are tipping on the dense sand layer.

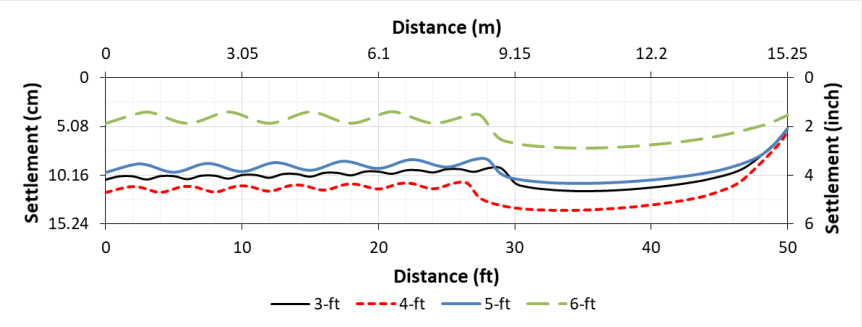


Figure 6.121. Settlement along the base of embankment after 2 years of consolidation for each pile spacing.

Figure 6.122 shows the settlement with time for each pile spacing at the very loose sand between the piles under the embankment centerline, and at the pile head under the embankment centerline. Both Figure 6.122a and Figure 6.122b show a fast consolidation settlement rate. This is attributed to the inclusion of the GRLTP and the pile foundation in which the settlement is improved, and a faster consolidation rate is achieved. It can be noted that almost all excess pore water pressure is dissipated during the embankment construction for the "6-ft" as the average increase in the settlement between the end of construction (EOC) and the settlement observed at 40 days is only 1.2%. However, the rest of the proposed pile spacings show an increase in the settlement between the end of construction (EOC) and the settlement observed at 40 days of 64.1%. This is attributed to the high excess pore water pressure induced as piles are not penetrating the soft clay layer (3$^{rd}$ layer) compared to the "6-ft" pile spacing.

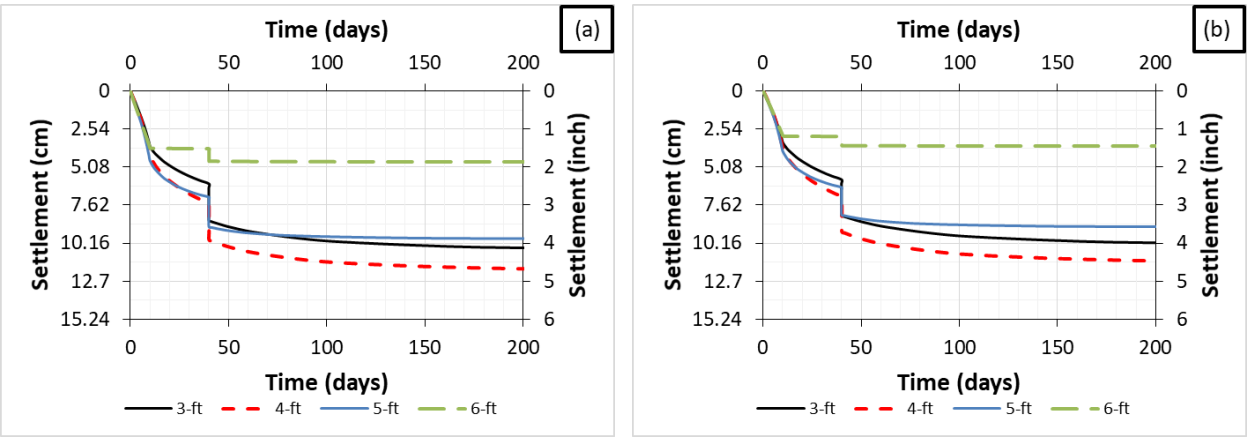


Figure 6.122. Settlement vs. time for each pile spacing at (a) the very loose sand between the piles at the embankment centerline; (b) the pile head under the embankment centerline.

### 6.7.1.3.2. Excess Pore Water Pressure

Figure 6.123. shows the maximum excess pore water pressure induced due to embankment loading at two different locations: under the embankment centerline and under the unsupported zone at the middle of slope at the bottom of the stiff clay layer and at the middle of the stiff clay layer, respectively. These values are observed at the end of construction (EOC). Results show significant excess pore water pressure observed in the stiff clay and soft clay layers for the first three proposed pile spacing as piles are tipped on them, whereas very low value is observed at the same location for the "6-ft" model as the piles are penetrating the clay layers and tipping on the dense sand. In contrast, the excess pore water pressure in the unsupported area depends on the distance $x$ (Figure 6.83) and the location of the pile tip. Excess pore water pressure at point B is almost the same for all pile spacing.

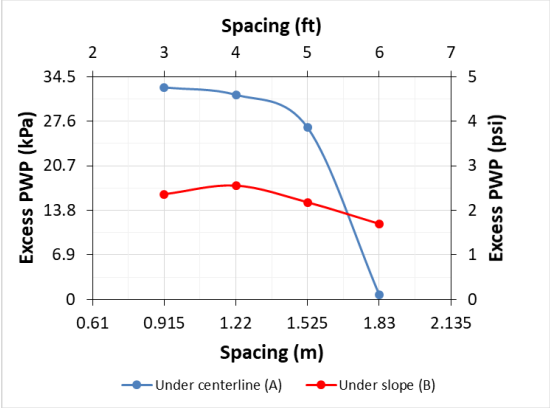


(a)

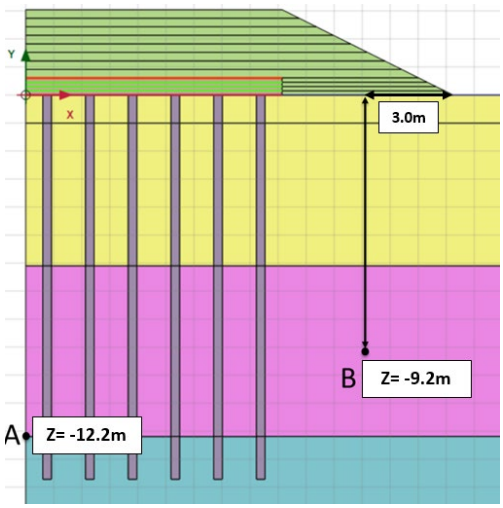


(b)

Figure 6.123. (a) Maximum excess pore water pressure observed at the end of construction under the centerline of the embankment (Point A), and the unsupported area (Point B); and (b) its location.

### 6.7.1.3.3. Vertical Stress

Figure 6.124 shows vertical stress observed at the base of the embankment for the 1.83 m (6 ft) pile spacing at two different times: the end of construction (EOC), and after 2 years of consolidation. Results show higher vertical stress observed on the pile heads compared to the very loose sand between piles. It can also be noted that vertical stresses on top of piles are higher after 2 years of consolidation than those observed at the EOC. Conversely, vertical stresses on the very loose sand between the piles are almost the same at the two times. The stress concentration ratio

(SCR) is found to be 9 and 10 at the EOC and after 2 years of consolidation, respectively. These values almost fall within the lower range of the SCR reported by Han and Wayne (2000) of 10 to 30 for pile-supported embankments with timber piles and a GRLTP. This is very close to the results obtained in Case 3 for the same embankment height and pile spacing (8 and 12 for Case 3).

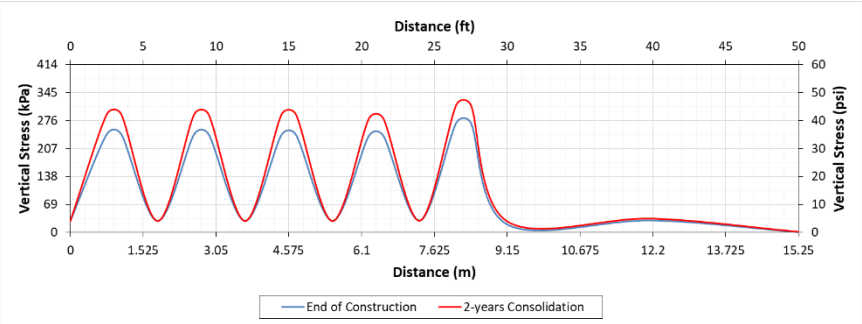


Figure 6.124. Vertical Stress along the base of the embankment at the end of construction (EOC) and after 2 years of consolidation.

### 6.7.1.3.4. Lateral Displacement

Figure 6.125 shows the lateral displacement profile along depth at the toe of the embankment after 2 years of consolidation. The maximum lateral displacement in all the pile spacing is observed in the bottom of the stiff clay layer near the soft clay layer for all pile spacing except for the "6-ft" in which the maximum value is observed at the top of the stiff clay layer. Computed values are 14.22 mm, 16.00 mm, 11.12 mm, and 7.27 mm for the pile spacing from the smallest to the largest. The difference in performance is caused by the different locations of the pile tip for each case. The lowest lateral displacement is observed in the "6-ft" model, while the maximum value is observed in the "4-ft" model. The lateral displacement is diminished at deeper depths after the soft clay layer.

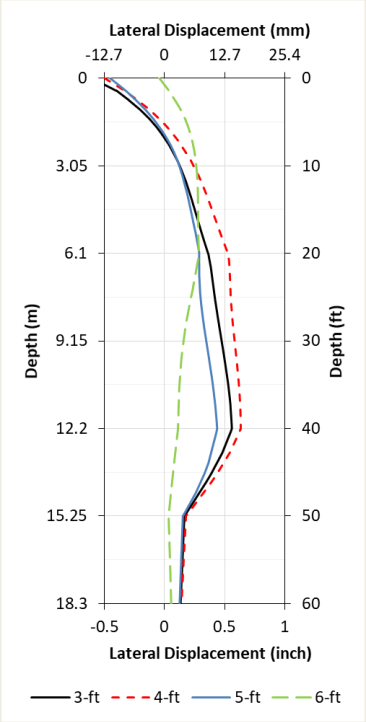


Figure 6.125. Lateral displacement profile along depth at the embankment toe after 2 years of consolidation.

### 6.7.1.3.5. Strain in Geosynthetics

Figure 6.126 shows the strain profile along the base of the embankment for the 1.83 m (6 ft) pile spacing after 2 years of consolidation for the 5 geosynthetic layers. Results show a peak-trough profile for all the geosynthetic layers. The peak is observed on top of the very loose sand between the piles for the bottom geotextile layer (Haring et al., 2008), whereas the peak is found on top of the pile heads for the rest of the geosynthetic layers, as observed in all previous cases. It can also be noted that the maximum strain percentage along each geosynthetic layer is observed near the end of the GRLTP because of the higher stresses experienced by the GRLTP due to differential settlement between the supported and unsupported zone. Figure 6.127 shows a closer look of the strain profile for the 1.83 m (6 ft) pile spacing in the 1$^{st}$ and 2$^{nd}$ geosynthetic layers.

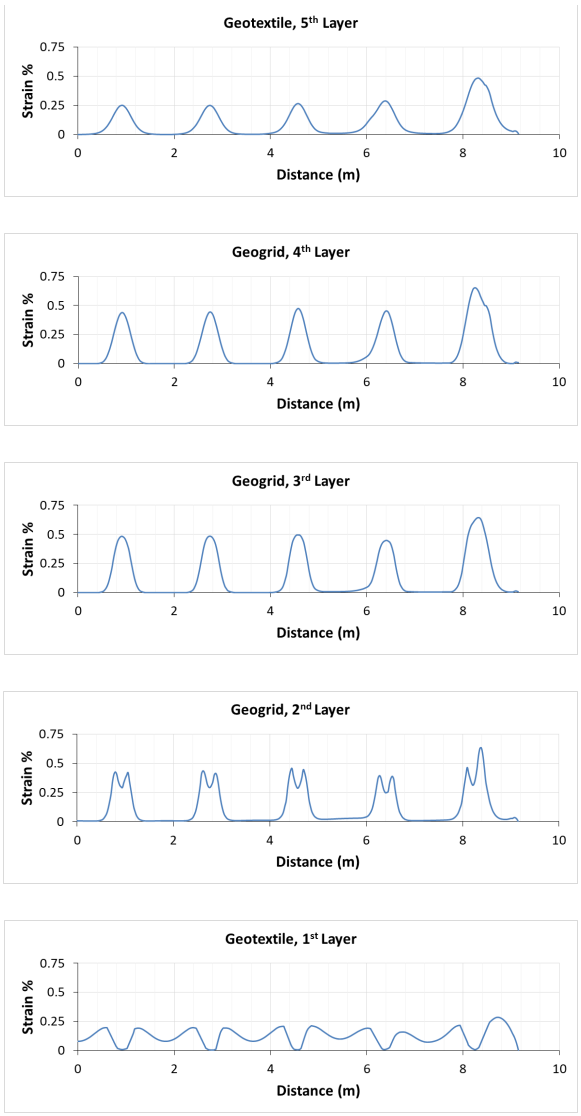


Figure 6.126. Strain profile along the base of embankment in the geosynthetic layers after 2 years of consolidation for the "6-ft" pile spacing.

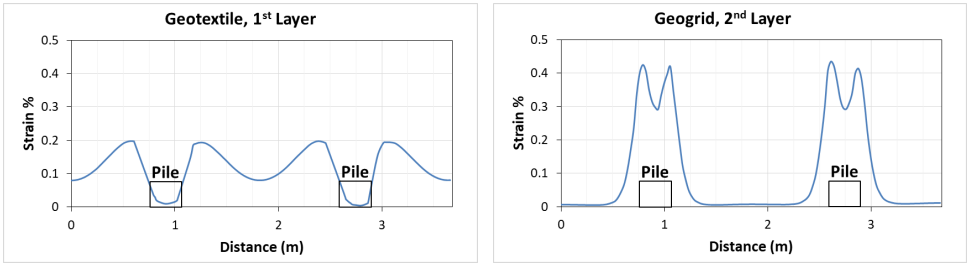


Figure 6.127. Closer look of the strain profile in the 1st and 2nd geosynthetic layers after 2 years of consolidation for the "6-ft" pile spacing.

Figure 6.128 shows the maximum strain observed in the geosynthetic layers after 2 years of consolidation for each pile spacing. The maximum strain among all the pile spacing is observed in the 1.83 m (6 ft) pile spacing. The piles in "6-ft" pile spacing are tipping on the dense sand layer, whereas the rest of the piles are tipping on the stiff clay layer. As a result, piles are restrained by the dense sand layer, so larger differential settlement between the pile head and the very loose sand between the piles is expected to occur for this pile spacing, meaning higher strain in the geosynthetics. In addition, the "4-ft" pile spacing has strain levels almost equal to or larger than those of the "5-ft" pile spacing. This may be attributed to the larger distance between the far end of the last pile and the GRLTP edge for the "4-ft" than the "5-ft" pile spacing. Moreover, maximum observed strain is computed in the 3rd geosynthetic layer for the 1.83 m (6 ft) pile spacing which is 0.64%.

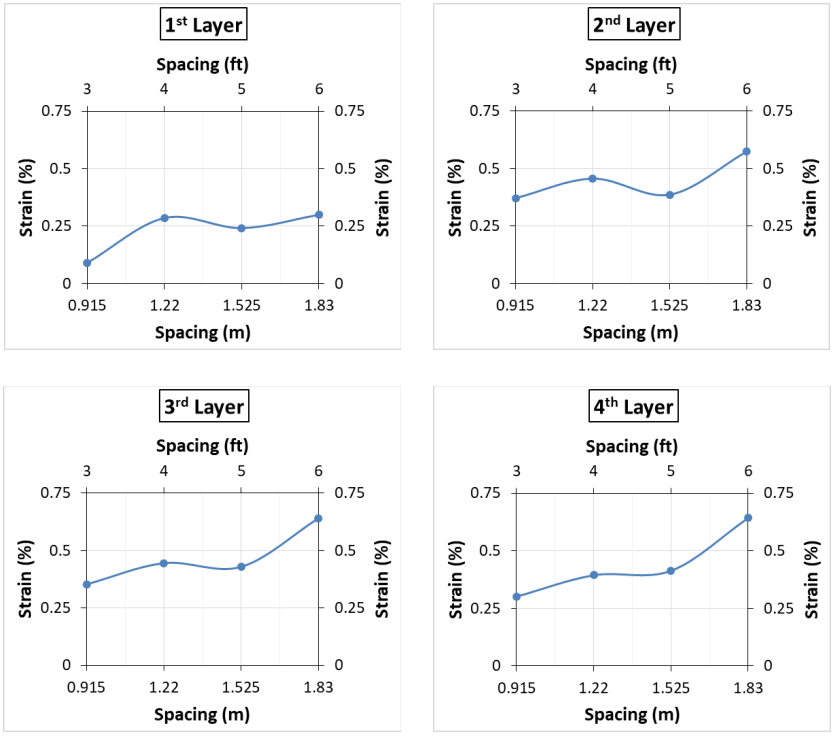

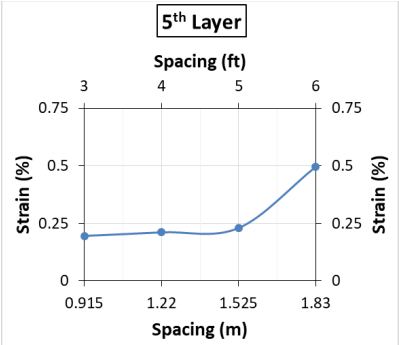


Figure 6.128. Maximum strain in geosynthetic layers for each pile spacing after 2 years of consolidation.

### 6.7.2. Embankment Height (H)= 6.10 m (20 ft)

#### 6.7.2.1. Pile Design

Piles are designed to carry the whole embankment load plus the surcharge load for each corresponding pile spacing. Estimated factored loads are 138 kN, 246 kN, 384 kN, and 552 kN for 0.915 m (3 ft), 1.22 m (4 ft), 1.525 m (5 ft), and 1.83 m (6 ft) pile spacing, respectively. Table 6.24 shows the pile design information including the pile diameter (D) and pile length (L) for each corresponding pile spacing. The piles in the 0.915 m (3 ft) pile spacing are tipped on the stiff clay layer, while the rest of the proposed pile spacing penetrated the clay layers and tipped on the dense sand layer to satisfy the geotechnical capacity. However, an extra 0.61 m is added to the pile lengths for the last three proposed pile spacing to account for the irregularity of the soil layers in the field.

Table 6.24. Pile Design for Case 4, H= 6.10 m (20 ft).

| Spacing | Pile Diameter (D) | Pile Length (L) |
|---|---|---|
| 0.915 m (3 ft) | 0.305 m (1 ft) | 9.76 m (32 ft) |
| 1.220 m (4 ft) | 0.305 m (1 ft) | 15.86 m (52 ft) |
| 1.525 m (5 ft) | 0.305 m (1 ft) | 15.86 m (52 ft) |
| 1.830 m (6 ft) | 0.305 m (1 ft) | 15.86 m (52 ft) |

#### 6.7.2.2. Stability Analysis

The GRLTP and piles' extent under the embankment slope is adopted from the stability analysis of Case 3 as the subsoil condition underneath the embankment is exactly the same as Case 3. However, the factor of safety is determined for each pile spacing to ensure that the safety factor for the short and long term is more than the minimum required factor of safety of 1.5. Accordingly, the GRLTP and pile are extended up to mid-slope (1.0H). The average factor of safety of all the pile spacing with the adopted GRLTP and piles' extent is 1.6. Therefore, the extent of the GRLTP and the piles is chosen to be 1.0H. Accordingly, the required number of piles per row for the NC soil case is 34, 24, 20, and 17 for the 0.915 m, 1.22 m, 1.525 m, and 1.83 m pile spacing, respectively.

#### 6.7.2.3. Spacing Parametric Study

The system's performance is investigated with changing the center-to-center pile spacing with the GRLTP and the piles extended up mid-slope area (1.0H). Pile spacing will be ranged from 3D to 6D as follows: 0.915 m (3 ft), 1.22 m (4 ft), 1.525 m (5 ft), and 1.83 m (6 ft). The designed pile length for each corresponding pile spacing, from the smallest to the largest, is 9.76 m (32 ft), 15.86 m (52 ft), 15.86 m (52 ft), and 15.86 m (52 ft).

##### 6.7.2.3.1. Settlement

Figure 6.129 shows the settlement at the base of the embankment after 2 years of consolidation for each pile spacing. The maximum observed settlement under the centerline of the embankment is 22.87 cm, 6.14 cm, 8.11 cm, and 10.5 cm for each corresponding spacing from the smallest to the largest. It can be observed that with increasing the pile length, the settlement at the very loose sand between the piles tends to increase except for the "3-ft" pile spacing. This is attributed to the location of the pile tip in each case. The "3-ft" pile spacing is tipped on the stiff clay layer, while

the rest of the piles are tipped on the dense sand layer. As a result, higher settlement is observed for the "3-ft" pile spacing. Furthermore, less settlement is observed under the unsupported zone compared to the supported area as the stress increase under the GRLTP is more significant than that under the slope with an extent of 1.0H of GRLTP and piles (i.e., the unsupported area carries a small embankment load). The maximum settlement observed under the unsupported zone is 14.92 cm, 8.24 cm, 7.74 cm, and 7.96 cm for each corresponding spacing from the smallest to the largest. Settlement in this area is the highest for the "3-ft" pile spacing. The rest of the pile spacings have almost the same settlement in the unsupported area as they all have the same length.

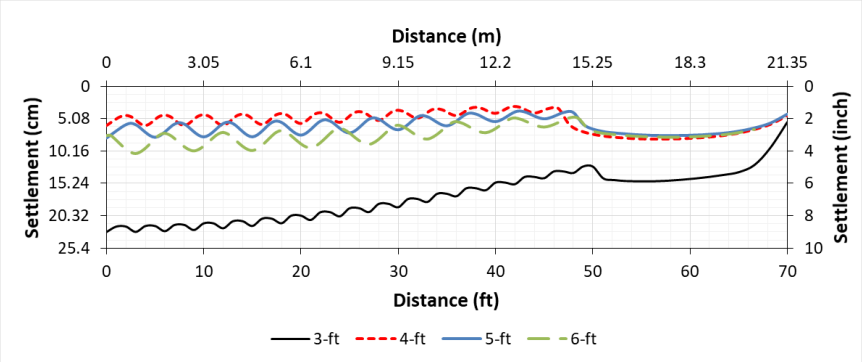


Figure 6.129. Settlement along the base of the embankment after 2 years of consolidation for each pile spacing.

Figure 6.130 shows the settlement with time for each pile spacing at the very loose sand between the piles under the embankment centerline, and at the pile head under the embankment centerline. Figure 6.130a and Figure 6.130b show a fast consolidation settlement rate for the last three proposed pile spacing. However, the "3-ft" pile spacing experiences significant settlement in the consolidation period after the end of construction. For instance, the average increase in the settlement between the end of construction and the settlement observed at 50 days is only 1.0% for the last three pile spacing, whereas the same increase is 56% for the "3-ft" pile spacing.

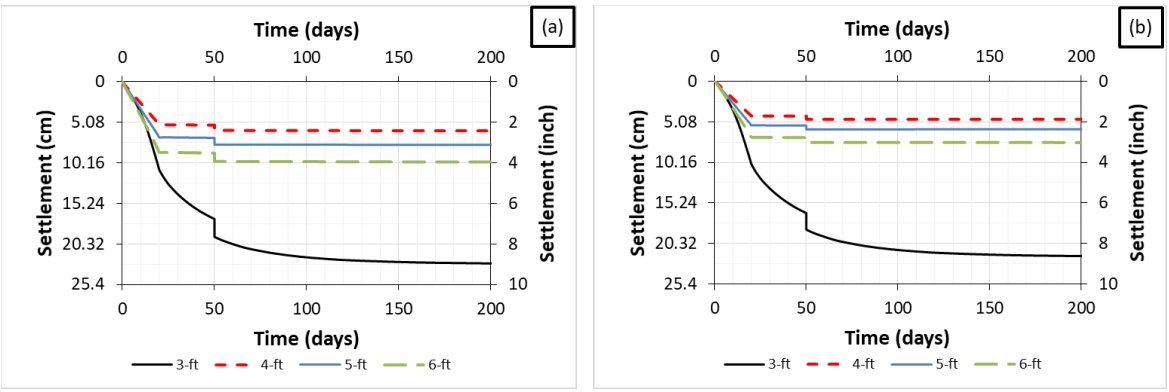


Figure 6.130. Settlement vs. time for each pile spacing at (a) the very loose sand between the piles at the embankment centerline; (b) the pile head under the embankment centerline.

### 6.7.2.3.2. Excess Pore Water Pressure

Figure 6.131. shows the maximum excess pore water pressure induced due to embankment loading at two different locations: under the embankment centerline and under the unsupported zone near the toe at the bottom of the stiff clay layer and at the middle of the stiff clay layer, respectively. These values are observed at the end of construction (EOC). Results show that the excess pore water pressure values increase with the pile spacing increase under the supported and unsupported zones except for the "3-ft" model. The piles in the "3-ft" pile spacing are tipping on the stiff clay layer which is underlain by the soft clay layer. As a result, significant stresses are transferred to these layers by the piles producing large excess pore water pressure. Moreover, it can be noted that the induced pore water pressure at the centerline of the embankment due to the stress increase is higher than that in the unsupported area.

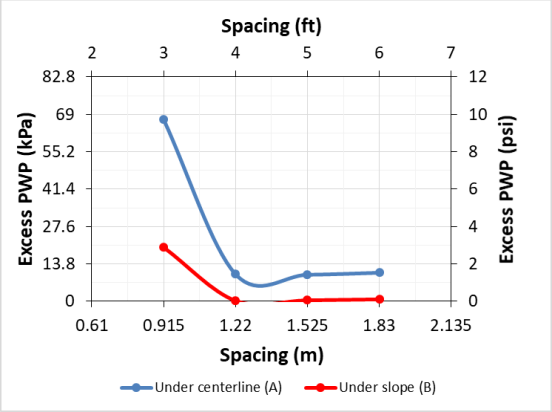


(a)

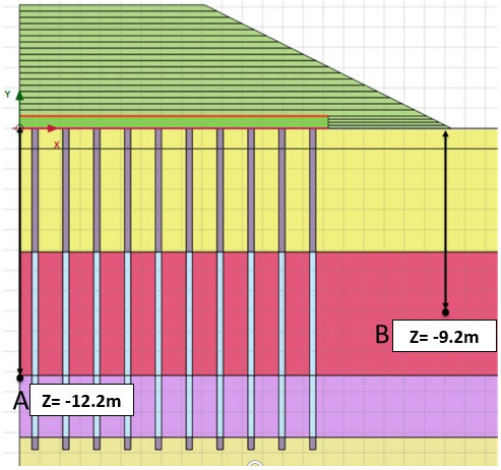


(b)

Figure 6.131. (a) Maximum excess pore water pressure observed at the end of construction under the centerline of the embankment (Point A), and the unsupported area (Point B); and (b) its location.

### 6.7.2.3.3. Vertical Stress

Figure 6.132 shows vertical stress observed at the base of the embankment for the 1.83 m (6 ft) pile spacing at two different times: the end of construction (EOC), and after 2 years of consolidation. Results show higher vertical stress observed on the pile heads compared to the very loose sand between piles. It can also be noted that vertical stresses on top of piles are higher after 2 years of consolidation than vertical stresses observed at the EOC. Conversely, vertical stresses on the very loose sand between the piles are almost the same at the EOC and after 2 years of

consolidation. The SCR is found to be 11 and 12 at the end of construction and after 2 years of consolidation, respectively. These values fall within the lower range of the SCR reported by Han and Wayne (2000) of 10 to 30 for pile-supported embankments with timber piles and a GRLTP, and coincides with the values determined for the same embankment height and same pile spacing in Case 3.

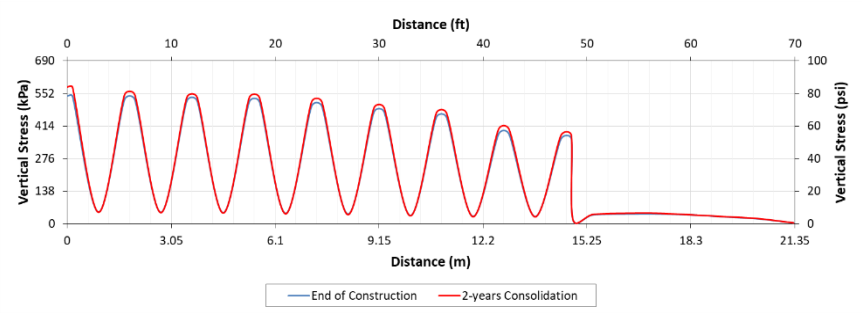


Figure 6.132. Vertical Stress along the base of the embankment at the end of construction (EOC) and after 2 years of consolidation.

### 6.7.2.3.4. Lateral Displacement

Figure 6.133 shows the lateral displacement profile along depth at the toe of the embankment after 2 years of consolidation. The lateral displacement for the last three proposed pile spacing is at its greatest at the middle of the very loose sand layer and starts to decrease with depth up to reaching zero. However, the "3-ft" pile spacing has different behavior as piles are tipped on the stiff clay layer which is underlain by another soft clay layer.

The soil mass near the ground surface for this pile spacing tends to move to the left due to the location of the pile tip. The settlement experienced by the stiff and soft clay layers under the supported zone is more than that under the unsupported area because piles transmitted more stresses to the stiff and soft clay layers. Consequently, the soil mass tends to move downward and to the left because of the differential settlement between the supported and the unsupported zones. However, this is not observed for the rest of the proposed pile spacing as all piles tipped on the

dense sand layer. Maximum observed lateral displacements are 23.27 mm, 11.49 mm, 13.49 mm, and 16.11 mm for the pile spacing from the smallest to the largest.

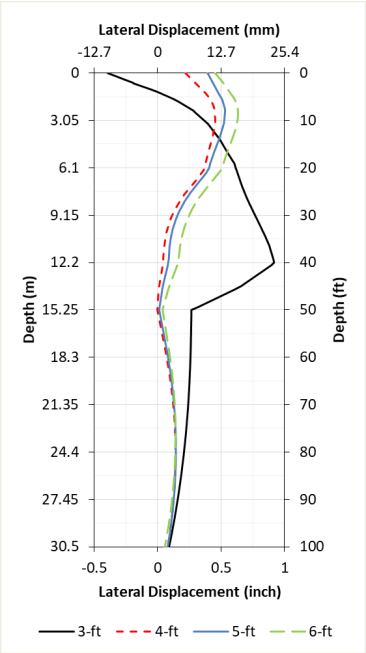


Figure 6.133. Lateral displacement profile along depth at the embankment toe after 2 years of consolidation.

### 6.7.2.3.5. Strain in Geosynthetics

Figure 6.134 shows the strain profile along the base of the embankment for the 1.83 m (6 ft) pile spacing after 2 years of consolidation for the 5 geosynthetic layers. Results show a peak-trough profile for all the geosynthetic layers. The peak is observed on top of the very loose sand between the piles for the bottom geotextile layer (1$^{st}$ layer), whereas the peak is found on top of the pile heads for the rest of the geosynthetic layers as observed before. All layers show an abrupt change in the strain at the pile edges. It can also be noted that the maximum strain percentage along each geosynthetic layer is observed almost at the middle of the embankment where the maximum load exists. Figure 6.135 shows a closer look of the strain profile for the 1.83 m (6 ft) pile spacing in the 1$^{st}$ and 2$^{nd}$ geosynthetic layers.

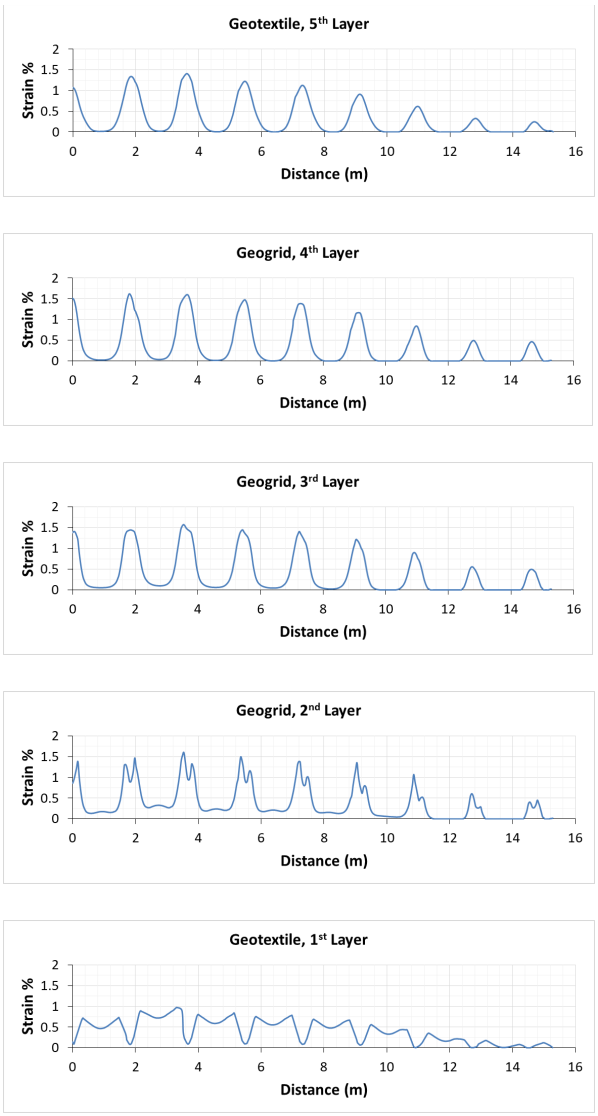


Figure 6.134. Strain profile along the base of embankment in the geosynthetic layers after 2 years of consolidation for the "6-ft" pile spacing.

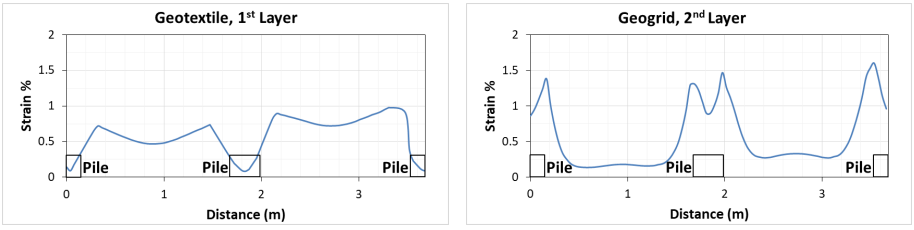


Figure 6.135. Closer look of the strain profile in the 1st and 2nd geosynthetic layers after 2 years of consolidation for the "6-ft" pile spacing.

Figure 6.136 shows the maximum strain observed in the geosynthetic layers after 2 years of consolidation for each pile spacing. All the layers have an almost linear relationship between the

strain in each layer and the corresponding pile spacing. Strain levels are much lower than the maximum allowable limit (5%) compared to the same embankment load in Cases 1 and 2, in which the strain almost reached the maximum allowable limit. The maximum observed strain is computed in the 4th geosynthetic layer for the 1.83 m (6 ft) pile spacing which is 1.62%.

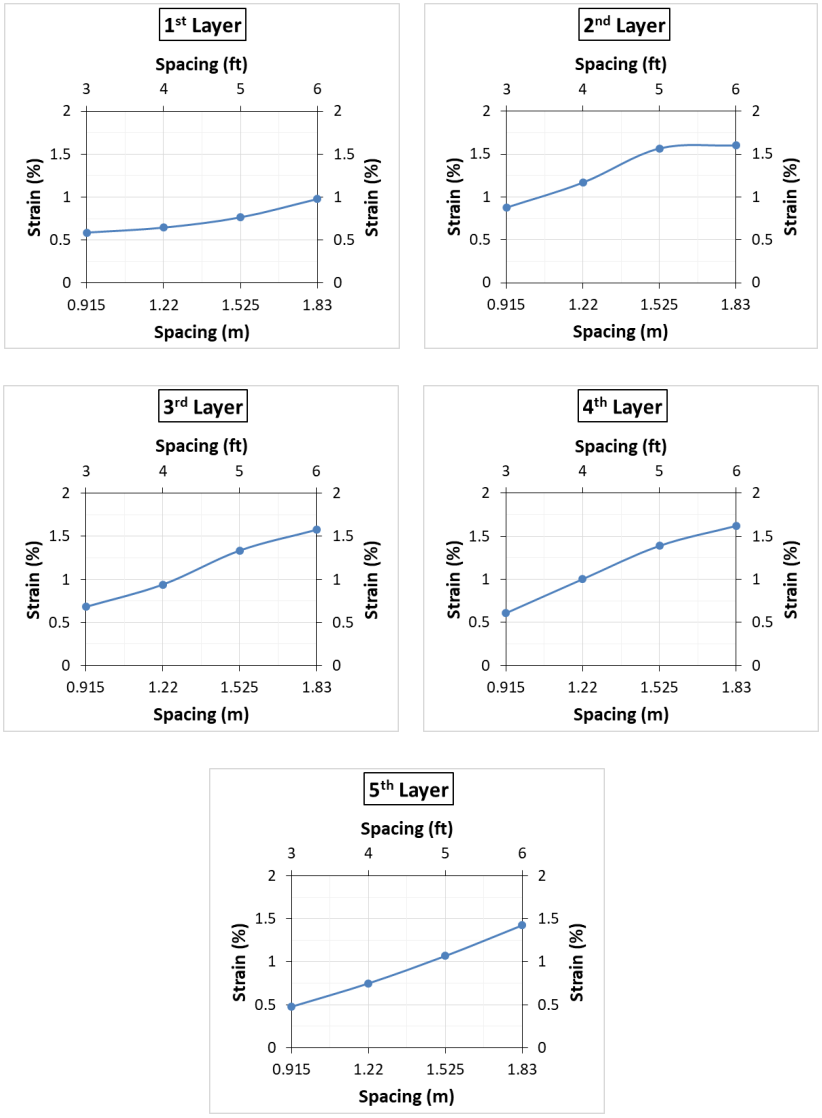


Figure 6.136. Maximum strain in geosynthetic layers for each pile spacing after 2 years of consolidation.

### 6.7.3. Embankment Height (H)= 9.15 m (30 ft)

#### 6.7.3.1. Pile Design

Piles are designed to carry the whole embankment load plus the surcharge load for each corresponding pile spacing. Estimated factored loads are 196 kN, 348 kN, 543 kN, and 782 kN for 0.915 m (3 ft), 1.22 m (4 ft), 1.525 m (5 ft), and 1.83 m (6 ft) pile spacing, respectively. Table 6.25 shows the pile design information including the pile diameter (D) and pile length (L) for each corresponding pile spacing. For this embankment height, all the piles are end bearing piles tipping on either the stiff clay layer or the dense sand layer. Moreover, an extra 0.61 m is added to the pile lengths for the ”4-ft” and “5-ft” pile spacing models.

Table 6.25. Pile Design for Case 4, H= 9.15 m (30 ft).

| Spacing | Pile Diameter (D) | Pile Length (L) |
|---|---|---|
| 0.915 m (3 ft) | 0.305 m (1 ft) | 10.98 m (36 ft) |
| 1.220 m (4 ft) | 0.305 m (1 ft) | 15.86 m (52 ft) |
| 1.525 m (5 ft) | 0.305 m (1 ft) | 15.86 m (52 ft) |
| 1.830 m (6 ft) | 0.305 m (1 ft) | 17.69 m (58 ft) |

#### 6.7.3.2. Stability Analysis

The GRLTP and piles’ extent under the embankment slope is adopted from the stability analysis of Case 3 as the subsoil condition underneath the embankment is exactly the same as Case 3. However, the factor of safety is determined for each pile spacing to ensure that the safety factor for the short and long term is more than the minimum required factor of safety of 1.5. Accordingly, the GRLTP and pile are extended up to three-quarters of the slope (1.5H). The average factor of safety of all the pile spacing with the adopted GRLTP and piles’ extent is 1.75. Therefore, the extent of the GRLTP and the piles is chosen to be 1.5H. Accordingly, the required number of piles

per row for the NC soil case is 50, 38, 30, and 25 for the 0.915 m, 1.22 m, 1.525 m, and 1.83 m pile spacing, respectively.

#### 6.7.3.3. Spacing Parametric Study

The performance of the system is investigated with changing the center-to-center pile spacing with the GRLTP and the piles extended up mid-slope area (1.0H). Pile spacing will be ranged from 3D to 6D as follows: 0.915 m (3 ft), 1.22 m (4 ft), 1.525 m (5 ft), and 1.83 m (6 ft). The designed pile length for each corresponding pile spacing, from the smallest to the largest, is 10.98 m (36 ft), 15.86 m (52 ft), 15.86 m (52 ft), and 17.69 m (58 ft).

##### 6.7.3.3.1. Settlement

Figure 6.137 shows the settlement at the base of the embankment after 2 years of consolidation for each pile spacing. The maximum observed settlement under the centerline of the embankment is 31.09 cm, 12.85 cm, 15.22 cm, and 19.14 cm for each corresponding spacing from the smallest to the largest. It can be observed that with increasing the pile length, the settlement at the very loose sand between the piles tends to increase for the "3-ft" pile spacing. This is attributed to the location of the pile tip in each case. The "3-ft" pile spacing is tipped on the stiff clay layer, while the rest of the piles are tipped on the dense sand layer. As a result, higher settlement is observed for the "3-ft" pile spacing. In addition, less settlement is observed under the unsupported zone compared to the supported area as the stress increase under the GRLTP is more significant than that under the slope with an extent of 1.5H of GRLTP and piles (i.e., the unsupported area carries a small embankment load). The maximum settlement observed under the unsupported zone is 9.67 cm, 6.41 cm, 7.52 cm, and 8.08 cm for each corresponding spacing from the smallest to the largest. Settlement in this area is the highest for the "3-ft" pile spacing. The rest of the pile spacings have almost the same settlement in this area as they all have the same pile configuration.

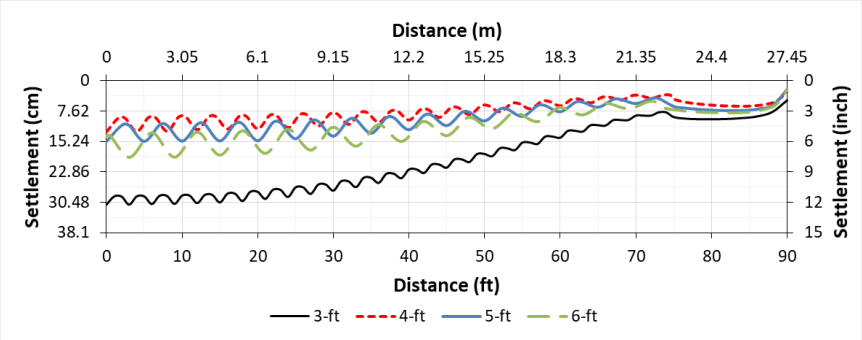


Figure 6.137. Settlement along the base of the embankment after 2 years of consolidation for each pile spacing.

Figure 6.138 shows the settlement with time for each pile spacing at the very loose sand between the piles under the embankment centerline, and at the pile head under the embankment centerline. Figure 6.138a and Figure 6.138b show a fast consolidation settlement rate for the last three proposed pile spacing. However, the "3-ft" pile spacing experiences significant settlement in the consolidation period after the end of construction. For instance, the average increase in the settlement between the end of construction and the settlement observed at 60 days is only 0.9% for the last three pile spacing, whereas the settlement increase is 33.6% for the "3-ft" pile spacing.

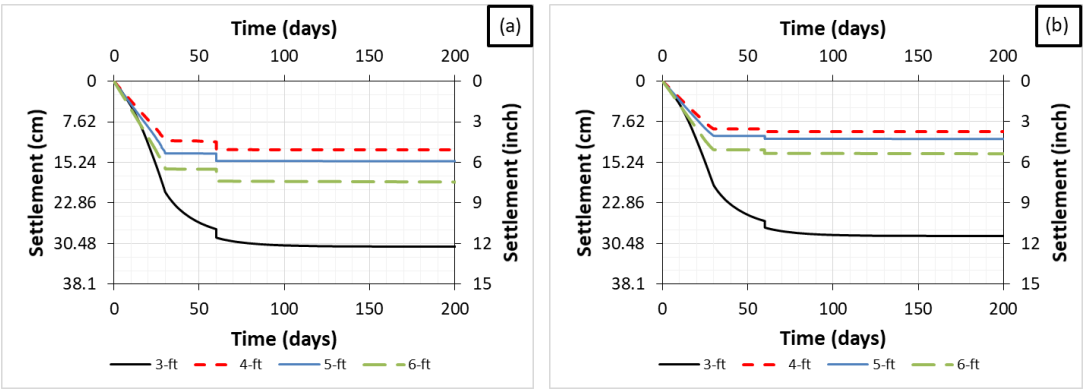


Figure 6.138. Settlement vs. time for each pile spacing at (a) the very loose sand between the piles at the embankment centerline; (b) the pile head under the embankment centerline.

### 6.7.3.3.2. Excess Pore Water Pressure

Figure 6.139 shows the maximum excess pore water pressure induced due to embankment loading at two different locations: under the embankment centerline and under the unsupported zone near

the toe at the bottom of the middle of the soft clay layer and at the middle of the stiff clay layer, respectively. These values are observed at the end of construction (EOC). Results show that the excess pore water pressure values increase with the pile spacing increase under the supported and unsupported zones except for the "3-ft" model. The piles in the "3-ft" pile spacing are tipping on the stiff clay layer which is underlain by the soft clay layer. As a result, significant stresses are transferred to these layers by the piles producing large excess pore water pressure. Moreover, it can be noted that the induced pore water pressure at the centerline of the embankment due to the stress increase is higher than that in the unsupported area.

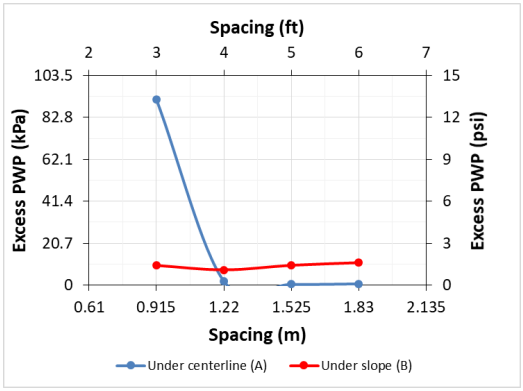


(a)

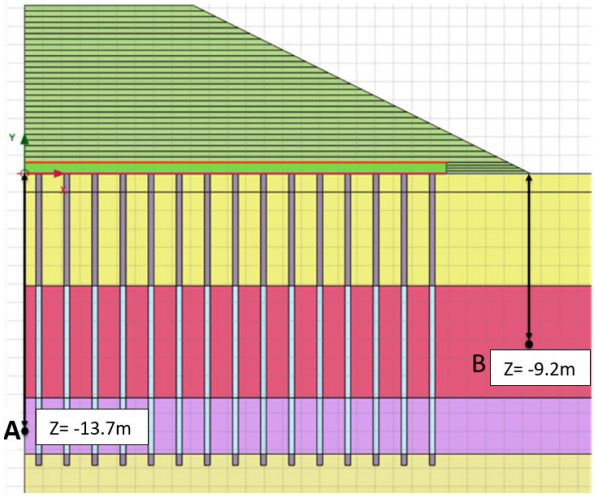


(b)

Figure 6.139. (a) Maximum excess pore water pressure observed at the end of construction under the centerline of embankment (Point A), and the unsupported area (Point B); and (b) its location.

#### 6.7.3.3.3. Vertical Stress

Figure 6.140 shows vertical stress observed at the base of the embankment for the 1.83 m (6 ft) pile spacing at two different times: the end of construction (EOC), and after 2 years of consolidation. Results show higher vertical stress observed on the pile heads compared to the very loose sand between piles. It can also be noted that vertical stresses on top of piles are higher after 2 years of consolidation compared to vertical stresses observed at the EOC. Conversely, vertical stresses on the very loose sand between the piles are almost the same at the EOC and after 2 years of consolidation. The SCR is found to be 13 and 14 at the end of construction and after 2 years of consolidation, respectively. These values fall within the range of the SCR reported by Han and Wayne (2000) of 10 to 30 for pile-supported embankments with timber piles and a GRLTP, and are almost the same as observed in the lower embankment height (H= 6.1 m).

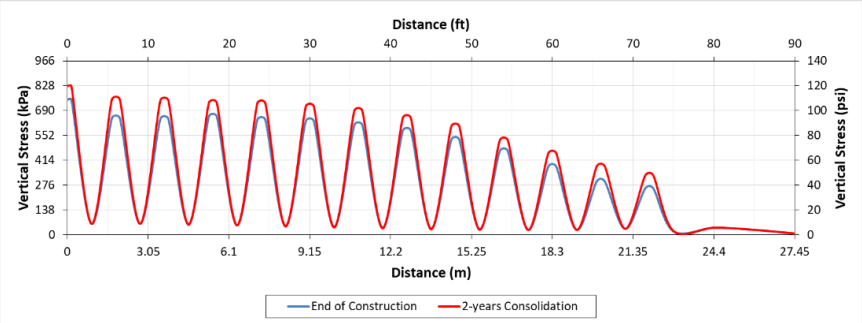


Figure 6.140. Vertical Stress along the base of the embankment at the end of construction (EOC) and after 2 years of consolidation.

#### 6.7.3.3.4. Lateral Displacement

Figure 6.141 shows the lateral displacement profile along depth at the toe of the embankment after 2 years of consolidation. The lateral displacement for the last three proposed pile spacing is at its most at the ground surface in the very loose sand layer, and then it starts to decrease with depth up to the point where it changes direction to the left near the end of the medium stiff clay layer. Then the lateral displacement changes direction again to the right and starts to decrease again until it

reaches almost zero in the dense sand layer. However, since the piles in "3-ft" pile spacing are not penetrating the soft clay layer (3rd layer), different behavior is observed from the rest of the pile spacing. The maximum lateral displacement for this pile spacing is at the ground surface, then it changes direction up to the second soft clay layer. The lateral displacement changes direction again at that depth as no support exists at the soft clay layer. Maximum observed lateral displacements are 20.32 mm, 35.56 mm, 40.64 mm, and 44.45 mm for the pile spacing from the smallest to the largest showing an increase with increasing the pile spacing.

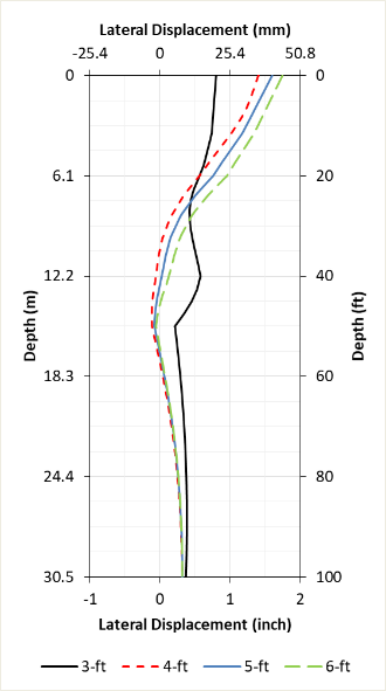


Figure 6.141. Lateral displacement profile along depth at the embankment toe after 2 years of consolidation.

**6.7.3.3.5. Strain in Geosynthetics**

Figure 6.142 shows the strain profile along the base of the embankment for the 1.83 m (6 ft) pile spacing after 2 years of consolidation for the 5 geosynthetic layers. Results show a peak-trough profile for all the geosynthetic layers. The peak is observed on top of the very loose sand between the piles for the bottom geotextile layer (1st layer), whereas the peak is found on top of the pile heads for the rest of the geosynthetic layers as observed before. All layers show a rapid change in

the strain at the pile edges. It can also be noted that the maximum strain percentage along each geosynthetic layer is observed almost at the middle of the embankment where the maximum load exists. Figure 6.143 shows a closer look of the strain profile for the 1.83 m (6 ft) pile spacing in the 1st and 2nd geosynthetic layers.

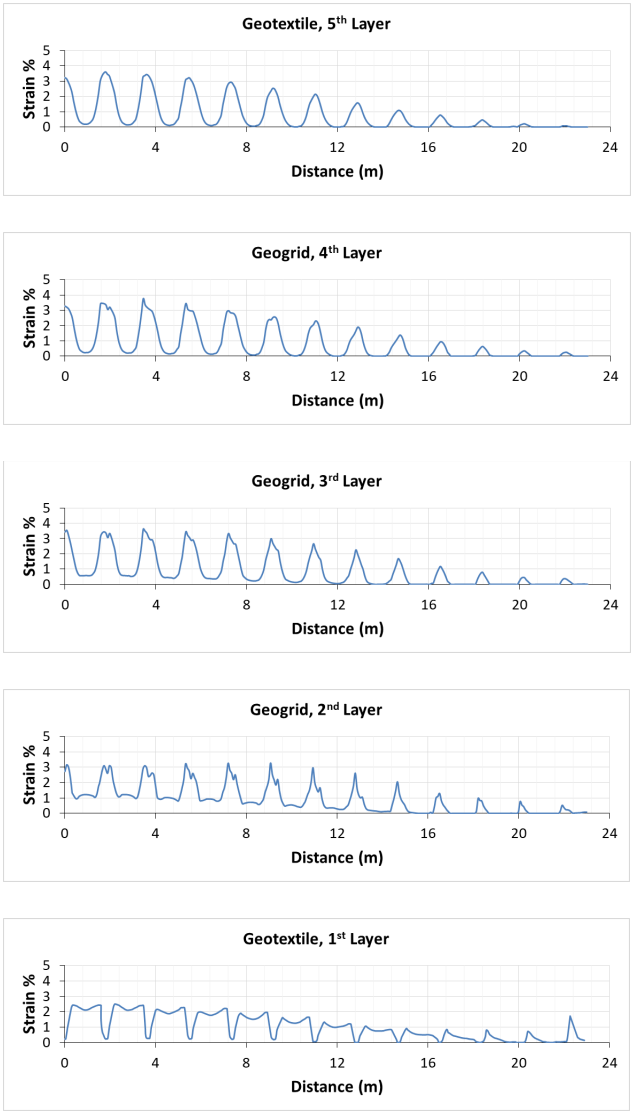


Figure 6.142. Strain profile along the base of the embankment in the geosynthetic layers after 2 years of consolidation for the "6-ft" pile spacing.

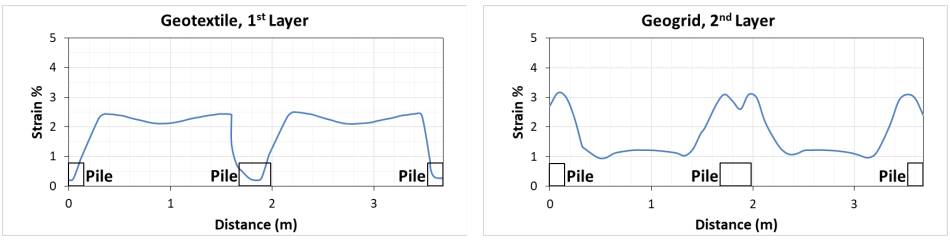


Figure 6.143. Closer look of the strain profile in the 1st and 2nd geosynthetic layers after 2 years of consolidation for the "6-ft" pile spacing.

Figure 6.144 shows the maximum strain observed in the geosynthetic layers after 2 years of consolidation for each pile spacing. All the layers have an almost linear relationship between the strain in each layer and the corresponding pile spacing. Strain levels are less than the maximum allowable limit (5%) compared to the same embankment load in Cases 1 and 2 in which the strain exceeded the maximum allowable limit for the majority of the cases. The maximum observed strain is computed in the 4th geosynthetic layer for the 1.83 m (6 ft) pile spacing which is 3.78%.

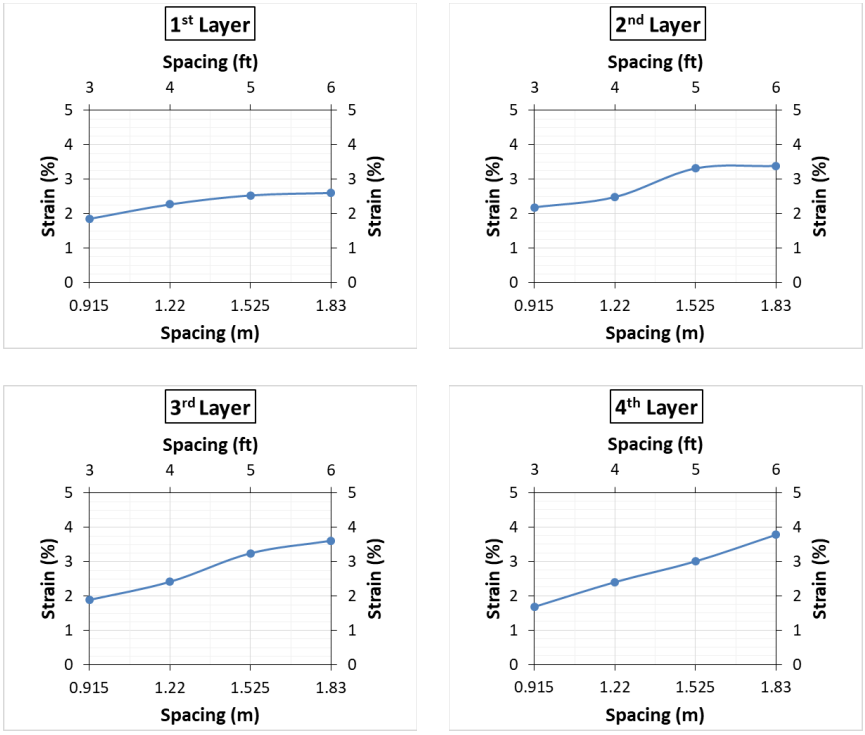

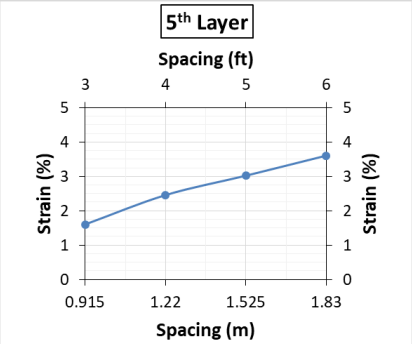


Figure 6.144. Maximum strain in geosynthetic layers for each pile spacing after 2 years of consolidation.

### 6.7.4. Discussion

The performance of the pile-supported system must satisfy both the strength and serviceability limit state requirements. For the strength limit state, the geotechnical capacity of the piles is maintained through the design with taking into consideration the pile length requirement. All the designed pile lengths with changing the embankment load (H= 3.05 m, 6.1 m, and 9.15 m) for each pile spacing (0.915 m, 1.22 m, 1.525 m, and 1.83 m) satisfy the minimum and maximum timber pile length requirement as all the pile lengths fall within the range of 9.15-18.30m (30-60 ft). Furthermore, the global stability of the system is maintained on the short-term and long-term provided that the GRLTP and piles are extended up to the embankment crest (0.0H), up to mid-slope (1.0H), and up to three-quarters of the slope (1.5H) for the lowest, intermediate, and highest embankment loads (H= 3.05 m, 6.10 m, and 9.15m), respectively. The calculated factor of safety at all embankment loads with each pile spacing is more than 1.5 for the short-term and long-term analyses. For the serviceability limit state, the foundation settlement must not exceed a maximum upper limit which is defined as 15.24 cm (6 inches) in this study. The settlement of the foundation soil requirement is maintained at the lowest embankment height. For the intermediate embankment height, all the pile spacings satisfy the settlement requirement except for the 0.915 m (3 ft). Thus, this pile spacing will be excluded from the design recommendation at this embankment height.

Moreover, both the 0.915 m (3 ft) and the 1.83 m (6 ft) violate the settlement requirement as they exceed the maximum allowable limit. Therefore, these pile spacings will be excluded from the design recommendation at this embankment height as well. Moreover, the strain of the geosynthetic reinforcement must be less than or equal to a maximum upper limit of 5%. The strain percentage requirement is maintained for each pile spacing at all embankment heights. This confirms the low values of the SCR observed in the vertical stress sections. The arching mechanism is not fully developed for the condition where there is a very loose sand layer underneath the embankment. This may be attributed to the lesser settlement experienced by the very loose sand, so no significant differential settlement occurs between the rigid inclusions (piles) and the very loose sand layer preventing the arching mechanism from being fully developed. As a result, the very loose sand does provide support for the embankment load leaving the GRLTP and the piles with lesser loads than that observed in Cases 1 and 2, where a very soft clay layer exists underneath the embankment. It should also be noted that no requirement is set on the lateral displacements near the toe of the embankment as the movement is in the foundation soil and does not appear on the ground surface. Meanwhile, excessive lateral displacements are not allowed if these movements cause a problem in the global stability of the system, which was checked in the stability analysis. Table 6.26 shows the cost evaluation depending mainly on the required timber pile length per row to maintain a stable system with all requirements being satisfied. Based on Table 6.26, recommended pile spacing for the lowest, intermediate, and highest embankment loads is 1.22 m (4 ft), 1.83 m (6 ft), and 1.525 m (5 ft), respectively. The same GRLTP configuration with the original tensile stiffness is adopted for all cases.

Table 6.26. Cost evaluation for Case 3 soil profile.

| H (m) | Valid Pile Spacing (m) | Pile Length (m) | Number of Piles per Row | Total Required Pile length per Row (m) |
|---|---|---|---|---|
| 3.05 (10 ft) | 0.915 (3 ft) | 9.15 m (30 ft) | 20 | 183 |
| | 1.220 (4 ft) | 9.76 m (32 ft) | 14 | 137 |
| | 1.525 (5 ft) | 11.59 m (38 ft) | 12 | 140 |
| | 1.830 (6 ft) | 15.86 m (52 ft) | 10 | 159 |
| 6.10 (20 ft) | 1.220 (4 ft) | 15.86 m (52 ft) | 24 | 381 |
| | 1.525 (5 ft) | 15.86 m (52 ft) | 20 | 318 |
| | 1.830 (6 ft) | 15.86 m (52 ft) | 17 | 270 |
| 9.15 (30 ft) | 1.220 (4 ft) | 15.86 m (52 ft) | 38 | 603 |
| | 1.525 (5 ft) | 15.86 m (52 ft) | 30 | 476 |

## 6.8. FHWA Design Comparison with Finite Element Modeling

This section discusses the difference between the design recommendations adopted in the FHWA Ground Modification Methods – Reference Manual (Schaefer et al., 2017) and the design recommendations of this FEM parametric study. The comparison mainly focuses on the piles' extent under the slope, the stress reduction ratio (SRR) to account for the arching effect, and the required tensile stiffness due to vertical loads and the lateral spreading effect. A case of 4D pile spacing, 1.22 m (4 ft), with 5 layers of GRLTP is considered a base case for the comparison. The comparison will be made for Cases 1 and 3 as a representative for the very soft clay and very loose sand layers, respectively. Embankment heights of 3.05 m (10 ft), 6.10 m (20 ft), and 9.15 m (30 ft) will be included as a parameter in the comparison. Equations from Chapter 2 are repeated in this chapter for convenience.

### 6.8.1. Lateral Extent of Piles

The piles under the embankment slope should extend a distance under the slope to maintain the stability of the system. A comparison will be made between the lateral extent of piles computed

with the FHWA design recommendations and the recommendations of this FEM parametric study. The FHWA design recommendation adopts the British Standards Institution Code of Practice. BS 8006 (2010) suggested a maximum required horizontal distance between the extreme edge of the pile or the pile cap and the embankment toe, $L_p$, as follows:

$$L_p = H(n - tan\theta \mathrm{p}) \quad (6.1)$$

The computed results from the equation above are compared with the values obtained from the FEM results with the same geometry provided throughout the study and are summarized in Table 6.27.

Table 6.27. Lateral extent of piles under the slope comparison.

| Soil Profile | H (m) | Horizontal Distance (HD) (m) | $L_p$ (BSI, 2010) (m) | Percent of HD (%) | $L_p$ (FEM) (m) | Percent of HD (%) |
|---|---|---|---|---|---|---|
| Case 1 | 3.05 | 6.1 | 4.30 | 71.1 | 2.28 | 37.5 |
| | 6.10 | 12.2 | 8.67 | 71.1 | 0.61 | 5.0 |
| | 9.15 | 18.3 | 13.00 | 71.1 | 1.07 | 5.9 |
| Case 3 | 3.05 | 6.1 | 4.34 | 71.1 | 7.16 | 117.5 |
| | 6.10 | 12.2 | 8.67 | 71.1 | 7.16 | 58.8 |
| | 9.15 | 18.3 | 13.00 | 71.1 | 4.72 | 25.8 |

The computed results by the BSI (2010) recommendation overestimate the values obtained in the FEM parametric study for Case 1, where a very soft clay layer exists underneath the embankment. For instance, the maximum required horizontal distance ($L_p$) for a 6.10 m embankment height is 8.67 m and 0.61 m for the recommended value by the BS (2010) and by the FEM parametric study, respectively. The computed values by the BSI (2010) recommendation is increasing with increasing the embankment height. This is attributed to the dependency of the side slope and the friction angle of the embankment material resulting in a constant percent of the horizontal distance

(HD) of 71.1%. It should be noted that increasing the embankment height will make the system vulnerable to instability problems compared to lower embankment heights. Thus, the horizontal required distance ($L_p$) should decrease with increasing the embankment height. This is observed in the computed values of the FEM parametric study of Case 1 except for a discrepancy between the 6.10 m and 9.15 m. Both embankment heights are recommended to have piles and GRLTP along the whole embankment slope, so the location of the last pile is governed by the pile spacing which caused this discrepancy. However, the percent of the horizontal distance is so close for both scenarios (5.0 % and 5.9 % for 6.10 m and 9.15 m, respectively). For Case 3 where a very loose sand layer exists underneath the embankment, the same computed results by the BSI (2010) recommendation are observed for both Cases 1 and 3 as the subsoil condition under the embankment is not accounted for. Conversely, the percent of the horizontal distance of the FEM modeling is decreasing with increasing the embankment height. In addition, the computed result by the BSI (2010) recommendation for the lowest embankment height underestimates the recommended value obtained in the FEM results. In contrast, the computed results by the BSI (2010) recommendation for the rest of the embankment loads overestimate the values obtained in the FEM study. This is attributed to the dependency of the geometry of the slope and the embankment filling material only.

### 6.8.2. Stress Reduction Ratio (SRR)

The SRR is the average stress on the subgrade soil or geosynthetic reinforcement to the average vertical stress at the base of the embankment consisting of the embankment weight and the surcharge load. The SRR value is evaluated using the Generalized Adapted Terzaghi Method recommended by the FHWA as explained in Chapter 2. This method is a revised version of the Adapted Terzaghi Method (Russell and Pierpoint, 1997; Russell et al., 2003) in which any pile

arrangement is adopted, and the GRTLP material and the critical height of embankment are accounted for as well. The average stress acting up on the base of the embankment in the area underlain by soil, which is $\sigma_{soil,geotop}$ and which can be expressed as $\sigma_{soil}$ for a pile-supported embankment without geosynthetic reinforcemen is:

$$\sigma_{soil,geotop}\ or\ \sigma_{soil} = \frac{\gamma_1}{\alpha_1}(1 - e^{-\alpha_1 H_1}) + \frac{\gamma_2}{\alpha_2}(e^{-\alpha_1 H_1})\left(1 - e^{-\alpha_2 (H_{crit} - H_1)}\right)$$
$$+[q + (H_1 + H_2 - H_{crit})\gamma_2](e^{-\alpha_1 H_1})\left(e^{-\alpha_2 (H_{crit} - H_1)}\right) \quad (6.2)$$

And,

$$H_{crit} = \max\begin{Bmatrix} 1.5\ (s - a) \\ 1.15\ s' + 1.44\ d \end{Bmatrix} \quad (6.3)$$

$$\alpha_{1,2} = \frac{p\ K_{1,2}\ tan\phi_{1,2}}{A_{soil}} \quad (6.4)$$

Assuming that no reaction is provided from the subsoil underneath the embankment, the SRR is computed as follows:

$$SRR = \frac{\sigma_{soil,geotop}}{\gamma H + q} \quad (6.5)$$

Parameters used to evaluate the SRR are summarized in table 6.28. It should be noted that the 1 and 2 subscripts represent the properties of the GRLTP and embankment fill materials, respectively. In addition, the equivalent pile width, $a_{eq}$, is 0.886 times the diameter of the pile ($d$). Moreover, the values of the lateral earth pressure coefficient are assumed to be 1.0 as suggested by Rowe and Liu (2015). The computed values of $H_{crit}$ and $\alpha_{1,2}$ for each embankment height are reported in Table 6.29. The SRR obtained from the FHWA recommendations is compared with values obtained from the FEM parametric study using the 1.22 m (4 ft) pile spacing for Case 1 and Case 3. The SRR values are reported for all the five geosynthetic layers except for Case 1 with an embankment height of 9.15 m in which a GRLTP with 7 layers is recommended for use in this

case. Table 6.30 shows the computed results by the FHWA design recommendation and the values obtained from the FEM models.

Table 6.28. Parameters used to compute the SRR.

| | |
|---|---|
| $d$ (m) | 0.305 |
| $s$ (m) | 1.22 |
| $a_{eq}$ (m) | 0.27 |
| $K_{1,2}$ | 1.0 |
| $\phi_{1,2}$ | 45°, 30° |
| $\gamma_{1,2}$ (kN/m$^3$) | 18.5 |
| $q$ (kPa) | 12 |

Table 6.29. Computed values of $H_{crit}$, and $\alpha_{1,2}$.

| H (m) | $H_1$ (m) | $H_2$ (m) | $H_{crit1}$ (m) | $H_{crit2}$ (m) | Adopted $H_{crit}$ (m) | $\alpha_1$ | $\alpha_2$ |
|---|---|---|---|---|---|---|---|
| 3.05 | 0.610 | 2.440 | 1.45 | 1.26 | 1.45 | 0.764 | 0.440 |
| 6.10 | 0.610 | 5.490 | | | | | |
| 9.15 | 0.915 | 8.235 | | | | | |

Table 6.30. SRR values.

| Soil Profile | H (m) | $SRR$ (FH-WA) | $SSR_1$ (FEM) | $SSR_2$ (FEM) | $SSR_3$ (FEM) | $SSR_4$ (FEM) | $SSR_5$ (FEM) | $SSR_6$ (FEM) | $SSR_7$ (FEM) |
|---|---|---|---|---|---|---|---|---|---|
| Case 1 | 3.05 | 0.52 | 0.2 | 0.32 | 0.49 | 0.58 | 0.66 | - | - |
| | 6.10 | 0.48 | 0.14 | 0.30 | 0.45 | 0.55 | 0.62 | - | - |
| | 9.15 | 0.43 | 0.11 | 0.26 | 0.41 | 0.56 | 0.67 | 0.75 | 0.78 |
| Case 3 | 3.05 | 0.52 | 0.32 | 0.58 | 0.68 | 0.71 | 0.73 | - | - |
| | 6.10 | 0.48 | 0.21 | 0.56 | 0.62 | 0.69 | 0.68 | - | - |
| | 9.15 | 0.43 | 0.19 | 0.54 | 0.59 | 0.66 | 0.60 | - | - |

Results of the FHWA recommendations are the same for Case 1 and Case 3, showing a decrease in value with increasing the embankment heights. It is also noted that the $SRR$ value is evaluated for the entire platform. Computed values are 0.52, 0.48, and 0.43 for the lowest, intermediate, and

highest embankment heights. The same results are observed for Cases 1 and 3 as the SRR evaluation by the Generalized Adapted Terzaghi Method does not account for the condition of the subsoil underneath the embankment. Conversely, the $SRR$ value for each reinforcement layer can be evaluated using the FEM of the simulated case. The FEM results for Case 1 showed an increase in the SRR values from the bottom geosynthetic layer to top geosynthetic layer, meaning that the lower geosynthetic layers experience lesser vertical loads than the upper ones attributed to the arching effect. Values ranged from 0.2 to 0.66 from the bottom to the top layer with the lowest embankment height. The SRR from the FHWA recommendations for the same condition falls within this range. Furthermore, a comparison is made between the lowest and intermediate embankment heights for Case 1 as 7 layers are adopted for the highest embankment height. The SRR showed a decrease with increasing the embankment height as observed in the adopted method by the FHWA. Similarly, results from the FHWA recommendations for Case 3 show a reduction in the SSR with increasing the embankment height. This is also observed in the results of the FEM of Case 3 as well. Meanwhile, all the SRR values obtained from the FHWA manual fall within the reported range of the FEM parametric study. However, comparing the FEM results in both Cases 1 and 3, results show higher SSR values for the same embankment height and same geosynthetic layer, meaning that the arching effect is more developed for the case of the very soft clay layer compared to that of the very loose sand layer. This confirms the higher stress concentration ratios (SCR) for the very soft clay layer than that of the very loose sand as observed throughout the parametric study.

### 6.8.3. Tension in Geosynthetics

The tension ($T$) in the geosynthetic layers due to vertical loads can be evaluated as suggested by Filz et al. (2019) as follows:

$$6T^3 - 6T\left(\frac{\sigma_{net}A_{soil}}{p}\right)^2 - J\left(\frac{\sigma_{net}A_{soil}}{p}\right)^2 = 0 \quad (6.6)$$

The bottom soil reaction is assumed to be zero, so the net vertical stress acting on the geosynthetic is the same evaluated in the SRR section above, and it will be used here.

Furthermore, the tension in the geosynthetics due to the lateral spreading effect is evaluated as follows:

$$P_{Lat} = K_a\left[\gamma\left(H^2/_2\right) + qH\right] \quad (6.7)$$

The computed tension from the equations above is used with a strain level of 5% to evaluate the required tensile stiffness ($J$) for the geosynthetics, and then compared with the axial stiffness used in the FEM to obtain a maximum allowable strain limit of 5%. For Case 1 soil profile, the lowest and intermediate embankment heights have 5 layers of geosynthetics with a total tensile stiffness of 2325 kN/m, whereas the highest embankment height is reinforced with 7 layers of geosynthetics with a total tensile stiffness of 3300 kN/m. Similarly, all embankment heights in Case 3 are reinforced with 5 layers of geosynthetics with a total tensile stiffness of 2325 kN/m. Table 6.31 shows the computed values of tension and tensile stiffness due to the vertical loads and the lateral spreading effect.

Table 6.31. Tension and tensile stiffness in the geosynthetic layers.

| Soil Profile | H (m) | $T$ (kN/m) | $P_{lat}$ (kN/m) | Total Tension= $T + P_{lat}$ (kN/m) | Required $J$ (kN/m) | FEM $J$ (kN/m) |
|---|---|---|---|---|---|---|
| Case 1 | 3.05 | 101.7 | 40.9 | 142.6 | 2852 | 2325 |
| | 6.10 | 149.3 | 139.1 | 288.4 | 5768 | 2325 |
| | 9.15 | 198.2 | 294.7 | 492.9 | 9858 | 3300 |
| Case 3 | 3.05 | 101.7 | 40.9 | 142.6 | 2852 | 2325 |
| | 6.10 | 149.3 | 139.1 | 288.4 | 5768 | 2325 |
| | 9.15 | 180.8 | 294.7 | 475.5 | 9510 | 2325 |

Results of the tension from the vertical loads and the lateral spreading is increasing with increasing the embankment height. The lateral spreading effect is the lowest among the two sources for the lowest and intermediate embankment heights, while it outweighs the tension from vertical loads at the highest embankment height. In addition, both computed results of $T$ and $P_{lat}$ are the same in Cases 1. The required axial stiffness to keep the strain levels in the geosynthetics under 5% overestimates the values obtained from the FEM modeling. This overestimation increases with increases the embankment height. For instance, the required axial stiffness according to the FHWA design recommendations overestimates the FEM values by a percentage of 22% and 198% for the lowest and highest embankment heights. This is also observed for the required tensile stiffness in Case 3.

# CHAPTER 7.
# CONCLUSIONS AND RECOMMENDATIONS

## 7.1. Conclusions

A 2D Finite Element numerical modeling study was carried out to simulate the performance of the pile-supported embankment system utilizing a geosynthetic reinforced load transfer platform (GRLTP) which was verified by well-documented case studies for this system, and to conduct an extensive Finite Element Modeling (FEM) parametric study of different parameters to investigate the effect of these parameters on the performance of the system. The parameters included changing the soil profile, changing the GRLTP and piles' extent under the slope, changing the embankment height (H), and changing the center-to-center pile spacing with different GRLTP configurations. The soil profiles consisted mainly of bad quality soils such as very soft clay and very loose sand layers. The rest of the layers are good quality soils to maintain an end bearing pile condition where piles are tipped on medium dense sand, dense sand, or stiff clay layers. Furthermore, the GRLTP and piles' extent were investigated by conducting a safety analysis of the system with changing the GRLTP and piles' extent under the slope which were 0.0H (at the embankment crest), 0.5H (one-quarter of the slope), 1.0H (mid-slope), 1.5H (three-quarters of the slope), and 2.0H (full length up to the embankment toe). Embankment heights were varied to be 3.05 m (10 ft), 6.10 m (20 ft), and 9.15 m (30 ft). Finally, the center-to-center pile spacing was varied as three to six times the pile diameter (3D-6D) to maintain a stable and economic system. The main performance measures were the settlement, the time rate of consolidation, the vertical stress, the lateral displacement, and the strain in the geosynthetic reinforcement. Based on the numerical modeling simulation and the FEM parametric study, the following conclusions can be made:

- The pile-supported embankment technique utilizing a GRLTP improves the overall performance of the system in terms of time and stability of the system.

- Generally, results of this study helped the LA DOTD to be more confident in designing this system in the state of Louisiana.
- An increase in the pile length of twice the pile diameter (2D) was suggest and adopted for cases where piles are tipped on a good quality layer which was overlaid by a bad quality layer to account for the irregularity of the soil layers in the field.
- The stability analysis in the system was mainly governed by the soil condition underneath the embankment and the GRLTP and piles' extent under the slope.
- The stability of the system at an embankment height of 3.05 m (10 ft) was maintained with a GRLTP and piles' extent of 1.5H and 0.5H for a normally consolidated (NC) and overconsolidated (OC) very soft clay layer underneath the embankment, respectively.
- The stability of the system at an embankment height of 6.10 m (20 ft) and 9.15 m (30 ft) was maintained with a GRLTP and piles' extent of 2.0H and 1.5H for a normally consolidated (NC) and overconsolidated (OC) very soft clay layer underneath the embankment, respectively.
- The stability of the system was maintained with a GRLTP and piles' extent of 0.0H, 1.0H, and 1.5H for a very loose sand layer underneath the embankment at embankment heights of 3.05 m (10 ft), 6.10 m (20 ft), and 9.15 m (30 ft), respectively.
- Factor of safety increased with time between the short term and long term analysis for cases where failure plane (slip surface) was initiated in the very soft clay layer due to the strength gain with the consolidation process.
- Factor of safety was almost the same for the short and long-term analyses when the failure plane (slip surface) was initiated in the embankment material only.

- Better overall performance of the system was observed for the cases where a very loose sand existed underneath the embankment compared to that of a very soft clay layer.
- Better performance was expected in the field than the performance predicted in this study for Cases 1 and 2 as the effect of pile driving on the strength of the very soft clay was not considered.
- The effect of increasing the lateral earth pressure coefficient due to pile driving resulted in no significant improvement on the settlement, but the lateral displacement was improved significantly.
- Heaving was observed near the embankment toe, where a very soft clay layer existed underneath the embankment due to the movement of the slope near the embankment toe with the undrained loading of the soft clay layer.
- Vertical stress on the pile heads increased with time, while vertical stress acting on the soil between the piles decreased with time due to the arching effect.
- Better arching effect development was observed for the very soft clay than that of the very loose sand layer due to the larger differential settlement between the piles and the very soft clay between the piles.
- Stress concentration ratio (SCR) for the cases where a very soft clay layer existed underneath the embankment outweighed the SCR values for a subsoil condition of very loose sands under the same embankment load and pile spacing.
- Higher SCR values were observed after 2 years of consolidation than that observed at the end of construction (EOC) for all soil profiles due to the arching mechanism.
- The strain profiles along the geosynthetic layers demonstrated a peak-trough profile where peaks were observed on top of the soil surrounding the piles for the bottom geotextile,

whereas the peak is found on top of the pile heads for the rest of the geosynthetic layers at all embankment heights as the bottom layer was supported by the piles and the rest of the layers had lack of support underneath them.

- A rapid change in the strain value occurred at the edges of the pile as a largest curvature of the geosynthetics occurred at the pile edges due to lack of support resulting in maximum strain values at the pile edges.
- The lateral extent of the piles under the embankment slope evaluated by the FHWA design recommendations provided by the British Standards Institution Code of Practice overestimated the maximum allowable horizontal distance between the extreme edge of the pile or the pile cap and the embankment toe compared to the obtained values from the FEM parametric study as the recommendation depended on the embankment height and the embankment fill material only.
- The stress reduction ratio (SRR) evaluated from the FHWA design recommendations fell within the SRR range provided by the FEM modeling for each geosynthetic layer with a decrease in the SRR value with increasing the embankment height for all soil profiles.
- The required tensile stiffness of geosynthetics to resist vertical loads and lateral spreading was overestimated by the FHWA design recommendations compared to the obtained values from the FEM parametric study, and this overestimation increased with increasing the embankment height.
- It was suggested that the edge of the last pile coincide with the GRLTP edge for convenience. This can be achieved by changing the spacing of the last pile or the piles under the slope until this condition is satisfied. Otherwise, the maximum distance between

the far end of the last pile and the GRLTP should not exceed 1.07 m (3.5 ft), which was the largest distance observed for all cases in this study.

## 7.2. Recommendations

- Additional research effort is needed to investigate the performance of the system with a triangular piles arrangement under the embankment.
- Studying the performance of the pile-supported embankment system utilizing the GRLTP under a floating piles configuration.
- Further experimental investigation is needed to study the effect of pile driving on the soft soil shear strength before the start of construction.
- There is a need for a full-scale testing to evaluate and verify the findings of this numerical modeling study.
- Additional numerical modeling research is needed to investigate the buckling of very long timber piles so that the timber pile length requirement is improved.
- Conducting experimental tests to evaluate the thickness of the GRLTP to increase the arching efficiency.

# REFERENCES


Abu-Farsakh, M. Y., Yoon, S., & Tsai, C. (2009). Calibration of resistance factors needed in the LRFD design of driven piles (No. FHWA/LA. 09/449). Louisiana Transportation Research Center.

Abusharar, S. W., Zheng, J. J., Chen, B. G., & Yin, J. H. (2009). A simplified method for analysis of a piled embankment reinforced with geosynthetics. Geotextiles and Geomembranes, 27(1), 39-52.

Almeida, M. S. S., Ehrlich, M., Spotti, A. P., & Marques, M. E. S. (2007). Embankment supported on piles with biaxial geogrids. Proceedings of the Institution of Civil Engineers-Geotechnical Engineering, 160(4), 185-192.

Ambily, A. P., & Gandhi, S. R. (2007). Behavior of stone columns based on experimental and FEM analysis. Journal of geotechnical and geoenvironmental engineering, 133(4), 405-415.

Ameratunga, J., Sivakugan, N., & Das, B. M. (2016). Correlations of soil and rock properties in geotechnical engineering. New Delhi: Springer India.

Ardah, A. I. (2018). Field Instrumentations and Numerical Analysis of Geosynthetic Reinforced Soil's Integrated Bridge System (GRS-IBS) (Doctoral dissertation, Louisiana State University).

Ariyarathne, P., Liyanapathirana, D. S., & Leo, C. J. (2013). Comparison of different two-dimensional idealizations for a geosynthetic-reinforced pile-supported embankment. International Journal of Geomechanics, 13(6), 754-768.

Bhasi, A., & Rajagopal, K. (2015). Geosynthetic-reinforced piled embankments: comparison of numerical and analytical methods. International Journal of Geomechanics, 15(5), 04014074.

Bosscher, P. J., & Gray, D. H. (1986). Soil arching in sandy slopes. Journal of Geotechnical Engineering, 112(6), 626-645.

Briançon, L., & Simon, B. (2012). Performance of pile-supported embankment over soft soil: full-scale experiment. Journal of Geotechnical and Geoenvironmental Engineering, 138(4), 551-561.

Broms, B. B., & Boman, P. (1979). Lime columns-a new foundation method. Journal of Geotechnical and Geoenvironmental engineering, 105(ASCE 14543).

BSI. (2010). BS 8006-1: 2010: Code of practice for strengthened/reinforced soils and other fills. Design of embankments with reinforced soil foundations on poor ground.

Budhu, M. (2010). Soil Mechanics and Foundation–3rd Edition" John Wiley & Sons Inc. ISBN 978-040-55684-9.

Carlson, B. O. (1987). Armerad Jord beräkningsprinciper för banker på pålar. Terranova, Distr. SGI., Linköping (in Swedish).

Chai, J. C., Shrestha, S., Hino, T., Ding, W. Q., Kamo, Y., & Carter, J. (2015). 2D and 3D analyses of an embankment on clay improved by soil–cement columns. Computers and Geotechnics, 68, 28-37.

Cheng, Q., Wu, J., Zhang, D., & Ma, F. (2014). Field testing of geosynthetic-reinforced and column-supported earth platforms constructed on soft soil. Frontiers of Structural and Civil Engineering, 8(2), 124-139.

Chen, R. P., Chen, Y. M., Han, J., & Xu, Z. Z. (2008). A theoretical solution for pile-supported embankments on soft soils under one-dimensional compression. Canadian Geotechnical Journal, 45(5), 611-623.

Chen, R. P., Xu, Z. Z., Chen, Y. M., Ling, D. S., & Zhu, B. (2010). Field tests on pile-supported embankments over soft ground. Journal of Geotechnical and Geoenvironmental Engineering, 136(6), 777-785.

Coduto, D. P., Kitch, W. A., & Yeung, M. C. R. (2001). Foundation design: principles and practices (Vol. 2). USA: Prentice Hall.

Collin, J. G. (2004, February). Column supported embankment design considerations. In Proceedings of the 52nd annual geotechnical engineering conference (pp. 51-78). Minnesota.

Collin, J. G., Han, J., & Huang, J. (2005). Geosynthetic reinforced column support embankment design guidelines. In Proceedings, the North America Geosynthetics Society Conference (pp. 1-15).

Das, B., Sobhan, K., & Das, B. (2016). Principles of Geotechnical Engineering 8th Ed. Instructor, 201601.

Filz, G. M., Sloan, J. A., McGuire, M. P., Smith, M., & Collin, J. (2019). Settlement and vertical load transfer in column-supported embankments. Journal of Geotechnical and Geoenvironmental Engineering, 145(10), 04019083.

Filz, G. M., & Smith, M. E. (2006). Design of bridging layers in geosynthetic-reinforced, column-supported embankments. Virginia Center for Transportation Innovation and Research.

Filz, G. M., & Smith, M. E. (2007). Net vertical loads on geosynthetic reinforcement in column-supported embankments. In Soil Improvement (pp. 1-10).

Gibbs, H. J., & Holtz, W. G. (1957). Research on Determining Density of Sands by Spoon Penetration Standart. In Proc. Int. Conf. Soil Mech. Found. Eng. 4 th, London, 1: 35 (Vol. 39).

Guido, V. A. (1987). Plate loading tests on geogrid-reinforced earth slab. In Geosynthetic'87 Conf. (pp. 216-225).

Halvordson, K. A., Plaut, R. H., & Filz, G. M. (2010). Analysis of geosynthetic reinforcement in pile-supported embankments. Part II: 3D cable-net model. Geosynthetics International, 17(2), 68-76.

Han, J. (1999). Design and construction of embankments on geosynthetic reinforced platforms supported by piles. In Proceedings of (pp. 66-84).

Han, J., Bhandari, A., & Wang, F. (2012). DEM analysis of stresses and deformations of geogrid-reinforced embankments over piles. International Journal of Geomechanics, 12(4), 340-350.

Han, J., & Gabr, M. A. (2002). Numerical analysis of geosynthetic-reinforced and pile-supported earth platforms over soft soil. Journal of geotechnical and geoenvironmental engineering, 128(1), 44-53.

Han, J., Zhou, H. T., & Ye, F. (2002). State-of-practice review of deep soil mixing techniques in China. Transportation research record, 1808(1), 49-57.

Hannigan, P. J., Rausche, F., Garland, L. E., Robinson, B. R., Becker, M. L., & Shelsta, H. (2016). Design and construction of driven pile foundations. US Department of Transportation, Federal Highway Administration.

Haring, W., Profittlich, M., & Hangen, H. (2008). Reconstruction of the national road N210 Bergambacht to Krimpen ad IJssel, NL: design approach, construction experiences and measurement results. In Proceedings 4th European Geosynthetics Conference.

Hewlett, W. J., & Randolph, M. F. (1988). Analysis of piled embankments. In International Journal of Rock Mechanics and Mining Sciences and Geomechanics Abstracts (Vol. 25, No. 6, pp. 297-298). Elsevier Science.

Hinchberger, S. D., & Rowe, R. K. (1998). Modelling the rate-sensitive characteristics of the Gloucester foundation soil. Canadian Geotechnical Journal, 35(5), 769-789.

Huang, J., & Han, J. (2009). 3D coupled mechanical and hydraulic modeling of a geosynthetic-reinforced deep mixed column-supported embankment. Geotextiles and Geomembranes, 27(4), 272-280.

Huang, J., & Han, J. (2010). Two-dimensional parametric study of geosynthetic-reinforced column-supported embankments by coupled hydraulic and mechanical modeling. Computers and Geotechnics, 37(5), 638-648.

Huang, J., Han, J., & Oztoprak, S. (2009). Coupled mechanical and hydraulic modeling of geosynthetic-reinforced column-supported embankments. Journal of Geotechnical and Geoenvironmental Engineering, 135(8), 1011-1021.

Hunt, C. E., Pestana, J. M., Bray, J. D., & Riemer, M. (2002). Effect of pile driving on static and dynamic properties of soft clay. Journal of geotechnical and geoenvironmental engineering, 128(1), 13-24.

Hwang, J. H., Liang, N., & Chen, C. H. (2001). Ground response during pile driving. Journal of Geotechnical and Geoenvironmental Engineering, 127(11), 939-949.

Jaky, J. (1944). The coefficient of earth pressure at rest. J. of the Society of Hungarian Architects and Engineers, 355-358.

Jamsawang, P., Yoobanpot, N., Thanasisathit, N., Voottipruex, P., & Jongpradist, P. (2016). Three-dimensional numerical analysis of a DCM column-supported highway embankment. Computers and Geotechnics, 72, 42-56.

Jenck, O., Dias, D., & Kastner, R. (2005). Soft ground improvement by vertical rigid piles two-dimensional physical modelling and comparison with current design methods. Soils and Foundations, 45(6), 15-30.

Jenck, O., Dias, D., & Kastner, R. (2009). Discrete element modelling of a granular platform supported by piles in soft soil–Validation on a small scale model test and comparison to a numerical analysis in a continuum. Computers and Geotechnics, 36(6), 917-927.

Johnson, A., 2011. Recommendations for Design and Analysis of Earth Structures Using Geosynthetic Reinforcements-EBGEO. Wiley, Hoboken.

Jones, B. M., Plaut, R. H., & Filz, G. M. (2010). Analysis of geosynthetic reinforcement in pile-supported embankments. Part I: 3D plate model. Geosynthetics International, 17(2), 59-67.

Jones, C.J.F.P., Lawson, C.R. & Ayres, D.J., 1990. Geotextile reinforced piled embankments, Geotextiles, Geomembranes and Related Products, G. den Hoedt (ed.), 1990, Balkema, Rotterdam, ISBN 90 6191 119 2, pp. 155-160.

Kempfert, H. G., Stadel, M., & Zaeske, D. (1997). Berechnung von geokunststoffbewehrten Teagschichten über Pfahlelementen. Bautechnik (Berlin, 1984), (12), 818-825.

Kempton, G., Russell, D., Pierpoint, N. D., & Jones, C. J. F. P. (1998, March). Two-and three-dimensional numerical analysis of the performance of piled embankments. In Proceedings, 6th International Conference on Geosynthetics (Vol. 2, pp. 767-772).

Kulhawy, F. H., & Mayne, P. W. (1990). Manual on estimating soil properties for foundation design (No. EPRI-EL-6800). Electric Power Research Inst., Palo Alto, CA (USA); Cornell Univ., Ithaca, NY (USA). Geotechnical Engineering Group.

Lai, H. J., Zheng, J. J., Cui, M. J., & Chu, J. (2020). “Soil arching” for piled embankments: insights from stress redistribution behaviour of DEM modelling. Acta Geotechnica, 15(8), 2117-2136.

Lai, H. J., Zheng, J. J., Zhang, J., Zhang, R. J., & Cui, L. (2014). DEM analysis of "soil"-arching within geogrid-reinforced and unreinforced pile-supported embankments. Computers and Geotechnics, 61, 13-23.

Lai, H. J., Zheng, J. J., Zhang, R. J., & Cui, M. J. (2018). Classification and characteristics of soil arching structures in pile-supported embankments. Computers and Geotechnics, 98, 153-171.

Le Hello, B., & Villard, P. (2009). Embankments reinforced by piles and geosynthetics—Numerical and experimental studies dealing with the transfer of load on the soil embankment. Engineering Geology, 106(1-2), 78-91.

Lin, K. Q., & Wong, I. H. (1999). Use of deep cement mixing to reduce settlements at bridge approaches. Journal of geotechnical and geoenvironmental engineering, 125(4), 309-320.

Liu, H. L., Chu, J., & Deng, A. (2009). Use of large-diameter, cast–in situ concrete pipe piles for embankment over soft clay. Canadian Geotechnical Journal, 46(8), 915-927.

Liu, H. L., Ng, C. W., & Fei, K. (2007). Performance of a geogrid-reinforced and pile-supported highway embankment over soft clay: case study. Journal of Geotechnical and Geoenvironmental Engineering, 133(12), 1483-1493.

Liu, K. W., & Rowe, R. K. (2015). Numerical modelling of prefabricated vertical drains and surcharge on reinforced floating column-supported embankment behaviour. Geotextiles and Geomembranes, 43(6), 493-505.

Liu, S. Y., Du, Y. J., Yi, Y. L., & Puppala, A. J. (2012). Field investigations on performance of T-shaped deep mixed soil cement column–supported embankments over soft ground. Journal of Geotechnical and Geoenvironmental Engineering, 138(6), 718-727.

Low, B. K., Tang, S. K., & Choa, V. (1994). Arching in piled embankments. Journal of Geotechnical Engineering, 120(11), 1917-1938.

Magnan, J. P. (1994). Methods to reduce the settlement of embankments on soft clay: a review. In Vertical and Horizontal Deformations of Foundations and Embankments (pp. 77-91). ASCE.

Marston, A. (1913). The theory of loads on pipe in ditches and tests of cement and clay drain tile and sewer pipe. Bulletin, 31.

Mayne, P. W., & Kulhawy, F. H. (1982). Ko-OCR relationships in soil. Journal of the Geotechnical Engineering Division, 108(6), 851-872.

McGuire, M., Sloan, J., Collin, J., & Filz, G. (2012). Critical height of column-supported embankments from bench-scale and field-scale tests. In ISSMGE-TC 211 International Symposium on Ground Improvement IS-GI Brussels.

Meyerhof, G. G. (1976). Bearing capacity and settlement of pile foundations. Journal of the Geotechnical Engineering Division, 102(3), 197-228.

Murugesan, S., & Rajagopal, K. (2010). Studies on the behavior of single and group of geosynthetic encased stone columns. Journal of Geotechnical and Geoenvironmental Engineering, 136(1), 129-139.

Nordlund, R. L. (1963). Bearing capacity of piles in cohesionless soils. Journal of the Soil Mechanics and Foundations Division, 89(3), 1-35.

Oh, Y. I., & Shin, E. C. (2007). Reinforcement and arching effect of geogrid-reinforced and pile-supported embankment on marine soft ground. Marine Georesources and Geotechnology, 25(2), 97-118.

O'Neill, M. W., Hawkins, R. A., & Mahar, L. J. (1981). Field study of pile group action. Materials Div., Federal Highway Administration Offices of Research and Development, Washington, DC Rep. No. FHWA RD-81/002.

Orrje, O., & Broms, B. B. (1967). Effects of pile driving on soil properties. Journal of the Soil Mechanics and Foundations Division, 93(5), 59-73.

Peck, R. B., Hanson, W. E., & Thornburn, T. H. (1974). Foundation Engineering''2nd Edition, John Wiley and Sons, New York.

Pham, T. A., Tran, Q. A., Villard, P., & Dias, D. (2021). Geosynthetic-reinforced pile-supported embankments− 3D discrete numerical analyses of the interaction and mobilization mechanisms. Engineering Structures, 242, 112337.

Plaut, R. H., & Filz, G. M. (2010). Analysis of geosynthetic reinforcement in pile-supported embankments. Part III: Axisymmetric model. Geosynthetics International, 17(2), 77-85.

Pongsivasathit, S., Chai, J., & Ding, W. (2013). Consolidation settlement of floating-column-improved soft clayey deposit. Proceedings of the Institution of Civil Engineers-Ground Improvement, 166(1), 44-58.

Rowe, R. K., & Liu, K. W. (2015). Three-dimensional finite element modelling of a full-scale geosynthetic-reinforced, pile-supported embankment. Canadian Geotechnical Journal, 52(12), 2041-2054.

Russell, D. and Pierpoint, N. (1997). An Assessment of Design Methods for Piled Embankments. Ground Engineering, 30(11): pp. 39-44.

Russell, D., Naughton, P.J., and Kempton, G. (2003). A New Design Procedure for Piled Embankments. Proc. 56th Canadian Geotechnical Conference and 2003 NAGS Conference, Vol. 1, Winnipeg, MB, pp. 858-865.

Schaefer, V. R., Berg, R. R., Collin, J. G., Christopher, B. R., DiMaggio, J. A., Filz, G. M., ... & Ayala, D. (2017). Ground Improvement Methods–Reference Manual Vols. I and II. FHWA-NHI-16-027 and FHWA-NHI-16-028.

Shen, P., Xu, C., & Han, J. (2018). Model tests investigating spatial tensile behavior of simulated geosynthetic reinforcement material over rigid supports. Journal of Materials in Civil Engineering, 30(2), 04017288.

Sloan, J. A. (2011). Column-supported embankments: full-scale tests and design recommendations (Doctoral dissertation, Virginia Tech).

Smith, M. E. (2005). Design of bridging layers in geosynthetic-reinforced column-supported embankments (Doctoral dissertation, Virginia Tech).

Smith, M., & Filz, G. (2007). Axisymmetric numerical modeling of a unit cell in geosynthetic-reinforced, column-supported embankments. Geosynthetics International, 14(1), 13-22.

Standards Australia (2002) AS 4678 earth retaining structures, Sydney.

Stuedlein, A. W., & Holtz, R. D. (2013). Bearing capacity of spread footings on aggregate pier reinforced clay. Journal of geotechnical and geoenvironmental engineering, 139(1), 49-58.

Van Eekelen, S. J., Bezuijen, A., & Van Tol, A. F. (2013). An analytical model for arching in piled embankments. Geotextiles and Geomembranes, 39, 78-102.

Van Eekelen, S. J., Bezuijen, A., Lodder, H. J., & Van Tol, A. F. (2012a). Model experiments on piled embankments. Part I. Geotextiles and Geomembranes, 32, 69-81.

Van Eekelen, S. J., Bezuijen, A., Lodder, H. J., & Van Tol, A. F. (2012b). Model experiments on piled embankments. Part II. Geotextiles and Geomembranes, 32, 82-94.

Van Eekelen, S. V., Bezuijen, A., & Van Tol, A. F. (2011). Analysis and modification of the British Standard BS8006 for the design of piled embankments. Geotextiles and Geomembranes, 29(3), 345-359.

Taechakumthorn, C., & Rowe, R. K. (2012). Performance of a reinforced embankment on a sensitive Champlain clay deposit. Canadian Geotechnical Journal, 49(8), 917-927.

Tavenas, F., Mieussens, C., & Bourges, F. (1979). Lateral displacements in clay foundations under embankments. Canadian Geotechnical Journal, 16(3), 532-550.

Terzaghi, K. (1943). Arching in ideal soils. Theoretical soil mechanics, 66-76.

Terzaghi, K. (1943). Theoretical soil mechanics. John wiley & sons. New York, 11-15.

Terzaghi, K., Peck, R. B., & Mesri, G. (1996). Soil mechanics in engineering practice. John Wiley & Sons.

Tomlinson, M. J. (1957, August). The adhesion of piles driven in clay soils. In Proceedings of the 4th international conference on soil mechanics and foundation engineering (Vol. 2, pp. 66-71).

Wolff, T. F. (1989). Pile capacity prediction using parameter functions. In Predicted and observed axial behavior of piles: results of a pile prediction symposium (pp. 96-106). ASCE.

Xing, H., Zhang, Z., Liu, H., & Wei, H. (2014). Large-scale tests of pile-supported earth platform with and without geogrid. Geotextiles and Geomembranes, 42(6), 586-598.

Ye Yang-sheng, Cai De-gou, Zhang Qian-li, & Yan Hong-ye, 2009. Calculating method of reinforced bedding in the geosynthetics reinforced and pile supported embankment, Proceedings of the 17th International Conference on Soil Mechanics and Geotechnical Engineering (Volumes 1, 2, 3 and 4), 933 – 937. DOI:10.3233/978-1-60750-031-5-933.

Yoo, C., & Kim, S. B. (2009). Numerical modeling of geosynthetic-encased stone column-reinforced ground. Geosynthetics International, 16(3), 116-126.

Yu, Y., & Bathurst, R. J. (2017). Modelling of geosynthetic-reinforced column-supported embankments using 2D full-width model and modified unit cell approach. Geotextiles and Geomembranes, 45(2), 103-120.

Zhang, C., Jiang, G., Liu, X., & Buzzi, O. (2016). Arching in geogrid-reinforced pile-supported embankments over silty clay of medium compressibility: Field data and analytical solution. Computers and Geotechnics, 77, 11-25.

Zhang, C., Jiang, G., Liu, X., & Wang, Z. (2015). Deformation performance of cement-fly ash-gravel pile-supported embankments over silty clay of medium compressibility: a case study. Arabian Journal of Geosciences, 8(7), 4495-4507.

Zhang, J., Zheng, J. J., Chen, B. G., & Yin, J. H. (2013). Coupled mechanical and hydraulic modeling of a geosynthetic-reinforced and pile-supported embankment. Computers and Geotechnics, 52, 28-37.

Zheng, G., Jiang, Y., Han, J., & Liu, Y. F. (2011). Performance of cement-fly ash-gravel pile-supported high-speed railway embankments over soft marine clay. Marine Georesources and Geotechnology, 29(2), 145-161.

Zhou, Y., & Kong, G. (2019). Deformation analysis of geosynthetic-encased stone column–supported embankment considering radial bulging. International Journal of Geomechanics, 19(6), 04019057.

Zhuang, Y., Wang, K. Y., & Liu, H. L. (2014). A simplified model to analyze the reinforced piled embankments. Geotextiles and Geomembranes, 42(2), 154-165.

# VITA

Abdallah Ikbarieh was born on November 6, 1996, in Irbid, Jordan. He finished his high school from King Abdullah II School for Excellence, Irbid, Jordan, in June 2014. He received his bachelor's degree in civil engineering from Jordan University of Science and Technology, Irbid, Jordan, in August 2018, and worked for a year as a site civil engineer, in Irbid, Jordan. He came to the United States on August of 2019 to pursue his graduate studies in civil engineering at Louisiana State University, Baton Rouge, Louisiana. Abdallah Ikbarieh is anticipated to fulfill the requirements of the degree of Master of Science in civil engineering in August 2021.